Subcellular location and protein interactions of the infectious bronchitis virus gene 3 and 5 accessory proteins

Marc Tudor Davies

A thesis submitted for the degree of Doctor of Philosophy

Department of Biological Sciences, University of Warwick

Institute for Animal Health

September 2009

Contents

List of figures

List of tables

Acknowledgements

I am indebted to the following people whose advice and contributions have made the work in this thesis possible:

- Dr. Paul Britton. As supervisor I would like to thank him for all the support and discussions over the last four years.
- Prof. Dave Cavanagh for originally setting out the idea behind the project and also discussions early on in the work.
- Dr. Andrew C Gill for all the help with mass spectrometry and especially with confirming the identity of two of the generated proteins.
- Dr. Lawrence Hunt for his advice with the identification of the protein-protein interactions and performing some of the tandem mass spectrometry experiments.
- Dr. Dominic Kurian for his practical knowledge of identifying protein interactions by mass spectrometry and performing some of the tandem mass spectrometry experiments.
- Ruth Hennion and Gillian Hill for their contributions in preparing most of the primary cells and continuous cell lines.

Declaration

I declare that the work in this thesis is original, except where stated by special reference, and that it has not been presented previously to support another degree. The work performed is the author's sole efforts, except the acquisition of data pertaining to the identification of proteins by mass spectrometry.

Summary

The avian coronavirus infectious bronchitis virus (IBV) expresses four non-structural, non-gene 1 proteins (3a, 3b, 5a and 5b) which have been shown to be dispensable for virus replication in cell culture. These IBV accessory proteins have no sequence homology to any of the accessory proteins of the group I and II coronaviruses but are highly conserved among the group III coronaviruses. Characterisation of naturally occurring strains of IBV which do not express two or more of the accessory proteins and of genetically modified recombinant IBVs has demonstrated that these accessory proteins contribute at most a minor role to the pathogenicity of the virus. To understand the relevance of these proteins for IBV the subcellular location of the 3a, 5a and 5b proteins have been characterised along with the identification of potential protein-protein interactions for the 3a protein. The subcellular location and protein-protein interactions of the 3b protein were attempted but specific problems were encountered.

Indirect immunofluorescence with confocal microscopy of IBV-infected chick kidney cells was used to study the subcellular location of the accessory proteins. The 3a protein displayed a punctate, cytoplasmic distribution pattern which colocalised with virally-induced double-stranded RNA. A diffuse, cytoplasmic distribution was observed for the 5b protein which produced limited colocalisation with an IBV structural protein. Expression of a FLAG-tagged 5a protein in transfected Vero cells resulted in a punctate, cytoplasmic pattern. The protein interactions of the 3a protein were identified using FLAG-tag pull-down experiments with tandem mass spectrometry. Six cellular proteins were identified as interacting with the FLAG/3a protein within transfected Vero cells, three of which, GCN1, PP2A and Exportin-1, may interact with native 3a protein in IBV-infected cells.

The 3a protein could sequester the viral dsRNA to hide it from the innate immune system and the potential interactions with three cellular proteins indicate that the IBV 3a protein may contribute to attenuation of host cell translation, induce cell cycle arrest and/or attenuate the nuclear export of a specific subset of mRNAs.

Table of abbreviations

BAP	Bacterial alkaline phosphatase
Beau	IBV Beaudette (wild-type)
Beau-CK	Chick kidney cell-adapted IBV Beaudette (wild-type)
Beau-R	IBV Beaudette-R (recombinant virus based upon Beau-CK)
BSA	Bovine serum albumen
cDNA	Complementary DNA
CK	Chick kidney
CoV	Coronavirus
c.p.e.	Cytopathic effect
DDW	Double distilled water
DMV	Double membrane vesicle
DNA	Deoxyribonucleic acid
dsRNA	Double-stranded RNA
E	Envelope (protein)
eIF	Eukaryotic initiation factor
EMEM	Eagle’s minimum essential medium
ER	Endoplasmic reticulum
ERGIC	ER-Golgi intermediate compartment
ESI	Electrospray ionisation
GCN	General control non-derepressible
h p.i.	Hour(s) post infection
HE	Haemagglutinin-esterase
HIS	Polyhistidine (epitope)
HIV	Human immunodeficiency virus
HRP	Horseradish peroxidise
HTLV	Human T-cell lymphotropic virus
IBV	Infectious bronchitis virus
IFN	Interferon
IPTG	Isopropyl ß-D-1-thiogalactopyranoside
IRES	Internal ribosome entry site

IRF	Interferon regulatory factor
LB	Luria-Bertani
M	Membrane (protein)
m.o.i.	Multiplicity of infection
MHV	Murine hepatitis virus
MS	Mass spectrometry
N	Nucleocapsid (protein)
Nef	Negative factor
nsp	nonstructural protein
ORF	Open reading frame
PAGE	Polyacrylamide gel electrophoresis
PBS	Phosphate buffered saline
PCR	Polymerase chain reaction
PP2A	Protein phosphatase 2A
PVDF	Polyvinylidene Fluoride
RdRp	RNA-dependent RNA polymerase
RNA	Ribonucleic acid
RTC	Replication-transcription complex
RT-PCR	Reverse-transcriptase polymerase chain reaction
S	Spike (protein)
SARS-CoV	Severe acute respiratory syndrome coronavirus
sg	Subgenomic
STAT	Signal transduction and activator of transcription
SUMO	Small ubiquitin modifier
TAS	Transcription associated sequence
TOC	Tracheal organ culture
UPR	Unfolded protein response
UTR	Untranslated region
V	Virus
Vif	Viral infectivity factor
Vpr	Viral protein R
Vpu	Viral protein U

Introduction

The *Coronavirinae*

Infectious bronchitis virus (IBV) is a member of the *gammacoronavirus* genus in the *coronavirinae* subfamily. The *Coronavirinae* and *Torovirinae* subfamilies comprise the *Coronaviridae* family, which along with the *Arteriviridae* and *Roniviridae* families, constitute the order *Nidovirales* (Fig. 1.1).

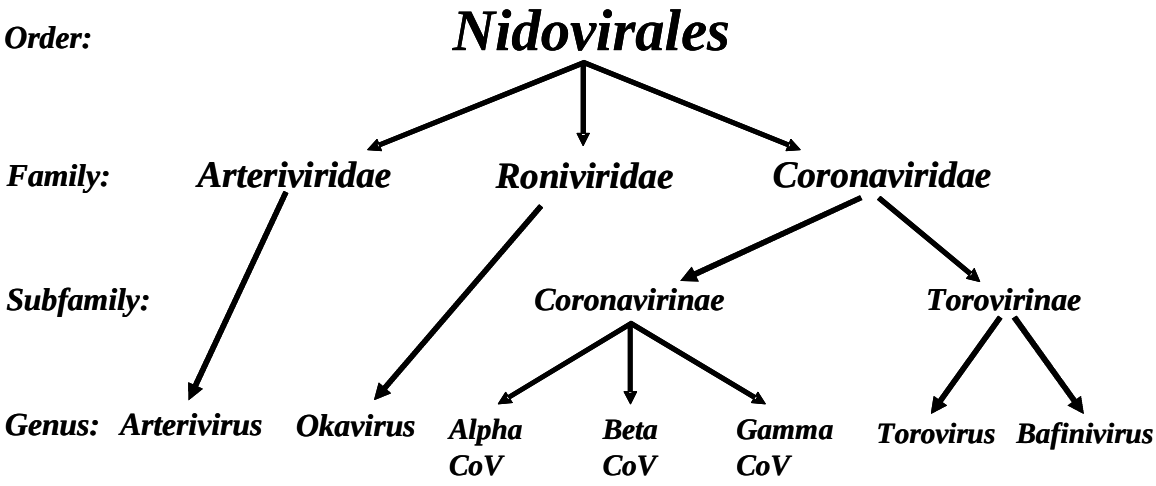

Figure 1.1. Taxonomy of the *Nidovirales*.

The taxonomy of order Nidovirales has recently changed (ICTV – Virus taxonomy 2009). The *coronavirinae* subfamily is now divided into three genera but was originally classified into three groups within the *coronavirus* genus based upon antigenic characteristics. These groups were later confirmed by phylogenetic analysis as coronavirus genome sequences became available. As more coronaviruses are discovered and their genomes sequenced distinctions are becoming evident between members of each genus. The *alphacoronaviruses* (previously group 1) were split into subgroups 1a and 1b (Gonzalez *et al.*, 2003). The *betacoronaviruses* (previously group 2) were divided into groups 2a and 2b (Snijder *et al.*, 2003) of which MHV and SARS-CoV were respective members. Putative groups 2c and 2d were proposed by Woo *et al*. (2007) to include various bat coronaviruses and groups

3b and 3c were proposed to incorporate newly discovered IBV-like coronaviruses (Mihindukulasuriya *et al.*, 2008; Woo *et al.*, 2009) (Table 1.1).

Table 1.1. The coronavirus groups, subgroups and coronavirus species.

Group	Subgroup	Coronavirus species[1]
Group 1	Group 1a	Porcine transmissible gastroenteritis (TGEV) Feline coronavirus (FCoV) Canine coronavirus (CCoV) Porcine respiratory coronavirus (PRCV)
	Group 1b	Human coronavirus (HCoV) 229E & NL63 Porcine epidemic diarrhoea virus (PEDV) *Miniopterus* bat coronavirus (Bat-CoV)
Group 2	Group 2a	Murine hepatitis virus (MHV) Bovine coronavirus (BCoV) Human coronavirus (HCoV) OC43, HKU1
	Group 2b	Severe acute respiratory coronavirus (SARS-CoV) Horse shoe bat coronavirus (SARS-CoV-Like, SL-BAT-CoV))
	Group 2c[2]	Bat coronavirus HKU4 (Bat-CoV HKU4) Bat coronavirus HKU5 (Bat-CoV HKU5)
	Group 2d[2]	Bat coronavirus HKU9 (Bat-CoV HKU9)
Group 3	Group 3a	Infectious bronchitis virus (IBV) Turkey coronavirus (TCoV) Partridge coronavirus (PrCoV) Peafowl coronavirus (PfCoV)
	Group 3b[2]	Beluga whale coronavirus (BeCoV)
	Group 3c[2]	Bullbul coronavirus (BuCoV) Thrush coronavirus (ThCoV) Munia coronavirus (MuCoV)

[1] Representatives from each subgroup
[2] Putative subgroups

Structure and morphology

The coronavirus particle consists of a single genome packaged into a helical structure by multiple copies of the N protein surrounded by an envelope into which the S, M and E proteins are inserted (Fig. 1.2). The spherical virions, approximately 120 nm in diameter (Davies and Macnaughton, 1979), appear surrounded by a

corona of protruding structures when observed by electron microscopy. These formations are the S proteins and give rise to the name of the genus.

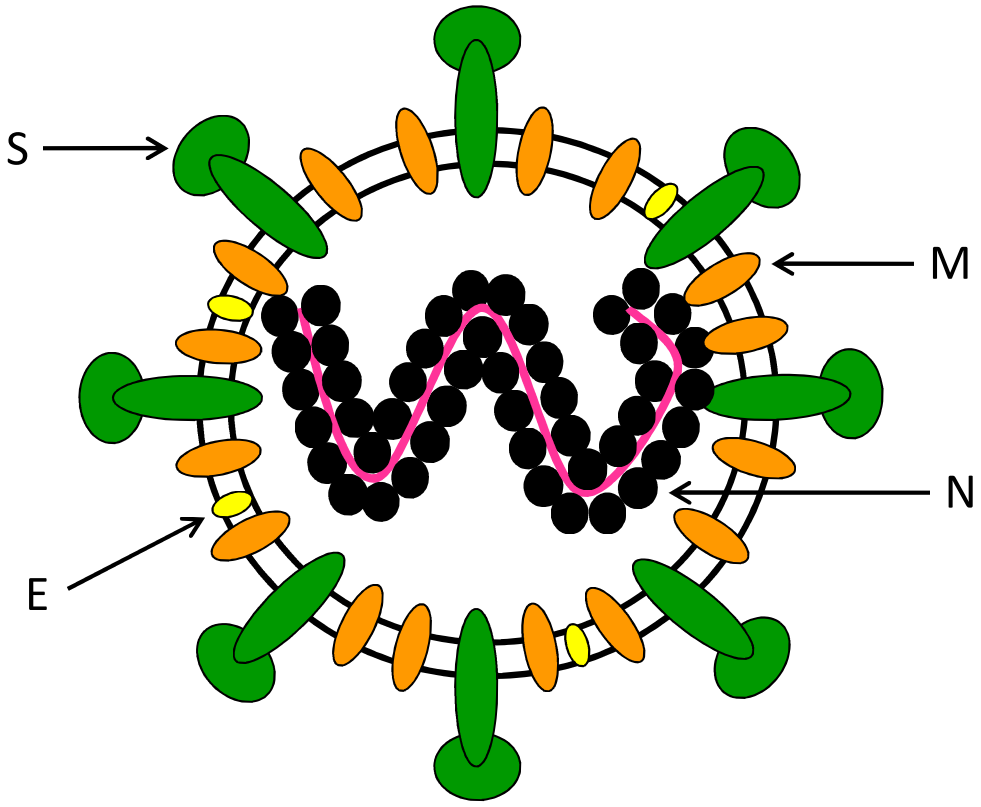

Figure 1.2. Structure of IBV. The non-segmented RNA genome (pink) is wrapped up in multiple copies of the N protein (black). Enclosing the genome is a membrane containing the M (orange), S (green) and E (yellow) proteins. The M protein interacts with the S, E and N proteins acting as the building block of the virion.

Genome organisation

The single stranded, non-segmented, positive-sense RNA genome varies in size from 27,317 nucleotides (nt) for human coronavirus (HCoV) – 229E to 31,357 nt for MHV-A59.

Features common to all coronavirus genomes include a 5’ cap, 5’ untranslated region (UTR), a large replicase gene (two-thirds of the genome), structural and non-structural genes (one-third of the genome) and a 3’UTR with poly(A) tail. The

minimum gene order is always: replicase, spike (S), envelope (E), membrane (M), nucleocapsid (N) (5' → 3') with a varying number of accessory genes dispersed between them (Fig. 1.3).

The terminal ends of the genome consist of an UTR which contains *cis*-acting sequences and structural elements important for viral transcription and replication (Dalton *et al.*, 2001; Liao and Lai, 1994; Lin *et al.*, 1994; Zhang *et al.*, 1994). The 5' UTR ranges from 209 – 528 nt in length for coronaviruses and toroviruses. The 3' UTR ranges from 288 – 506 nt in length for coronaviruses and toroviruses. Gene 1 (replicase) contains around 20 kb and encodes the proteins involved in viral RNA synthesis. It consists of two open reading frames (ORFs) (ORF 1a and 1b) that are translated into polyproteins 1a and 1ab (pp1a and pp1ab). Production of the downstream ORF, ORF 1b, requires a (-1) ribosomal frame-shift to produce the 1ab polyprotein (Brierley *et al.*, 1987). This frame-shift requires a pseudoknot in the form of a hairpin-type conformation for IBV (Brierley *et al.*, 1989), MHV and bovine coronavirus (BCoV). The slippery sequence which allows the pp1ab to be fully translated is UUUAAAC for IBV (Brierley *et al.*, 1992). The 3' one-third of the genome contains the structural and a variable number of additional non-structural accessory genes. Upstream of each gene there is a transcription associated sequence (TAS) (also known as transcriptional regulatory sequences – TRS) which serves as the signal for transcription of the negative sense subgenomic RNAs (sgRNA) (Makino *et al.*, 1991). The core TAS for MHV contains the sequence UCUAAAC (Shieh *et al.*, 1987), while the canonical octameric IBV TAS consists of CT(T/G)AACAA.

Figure 1.3. Genome organisation of coronaviruses. The diagrams illustrate the genomes of representative coronaviruses from each of the three groups. The 5' two/thirds of the genome is comprised of gene 1 (blue) which is translated into a polyprotein. The ribosomal frame shift (RFS) is required for translation of the ORF1b proteins. Genes encoding structural and accessory proteins are contained in the 3' one/third of the genomes, with the S protein (green), E protein (yellow), M protein (orange) and N protein (black) being common to all coronaviruses. The genome location and sequence of the accessory proteins (red) differ between coronaviruses in the three groups. MHV encodes an additional structural protein, HE. Some of the accessory proteins of SARS-CoV have also been reported to be associated with virions.

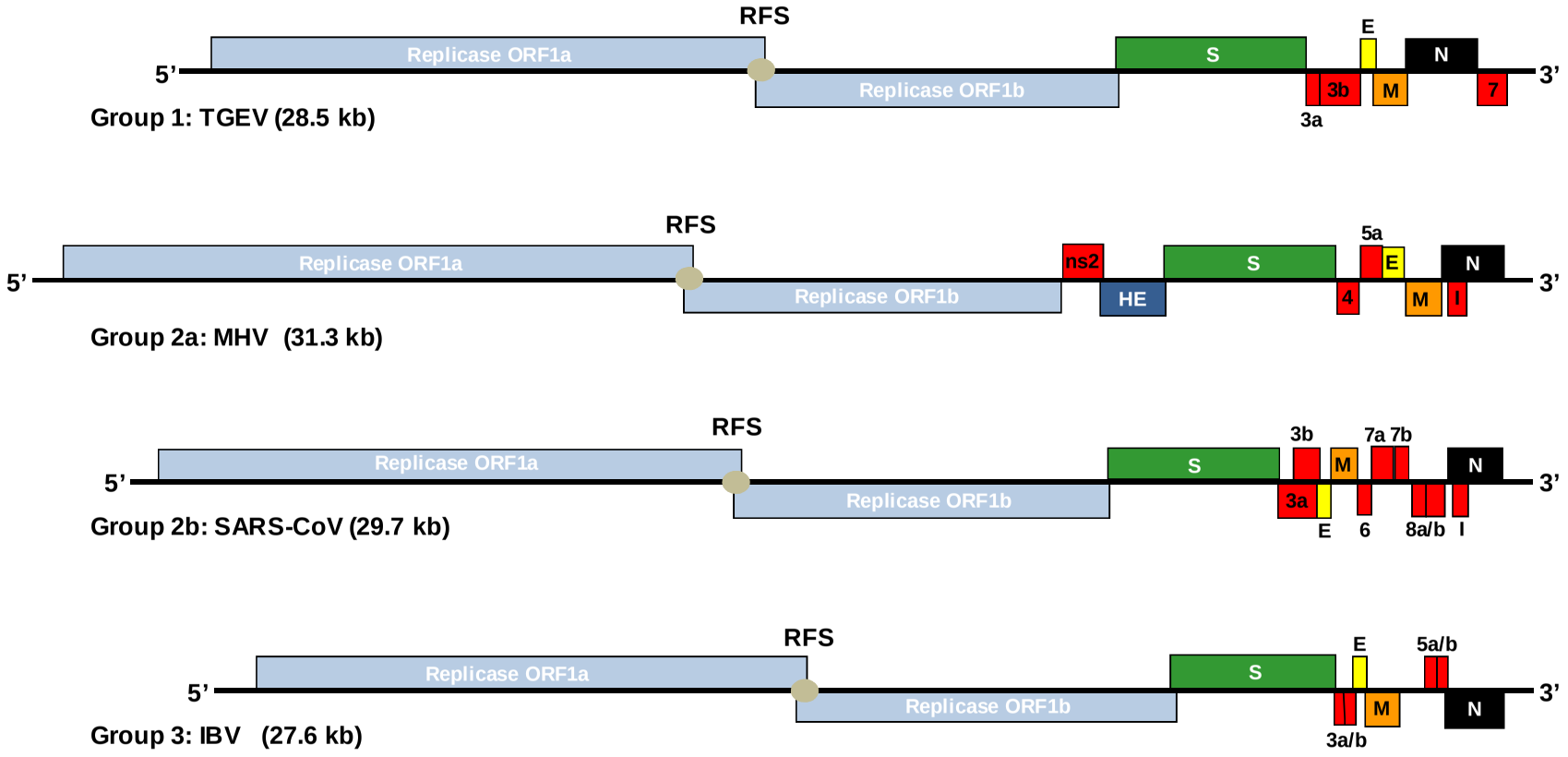
RFS
Replicase ORF1a
Replicase ORF1b
S
E
N
5'
3'
3b
M
7
3a
Group 1: TGEV (28.5 kb)
RFS
5a
Replicase ORF1a
ns2
S
E
N
5'
3'
Replicase ORF1b
HE
4
M
I
Group 2a: MHV (31.3 kb)
RFS
3b
7a 7b
Replicase ORF1a
S
M
N
5'
3'
Replicase ORF1b
3a
E
6
8a/b
I
Group 2b: SARS-CoV (29.7 kb)
RFS
E
5a/b
Replicase ORF1a
S
5'
3'
Replicase ORF1b
M
N
3a/b
Group 3: IBV (27.6 kb)

Gene 1 proteins

The replicase proteins of coronaviruses are encoded in the first two-thirds of the plus-strand RNA genome, referred to as gene 1. Transcription of the viral genome produces a genomic-length mRNA 1 and a 3'-coterminal nested set of mRNAs. mRNA 1 is functionally bicistronic containing two large open reading frames (ORFs), ORF1a and ORF1b. Translation of the 1a ORF results in a polyprotein (pp1a) of 450-500 kDa. A (-1) ribosomal frame-shift event near the ORF1a/1b junction results in the production of polyprotein 1ab (750-800 kDa) which contains the ORF1b-encoded proteins. The group 1 and 2 coronaviruses can generate 16 non-structural proteins (nsp1-16), however IBV does not have the equivalent of nsp1 but does have the equivalent of nsps 2-16 and thus the same nomenclature is used as for the other coronaviruses.

Processing of the polyproteins requires a mechanism of proteolytic cleavage. This process is facilitated with one main proteinase (3CLpro/nsp5) (Lu and Denison, 1997; Pinon *et al.*, 1999; Tibbles *et al.*, 1999; Ziebuhr and Siddell, 1999) and one (e.g. IBV and SARS-CoV) or two (e.g. HCoV-229E and MHV) accessory proteinases (contained in nsp3). The main proteinase is a cysteine proteinase with a serine proteinase-like structure. It cleaves at 11 conserved sites from the nsp4-nsp5 junction through to the nsp15-nsp16 junction. Within the pp1ab the cleavage site for the nsp10-nsp11 junction is absent due to the ribosomal frame-shift occurring at this point. Nsp11 is only produced from the 1a polyprotein. Nsp10 and nsp12 are adjacent on the 1ab polyprotein.

The gene 1 non-structural proteins perform a diverse range of functions. Nsp1 suppresses host gene expression (Kamitani *et al.*, 2006), while nsp2 is dispensable for viral replication but attenuates the modified virus (Graham *et al.*, 2005). Nsp3 is a large multidomain protein which includes adenosine diphosphate ribose 1″ phosphatase activity (Saikatendu *et al.*, 2005), a papain-like protease and two membrane spanning domains (Kanjanahaluethai *et al.*, 2007, Oostra *et al.*, 2008). Nsp4 contains four putative transmembrane sections, three of which appear essential for productive viral replication (Sparks *et al.*, 2007). Nsp6 contains seven putative transmembrane domains with potentially only six being functional (Oostra *et al.*,

2008). Both these proteins, along with nsp3 which also contains a transmembrane domain, have been implicated in anchoring the replicase complex to membranes. Nsp8 interacts with nsp7 to form a hexadecamer (Zhai *et al.*, 2005) and possibly is a second RNA-dependent RNA polymerase (RdRp) which produces primers for the main RdRp (Imbert *et al.*, 2006). Nsp12 is the main RdRp and nsp13 is a helicase with RNA and DNA duplex unwinding activities (Ivanov *et al.*, 2004; Seybert *et al.*, 2000). Nsp14 has been shown to have exoribonuclease (Minskaia *et al.*, 2006) and cap N7 methyltransferase (Chen *et al.*, 2009) activity. Nsp15 is an RNA endonuclease (Bhardwaj *et al.*, 2004; Ricagno *et al.*, 2006) while nsp16 has methyltransferase activity and cap-0 binding properties (Decroly *et al.*, 2008). Studies into these proteins have also examined their subcellular location by indirect immunofluorescence of coronavirus infected cells. Nsps 1-3 colocalise with newly synthesised viral RNA, displaying a punctate, cytoplasmic staining pattern (Harcourt *et al.*, 2004). Similarly nsps 4, 8, 9 and 13 all displayed a punctate, cytoplasmic staining pattern (Prentice *et al.*, 2004b) indicating that this subcellular distribution pattern represents the location of the coronavirus replication/transcription complexes (RTCs).

Structural proteins

All coronaviruses contain a common set of four structural proteins, spike (S), envelope (E), membrane (M) and nucleocapsid (N). Some of the group 2 coronaviruses also contain a fifth structural protein in the form of the haemagglutinin-esterase (HE) protein.

Spike protein

The S protein is a type I transmembrane protein consisting of 1162 amino acids (for IBV) with a N-terminal signal sequence, a large ectodomain, a single transmembrane domain and a short cytoplasmic tail. It consists of two regions: S1 and S2. S1 interacts with cellular receptors (Kubo *et al.*, 1994) and S2 is responsible for fusion of the virus envelope with the cell membrane (Yoo *et al.*, 1991). It is synthesized as a single polypeptide precursor that oligomerize in the ER to form a trimer (Delmas

and Laude, 1990). S proteins are transported from the rough endoplasmic reticulum (ER) to the ER-Golgi intermediate compartment (ERGIC) (Lontok *et al.*, 2004) where it interacts with the M protein (Nguyen and Hogue, 1997; Opstelten *et al.*, 1995) and is incorporated into the virion (de Haan *et al.*, 1999). Excess S protein can be transported to the plasma membrane where it may participate in cell-cell fusion (Vennema *et al.*, 1990). The subcellular location of IBV S protein is influenced by two known signal motifs. It has been shown to contain a canonical dilysine ER retrieval signal (-KKXX-COOH) (Youn *et al.*, 2005) and a tyrosine-based endocytosis signal in its cytoplasmic tail (Lontok *et al.*, 2004). Immunofluorescence microscopy has shown the S protein to be localised in a perinuclear area colocalising with markers for the ER, ERGIC and Golgi apparatus (Winter *et al.*, 2008b).

Envelope protein

The E protein is a minor component of the virus envelope, but seems to have an important role in viral budding. The cytoplasmic tail of E protein is necessary and sufficient for Golgi targeting (Corse and Machamer, 2002) which is displayed on the cytoplasmic face of the ER or Golgi apparatus (Corse and Machamer, 2000). It has also been reported to form ion channels leading to enhanced membrane permeability and supporting budding of the virions (Madan *et al.*, 2005; Wilson *et al.*, 2004). TGEV cannot productively replicate without the E protein present (Ortego *et al.*, 2007), but MHV and SARS-CoV can replicate, although severely impaired, without the E protein (Dediego *et al.*, 2008; Kuo and Masters, 2003) highlighting the almost essential role this protein plays in coronavirus replication.

Membrane protein

The M protein is the most abundant envelope protein in virions. It is a glycoprotein with three transmembrane domains (Rottier *et al.*, 1986) and a large C-terminal domain that binds to the N protein during virus particle assembly (Narayanan *et al.*, 2000). The M protein also interacts with the S protein retaining it in the ERGIC instead of the S protein being transported to the plasma membrane (Opstelten *et al.*, 1995). Before budding of the virus the M proteins are targeted to the Golgi apparatus (Rottier and Rose, 1987), where they become anchored within the membrane, and

are not transported to the plasma membrane. The MHV M protein is concentrated to the *trans* Golgi compartments, whereas the IBV M protein localised to the *cis* side of the Golgi complex (Klumperman *et al.*, 1994). Co-expression of M and E resulted in the formation of virus-like particles (Vennema *et al.*, 1996) suggesting that these two proteins are the main building blocks of the coronavirus particle. The M protein colocalised with the E protein, which colocalised with markers for the Golgi (Bost *et al.*, 2001; Corse and Machamer, 2000).

Nucleocapsid protein

The N protein is a phosphorylated, highly basic structural protein which is known to bind RNA to form the helical core structure (Kennedy and Johnson-Lussenburg, 1975; Macneughton and Davies, 1978). This binding is thought to centre on the TAS (Baric *et al.*, 1988; Nelson *et al.*, 2000; Stohlman *et al.*, 1988). It lacks a membrane-spanning domain and was observed throughout the cytoplasm of an infected cell (Sims *et al.*, 2000; Wurm *et al.*, 2001), but can be found in association with membranes, particularly the membrane-associated viral RTCs (Sims *et al.*, 2000). Combining the information that the N protein colocalises with the viral RTCs with observations from the use of an *in vitro* replication system for MHV where antibodies directed towards the N protein inhibited viral RNA synthesis by 90% (Compton *et al.*, 1987) suggests a direct role for the N protein in coronavirus RNA replication/transcription. Additionally, translation of MHV subgenomic (sg) RNAs was also reported to be enhanced by the N protein (Tahara *et al.*, 1998). Consistent with the diffuse cytoplasmic distribution of the N protein was the indication that the N ORF was translated on free ribosomes, whereas the M and S ORFs were translated on the rough ER (Niemann *et al.*, 1982).

A nucleolus localisation pattern for the N protein has been observed in some infected cells (Hiscox *et al.*, 2001; Rowland *et al.*, 1999; Wurm *et al.*, 2001) but was found excluded from the nucleus in SARS-CoV-infected cells (Bussmann *et al.*, 2006; Rowland *et al.*, 2005; You *et al.*, 2005). The nuclear localisation of some coronavirus N proteins does not appear to be essential due to the observations that nuclear localisation of the N protein does not occur in every infected cell and that

MHV is able to replicate efficiently in enucleated cells (Brayton *et al.*, 1981; Wilhelmsen *et al.*, 1981).

Coronavirus replication cycle

Attachment and entry

Coronavirus attachment to the host cell occurs via binding of the S1 portion of the S protein to the host cell receptor. The S2 portion of the S protein causes fusion of the virus envelope with the cellular membrane. The viral genome is then released into the cell by disassembly of the viral particle.

Group 1 coronaviruses use aminopeptidase N as their receptor (Delmas *et al.*, 1992; Tresnan *et al.*, 1996; Yeager *et al.*, 1992) which is highly expressed in the small intestinal mucosa. Carcinoembryonic antigen-related cell adhesion molecule (CEACAM) is used by MHV (Williams *et al.*, 1991) and is found in the intestinal and hepatocyte membranes. The SARS S protein attaches to ACE2 (Li *et al.*, 2003). The receptor for IBV has not been identified but it has been proposed that receptor attachment is dependent upon α2,3-linked sialic acid (Schultze *et al.*, 1992; Winter *et al.*, 2008a; Winter *et al.*, 2006).

Coronavirus entry appears to rely upon endocytosis (Chu *et al.*, 2006; Eifart *et al.*, 2007; Kawase *et al.*, 2009; Yang *et al.*, 2004) and a low-pH environment to either act directly upon the virion (Chu *et al.*, 2006) or to use proteases active at a low pH to initiate the fusion potential of the S protein (Kawase *et al.*, 2009).

Subcellular location of transcription/replication

Upon virus entry and uncoating the plus-sense genome is directly translated to produce the replicase polyproteins. These large polyproteins are then cleaved by viral proteases to produce 15 (for IBV) and 16 (for the other coronaviruses) subunits that function, in unknown combinations, as transcription and replication complexes. The nsps assemble into complexes associated with double-membrane vesicles (DMVs), where newly-synthesised viral RNA can be found (Gosert *et al.*, 2002; Knoops *et al.*, 2008; Shi *et al.*, 1999; Snijder *et al.*, 2006). The source of membrane used by coronaviruses to form the DMVs is most probably the ER (Knoops *et al.*,

2008; Snijder *et al.*, 2006), although autophagy has also been implicated (Prentice *et al.*, 2004a) and excluded (Zhao *et al.*, 2007) in DMV formation. These particular membrane structures may serve to protect the nsps and virally-produced dsRNA from detection by the host cell's innate immune response (van Hemert *et al.*, 2008). Three of the nsps with predicted transmembrane domains (nsp3, nsp4 and nsp6) have been implicated in anchoring the replication/transcription complex to the DMVs (Clementz *et al.*, 2008; Oostra *et al.*, 2008; Oostra *et al.*, 2007b).

Genome replication and transcription

Coronaviral transcription produces a 3' co-terminal, nested set of six to eight mRNAs (six for IBV). The 5' end of the genome contains a 55-92 nt leader sequence and at the 3' end of this leader sequence and at the 5' end of each gene is found a short, AU-rich motif called the TAS. This sequence is not required to generate sgmRNA but its presence leads to higher transcription levels (Zuniga *et al.*, 2004). The TRS/TAS is both necessary and sufficient for sgmRNA production in arterivirus (van Marle *et al*., 1999) Two models for the generation of coronavirus mRNAs have been proposed, although there is increasing evidence for the discontinuous extension during subgenome-length minus-strand synthesis model. The favoured model for generation of the sgmRNAs suggests that transcription begins at the 3' end of the genome and proceeds until the RTC arrives at a TAS. This sequence causes the RTC to pause and either continue onto the next TAS or switch to the TAS at the 3' end of the leader sequence and continue transcription to produce the completed negative sense template for the sgmRNA. The 5' end of the genome has been proposed to have curled round by this point so that the leader sequence with the downstream TAS could base-pair with the complementary TAS on the newly transcribed sequence. The discontinuous negative sense sgmRNA is then used to produce positive sense sgmRNAs (Fig. 1.4).

Figure 1.4. Proposed model for coronavirus transcription. The discontinuous extension during subgenome-length minus-strand synthesis model implies that transcription begins at the 3’ end of the genome. This continues until the transcription complex encounters a TAS (purple box) where the complex may pause or continue on until the next TAS is located (stage 1). If the complex stops the negative sense transcript with the 3’ anti-TAS sequence (in this diagram the anti-TAS comes from the TAS for the M protein) binds to the TAS (dark pink box) in the leader sequence (yellow box) at the 5’ end of the genome (stage 2). Transcription restarts to generate a negative sense transcript with the anti-leader sequence at the 3’ end (stage 3). The completed negative sense RNA is used to generate a positive sense RNA transcript which will express the 5’ most gene (the M protein in this case) (stage 4).

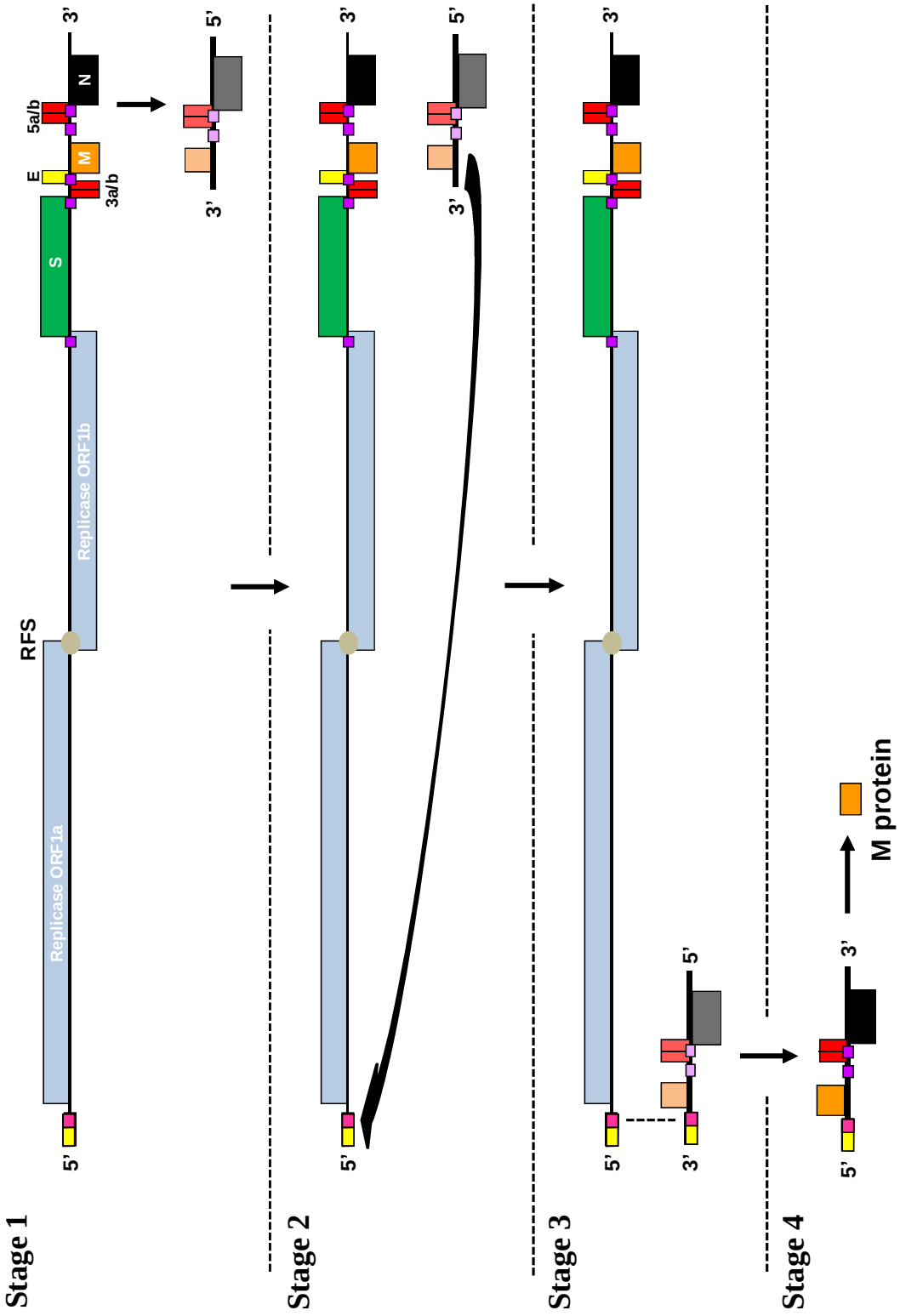
Stage 1
Stage 2
Stage 3
Stage 4
RFS
Replicase ORF1a
Replicase ORF1b
S
E
M
N
5a/b
3a/b
5'
3'
M protein

Translation

Most of the sgmRNAs produced by coronaviruses are functionally monocistronic and only result in the cap-dependent translation of the 5'-most ORF. Some of the sgmRNAs are bicistronic and tricistronic and express their 3' ORFs by leaky scanning of the ribosome or via an IRES-like structure. Internal entry of ribosomes has been suggested for expression of the IBV E protein (Liu and Inglis, 1992b) and the MHV E protein (Thiel and Siddell, 1994).

Translation occurs on the rough ER for S and M proteins and on free ribosomes for the N protein (Niemann *et al.*, 1982) using the host cell's machinery. A preference for the translation of viral sgmRNA within coronavirus-infected cells has been observed (Tahara *et al.*, 1994) and this may be in part due to the interaction of the N protein with the TAS (Tahara *et al.*, 1998).

Assembly and budding

The coronavirus particle is formed by the interaction of the M protein with the S, E and N proteins (with the possible inclusion of other accessory proteins, e.g. HE, for MHV and the 3a protein for SARS-CoV). Only the M and E proteins are required for virus-like particle formation and the S protein will be incorporated if present (Vennema *et al.*, 1996). The N protein will only be incorporated into the virion in combination with genomic RNA (Narayanan *et al.*, 2000). Assembly of the viral particles occurs at the ERGIC (Goldsmith *et al.*, 2004; Klumperman *et al.*, 1994), although the M protein can be found to accumulate in the cis- (IBV) and trans-Golgi (MHV) cisternae (Klumperman *et al.*, 1994; Machamer *et al.*, 1990) (Fig. 1.5). Once assembled the viral particles use vesicles of the constitutive secretory pathway to reach the cell surface (Tooze *et al.*, 1987).

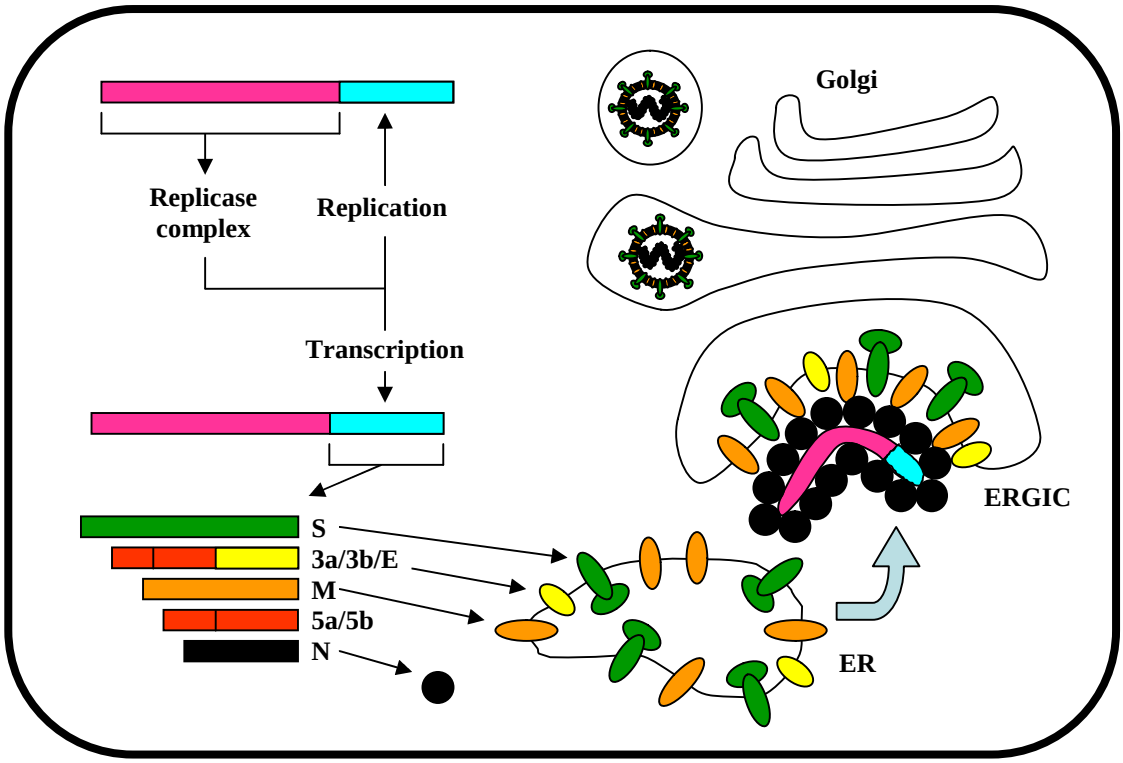

Figure 1.5. The IBV replication cycle. After viral attachment and fusion the genome (pink and blue bar) is directly translated to produce two large polyproteins, 1a and 1ab. These are cleaved into the constituent subunits which are involved in transcription and replication of the six mRNAs: genomic RNA and five 3'-coterminal mRNAs. The S (green), E (yellow) and M (orange) proteins are inserted into the rough ER where they are translocated to the ERGIC. The red bars represent the IBV accessory proteins. Multiple copies of the N protein (black) wrap up the viral genomic RNA and interact with the M protein, which along with the S and E protein constitute the viral particle. Assembled virions exit the cell via the constitutive secretory pathway.

Accessory proteins of coronaviruses

All viruses contain proteins that are essential for replication. These include proteins responsible for viral replication and virion structure. Many viruses also produce additional proteins that may be essential or dispensable. Essential refers to the requirement for viral replication in cell culture. Coronaviruses have been shown to produce non-essential, accessory proteins (Casais *et al.*, 2005; de Haan *et al.*, 2002; Ortego *et al.*, 2003). The genes for these accessory proteins are mainly interspersed between the genes for the structural proteins in the 3' one-third of the genome. Some of the accessory proteins have the same names between the different groups of

coronaviruses. This is due to nomenclature only and does not necessarily reflect any nucleotide or amino acid similarities.

Group 1

The Feline coronaviruses (FCoV) (Fig. 1.6) and Canine coronaviruses described to date share the same complement of accessory genes, three of which (ORF 3abc) are located between the S and E genes (Haijema *et al.*, 2004; Tekes *et al.*, 2008). These viruses also encode two remaining accessory proteins, 7a and 7b which are located at the 3'-end of the genome (Haijema *et al.*, 2004). In TGEV there are two ORFs between the S and E genes and one ORF downstream of the N gene. Other group 1 coronaviruses have a single non-structural gene located between the S and E genes (e.g. HCoV-NL63 (van der Hoek *et al.*, 2004) or Porcine epidemic diarrhoea virus (Duarte *et al.*, 1993). Transmissible gastroenteritis coronavirus (TGEV) contains the gene sequence 5'-Replicase-S-3a-3b-E-M-N-7-3'. A set of recombinant TGEVs (rTGEV) were constructed with restriction sites which separated the 3' genes and additionally had a deleted gene 7 (Ortego *et al.*, 2003). Virus growth in cell culture was unaffected and in the lungs of piglets the majority of the rTGEVs (no modification except separation of the genes) resulted in 80-90% survival. Infection with the rTGEV with a non-functional gene 7 showed 100% survival. There was a 0% survival outcome in piglets infected with a rTGEV which didn't have the separated genes indicating that the separation of the genes had a major effect on reducing pathogenicity of the virus but also that the deletion of the gene 7 further decreased the pathogenicity of the virus. The gene 7 protein has been shown to be capable of membrane association and to have a perinuclear distribution pattern (Tung *et al.*, 1992). The hypothesis put forward suggested that this protein may play a role in the membrane association of the gene 1 proteins.

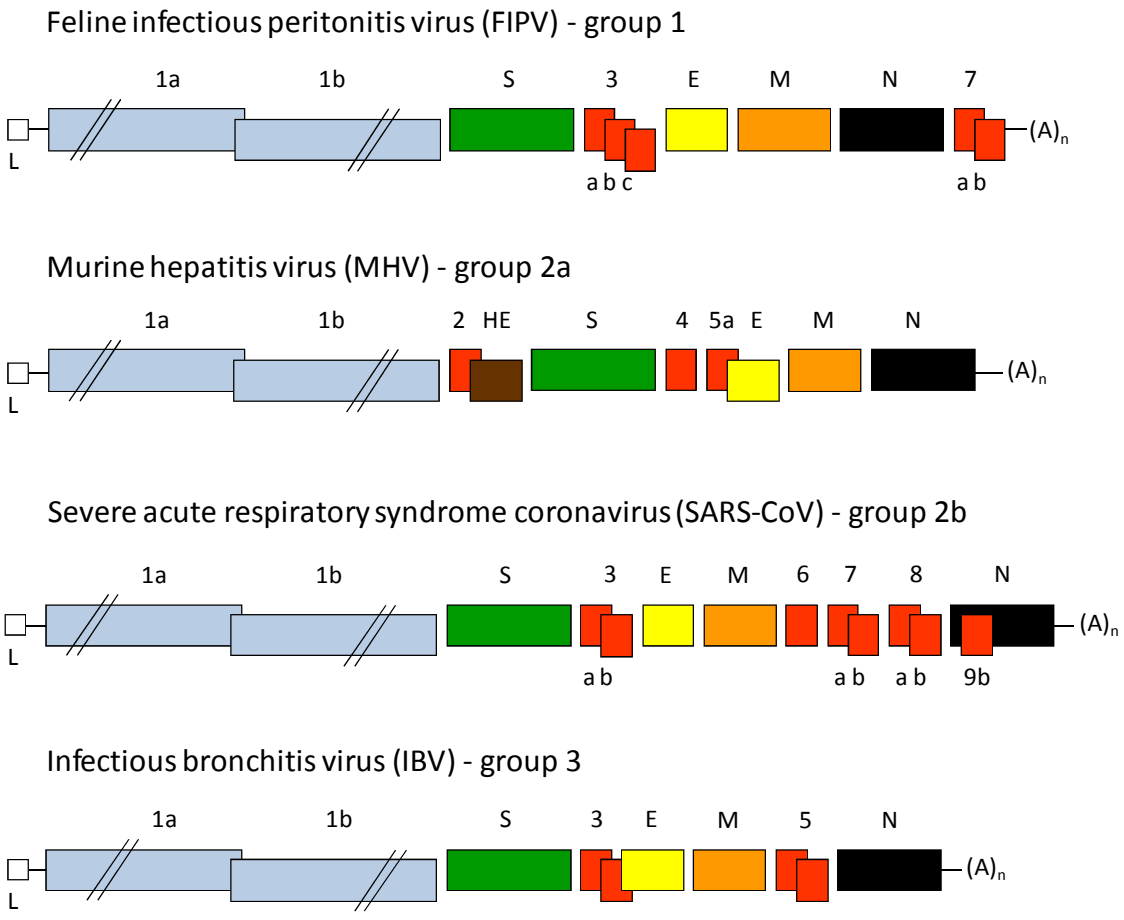

Figure 1.6. Genome arrangements of representatives from each of the coronavirus groups. The replicase gene is highlighted in blue. S protein in green, E protein in yellow, M protein in orange and the N protein in black. Accessory proteins are highlighted in red. L represents the 5' leader sequence and (A)n represents the poly(A) tail.

Similarly, a reduction in pathogenicity was observed for a TGEV which couldn't express the 3a ORF but was unaffected for replication in cell culture (Sola *et al.*, 2003; Woods, 2001). However, the correlation between an intact gene 3 and virulence of TGEV has been challenged by the isolation from the wild of virulent TGEVs with large deletions in the 3a ORF (McGoldrick *et al.*, 1999).

A FCoV with a deleted 3abc resulted in two- to five-fold higher viral titres in cell culture than the parent virus, whereas a FCoV with a deleted 7ab had 10-fold less titres. Kittens infected with either viruses developed no signs of disease and were protected against challenge with the pathogenic wild-type virus (Haijema *et al.*, 2004). Replacement of gene 3 with GFP was also viable and reached nearly the same titres as the parental strain in cell culture (Tekes *et al.*, 2008). As with TGEV,

virulent FCoV isolates have been found which lack an accessory gene (Lin *et al.*, 2008) and avirulent isolates which contain an intact accessory gene (Herrewegh *et al.*, 1995).

Group 2

The non-structural genes located in the 3' end of the MHV and SARS-CoV genomes have been studied. MHV has two clusters of potential accessory genes: 2a/ HE and 4/5a (Fig. 1.6). The 2a ORF is predicted to produce a cyclic phosphodiesterase (Mazumder *et al.*, 2002) which has a cytoplasmic cellular distribution (Bredenbeek *et al.*, 1990; Zoltick *et al.*, 1990). The MHV 2a protein was demonstrated to be less stable than the N protein (Bredenbeek *et al.*, 1990), while the Bovine CoV 2a protein was just as stable as the N protein (Cox *et al.*, 1991). The HE is a type I membrane protein (Kienzle *et al.*, 1990). Recombinant viruses were constructed which had combinations of the accessory genes deleted. Virus replication was unaffected in cell culture (although the rMHV deletion 4/5a consistently produced 10-fold less virus titres). Virus inoculation of mice resulted in death from the wild-type virus, but no death and less severe clinical signs from the modified viruses (de Haan *et al.*, 2002) indicating that the accessory proteins of MHV are determinants of pathogenicity. Another recombinant MHV was produced which could not express the gene 4 protein. Viral replication kinetics in cell culture were similar between the recombinant and recombinant/gene 4 deletion viruses and there was no observable difference in virulence, indicating there were other factors involved in disease progression. The loss of the 2a protein did not affect viral replication or the production of viral mRNAs and proteins in cell culture (Schwarz *et al.*, 1990), but mutation of conserved motifs in the catalytic site of this protein has been shown to produce attenuated replication in the liver but not in the brain of infected mice (Roth-Cross *et al.*, 2009). The interchange of structural and accessory proteins between two different strains of MHV also indicated that it is the 3' end of the MHV genome that encodes the determinants of pathogenicity (Navas-Martin *et al.*, 2007).

Severe acute respiratory syndrome coronavirus (SARS-CoV) produces eight accessory proteins, 3a/b, 6, 7a/b, 8a/b and 9b (Marra *et al.*, 2003; Yount *et al.*, 2005) (Fig. 1.6). Reverse genetics has been used to study the role of these accessory

proteins. Yount *el al*. (2005) deleted five of the eight accessory genes. All these recombinant viruses replicated to similar titres as the wild-type virus and they all replicated to similar titres in the murine model indicating that these ORFs play little role in replication in an organism or that the mouse model wasn't adequate to simulate a natural infection. Transgenic mice which expressed the ACE-2 receptor on their epithelial cells were used to assess the pathogenicity of accessory protein deletion SARS-CoVs (Dediego *et al.*, 2008). Progression of disease in these transgenic mice was similar to that observed in human during the SARS outbreak and closely simulated a natural infection. The absence of ORFs 6, 7a, 7b, 8a, 8b and 9b had very little effect upon the viral replication efficiency *in vitro* and *in vivo* and were not attenuating.

The individual accessory proteins have been characterised with varying levels of detail.

The 3a protein

The 3a protein has been demonstrated to be a structural protein (Ito *et al.*, 2005; Shen *et al.*, 2005) which can interact with the M, E and S proteins (Tan *et al.*, 2004b) and the 5'UTR of the viral genome (Sharma *et al.*, 2007). Interaction with caveolin-1 has also been identified (Padhan *et al.*, 2007) which may affect the functions of caveolin-1 such as cell signal transduction and endocytosis. DNA fragmentation and chromatin condensation followed transfection and expression of the 3a protein (Law *et al.*, 2005), as did activation of the mitochondrial death pathway (Padhan *et al.*, 2008) indicating that the 3a protein can induce apoptosis. It may do this by forming ion channels in membranes through homodimerization and homotetramerization (Chan *et al.*, 2009; Lu *et al.*, 2006). It has also been reported to up-regulate fibrinogen (Tan *et al.*, 2005) and induce G1-phase cell cycle arrest (Yuan *et al.*, 2007). A perinuclear and plasma membrane localisation pattern was observed within infected and transfected cells and the plasma membrane distribution was abolished when the C-terminal cytoplasmic domain, which contains the YxxΦ and dibasic motifs, was deleted (Tan *et al.*, 2004b). An epitope-tagged 3a protein expressed in transfected cells was reported to colocalise with an ER-marker protein (Law *et al.*, 2005) and to have a Golgi localisation pattern colocalising with the M protein (Yuan *et al.*, 2005a).

The 3b protein

A tagged-3b protein expressed in transfected cells localised to the nucleus (Freundt *et al.*, 2009; Khan *et al.*, 2006; Yuan *et al.*, 2005c) of which the C-terminal region was determined to be responsible for this cellular targeting (Yuan *et al.*, 2005c). A mitochondrial localisation pattern has also been observed, possibly as a late event in SARS replication (Freundt *et al.*, 2009; Yuan *et al.*, 2006a). It has been reported to arrest the cell cycle at the G0/G1 phase (Yuan *et al.*, 2005b), induce apoptosis (Khan *et al.*, 2006; Yuan *et al.*, 2005b) and act to antagonise the interferon response (Kopecky-Bromberg *et al.*, 2007).

The 6 protein

Introduction of the SARS-CoV ORF6 sequence into an attenuated murine coronavirus (MHV rJ2.2) converted it into a virus capable of enhanced replication in cell culture and inducing lethal encephalitis in mice (Pewe *et al.*, 2005). The rMHV with the SARS ORF6 sequence produced viral proteins and progeny virus earlier than rMHV and viral RNA levels were higher (Tangudu *et al.*, 2007) and expression of the ORF6 protein has been linked to optimal viral replication in cells infected with a low m.o.i. (Zhao *et al.*, 2009a). These observations along with immunofluorescence images indicating an ER localisation (Geng *et al.*, 2005) and colocalisation with viral RNA (Tangudu *et al.*, 2007) suggested that the ORF6 protein either positively affects viral RNA/protein synthesis or assists in forming suitable viral RNA replication sites. Mutation of the N-terminal hydrophobic sequence affected the ability of the ORF6 protein to enhance viral replication (Netland *et al.*, 2007). The localisation of the ORF6 protein to the ER/Golgi membrane was also reported by Frieman *et al*. (2007) who demonstrated that the ORF6 protein can bind to karyopherin tethering it to the membrane and thereby stopping karyopherin-mediated transport of STAT1 into the nucleus and inducing an interferon response (Frieman *et al.*, 2007). Kopecky-Bromberg *et al*. (2007) also observed an interferon antagonistic function for the ORF6 protein. This inhibition of the IFN response does not appear to be the main function of the ORF6 protein as levels of IFN induced in cell culture were not significantly different between rMHVs either expressing or not expressing the ORF6 protein (Pewe *et al.*, 2005), the ORF6 protein was not required for SARS-CoV to be resistant to IFN (Zhao *et al.*, 2009a) and the inhibition of STAT1 translocation to the nucleus, and subsequent

interference of the interferon response, was only observed at late times during the viral replication cycle (Frieman *et al.*, 2007; Zhao *et al.*, 2009a). Induction of apoptosis via the caspase-3 mediated, ER stress and JNK-dependent pathways was also found in transfected cells (Ye *et al.*, 2008).

The 7a protein

The 7a ORF was predicted to encode a type I transmembrane protein with an ER retrieval signal in the C-terminal tail (Fielding *et al.*, 2004). The crystal structure of the N-terminal ectodomain indicated a similarity with the Ig-like superfamily (Hanel *et al.*, 2006; Nelson *et al.*, 2005). Overexpression of the 7a protein was shown to induce apoptosis (Schaecher *et al.*, 2007b; Tan *et al.*, 2004a), possibly by interaction and inhibition of prosurvival proteins such as Bcl-X_L (Tan *et al.*, 2007) and/or by host cell protein translation inhibition and activation of the p38 mitogen-activated protein kinases (Kopecky-Bromberg *et al.*, 2006). Cell cycle arrest at G0/G1 has also been reported to be induced by this protein (Yuan *et al.*, 2006b). Expression of a tagged 7a protein within transfected cells indicated a perinuclear/cytoplasmic localisation pattern (Fielding *et al.*, 2004; Yuan *et al.*, 2006b) which could colocalise with markers for the ER, ERGIC and Golgi (Fielding *et al.*, 2004). Virion particle association has been observed (Huang *et al.*, 2006) and appears possible due to the cellular location at the sites of virion assembly and egress (i.e. the ERGIC and Golgi). Interactions with the cellular proteins lymphocyte function-associated antigen 1 (Hanel and Willbold, 2007) (possibly as a virus attachment factor) and small glutamine-rich tetratricopeptide repeat-containing protein (Fielding *et al.*, 2006) (possibly influencing virion assembly) have also been observed.

The 7b protein

A Golgi accumulation was seen with the 7b protein and this pattern was produced by the putative transmembrane domain (Schaecher *et al.*, 2008). It was demonstrated to be incorporated into SARS-CoV particles (Schaecher *et al.*, 2007a) and contributes to apoptosis (Schaecher *et al.*, 2007b).

The 8 protein

Viruses isolated from animals as well as some early-stage human isolates were found to possess a single ORF8 encoding a 122 amino acid polypeptide, whereas middle or

late-stage human isolates contained 29-nucleotide deletion that created two ORFs, ORF8a and ORF8b (Chinese, 2004). Expression of the 8a and 8ab proteins has been detected, but the 8b has either been shown to be highly unstable or to be expressed at undetectable amounts (Le *et al.*, 2007; Oostra *et al.*, 2007a). This may indicate that the 8a and 8b proteins are not actually required for efficient SARS-CoV infection within the human population or that only the 39 amino acid 8a protein is required as the 8a protein has been shown to enhance viral replication (Chen *et al.*, 2007). The 8ab protein has a distribution pattern similar to the ER and, if actually functional in the context of SARS-CoV infection, 8a has an ER-like pattern and 8b has a diffuse cytoplasmic cellular distribution (Keng *et al.*, 2006; Oostra *et al.*, 2007a). The 8ab protein found associated with the luminal surface of the ER and induces activation of ATF6 thus possibly activating the unfolded protein response (UPR) (Sung *et al.*, 2009) and shutting down host cell protein translation to favour viral protein synthesis.

The 9b protein

Contained within the N gene there is an internal ORF designated 9b which could express a 98 amino acid protein (Marra *et al.*, 2003). Antibodies to the 9b protein have been detected in the sera from SARS-CoV infected patients (Qiu *et al.*, 2005) and the protein has been detected in infected cells and clinical specimens (Chan *et al.*, 2005). An ER-like cellular distribution has been observed (Moshynskyy *et al.*, 2007) but also a punctate, cytoplasmic pattern (Meier *et al.*, 2006). The crystal structure suggested an intertwined dimer with an amphipathic outer surface and long hydrophobic tunnel which could bind lipid molecules (Meier *et al.*, 2006). These data combined with the suggested association of the 9b protein with virions (Xu *et al.*, 2009) provides evidence for a role of this accessory protein in SARS-CoV assembly.

Group 3

IBV encodes four group-specific proteins (Fig. 1.6) that are dispensable for replication in cell culture (Casais *et al.*, 2005; Hodgson *et al.*, 2006). Gene 3 contains three open reading frames (ORFs) that produce two non-essential proteins 3a and 3b, with the 3c ORF encoding for the E protein (Liu *et al.*, 1991). Gene 5 is functionally bicistronic (ORF 5a and ORF 5b), producing two proteins 5a and 5b (Liu and Inglis,

1992a). All four of these accessory proteins are small when compared to the other proteins encoded for by IBV, ranging in size from 57 to 82 amino acids in length. The nucleotide sequences of genes 3 and 5 are also highly conserved between members of the group 3 coronaviruses (Cavanagh *et al.*, 2001; Cavanagh *et al.*, 2002; Jia and Naqi, 1997). Retention and conservation of these genes would indicate an important role in the replication of the virus *in vivo*.

The 3a protein

The smallest of the IBV accessory proteins is the 57 amino acid 3a protein. Within IBV-infected Vero cells the 3a protein displayed a punctate cytoplasmic distribution where it colocalised with the interferon-induced MxA protein on the smooth ER (Pendleton and Machamer, 2005). Characterisation of a recombinant IBV which lacked the ability to express the 3a protein resulted in a virus which had very similar titres to a wild-type IBV upon replication in CK cells up to 96 h p.i. and embryonated eggs up to 36 h p.i. The only difference observed was a 10-fold reduction in virus titres compared to wild-type virus *ex vivo* after 25 hours (Hodgson *et al.*, 2006) which may be due to tracheal epithelial cell-specific inhibition. Field strains have been found with deletions and point mutations resulting in the production of truncated and non-expressing 3a proteins, respectively (Liu *et al.*, 2008). The IBV expressing a truncated 3a produced virus titres in embryonated eggs similar to viruses expressing intact 3a proteins and the non-expressing 3a had 10-fold less titres. Clinical signs of infection were observed for all the viruses examined indicating that a truncated or absent 3a protein did not affect viral pathogenesis (although gene 1 wasn't sequenced for these viruses which could have had an effect upon virus titres and disease outcome).

The 3b protein

The subcellular distribution of the 3b protein was cytoplasmic within IBV-infected avian cells with little or no staining observed within infected mammalian cells (Pendleton and Machamer, 2006). The absence of detectable 3b protein in mammalian cells was found to be a result of the short half-life of the 3b protein within mammalian cells compared to avian cells due to proteasomal degradation (Pendleton and Machamer, 2006). Pendleton and Machamer (2006) also found that

using vaccinia virus to express the T7 polymerase to enable expression of the 3b protein from a transfected plasmid resulted in nuclear accumulation of the 3b protein, similar to data presented by Shen *et al*. (2003). These data contrast greatly to the subcellular location of the 3b protein within an IBV-infected cell and highlight the subcellular changes which can arise upon the use of heterologous viruses to express proteins. Analysis of an IBV Beaudette strain expressing a truncated 3b protein displayed increased replication kinetics and an increase in virulence compared to the parent virus, although genome sequencing also found that there would be two amino acid changes in nsp3 and one in the S protein which may have contributed to an altered viral phenotype (Shen *et al.*, 2003). A recombinant IBV which lacked the ability to express the 3b protein produced similar virus titres in CK cells, embryonated eggs and tracheal organ cultures (TOCs) (Hodgson *et al.*, 2006).

The 5a and 5b proteins

The subcellular location of the 5a protein within IBV-infected Vero cells has been described as diffuse cytoplasmic with some concentration around the nucleus (Liu and Inglis, 1992a). The 5b protein had a diffuse cytoplasmic pattern but with a more granular appearance and perinuclear distribution than the 5a protein (Liu and Inglis, 1992a). Recombinant IBVs which couldn't express either or both of the gene 5 proteins produced similar titres to wild-type viruses in CK cells, embryonated eggs and TOCs (Casais *et al.*, 2005).

Attenuated IBVs have been sequenced and suggest that this reduction in pathogenicity was not due to an inhibition of the functions of the gene 3 or 5 accessory proteins. A virulent IBV Arkansas strain was attenuated by passage in eggs. Seventeen amino acid changes were found and only one of these was in an accessory protein (5b) (Ammayappan *et al.*, 2009). Similarly three IBV strains were attenuated and sequenced. There was one amino acid change in 5a for two of the strains (different amino acids) and one amino acid change in 5b for the other strain (Huang and Wang, 2007). Naturally occurring IBV strains have been discovered which lack some of the accessory ORFs (Mardani *et al.*, 2008). These strains had a X1 ORF instead of the 3a and 3b ORFs which had no significant sequence similarity to the 3a or 3b ORFs but did have a recognisable TRS. There was no 5a ORF and

two of the four strains also had no 5b ORF. All these novel strains had much reduced titres in embryonated eggs, TOCs and the trachea of infected chickens. However, they all induced histopathological lesions indistinguishable from the wild-type strains. As the gene 1 section of the genome wasn't sequenced the differences in virus titres cannot be solely attributed to the changes in the accessory genes. Additionally, in contrast to the situation presented for MHV whereby the MHV structural and accessory proteins are determinants of pathogenicity (de Haan *et al.*, 2002; Navas-Martin *et al.*, 2007) it would appear that for IBV the 5' end of the genome encodes the determinants of pathogenicity (Armesto *et al*., 2009). Exchange of the genes encoding the structural and accessory proteins from an apathogenic IBV strain (Beaudette) with those of a pathogenic IBV strain (M41) did not confer a pathogenic phenotype on the chimeric virus.

Accessory proteins of other RNA viruses

The functions of most of the accessory proteins of coronaviruses are as yet unknown and there are still many unknown details about their mode of action and relevance during the viral replication cycle. The known functions of accessory proteins from other viruses may be a guide to these unknown features. Details about the accessory proteins of other RNA viruses are presented to give examples of the functions which might be possessed by the accessory proteins of IBV.

Paramyxoviridae

Sendai virus is a member of the *Respirovirus* genus of the *Paramyxoviridae* family. Six mRNAs are transcribed from the genome template and they all, except the P gene mRNA, express a single primary translation product from a single ORF. Insertion of a G residue into the P mRNA creates the V ORF and an insertion of two Gs, leads to the production of the W protein. Additionally, there are four independently initiated C proteins expressed via a non-AUG start site (C') and both scanning dependent (C) and scanning independent (Y1/Y2) ribosomal initiation. A recombinant Sendai virus which was unable to express the V protein has been constructed and shown to produce consistently higher viral titres at early time-points

compared to the wild-type recombinant virus. This recombinant virus was also attenuated in mice, the natural host (Kato *et al.*, 1997). The C and C' proteins were also dispensable for virus replication but caused a reduction in virus titres of 10-100-fold in three different cell types (Kurotani *et al.*, 1998). Viruses lacking C/C' expression were attenuated in mice causing no death or clinical signs. This group also knocked-out the expression of the Y1 and Y2 proteins and virus was recovered although at severely reduced amounts. Expression of the C or V proteins could inhibit the activation of IRF-3 and NF-κB (Komatsu *et al.*, 2004), but it would appear as though the C proteins suppress the IFN response (Gotoh *et al.*, 1999) while the V protein counteracts an innate immune response activated by IRF-3 which isn't IFN (Kiyotani *et al.*, 2007). Sendai virus attenuation has also been associated with amino acid changes in the polymerase protein (L) and in the leader sequence (Fujii *et al.*, 2002; Itoh *et al.*, 1997).

Human respiratory syncytial virus (RSV) is a non-segmented, single-stranded, negative sense RNA virus in the genus *Pneumovirus* of the family *Paramyxoviridae*. Proteins in RSV that are not clearly homologous with other paramyxoviruses include SH (small hydrophobic), M2-1, M2-2 and the non-structural proteins NS1 and NS2. Using reverse genetics, the NS1, NS2, SH and M2-2 genes were deleted from the RSV genome and these deletion mutants were characterised *in vitro* and *in vivo* (Jin *et al.*, 2000b). Compared to viral titres of the unmodified recombinant RSV (rRSV) in Vero cells the largest decrease in virus titre was produced from the NS1 deletion virus whereas the largest decrease in virus titres in human epithelial cells compared to unmodified rRSV was produced by the M2-2 deletion virus. Replication of the rRSVs in the lower respiratory tracts of cotton rats indicated that inhibition of M2-2 expression led to a severely attenuated virus, as did deletion of NS1 or NS2. The M2-2 protein has been suggested to play a role in mediating the switch from viral transcription to genome replication to ensure high levels of viral mRNA initially then high levels of genomic RNA for virion assembly (Bermingham and Collins, 1999; Jin *et al.*, 2000a). Disruption of this event could have led to an insufficient number of genomes and a reduction in viral progeny. Deletion of the NS2 gene reduced the recombinant virus titres by 10-100-fold in cell culture (Teng and Collins, 1999). Work has been done to characterise the role of the accessory NS1 and NS2

proteins. rRSV with the NS1 and NS2 genes deleted, either singularly or in combination, induced high levels of alpha and beta interferon (IFN-α/β) (Spann *et al.*, 2004), although a wild-type RSV has been shown to produce high levels of type I IFN but was resistant to the antiviral state produced (Young *et al.*, 2000)). NS1 has been reported to degrade STAT2 via the proteasome (Elliott *et al.*, 2007) and NS2 interacts with RIG-I to inhibit the phosphorylation and translocation to the nucleus of IRF-3 (Ling *et al.*, 2009). The RSV NS genes have also been implicated in determining the viral host range as a bovine RSV with human RSV NS genes was severely attenuated in IFN-competent bovine cells (Bossert and Conzelmann, 2002).

Bunyaviridae

Bunyamwera virus is the prototype of both the family *Bunyaviridae* and the *Bunyavirus* genus. It is an enveloped virus comprising a genome of three segments of single-stranded, negative-sense RNA. Bunyamwera virus replicates in the cytoplasm and buds into the Golgi apparatus. There are four structural polypeptides and two non-structural proteins, NSs and NSm. The large RNA segment, L, encodes the polymerase (L) protein; the medium-sized RNA segment, M, encodes G1, G2 (two glycoproteins) and NSm; and the smallest RNA segment, S, encodes the nucleocapsid (N) protein and NSs. A mutant Bunyamwera virus lacking NSs has been generated (BUNdelNSs) by reverse genetics and used to begin characterising the NSs protein (Bridgen *et al.*, 2001). The mutant virus replicated to approximately 10-fold lower titres in cell culture and there also seemed to be a reduction in the inhibition of host cell protein synthesis compared to the complete inhibition in wild-type virus infected cells. Experiments in mice indicated that the mutant virus was attenuated, as the mice inoculated with the mutant virus survived for three days longer compared to those infected with the wild-type virus. Characterisation of the NSs protein indicated that it inhibits the induction of IFN (Bridgen *et al.*, 2001; Weber *et al.*, 2002).

Birnaviridae

Infectious bursal disease virus (IBDV) is a pathogen of economic importance to the poultry industry. It causes severe immunodeficiency in young chickens by destroying the precursors of antibody-producing B cells in the bursa of Fabricius. IBDV belongs to the genus *Avibirnavirus* of the *Birnaviridae* family. Its genome consists of two segments of double-stranded RNA. The smaller segment B encodes VP1, a multifunctional protein with polymerase and capping enzyme activities. The larger segment A encodes a precursor protein which is processed into mature VP2, VP3 and VP4 proteins. This segment also encodes a 17 kDa nonstructural (NS) protein from a small ORF partly preceding and overlapping the polyprotein ORF. Deletion of the NS protein produced a recombinant virus which consistently produced 10-fold fewer viruses over 6 days in cell culture and exhibited less of an apoptotic effect (Yao *et al.*, 1998). This virus also failed to produce any clinical signs of disease. This apoptotic effect was confirmed and shown to affect the release of progeny virus from the infected cell (Yao and Vakharia, 2001).

Picornaviridae

Theiler's murine encephalomyelitis virus (TMEV) belongs to the genus *Cardiovirus* in the family *Picornaviridae*. The single-stranded positive sense RNA genome is translated into a single, long polyprotein which is co-translationally cleaved. The first protein to be translated is the leader (L) protein which is unique to this genus and consists of 76 amino acids. An inability to express this protein was attenuating for the virus with a 10-fold reduction in viral titres in BHK cells compared to wt virus but was essential for persistence in the central nervous system of mice (Calenoff *et al.*, 1995). Inhibition of host cell protein synthesis by cardioviruses has been attributed to the L protein (Zoll *et al.*, 1996) as has inhibition of type I IFN (van Pesch *et al.*, 2001) and apoptosis (Romanova *et al.*, 2009).

Orthomyxoviridae

Influenza A viruses are enveloped viruses within the family *Orthomyxoviridae* comprising a single-stranded, negative sense, segmented genome encoding 11 proteins. The only non-structural protein is non-structural 1 (NS1) the expression of

which is not required for viral replication and deletion of which is attenuating, especially in innate-immune competent cells (Garcia-Sastre *et al.*, 1998). Nuclear (Marion *et al.*, 1997) and cytoplasmic (Newby *et al.*, 2007) subcellular distribution patterns have been observed for NS1 and may dependent upon cell type and/or strain of influenza A virus. NS1 has been shown to bind dsRNA and attenuate the activation of protein kinase RNA activated (PKR) (Hatada *et al.*, 1999), regulate viral mRNA splicing (Garaigorta and Ortin, 2007), induce efficient viral protein synthesis (Salvatore *et al.*, 2002) and to antagonise the IFN response (Hayman *et al.*, 2007; Kochs *et al.*, 2007; Opitz *et al.*, 2007). Naturally occurring Influenza A viruses have been found which possess C-terminally truncated NS1 proteins (Suarez and Perdue, 1998).

Retroviridae

Human immunodeficiency viruses (HIV) are enveloped viruses within the family *Retroviridae*. The genome consists of a dimer of single-stranded, positive sense RNA encoding nine proteins, four of which (Nef, Vpu, Vpr and Vif) are accessory proteins. Negative factor (Nef) down-regulates the expression of CD4 (Benson *et al.*, 1993), CD28 (Bell *et al.*, 2001) and MHC class I (Swigut *et al.*, 2000) as well as enhancing viral infectivity (Chowers *et al.*, 1994) and replication (Aiken and Trono, 1995). Nef is also a critical pathogenicity factor as demonstrated by the reduced pathogenicity exhibited by viruses which cannot express Nef (Daniel *et al.*, 1992; Jamieson *et al.*, 1994). Viral protein U (Vpu) is unique to HIV-1 and like Nef, down-regulates the cell surface expression of CD4 (Willey *et al.*, 1992). Vpu also facilitates the efficient release of virions (Klimkait *et al.*, 1990; Strebel *et al.*, 1989) and has a perinuclear distribution in infected cells (Klimkait *et al.*, 1990). Viral protein R (Vpr) is virion associated (Cohen *et al.*, 1990), arrests the cell cycle in the G2/M phase (Jowett *et al.*, 1995) and was shown to be important in transporting the pre-integration complex from the cytoplasm to the nucleus (Heinzinger *et al.*, 1994). Viral infectivity factor (Vif) has been shown to be dispensable for virus replication on certain cell lines (Sakai *et al.*, 1993) but is essential for virus replication in primary cells (Gabuzda *et al.*, 1992). The cellular protein which is responsible for inhibiting retroviral replication is apolipoprotein B mRNA-editing enzyme catalytic polypeptide-like 3G (APOBEC3G) (Sheehy *et al.*, 2002). Vif antagonises the

activity of APOBEC3G by targeting it for degradation in the ubiquitin-proteasome pathway (Mehle *et al.*, 2004).

Pathology of IBV

IBV is the major respiratory virus of the chicken throughout the world. Most countries are endemic for the virus which infects both large and small scale flocks.

Viral replication can occur in virtually all epithelial cells of the chicken (Janse *et al.*, 1994; Nakamura *et al.*, 1991; Purcell and Clarke, 1972). Disease is usually associated with lesions in the epithelium of the respiratory tract (Chen *et al.*, 1996; Geilhausen *et al.*, 1973; Nakamura *et al.*, 1991) and, less commonly, with lesions in the kidneys (Butcher *et al.*, 1990; Chen *et al.*, 1996). Upon infection of the chicken, IBV causes deciliation of the ciliated epithelia of the nose and trachea. Clinical signs occur within 36 hours and symptoms include a nasal discharge, snicking, watery eyes and lethargy. Infection is resolved within fourteen days with a rise in antibody titres. A latent infection can also occur in a small number of birds.

Virus is present in considerable titres in the tracheal mucus and faeces in the acute and recovery stages of the disease respectively and is highly infectious. Consequently, horizontal transmission to other birds is extremely probable. Juvenile and adult birds are less prone to death than younger chickens, but experience a slowing of growth and substantial decline in egg-laying ability. The death of the younger birds appears to be more commonly a result of secondary infection rather than as a direct consequence of viral replication and host immune response (Vandekerchove *et al.*, 2004).

Death of chickens is not the only economical factor brought about by IBV. The birds may survive but poor weight gain, condemnation at processing, suboptimal egg production and downgrading of eggs all contribute to ensure that IBV remains a major burden on the poultry industry.

Control of IBV

The major protein that resides on the external surface of IBV is the S glycoprotein. This molecule is responsible for viral attachment to the cell and also induces virus-

neutralizing antibodies (Cavanagh *et al.*, 1984). The S protein therefore confers the serotype and is the major factor involved when the molecular basis for vaccine efficacy is analysed.

A mature S protein consists of two subunits: S1 and S2. The S2 subunit anchors the S protein in the viral envelope while the S1 subunit forms the distal bulbous head which protrudes from the viral envelope. A new serotype can arise when there are amino acid changes in the S1 subunit, normally around 20-25%. A study on various strains of the Massachusetts serotype identified two hypervariable regions (HVRs). A single amino acid change in HVR 1 was found to be associated with resistance to neutralization by antibody (Cavanagh *et al.*, 1988). Additionally, recombination between viral genomes can occur (Cavanagh *et al.*, 1992). The possibly of a new S gene may result in a new serotype and therefore provide a very effective means to escape an antibody response.

A few vaccine strains have been developed in conjunction with varying vaccination strategies to offer protection against IBV-induced disease. However, protection trials have shown that commercially available vaccines can provide little protection upon challenge with a range of IBV field isolates (Muneer *et al.*, 1988) and that outbreaks of disease can still occur within vaccinated flocks (Alvarado *et al.*, 2005; Di Fabio *et al.*, 2000; Rimondi *et al.*, 2009). The most common approach used presently involves vaccinating young female birds two or more times with a live vaccine, followed by one dose of inactivated vaccine as the birds come into lay. This intensive strategy is required because protection of the respiratory tract following a single live attenuated virus vaccination has been found to be short-lived (Darbyshire and Peters, 1984). Attenuation of IBV for use as a vaccine occurs through serial passage in embryonated chicken eggs.

The presence of many serotypes and the inability to elicit a sustainable antibody response to a broad range of these serotypes ensures that IBV remains a major problem for the poultry industry.

Aims of the thesis

The roles of accessory proteins from non-coronaviruses mainly concern the subversion of the host's innate immune response. This would also appear to be applicable for the SARS-CoV in which two of the eight accessory proteins have been demonstrated to act as IFN antagonists whereas the other six SARS-CoV accessory proteins have been implicated in inducing apoptosis, regulating the cell cycle and host cell protein translation inhibition. The determinants of group I and II coronavirus pathogenicity also appear to correlate with proteins expressed from the 3' end of coronavirus genome which contains the structural and accessory protein ORFs. However unlike the group I and II coronaviruses the determinants of pathogenicity of the group III coronavirus IBV reside in the 5' end of the genome indicating that the accessory proteins contribute at most a minor role to the pathogenic phenotype of the virus. Additionally rIBVs which could not express one or more of the accessory proteins were not compromised for their replication efficiencies in IFN-competent cell culture implying that the accessory proteins do not play a major role in antagonising the IFN response *in vitro*.

In order to understand the roles the IBV accessory proteins play during virus replication the aims of this thesis were:

1) To assess the subcellular distribution of the individual accessory proteins as well as determine the cellular compartment to which they localise.
2) To determine the protein-protein interactions of one or more of the accessory proteins in order to provide a line of investigation into assigning a role to the accessory proteins.

Chapter 2: Materials and methods

Animal cell culture and virus stocks

All primary cells and continuous cell lines were prepared by the I.A.H. media and tissue culture department.

Chicken kidney (CK) cells were primary cells prepared by the trypsinisation of kidneys from two- to three-week-old, specific pathogen free (SPF), Rhode Island Red chicks.

Vero cells were continuous cell lines originating from African green monkey epithelial and fibroblast kidney cells

Vero and CK cell culture medium

For 100 ml of BES cell medium (final concentrations indicated in parentheses):

10 x Eagles's MEM (Sigma)	10 ml	(1x)
Tryptose Phosphate Broth	10 ml	(10%)
Bovine serum albumen (BSA) fraction V (10% w/v filter sterilised; Sigma)	10 ml	(1%)
N, N-bis[2-hydroxethyl]-2-Aminoethanesulfonic acid (BES, 1 M filter sterilised; Sigma)	2 ml	(20 mM)
Sodium bicarbonate	0.19 g	(1.9 g/l)
L-glutamine (100x; Gibco)	1 ml	(2 mM)
Nystatin (100,000 U/ml; Sigma)	0.25 ml	(250,000 U/l)
Penicillin and streptomycin (100,000 U/ml; Sigma)	0.1 ml	(100,000 U/l each)

Sterile water was added to a final volume of 100 ml.

Viruses

Beaudette-R (Beau-R) was an isogenic clone of Beaudette-CK (a CK cell-adapted Beaudette virus which had been passaged several times in chicken embryos and eight times in CK cells in our laboratory), except for two nucleotide substitutions. $C^{19666} \rightarrow U$ and $A^{27087} \rightarrow G$, in the ORF 1b and N genes respectively. R. Casais constructed Beau-R by cloning the IBV Beau-CK cDNA genome into the vaccinia virus, vNotI/tk to produce vNotI/IBV_{FL} (Casais *et al.*, 2001).

Bacterial cultures

SOC medium

SOC medium was used for culturing *E. coli* immediately following transformation with each plasmid.

20 g	Bacto tryptone	2 % w/v
5 g	Yeast extract	0.5 % w/v
0.5 g	NaCl	9 mM
5 g	MgSO4	20 mM
3.6 g	Glucose	20 mM

Double-distilled water (DDW) was added to a final volume of 1 L.

Luria-Bertani (LB) broth

10 g	Bacto tryptone	1 % w/v
5 g	Yeast extract	0.5 % w/v
10 g	NaCl	170 mM

DDW was added to a final volume of 1 L and the pH adjusted to 7.2 with NaOH before autoclaving at 121^{o}C for 15 minutes.

When culturing *E. coli* transformed with plasmids encoding β-lactamase (ampicillin resistance), ampicillin (Sigma-Aldrich) was added to the broth to a final concentration of 100 μg/ml.

When culturing *E. coli* transformed with plasmids encoding the *nptII* gene (kanamycin resistance), kanamycin (Sigma-Aldrich) was added to the broth to a final concentration of 50 μg/ml.

LB-agar plates

LB-agar/ampicillin was LB-broth containing 1.5 % Bacto agar plus 100 μg/ml ampicillin.

LB-agar/kanamycin was LB-broth containing 1.5 % Bacto agar plus 50 μg/ml kanamycin.

Plasmids

SUMO plasmids

The pET SUMO protein expression system (Invitrogen) (Fig. 2.1) was used to express the IBV 3b protein and IBV ADRP domain of nsp3 with a N-terminal small ubiquitin-like modifier (SUMO). Addition of the SUMO sequence has been shown to increase expression and enhance solubility of proteins (Zuo *et al.*, 2005). The plasmid was supplied in a linearised form with 3' deoxythymidine overhangs that prevented recircularisation of the plasmid and provided a one-step cloning strategy for the insertion of a PCR product with 3' deoxyadenosine overhangs. IPTG-inducible gene expression was facilitated by the T7*lac* promoter. Purification of the protein was assisted by the presence of a N-terminal polyhistidine (His) tag.

The pET SUMO/3b and pET SUMO/ADRP plasmids were constructed by reverse-transcriptase polymerase chain reaction (RT-PCR) amplification of the 3b ORF or ADRP domain of nsp3 from RNA isolated from Beau-R-infected CK cells using ORF or domain inclusive primers (Primer sequence in appendix table A.1). RT-PCR was performed using the polymerase from *Thermus aquaticus* (*Taq*) to generate 3'

deoxyadenosine overhangs. The 3' deoxyadenosine added by the *Taq* polymerase during the PCR step was ligated to the overlapping 3' deoxythymidine of the linearised pET SUMO vector. Sequencing confirmed the correct orientation of the PCR product.

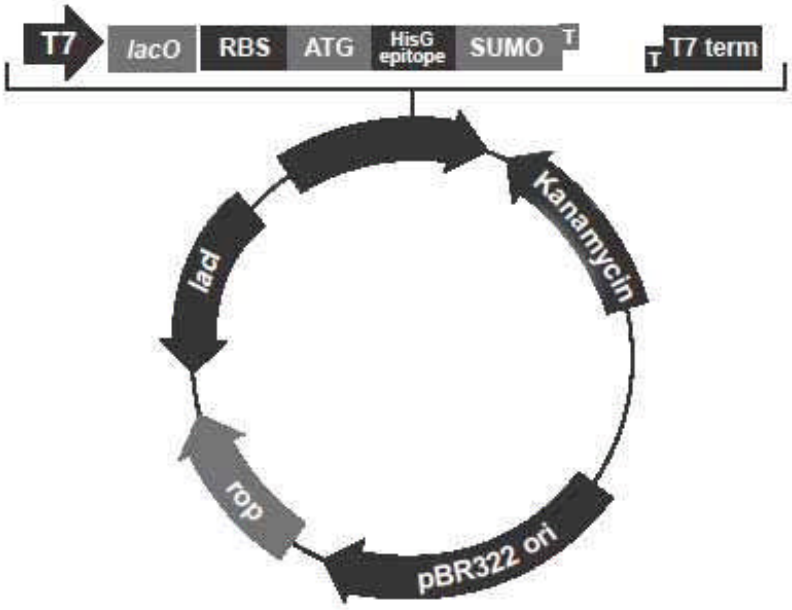

Figure 2.1. Map of the pET SUMO plasmid. The PCR product with 3' deoxyadenosine overhangs was ligated with the 3' deoxythymidine overhangs contained in the linearised plasmid. The T7lac promoter facilitated gene expression. The expressed protein would contain a His-tag and SUMO N-terminal to the protein of interest.

FLAG-tagged plasmids

The pFLAG-CMV-2 plasmid (Sigma-Aldrich) (Fig. 2.2) was used to express N-terminally FLAG-tagged IBV accessory proteins. This plasmid contained the FLAG sequence upstream of a multiple cloning site. Expression of the gene is facilitated by the cytomegalovirus immediate/early (CMV) promoter.

The Beau-R 3a, 3b, 5a and 5b ORFs were cloned by RT-PCR of RNA isolated from Beau-R-infected CK cells. Primers containing *Eco*RI sites upstream and downstream of the complete ORFs were used to amplify the sequence (Primer sequence in appendix table A.2). These restriction sites were used to clone the ORFs in frame with the upstream FLAG tag sequence of pFLAG-CMV-2 (Sigma), separated by 18 nucleotides to create pFLAG/3a, /3b, /5a and /5b. pFLAG/Bacterial alkaline phosphatase (BAP) was included with the pFLAG-CMV-2 vector.

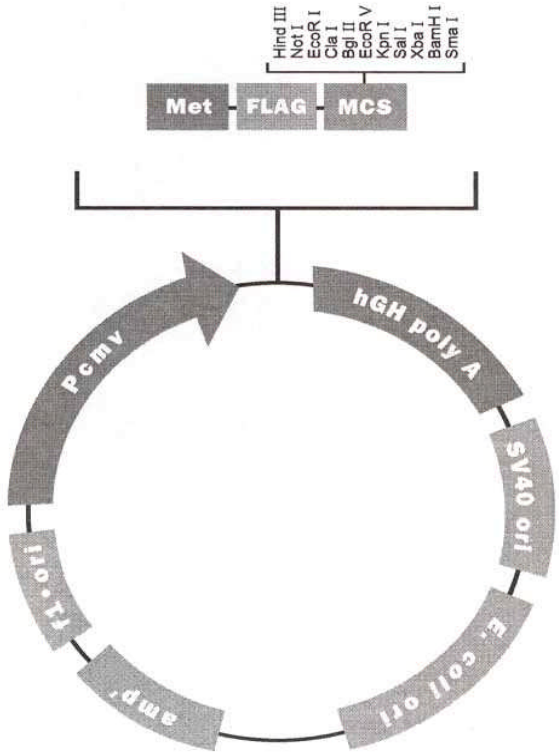

Figure 2.2. Map of the pFLAG-CMV-2 plasmid. Expression of the gene is facilitated by the CMV promoter. A methionine (Met) initiates the translation process which is N-terminal to the FLAG sequence and the protein of interest. The gene of interest is inserted into the multiple cloning site (MCS).

His-tagged plasmids

pDEST14-nsp8HN was a kind gift from Eric Snijder, Leiden University Medical Center, the Netherlands.

DNA-based methods

Small-scale plasmid DNA purification

Overnight cultures of *E. coli*, transformed with the required plasmid were grown in 5 ml of LB broth containing the desired antibiotic, either ampicillin (100 μg/ml) or kanamycin (50 μg/ml). The Qiaprep Spin Miniprep Kit (Qiagen) was used for the DNA purification and the recommendations of the manufacturer were followed.

Briefly, the bacterial cells undergo alkaline lysis before selective adsorption of plasmid DNA onto silica-gel columns in the presence of high salt. Bound plasmid DNA was washed with the supplied wash buffer to remove salts. Elution was performed with nuclease-free water (Sigma).

Large-scale plasmid DNA purification

Overnight 200 ml cultures of *E. coli*, transformed with the required plasmid were centrifuged at 2,000 x g for 25 min to pellet the bacteria before large-scale isolation and purification of DNA using either the HiSpeed plasmid maxi kit (Qiagen) or the Qiafilter plasmid maxi kit (Qiagen) according to manufacturer's instructions. These kits utilise the binding of DNA to diethylaminoethyl (DEAE) contained on a silica-based resin. Contaminants are removed with increased salt concentration and DNA is eluted with a high salt concentration. The DNA is concentrated and the salt removed by isopropanol precipitation.

PCR amplification of DNA fragments

PCR was used to amplify specific IBV cDNA sequences.

5 µl	10 x *Taq* DNA polymerase buffer
2 µl	50 mM $MgCl_2$
1 µl	10 mM dNTP mix
1 µl	forward oligonucleotide (10 pmol)
1 µl	reverse oligonucleotide (10 pmol)
5 µl	template DNA
34.75 µl	nuclease-free water (sigma)
0.25 µl	*Taq* polymerase

PCRs were performed using a Px2 thermal cycler, Thermo Electron corporation with hotlid with the following cycles:

96^{o}C x 2 min	1 cycle

96°C x 30 sec
X°C x 30 sec*
72°C x 1 min per kb of DNA to be amplified
} 30 cycles

* The annealing temperature was dependent upon the melting temperature of the primers – typically the lowest melting temperature of the two primers was used.

PCR products were analysed by electrophoresis of 5 µl on a 0.8 – 1.2 % agarose gel stained with ethidium bromide.

Agarose gel electrophoresis

DNA was routinely separated and visualised by agarose gel electrophoreses in 0.8 – 1.2 % agarose and 1 x Tris borate EDTA buffer (10 x TBE buffer (1M Tris, 0.9 M boric acid and 10 mM EDTA; Invitrogen) diluted with milli-Q water) with 0.1 µg ethidium bromide per ml of agarose gel. Cast gels were run in 1 x TBE buffer using a horizontal submarine gel apparatus at ~5 V/cm gel length. DNA was visualised by exposure of the gel to 260 nm UV light. DNA band sizes were established by comparison against 1 µg 1kb+ DNA ladder (Invitrogen).

DNA loading buffer

Glycerol	10 ml
0.5 M EDTA pH 8.0	4 ml
1 M Tris-HCL pH 8.0	1 ml
1% bromophenol blue	1 ml

Purification of DNA from PCR

Prior to ligation of the PCR products into the pET-SUMO or pFLAG vectors DNA from the PCRs was purified using the Qiaquick PCR purification kit (Qiagen) according to manufacturer's instructions.

DNA restriction enzyme digestion

Restriction enzyme digestions were performed at the conditions recommended by the manufacturer. *Eco*RI was sourced from New England Biolabs.

DNA dephosphorylation for cloning

After restriction enzyme digestion the plasmid DNA was dephosphorylated to prevent self-ligation. Shrimp alkaline phosphatase (Promega) was used according to the manufacturer's instructions.

DNA ligation

The quantities of vector DNA and PCR product were evaluated by comparison of the DNA band intensities on an ethidium bromide-stained agarose gel. A 3:1 insert to vector ratio was established to facilitate the ligation.

T4 DNA ligase (Invitrogen)	1 µl
10x DNA ligase buffer (Invitrogen)	3 µl
Vector DNA	1 µl
PCR DNA	18 µl

Nuclease-free water was added to a final volume of 30 µl.

Transformation of *E. coli* and plasmid screening

The ligation mixture was used to transform One shot Mach1-T1 *E. coli* as manufacturer's instructions. Aliquots of the transformed *E. coli* were plated out on LB plates containing ampicillin (100 µg/ml) and incubated for 16 h at 37^{o}C. Individual *E. coli* colonies were cultured in 5 ml LB containing ampicillin (100 µg/ml) for 16 h at 37^{o}C. DNA was extracted from the culture and sequenced to assess the correct insert.

RNA-based methods

Purification of RNA from cells

Cellular RNA was purified from CK cells using the RNeasy mini column system (Qiagen) following the manufacturer's protocol. Briefly, cells were lysed with a guanidine isothiocyanate lysis buffer (Qiagen). Ethanol was added to optimise RNA binding to the column. Bound RNA was washed and eluted with RNase-free water.

Protein expression and purification in bacteria

Expression of protein in bacteria

BL21 (DE3) One Shot *E.coli* (Invitrogen) were transformed with the appropriate plasmid according to the manufacturer's protocol. 10 ml overnight cultures were used to inoculate 500 ml LB plus appropriate antibiotic and cultured for two hours. Protein expression was then induced by growing cultures in 1 mM (final concentration) isopropyl-β-D-thiogalactopyranoside (IPTG) (Sigma) for four hours at 37^{o}C.

Lysis of bacteria

Bacteria were lysed using CelLytic B 2x (Sigma) supplemented with Benzonase Nuclease (Novagen), Lysozyme (Sigma) and protease inhibitors for purification of Histidine-tagged proteins (Sigma) following manufacturer's protocol.

Purification of the expressed protein

Purification of the His-tagged proteins was performed using the HisSelect gel (Sigma) and following the manufacturer's recommendations. Both the batch method and column purification were used. Higher levels of purification were obtained by eluting with increasing concentrations of Imidazole step-wise from 20 mM, 60 mM to 250 mM.

Quantitation of the expressed protein

The bicinchoninic acid (BCA) protein assay was used for the quantitation of protein samples. This process is based upon the biuret reaction whereby peptides containing three or more amino acid residues reduce cupric ions (Cu2+) to cuprous ions (Cu1+) in the presence of an alkaline solution. The generated cuprous ions are chelated by BCA and these complexes absorb light at 562 nm. This absorbance is nearly linear over a range of protein concentrations.

Generation of antibodies against 3b, ADRP domain and nsp8

Two rabbits were used for each of the SUMO/3b, SUMO/ADRP and nsp8HN proteins. Pre-immune sera were taken and 200 μg protein injections were given at day 0. Additional injections were given at 14, 28 and 56 days. Immune sera were taken at 38, 66 and 87 days. All procedures were performed by Eurogentec SA, Belgium.

Protein-based methods

PAGE

Technique performed using the 4-12% NuPAGE Novex Bis-Tris gels (Invitrogen) with 2-(N-Morpholino) ethanesulfonic acid (MES) or (N-Morpholino) propanesulfonic acid (MOPS) running buffer. Samples were prepared and separated according to the manufacturer's recommendations, which included sample reducing solution and heating the sample to 70^{o}C for 10 min.

Western blot

Proteins were electrophoretically transferred to polyvinylidene difluoride (PVDF) membrane (Invitrogen) using a CSL semi dry blotting unit (Cleaver Scientific) according to manufacturer's instructions. Membranes were rinsed in PBS and blocked with 2% dried milk powder in 0.1% Tween-20/PBS. All antibodies were diluted in the same to the concentrations listed in table 2.1. The membranes were

incubated with the antibody solutions on an orbital shaker for 1hr, rinsed once with 0.1% Tween-20 in PBS and 3 x 20 min in 0.1% Tween-20 in PBS.

HRP-conjugated secondary antibodies were diluted in 2% Marvel in 0.1% Tween-20/PBS, incubated and washed as described for the primary antibodies. HRP-conjugated antibodies were detected with the Immobilon Western detection system (Millipore) according to manufacturer's instructions.

Table 2.1. Antibodies used for performing Western blots

Name/antigen recognised		Species of origin	Dilution factor
5b SK71		Rat	1:5,000
3a 3480		Rabbit	1:5,000
M2 / FLAG (Stratagene[1])		Mouse	1:10,000
GCN1L1 (Bethyl Laboratories[1])		Rabbit	1:5,000
SUMO/3b	0525	Rabbit	1:5,000
	0526	Rabbit	1:5,000
SUMO/ADRP	0523	Rabbit	1:5,000
	0524	Rabbit	1:5,000
nsp8HN	0682	Rabbit	1:5,000
	0683	Rabbit	1:5,000

[1] Supplier

Coomassie staining

After protein separation by PAGE the gel was rinsed once with dH_2O and fixed with 50% ethanol and 7% acetic acid and stained with GelCode Blue stain (Thermo Scientific) according to the manufacturer's instructions.

Silver staining

After protein separation by PAGE the gel was rinsed once with dH_2O and fixed with 30% ethanol and 10% acetic acid overnight at 4^oC.

Sensitive method (not mass spectrometry compatible)

Sensitising solution:

Ethanol	15 mls	(30%)
25% Glutaraldehyde	250 µl	(0.125%)
Sodium thiosulphate	0.1 g	(0.008 M)
Sodium acetate	3.4 g	(0.83 M)
dH2O	35 mls	

Silver solution:

Silver nitrate	0.13 g	(0.015 M)
37% Formaldehyde solution	20 µl	(0.015%)
dH2O	50 mls	

Developing solution:

Sodium carbonate	1.25 g	(0.24 M)
37% Formaldehyde solution	40 µl	(0.03%)
dH2O	50 mls	

Stop solution:

EDTA	0.73 g	(0.05 M)
Total 50 mls		

Mass spectrometry compatible silver staining:

As above, except no glutaraldehyde is added to the sensitising solution, no formaldehyde is added to the silver solution and half the quantity of formaldehyde is added to the developing solution.

Transfection

Vero cells were seeded onto cover slips in 24-well cell culture plates (for immunofluorescence) or T25 cell culture flasks (for immunoprecipitation). The following day the cells were ~80% confluent. The transfections were performed using ICAFectin 441 (Eurogentec) according to the manufacturer's recommendations.

Immunoprecipitation

Twenty-four hours after transfection, ~6 x 10^7 Vero cells were washed once with ice-cold PBS and lysed on ice with non-denaturing lysis buffer (20 mM Tris·HCl pH 8, 137 mM NaCl, 10% glycerol, 1% Triton X-100, 2 mM EDTA) containing protease inhibitors (Cømplete protease inhibitor cocktail, Roche). The cell extract was centrifuged for 10 min, 13,000 x g, 4^{o}C. The cleared extract was incubated overnight at 4^{o}C with 100 µl Dynabeads Protein G (Invitrogen) cross-linked to 20 µg anti-FLAG M2 antibody (Stratagene). After extensive washing of the beads, the bound protein was eluted with 0.1 M glycine pH 3.4. The eluted proteins were neutralised with 1 M Tris pH 7.6 and concentrated using acetone precipitation.

Cross-linking antibody

Anti-FLAG antibodies were cross-linked to Dynabeads/Protein G (Invitrogen) using the manufacturer's instructions. Breifly 20 µg anti-FLAG M2 antibody was incubated with 50 µl Dynabeads/Protein G. The antibody/Protein G complex was washed with 0.2 M triethanolamine pH 8.2 and cross-linked using 20 mM dimethyl pimelimidate (DMP) in 0.2 M triethanolamine. The reaction was stopped using 50 mM Tris pH 7.5. DMP is a homobifunctional imidoester cross-linker which reacts with primary amines.

Acetone precipitation

Four times the sample volume of -20^{o}C acetone was added to the sample. After vortexing the sample and acetone was stored at -20^{o}C overnight. Sample was

centrifuged for 10 min, 13,000 x g, 4°C, the acetone was removed and the proteins were resuspended in 20 µl dH_2O.

Indirect immunofluorescence

Infection

Vero cells or CK cells were seeded onto cover slips in 24-well cell culture plates. The following day the cells were ~ 50% confluent. Beau-R at 1 x 10^5 pfu was used to infect these cells. The virus was allowed to absorb for 1 h at 37°C in a CO_2 incubator. The inoculum was drained and replaced with 0.5 ml 1 x BES medium.

Fixing, permeabilisation and blocking

Infected cells were fixed with 4% paraformaldehyde in PBS for 45 min. The paraformaldehyde was then replaced with PBS. Fixed cells were permeabilised with 0.5% Triton-X100 for 10 min and blocked with 0.5% BSA-PBS for 1 hr.

Immunolabelling

Fixed and permeabilised cells were immersed in diluted primary antibody for 1 h and washed with PBS. Diluted secondary antibody was applied for 1 h with the same wash procedure. The nuclei were stained with DAPI (Invitrogen) as manufacturer's recommendations. Cells on the cover slips were mounted in Vectashield Mounting Medium for Fluorescence (Vector Laboratories) and sealed with nail varnish.
Immunolabelled cells were examined using a Leica TCS SP5 DM6000 confocal microscope with the Leica Microsystems LAS AF software.

Antibodies

Primary antibodies were diluted in 0.5% BSA-PBS to a final volume of 200 µl (Table 2.2).

Table 2.2. Antibodies used for indirect immunofluorescence.

Name/antigen recognised	Species of origin	Dilution factor	Comments
SK71 / 5b	Rat	1:100	Polyclonal anti-C-terminal peptide
8194 / 3a	Rabbit	1:100	Polyclonal anti-N-terminal peptide
3480 / 3a	Rabbit	1:100	Polyclonal anti-C-terminal peptide
C5-124 / M	Mouse	1:10	Monoclonal against M41 membrane protein
A13-38 / S	Mouse	1:10	Monoclonal against M41 spike protein
SUMO-3b 0525	Rabbit	1:100	Polyclonal anti-protein
SUMO-3b 0526	Rabbit	1:100	Polyclonal anti-protein
SUMO-ADRP 0523	Rabbit	1:100	Polyclonal anti-protein
SUMO-ADRP 0524	Rabbit	1:100	Polyclonal anti-protein
nsp8HN 0682	Rabbit	1:100	Polyclonal anti-protein
nsp8HN 0683	Rabbit	1:100	Polyclonal anti-protein
Anti-Beaudette	Rabbit	1:500	Polyclonal anti-IBV
Anti-Beaudette	Chicken	1:500	Polyclonal anti-IBV
GM130 / Golgi apparatus	Mouse	1:1000	Monoclonal Golgi marker
FLAG / M2 (Stratagene)	Mouse	1:1000	Monoclonal anti-FLAG tag
dsRNA / J2 (English and Scientific Consulting)	Mouse	1:1000	Monoclonal anti-double stranded RNA
SPA-891 / PDI (Stressgen)	Mouse	1:1000	Monoclonal endoplasmic reticulum marker
ERGIC-53 (Alexis Biochemicals)	Mouse	1:1000	Monoclonal endoplasmic reticulum-Golgi intermediate compartment marker

Mass spectrometry

Confirmation of the identity of the SUMO/3b and SUMO/ADRP proteins

All mass spectrometry was performed at the Proteomics Facility, IAH Compton, by facility staff. Samples were analysed by on-line capillary HPLC-mass spectrometry. Briefly, samples were diluted to an estimated concentration of 1 pmole/ul in HPLC buffer A (95:5 H2O:acetonitrile & 0.05 % (v/v) trifluoracetic acid) and 25-30 µl was injected onto a homemade pre-concentration trap packed with C_{18} reversed phase sorbent (Jupiter, 300 Å pore size, 3.5 um bead size) (Homemade – column was packed and validated at the IAH Compton). The trap was washed with HPLC buffer A and bound components were eluted onto a capillary column, packed with the same sorbent, by means of a linear gradient of increasing HPLC buffer B (5:95 H2O:acetonitrile & 0.05 % (v/v) trifluoroacetic acid). The eluent from the column was passed directly to the nanospray source of a Q-ToF Premier mass spectrometer (Waters Ltd, Altrincham, UK). Full scan mass spectra (m/z 500-2100) were acquired every second. Protein mass spectra were smoothed and centroided and molecular masses calculated based on m/z values of peaks.

Identification of the FLAG/3a protein interacting proteins by LC-MS/MS

Results from the pull-down assays using the FLAG/3a and FLAG/BAP proteins indicated that six cellular proteins were interacting with the FLAG/3a sequence. The silver-stained protein bands were cut out from the gel and divided into cubes (~2 mm^3). Protein contained within the gel fragments were digested using a MassPREP workstation (Waters) during which they were washed with 100 mM ammonium bicarbonate and dehydrated with 100% (v/v) acetonitrile prior to reduction with 10 mM DTT / 100 mM ammonium bicarbonate for 30 min and alkylated with 55 mM iodoacetamide / 100 mM ammonium bicarbonate for 20 min. These were then washed again with 100 mM ammonium bicarbonate and dehydrated with 100% (v/v) acetonitrile. Proteins were digested with 6 ng/µl trypsin / 50 mM ammonium

bicarbonate for 5 hours at 37°C and peptides were extracted firstly in 1% (v/v) formic acid / 2% (v/v) acetonitrile and secondly in 50% (v/v) acetonitrile. Tryptic peptides (5 μl) were desalted and concentrated on a C18 TRAP (180 μm x 20 mm, 5 μm Symmetry, Waters), for 3 min at 10 μl/ min, and resolved on a 1.7 μm BEH 130 C18 column (100 μm x 100 mm, Waters) at 400 nl/ min attached to Waters UPLC Acquity HPLC. Peptides were eluted at 400 nl/ min with a linear gradient of 0-50% (v/v) acetonitrile/ 0.1% (v/v) formic acid over 30 min, followed by 85% (v/v) acetonitrile/ 0.1% (v/v) formic acid for 7 min. Ionised peptides were analysed by a Waters Quadrupole Time of Flight Premier Mass Spectrometer in data directed acquisition mode tuned using 200 fmol / μl human glutamate fibrinopeptide B in (v/v) 0.1% formic acid/ (v/v) 50% acetonitrile / water. Peaklists were created from raw spectral data with ProteinLynx Global Server version 2.2.5 (Waters), using the following criteria: external calibration with lockmass of 785.8426 ($M+H^{2+}$) of glutamate fibrinopeptide B, adaptive type background subtraction combining all scans and deisotoping with a threshold of 5%.

The resulting peak lists were submitted to MASCOT version 2.2 (Matrix Science, UK) and searched against the NCBInr database. Database search settings allowed one missed cleavage with the trypsin enzyme selected, carbamidomethylated cysteine as fixed modification, oxidised methionine as potential variable modification, peptide tolerance of ± 200 ppm, MS/MS tolerance of ± 0.2 Da and +2 and +3 peptide charge states.

Chapter 3: Cellular location of the gene 3 accessory proteins

Summary

The cellular location of the gene 3 accessory proteins was examined. Antibodies directed against the 3a protein indicated that the 3a protein had a punctate, cytoplasmic distribution pattern in infected avian cells. There were no colocalisation events seen between 3a and the Beau-R structural proteins or markers for the ER, ERGIC or Golgi. There were colocalisation events observed between the 3a protein and viral double-stranded RNA produced in infected cells.

Antibodies weren't available against the IBV 3b protein. Likewise, antibodies weren't available against the replicase proteins in order to compare the subcellular location of the gene 3 accessory proteins to the sites of genome replication. Strategies to generate antibodies directed against 3b, nsp8 proteins and the ADRP domain of nsp3 were unsuccessful.

Introduction

Very little was known about the cellular location of the gene 3 accessory proteins in infected mammalian and avian cells. In order to gain some insight into the functions of these proteins their subcellular location was analysed. Immunofluorescence with confocal microscopy was used to discern the distribution pattern and potentially highlight any colocalisation events. This technique examines the location of fluorescent molecules attached to antibodies, normally within a cell. The resolution of confocal microscopy is such that when two of these fluorescent molecules are within 250 nm of each other the same pixel in the digital image will contain two colours. These two colours together merge to make the combination, i.e. green and

red together make yellow. This isn't close enough to imply an interaction is occurring but does suggest a close spatial relationship.

Antibodies were available to the 3a protein and these were used in conjunction with other viral protein or cellular compartment markers to confirm the findings from IBV-infected mammalian cells and to specify their cellular location within infected avian cells. When an antibody to label a specific subcellular structure was unavailable for use in avian cells Vero cells were used instead. Although Beau-R replicates in Vero cells to the same titres as in CK cells the number of cells initially infected is lower. To achieve a similar number of infected cells for the immunofluorescence experiments Beau-R was left longer to continue replicating in Vero cells.

Where an antibody wasn't immediately available to detect a protein in immunofluorescence experiments, i.e. the 3b protein, a FLAG-tagged version was expressed from a plasmid which had been used to transfect cells. The FLAG tag is a hydrophilic octapeptide which is recognised by commercially available antibodies. A FLAG-tagged 3a protein was also used to identify the subcellular distribution of a tagged 3a protein and compare it to the subcellular distribution of the native, virally-expressed 3a protein.

Antibodies to detect the 3b protein were unavailable. Various procedures to raise suitable antibodies had been previously been unsuccessful. These included Keyhole Limpet Haemocyanin (KLH) -conjugated peptides, Glutathione-S-transferase (GST) -fusion proteins and DNA vaccinations. Consequently, recombinant proteins were generated which contained an N-terminal Small Ubiquitin modifier (SUMO) sequence. This tag has been reported to enhance expression and solubility (Malakhov *et al.*, 2004). Antibodies to the replicase proteins were also unavailable and a similar method of antibody production was performed.

Results

Immunofluorescence with anti-3a antibodies and subcellular markers

The subcellular location which the 3a protein occupied within IBV-infected cells was analysed using indirect immunofluorescence with confocal microscopy. A polyclonal antibody which recognised the N-terminal portion of the 3a protein was used in conjunction with antibodies which specifically labelled subcellular structures involved in the replication of Beau-R or which detected the viral structural proteins.

Images taken of indirect immunofluorescence experiments using Beau-R-infected Vero and CK cells indicated that in both mammalian and avian cells the 3a protein exhibited a punctate distribution spread throughout the cytoplasm and absence from the nucleus (Fig. 3.1). This distribution pattern was compared to protein markers for subcellular structures contained within the cell. There was no colocalisation or similar distribution pattern between 3a and the ER (Fig. 3.2), ERGIC (Fig. 3.3) or Golgi apparatus (Fig. 3.4).. The detection of 3a protein could be observed from 4 h p.i. onwards (Fig. 3.5) (Mock infected Fig. 3.6).

Due to a lack of antibodies which specifically labelled the ERGIC in avian cells, Vero cells were used to compare the subcellular distribution of the 3a protein with this site of virion assembly.

Figure 3.1. Indirect immunofluorescence analysis of the intracellular distribution of IBV 3a protein within Beau-R-infected CK cells. Subconfluent CK cells were infected with Beau-R and fixed at 10 h p.i. with paraformaldehyde. After making the cells permeable with Triton X-100 they were labelled with rabbit polyclonal anti-3a (8194). Secondary antibodies included Alexa Fluor 488 anti-rabbit (green) and nuclei were labelled with DAPI. A – Anti-3a antibody with DAPI. B – A magnified section of (A). C – The same magnified section as (B) but displaying the anti-3a antibody labelling only. D - The same magnified section as (B) but displaying the DAPI labelling only. The different wavelengths (colours) were scanned independently and digitally merged. Scale bar indicates 20 μm.

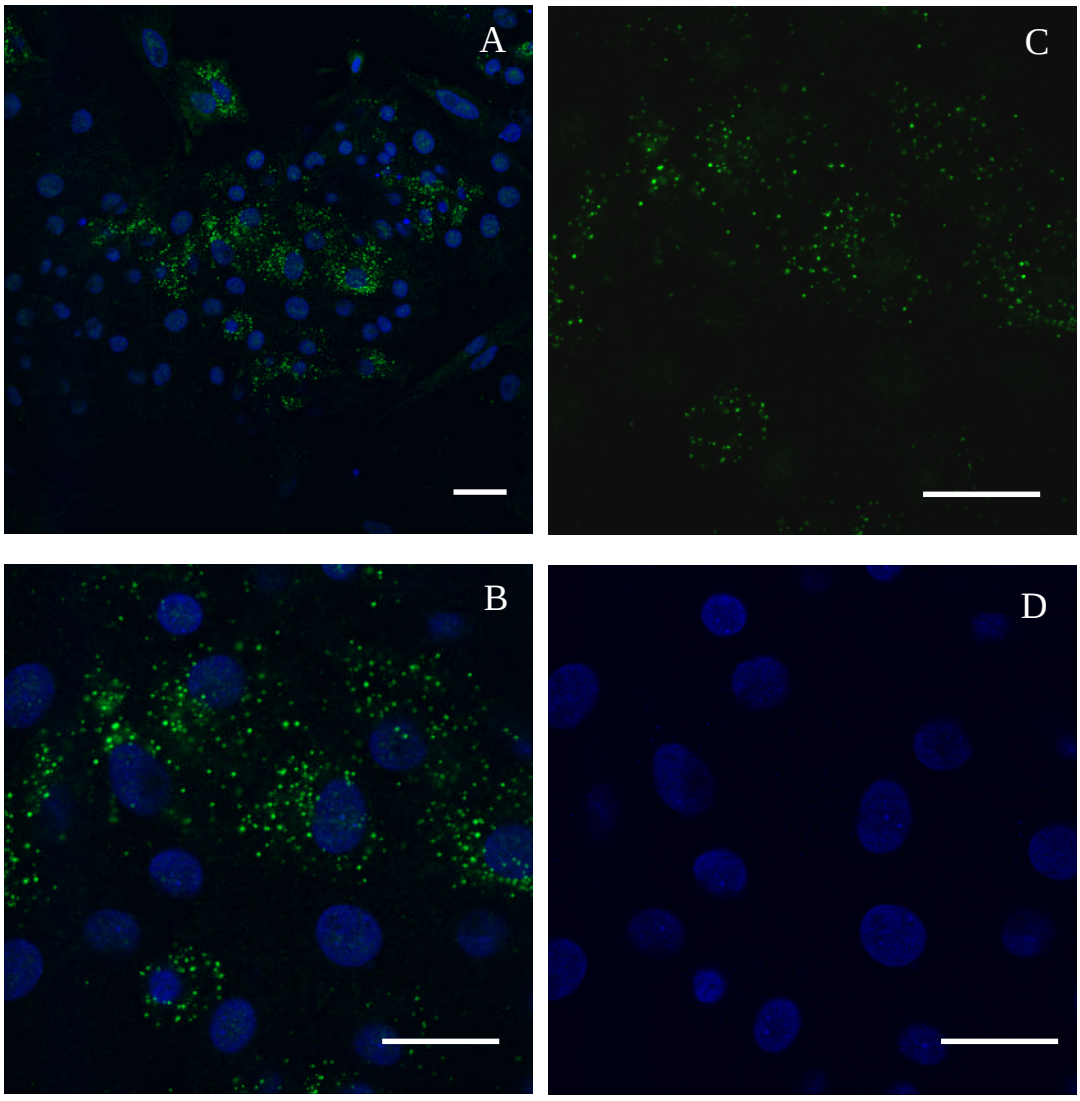
A
C
B
D

Figure 3.2. Indirect immunofluorescence analysis of the intracellular location of the 3a protein compared to ER. Subconfluent CK cells were infected with Beau-R and fixed at 10 h p.i. with paraformaldehyde. After making the cells permeable with Triton X-100 they were labelled with rabbit polyclonal anti-3a (8194) (A and D) and mouse anti-PDI (ER marker) (B and E). Secondary antibodies included Alexa Fluor 488 anti-rabbit (green) and Alexa Fluor 568 anti-mouse (red). Nuclei were labelled with DAPI. The different wavelengths (colours) were scanned independently and digitally merged (C and F). Images D, E and F are a magnified section of the images A, B and C. Scale bar indicates 20 μm.

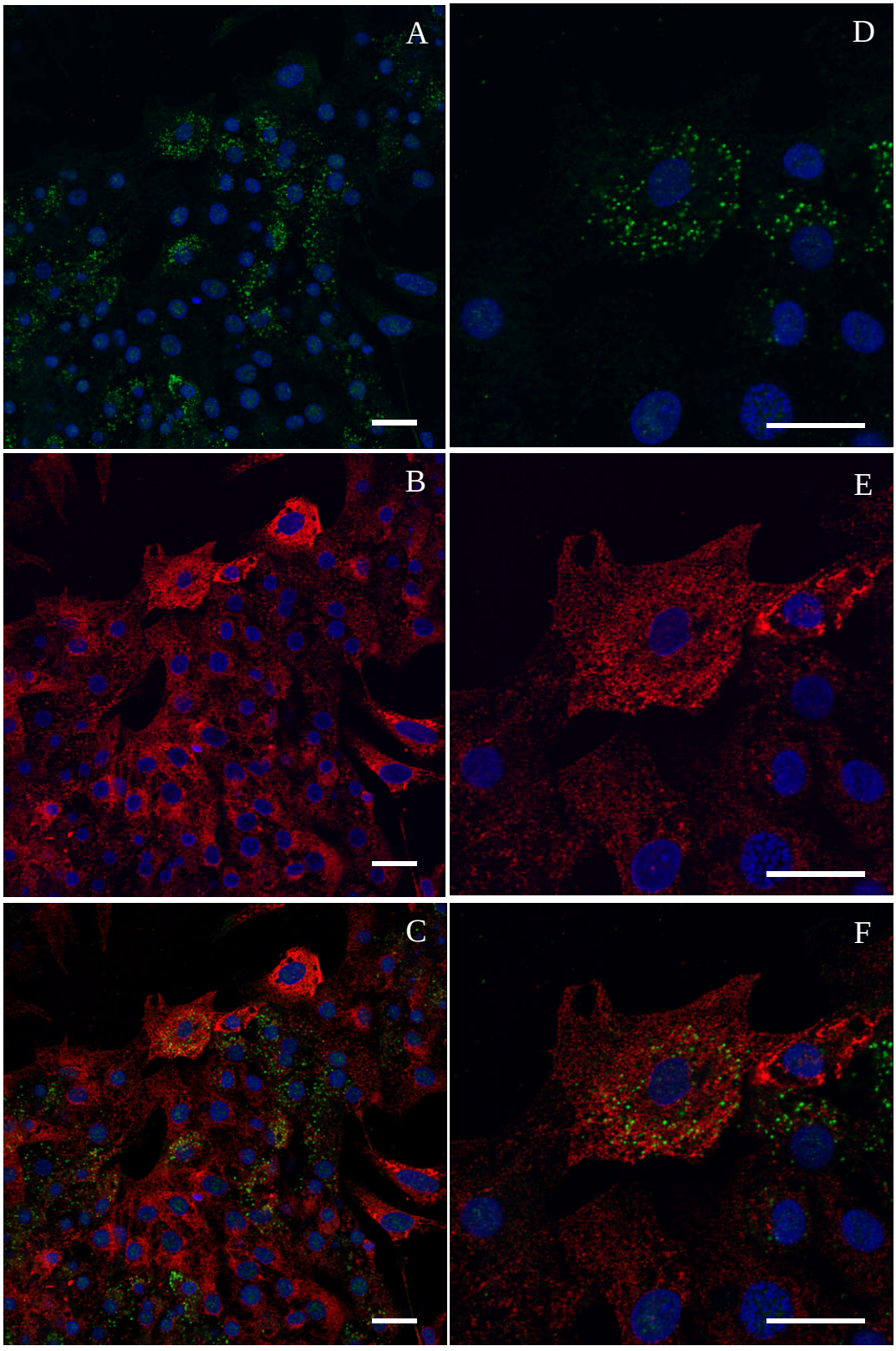
A
D
B
E
C
F

Figure 3.3. Indirect immunofluorescence analysis of the intracellular location of the 3a protein compared to ERGIC. Subconfluent Vero cells were infected with Beau-R and fixed at 8 h p.i. with paraformaldehyde. After making the cells permeable with Triton X-100 they were labelled with rabbit polyclonal anti-3a (8194) (A and D) and mouse anti-ERGIC-53 (ERGIC marker) (B and E). Secondary antibodies included Alexa Fluor 488 anti-rabbit (green) and Alexa Fluor 568 anti-mouse (red). Nuclei were labelled with DAPI. The different wavelengths (colours) were scanned independently and digitally merged (C and F). Images D, E and F are a magnified section of the images A, B and C. Scale bar indicates 20 μm.

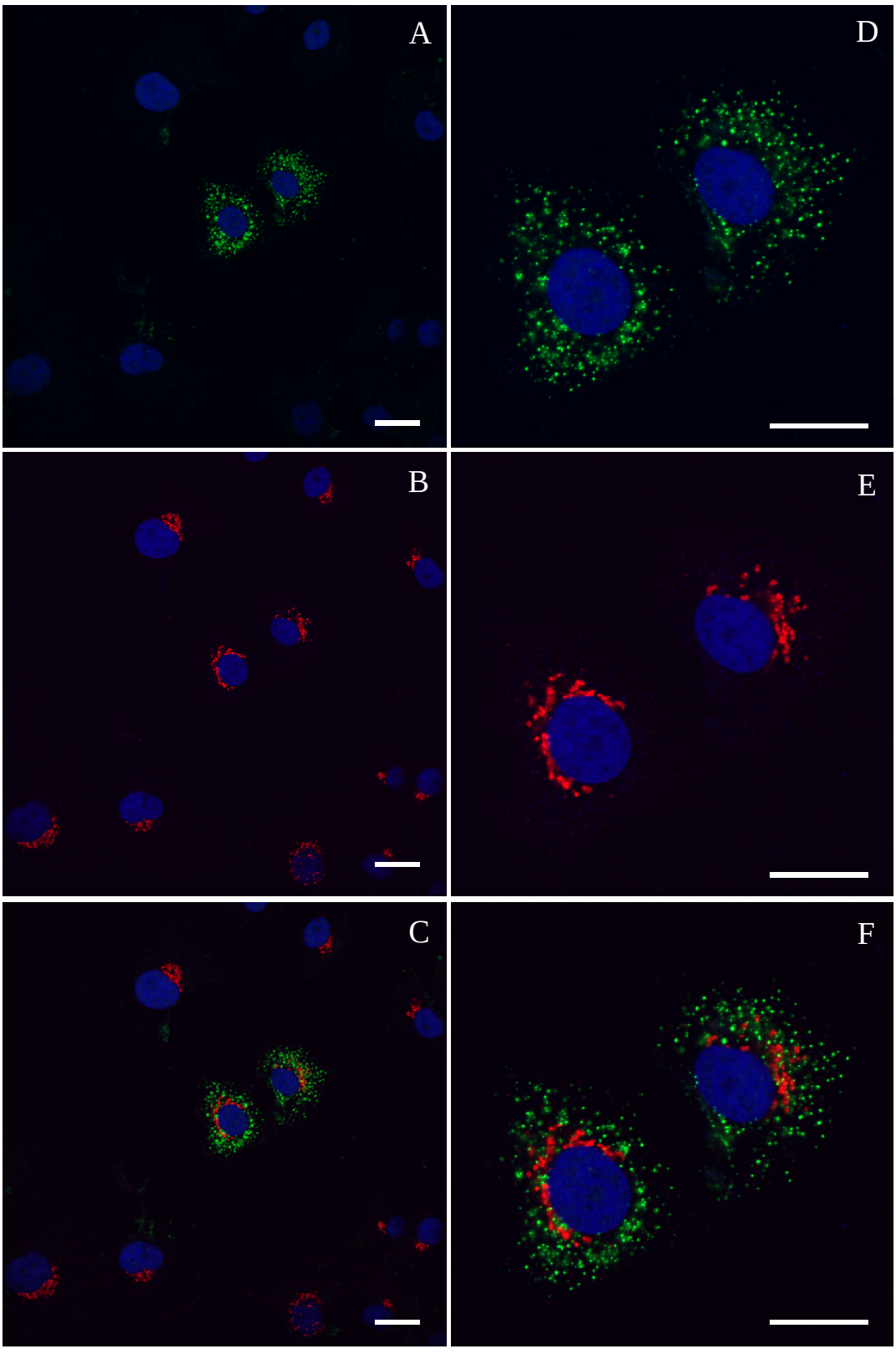
A
D
B
E
C
F

Figure 3.4. Indirect immunofluorescence analysis of the intracellular location of the 3a protein compared to Golgi apparatus. Subconfluent CK cells were infected with Beau-R and fixed at 10 h p.i. with paraformaldehyde. After making the cells permeable with Triton X-100 they were labelled with rabbit polyclonal anti-3a (8194) (A and D) and mouse anti-GM130 (Golgi marker) (B and E). Secondary antibodies included Alexa Fluor 488 anti-rabbit (green) and Alexa Fluor 568 anti-mouse (red). Nuclei were labelled with DAPI. The different wavelengths (colours) were scanned independently and digitally merged (C and F). Images D, E and F are a magnified section of the images A, B and C. Scale bar indicates 20 μm.

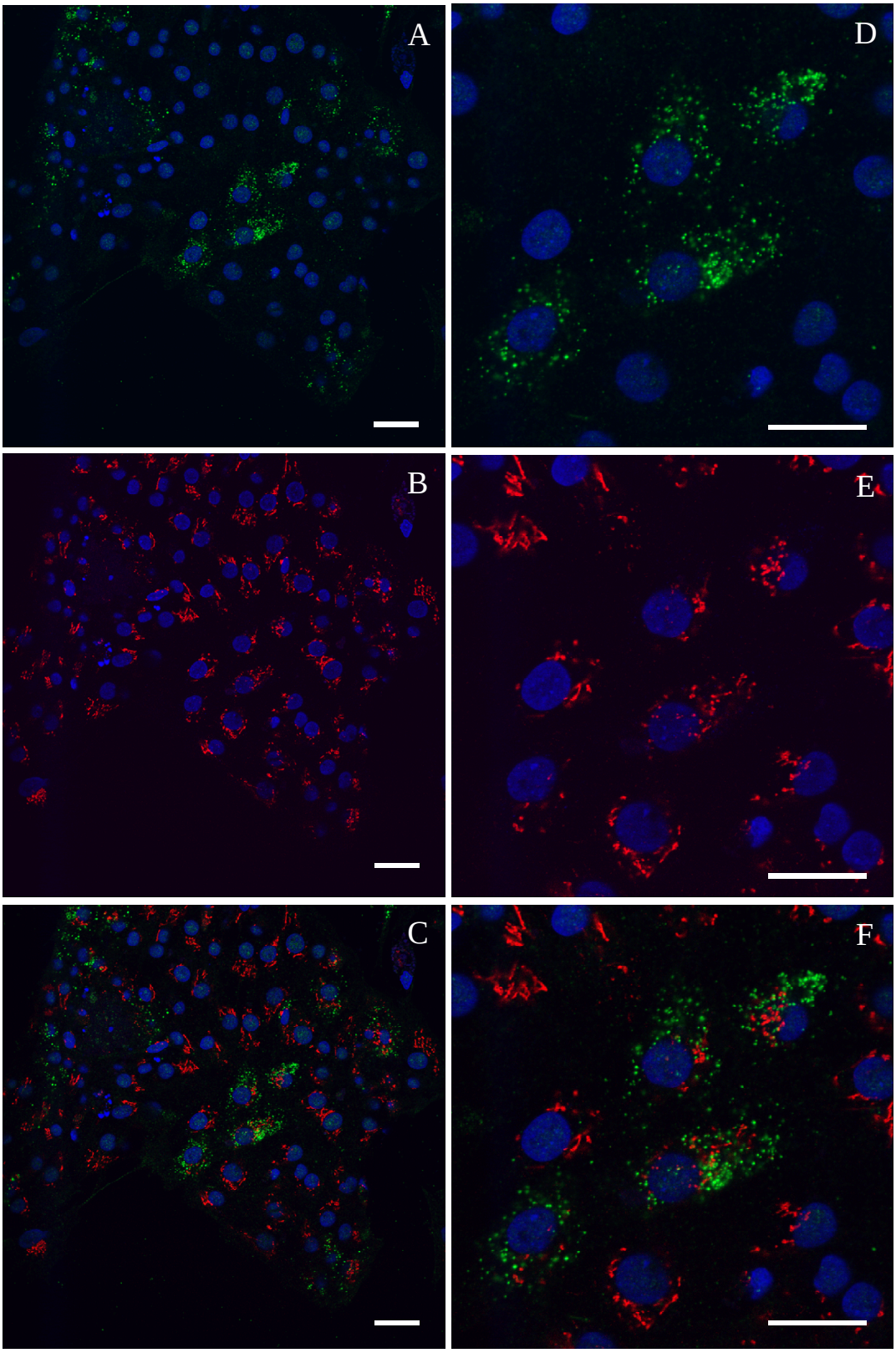
A
D
B
E
C
F

Figure 3.5. Indirect immunofluorescence analysis of the expression of the 3a protein at 4 and 6 h p.i. Subconfluent CK cells were infected with Beau-R and fixed at either 4 (A, B and C) or 6 h p.i. (D, E and F) with paraformaldehyde. After making the cells permeable with Triton X-100 they were labelled with rabbit polyclonal anti-3a (8194) (A and D) and mouse anti-M (C5/124) (B and E) protein antibodies. Secondary antibodies included Alexa Fluor 488 anti-rabbit (green) and Alexa Fluor 568 anti-mouse (red). Nuclei were labelled with DAPI. The different wavelengths (colours) were scanned independently and digitally merged (C and F). Scale bar indicates 20 μm.

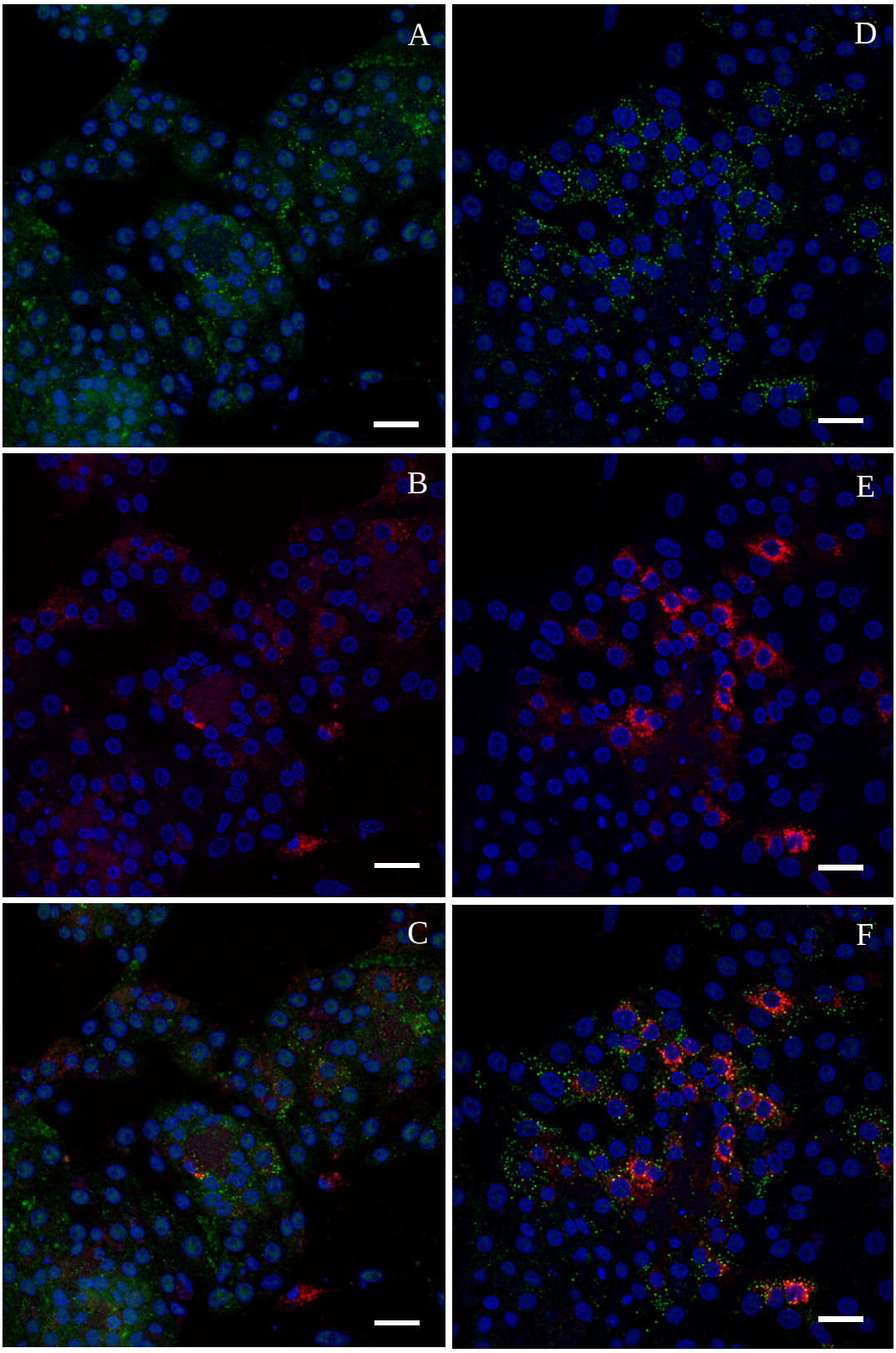
A
D
B
E
C
F

Figure 3.6. Indirect immunofluorescence analysis of the expression of the 3a protein at 4 and 6 h p.i in mock infected CK cells. Subconfluent CK cells were mock infected fixed at either 4 (A, B and C) or 6 h p.i. (D, E and F) with paraformaldehyde. After making the cells permeable with Triton X-100 they were labelled with rabbit polyclonal anti-3a (8194) (A and D) and mouse anti-M (C5/124) (B and E) protein antibodies. Secondary antibodies included Alexa Fluor 488 anti-rabbit (green) and Alexa Fluor 568 anti-mouse (red). Nuclei were labelled with DAPI. The different wavelengths (colours) were scanned independently and digitally merged (C and F). Scale bar indicates 20 μm.

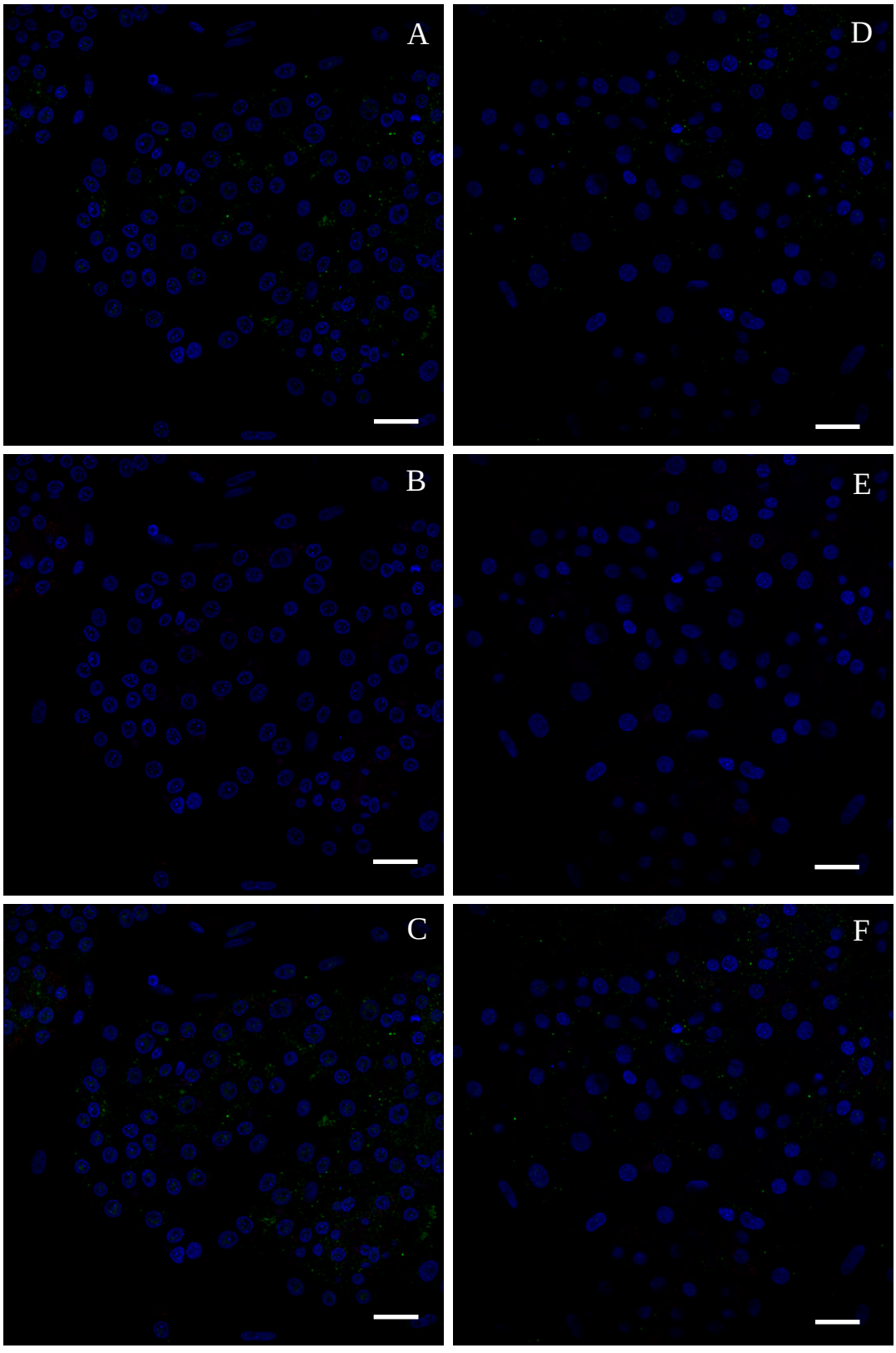
A
D
B
E
C
F

Immunofluorescence with anti-3a antibodies and IBV structural proteins

The distribution of 3a protein in Beau-R-infected Vero and CK cells was compared to the subcellular location of the S and M proteins. When observed individually the 3a, S and M protein labelling appeared as a punctate staining pattern, although the S and M proteins had a more perinuclear distribution than 3a (Fig. 3.7 and 3.8). The assumed subcellular location of the majority of the S and M proteins was the ERGIC and Golgi (Klumperman *et al.*, 1994; Winter *et al.*, 2008b). Dual labelling of the 3a protein with the S (Fig. 3.7) or M (Fig. 3.8) proteins revealed no colocalisation between the two proteins as would be expected by the different subcellular distribution patterns of the 3a and S or M protein puncta and the data indicating a lack of colocalisation between the 3a protein and markers for the ERGIC or Golgi apparatus (Fig. 3.3 and 3.4). (Mock infected CK cells labelled with anti-3a protein antibody with anti-S protein or anti-M protein antibody in Fig. 3.9)

Figure 3.7. Indirect immunofluorescence analysis of the intracellular location of the 3a protein compared to S protein. Subconfluent CK cells were infected with Beau-R and fixed at 10 h p.i. with paraformaldehyde. After making the cells permeable with Triton X-100 they were labelled with rabbit polyclonal anti-3a (8194) (A and D) and mouse anti-S (A13/38) (B and E). Secondary antibodies included Alexa Fluor 488 anti-rabbit (green) and Alexa Fluor 568 anti-mouse (red). Nuclei were labelled with DAPI. The different wavelengths (colours) were scanned independently and digitally merged (C and F). Images A, B, C and D, E, F are two different fields of view of the same experiment. Scale bar indicates 20 μm.

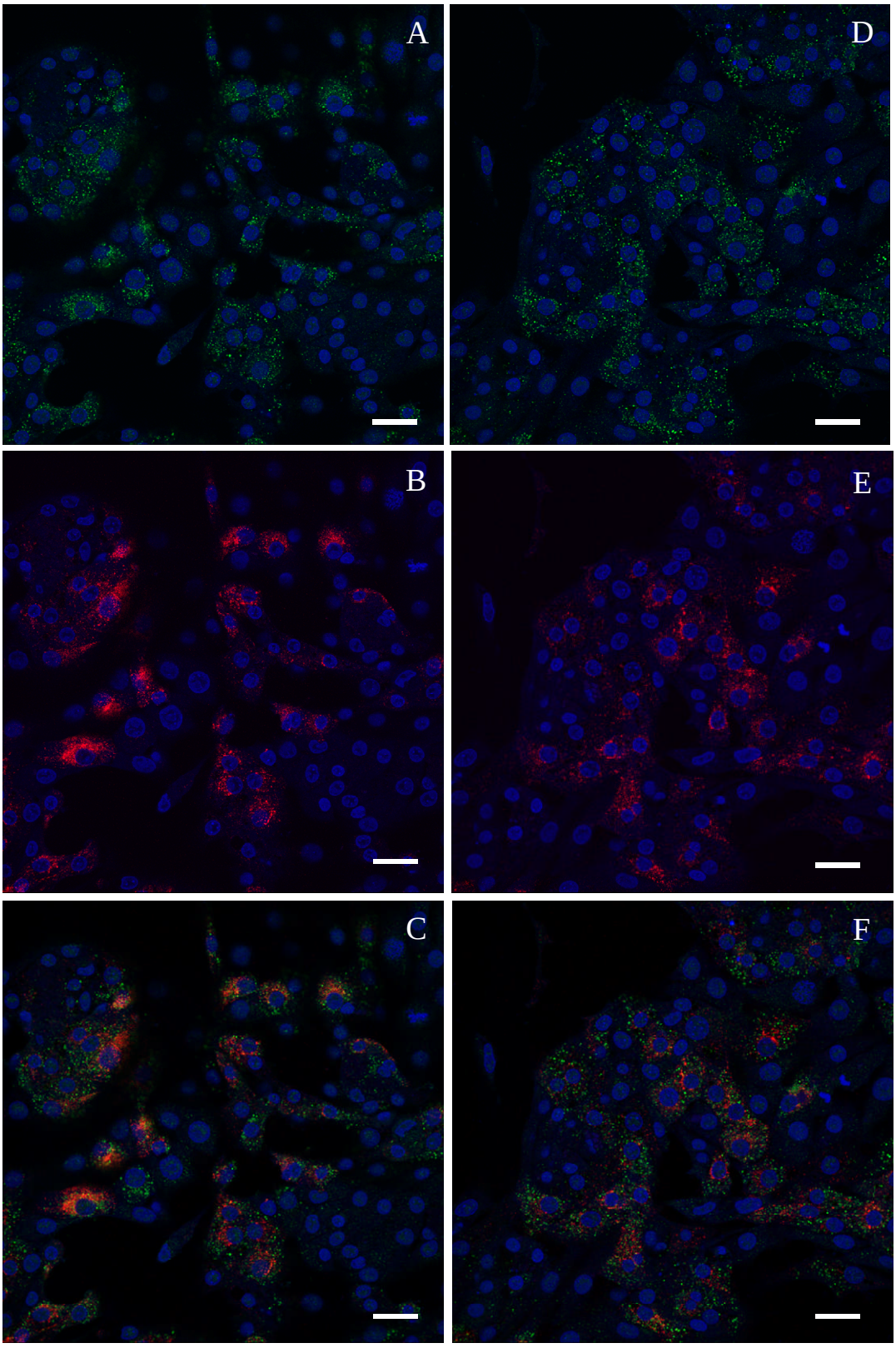
A
D
B
E
C
F

Figure 3.8. Indirect immunofluorescence analysis of the intracellular location of the 3a protein compared to M protein. Subconfluent CK cells were infected with Beau-R and fixed at 10 h p.i. with paraformaldehyde. After making the cells permeable with Triton X-100 they were labelled with rabbit polyclonal anti-3a (8194) (A and D) and mouse anti-M (C5/124) (B and E). Secondary antibodies included Alexa Fluor 488 anti-rabbit (green) and Alexa Fluor 568 anti-mouse (red). Nuclei were labelled with DAPI. The different wavelengths (colours) were scanned independently and digitally merged (C and F). Images D, E, F are from a magnified section of images A, B and C. Scale bar indicates 20 μm.

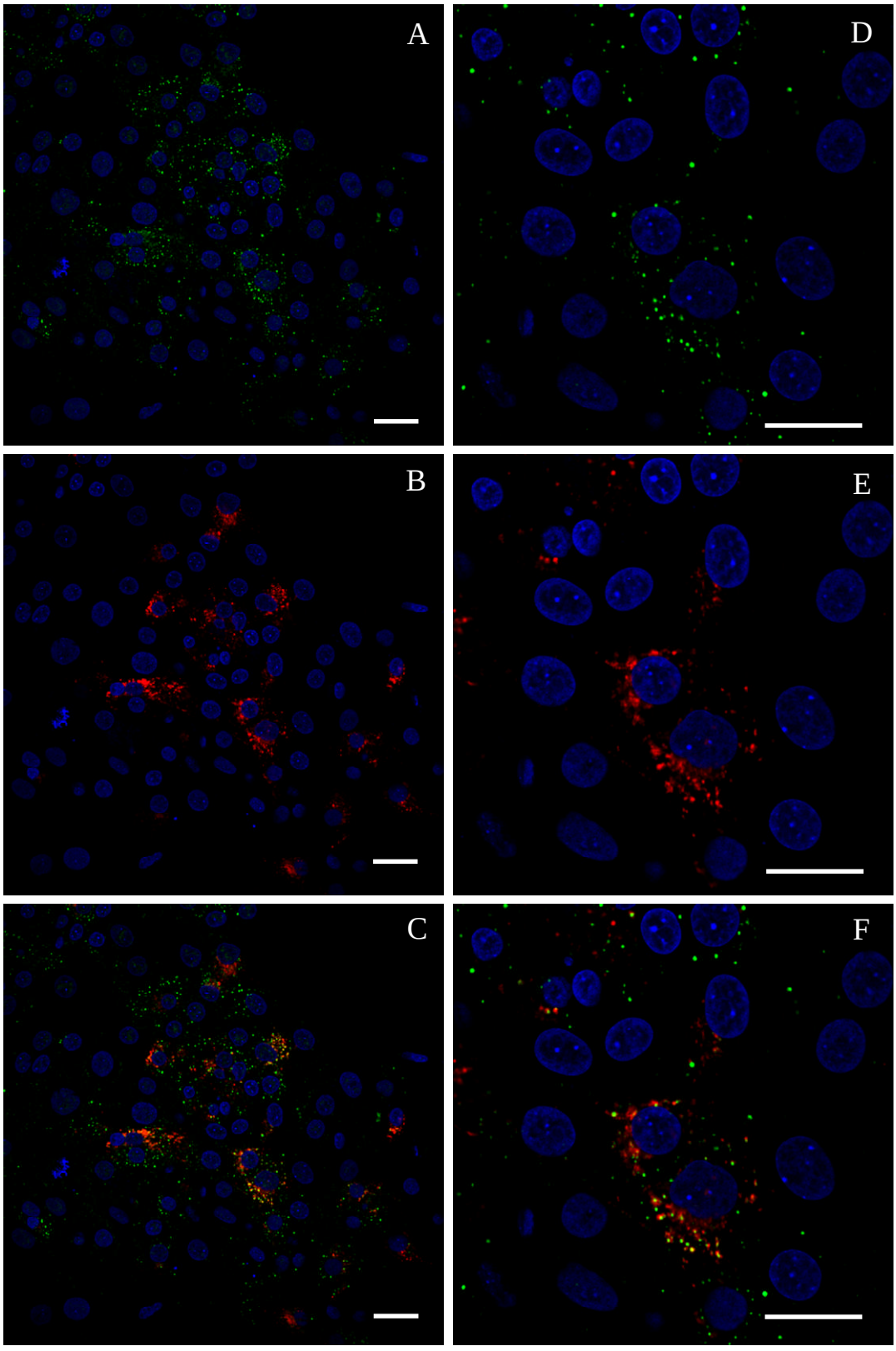
A
D
B
E
C
F

Figure 3.9. Indirect immunofluorescence analysis of the intracellular location of the 3a protein compared to the M and S proteins in mock infected CK cells. Subconfluent CK cells were mock infected and fixed at 10 h p.i. with paraformaldehyde. After making the cells permeable with Triton X-100 they were labelled with rabbit polyclonal anti-3a (8194) (A and D) and mouse anti-M (C5/124) (B) or mouse anti-S (A13/38) (E). Secondary antibodies included Alexa Fluor 488 anti-rabbit (green) and Alexa Fluor 568 anti-mouse (red). Nuclei were labelled with DAPI. The different wavelengths (colours) were scanned independently and digitally merged (C and F). Scale bar indicates 20 μm.

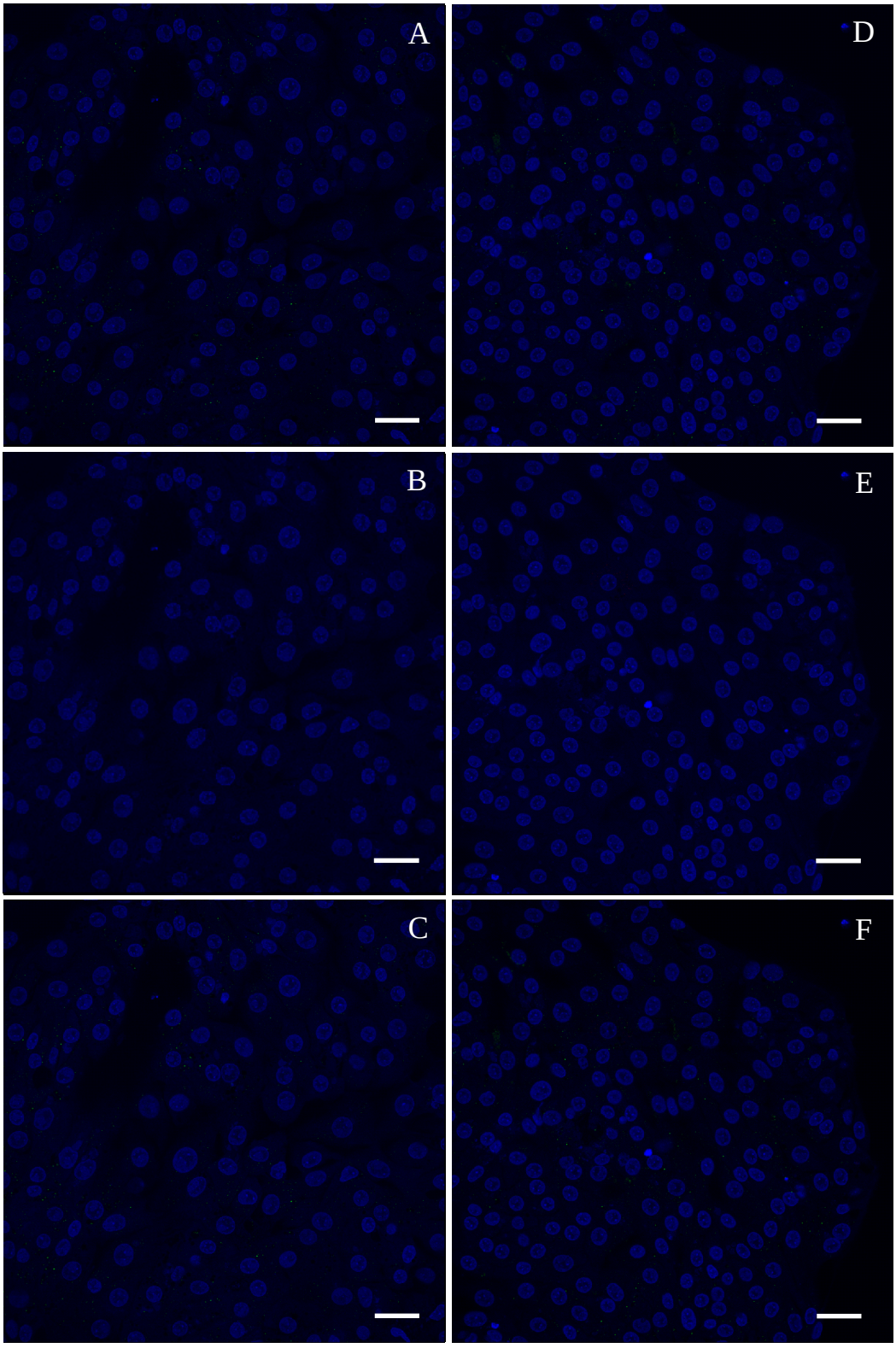
A
D
B
E
C
F

Beau-R 3a protein colocalises with viral dsRNA in infected cells

Observation of the subcellular distribution of the replicase proteins of coronaviruses published by other groups indicated that these proteins formed a punctate cytoplasmic pattern, without the semi-perinuclear distribution seen with the S and M proteins (Oostra *et al.*, 2007b; Snijder *et al.*, 2006; van der Meer *et al.*, 1999). A comparison between the subcellular location of the replication/transcription complexes and the 3a protein was conducted. Due to a lack of antibodies directed against the nsps, an antibody recognising double-stranded RNA (dsRNA) was used. This antibody only labelled punctate structures within infected cells, with the same cells also labelled with an antibody recognising the Beau-R structural proteins (Fig. 3.10 including images of mock infected cells). This indicated that the observed dsRNA was derived as a result of viral replication and assumed to be viral dsRNA. The subcellular location of the viral dsRNA should be found in a very close spatial relationship to the nsps involved in transcription and replication (Knoops *et al.*, 2008; Oostra *et al.*, 2007b) and therefore would provide an alternative way of observing the potential location of the nsps. Dual labelling of the 3a protein with viral dsRNA produced images displaying colocalisation between the two molecules in infected Vero (Fig. 3.11) and CK cells (Fig. 3.12) as displayed by the almost complete overlap between the two sets of labelled puncta. This colocalisation was not due to cross-reactivity between the primary and secondary antibodies used in the indirect immunofluorescence experiments as there was no fluorescence observed when the anti-mouse IgG Alexa fluor was used to detect the rabbit anti-3a protein antibody or when the anti-rabbit IgG Alexa Fluor was used to detect the anti-dsRNA antibody (Appendix Fig. A.1). (Mock infected CK cells labelled with anti-3a protein antibody and anti-dsRNA antibody in appendix Fig. A.1a)

Figure 3.10. Indirect immunofluorescence analysis comparing the location of the IBV structural proteins to the detection of dsRNA. Subconfluent CK cells were infected with Beau-R (A, B and C) or mock infected (D, E and F) and fixed at 16 h p.i. with paraformaldehyde. After making the cells permeable with Triton X-100 they were labelled with chicken polyclonal anti-IBV (A and D) and mouse anti-dsRNA J2 (B and E). Secondary antibodies included Alexa Fluor 488 anti-chicken (green) and Alexa Fluor 568 anti-mouse (red). Nuclei were labelled with DAPI. The different wavelengths (colours) were scanned independently and digitally merged (C and F). Scale bar indicates 20 μm.

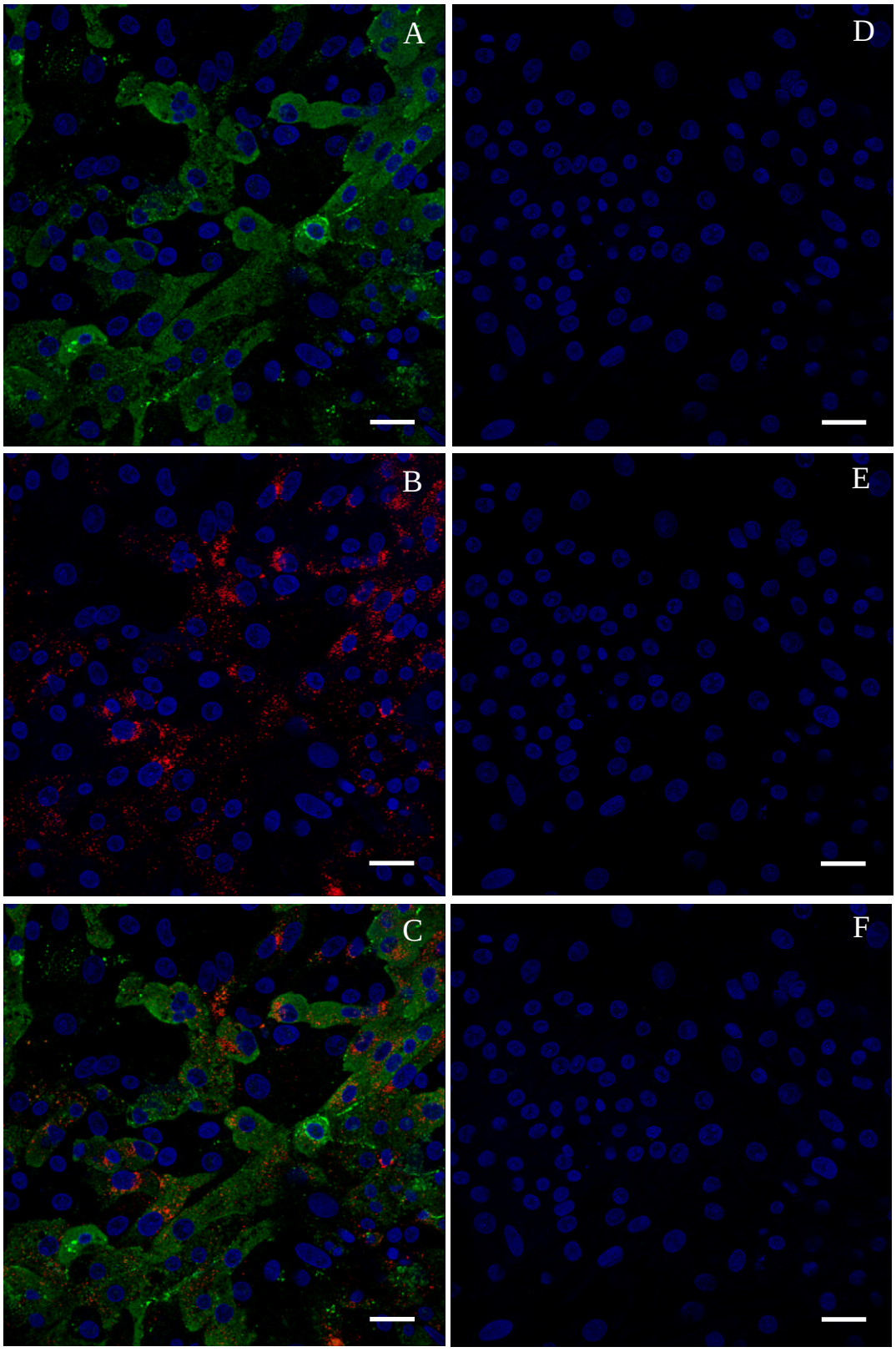
A
D
B
E
C
F

Figure 3.11. Indirect immunofluorescence analysis of the intracellular location of the 3a protein compared to dsRNA. Subconfluent Vero cells were infected with Beau-R and fixed at 10 h p.i. with paraformaldehyde. After making the cells permeable with Triton X-100 they were labelled with rabbit polyclonal anti-3a (8194) (A and D) and mouse anti-dsRNA J2 (B and E). Secondary antibodies included Alexa Fluor 488 anti-rabbit (green) and Alexa Fluor 568 anti-mouse (red). Nuclei were labelled with DAPI. The different wavelengths (colours) were scanned independently and digitally merged (C and F). Images D, E and F are a magnified section of the images A, B and C. Scale bar indicates 20 μm.

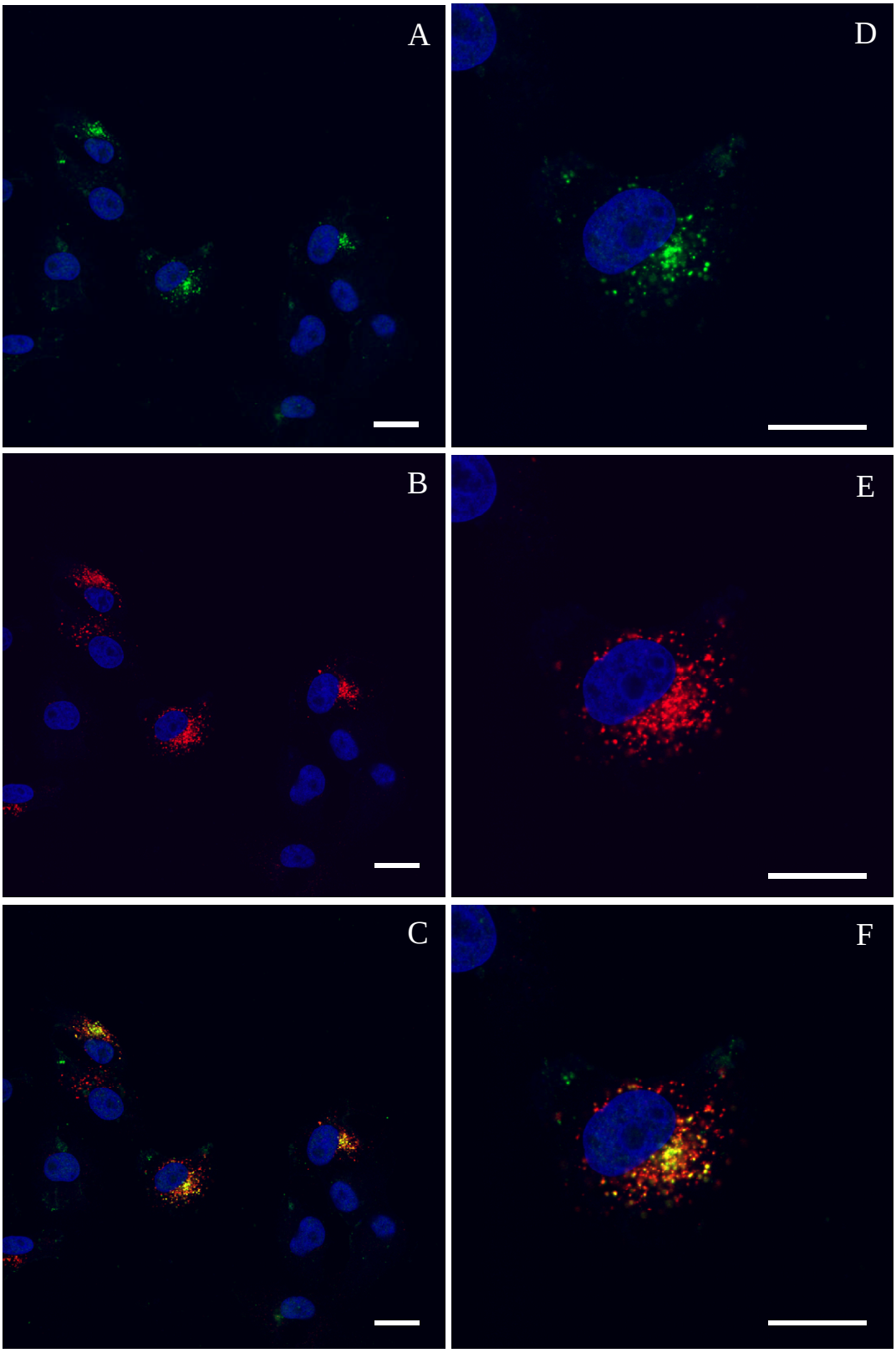
A
D
B
E
C
F

Figure 3.12. Indirect immunofluorescence analysis of the intracellular location of the 3a protein compared to dsRNA. Subconfluent CK cells were infected with Beau-R and fixed at 10 h p.i. with paraformaldehyde. After making the cells permeable with Triton X-100 they were labelled with rabbit polyclonal anti-3a (8194) (A and D) and mouse anti-dsRNA J2 (B and E). Secondary antibodies included Alexa Fluor 488 anti-rabbit (green) and Alexa Fluor 568 anti-mouse (red). Nuclei were labelled with DAPI. The different wavelengths (colours) were scanned independently and digitally merged (C and F). Images D, E and F are a magnified section of the images A, B and C. Scale bar indicates 20 μm.

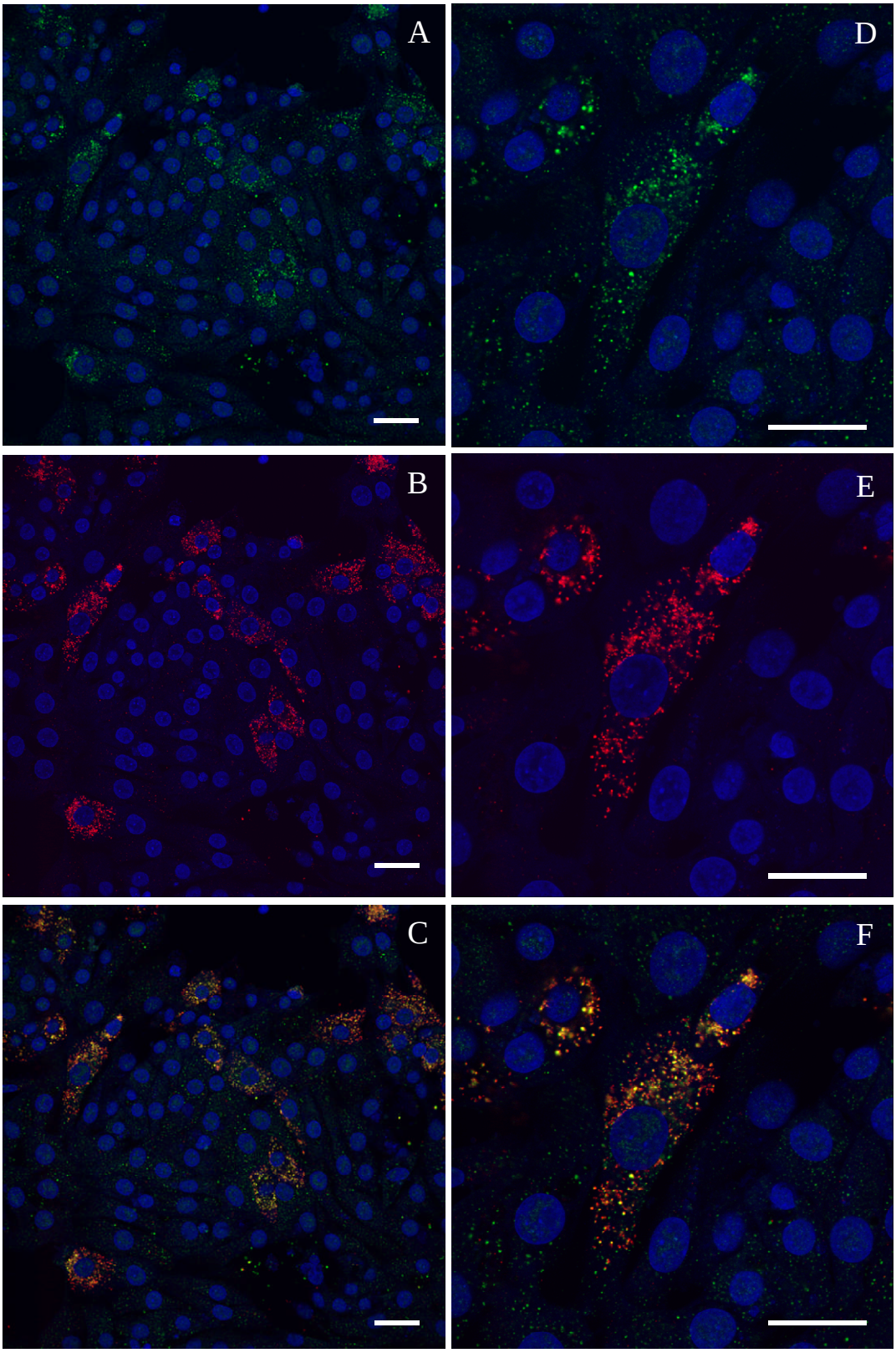
A
D
B
E
C
F

FLAG-tagged 3a protein has the same subcellular distribution pattern as virally expressed 3a protein

Determination of the distribution pattern of the 3a protein within Beau-R-infected cells had already been achieved. A distribution pattern for the 3b protein was undetermined due to the lack of a suitable antibody. To discover the subcellular location of the 3b protein and to confirm the subcellular distribution of a tagged 3a protein plasmids were constructed which would express FLAG tagged accessory proteins. The expression of these tagged proteins within transfected Vero cells would be detected using anti-FLAG monoclonal antibodies in indirect immunofluorescence experiments.

An unrelated protein, BAP, was FLAG-tagged to provide a control for expression and FLAG-tag-induced subcellular distribution. This recombinant protein produced a diffuse cytoplasmic staining pattern (Fig. 3.13).

Distribution of the FLAG-tagged 3b protein was analysed (Fig. 3.13). No detection of the FLAG tag could be achieved within Vero cells transfected with the pFLAG/3b plasmid possibly because of the reported rapid turnover of the IBV 3b protein when expressed in mammalian cells (Pendleton and Machamer, 2006).

Figure 3.13. Indirect immunofluorescence analysis of the intracellular location of FLAG-tagged BAP protein and FLAG/3b within transfected Vero cells. Subconfluent Vero cells were transfected with pFLAG/BAP (A) or pFLAG/3b (B). After 24 h of infection the cells were fixed with paraformaldehyde and permeabilised with Triton X-100. Cells were labelled with mouse anti-FLAG. Secondary antibodies included Alexa Fluor 568 anti-mouse (red). Nuclei were labelled with DAPI (blue). Each wavelength (colour) was scanned separately and the images digitally merged. Scale bar indicates 20 μm.

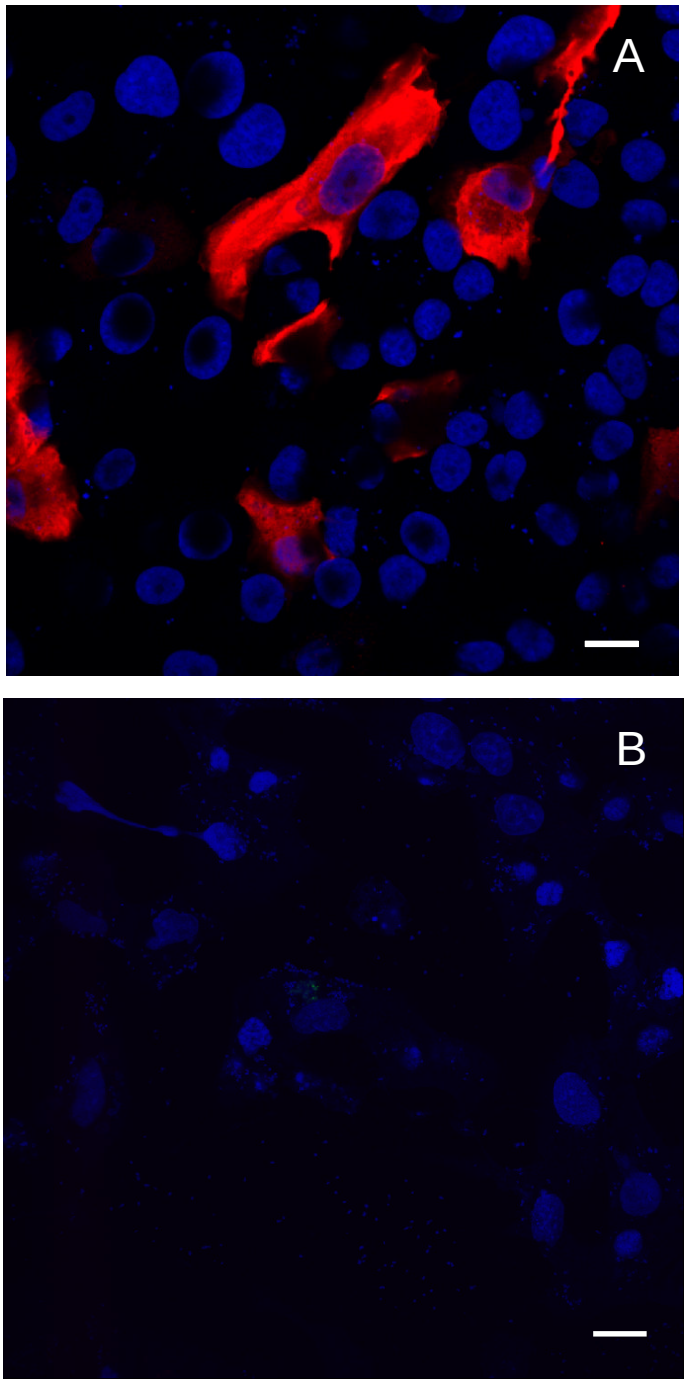
A
B

The same punctate, cytoplasmic distribution observed for the 3a protein within Beau-R-infected cells was evident when the FLAG tag was detected in cells transfected with the plasmid expressing the FLAG/3a protein (Fig. 3.14). This indicated that when expressed in cells without any other IBV proteins present the epitope tagged 3a protein occupied a similar subcellular location to 3a protein found in Beau-R-infected cells. The presence of heterologous sequence at the N-terminus of the expressed 3a protein (i.e. the FLAG tag and linker sequence) did not affect this subcellular distribution. Some images of pFLAG/3a transfected cells did show a perinuclear distribution for the FLAG/3a protein which was different from the 3a protein pattern displayed in Beau-R infected cells possibly due to the high level expression of heterologous protein saturating one subcellular compartment and occupying another.

Dual labelling of the 3a protein and dsRNA in Beau-R infected Vero and CK cells indicated that the 3a protein colocalised with virally-induced dsRNA. Images of dual-labelled infected and transfected Vero cells demonstrated that the FLAG/3a protein also colocalised with dsRNA (Fig. 3.15) implying that the FLAG/3a protein localised to the same compartment as the natively expressed 3a protein.

Figure 3.14. Indirect immunofluorescence analysis of the intracellular location of FLAG-tagged 3a protein within Beau-R infected Vero cells. Subconfluent Vero cells were infected with Beau-R and transfected with pFLAG/3a. After 24 h of infection the cells were fixed with paraformaldehyde and permeabilised with Triton X-100. Cells were labelled with chicken anti-IBV (A and D) and mouse anti-FLAG (B and E). Secondary antibodies included Alexa Fluor 488 anti-chicken (green) and Alexa Fluor 568 anti-mouse (red). Nuclei were labelled with DAPI (blue). Each wavelength (colour) was scanned separately and the images digitally merged (C and F). Images A, B, C and D, E, F are two different fields of view of the same experiment. Scale bar indicates 20 μm.

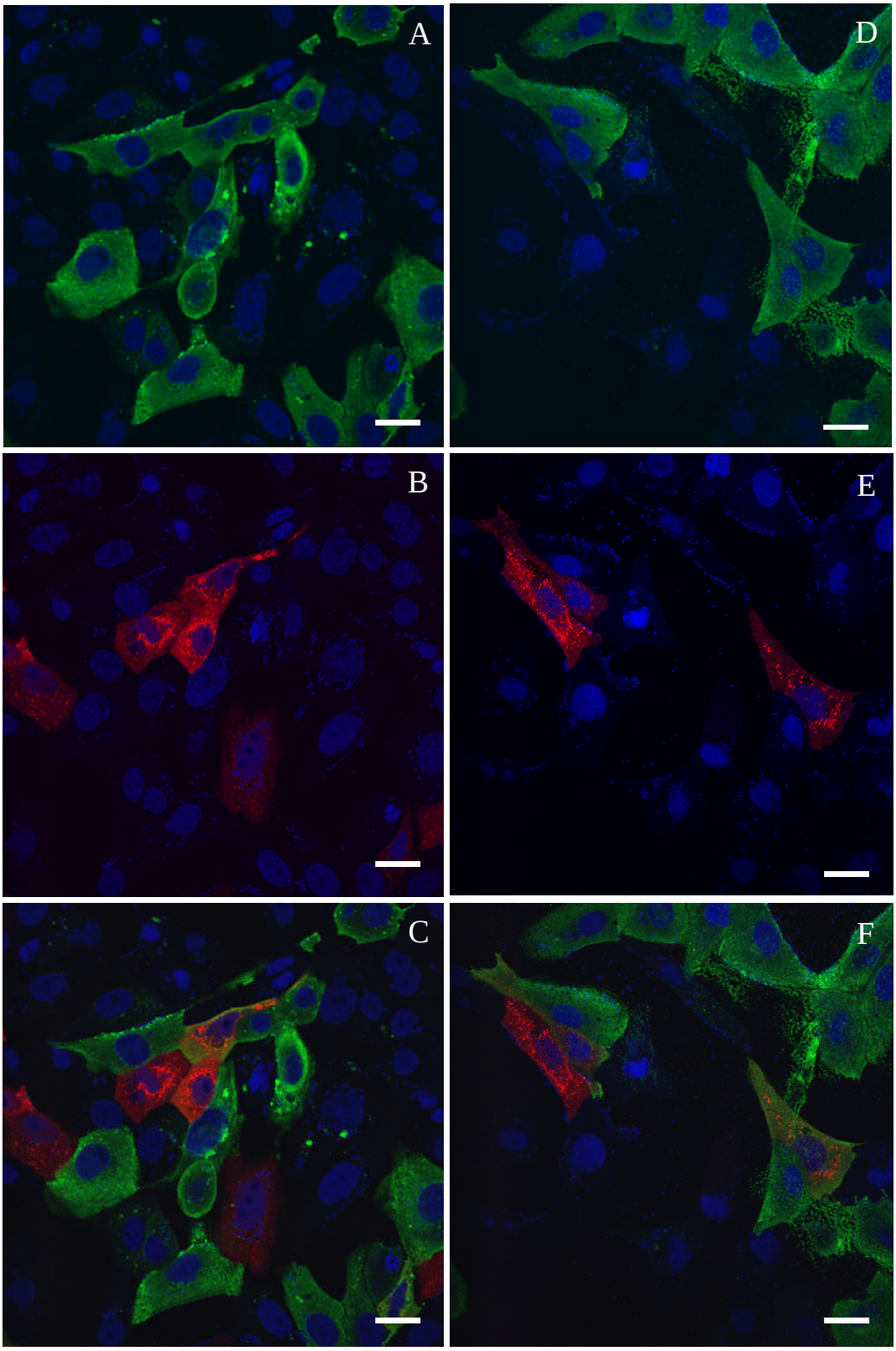
A
D
B
E
C
F

Figure 3.15. Colocalisation of the FLAG/3a protein with viral dsRNA. Subconfluent Vero cells were infected with Beau-R and transfected with pFLAG/3a. After 24 h of infection the cells were fixed with paraformaldehyde and permeabilised with Triton X-100. Cells were labelled with chicken anti-IBV (A and D) and mouse anti-FLAG (B and E). Secondary antibodies included Alexa Fluor 488 anti-chicken (green) and Alexa Fluor 568 anti-mouse (red). Nuclei were labelled with DAPI (blue). Each wavelength (colour) was scanned separately and the images digitally merged (C and F). Images A, B, C and D, E, F are two different fields of view of the same experiment. Scale bar indicates 20 μm.

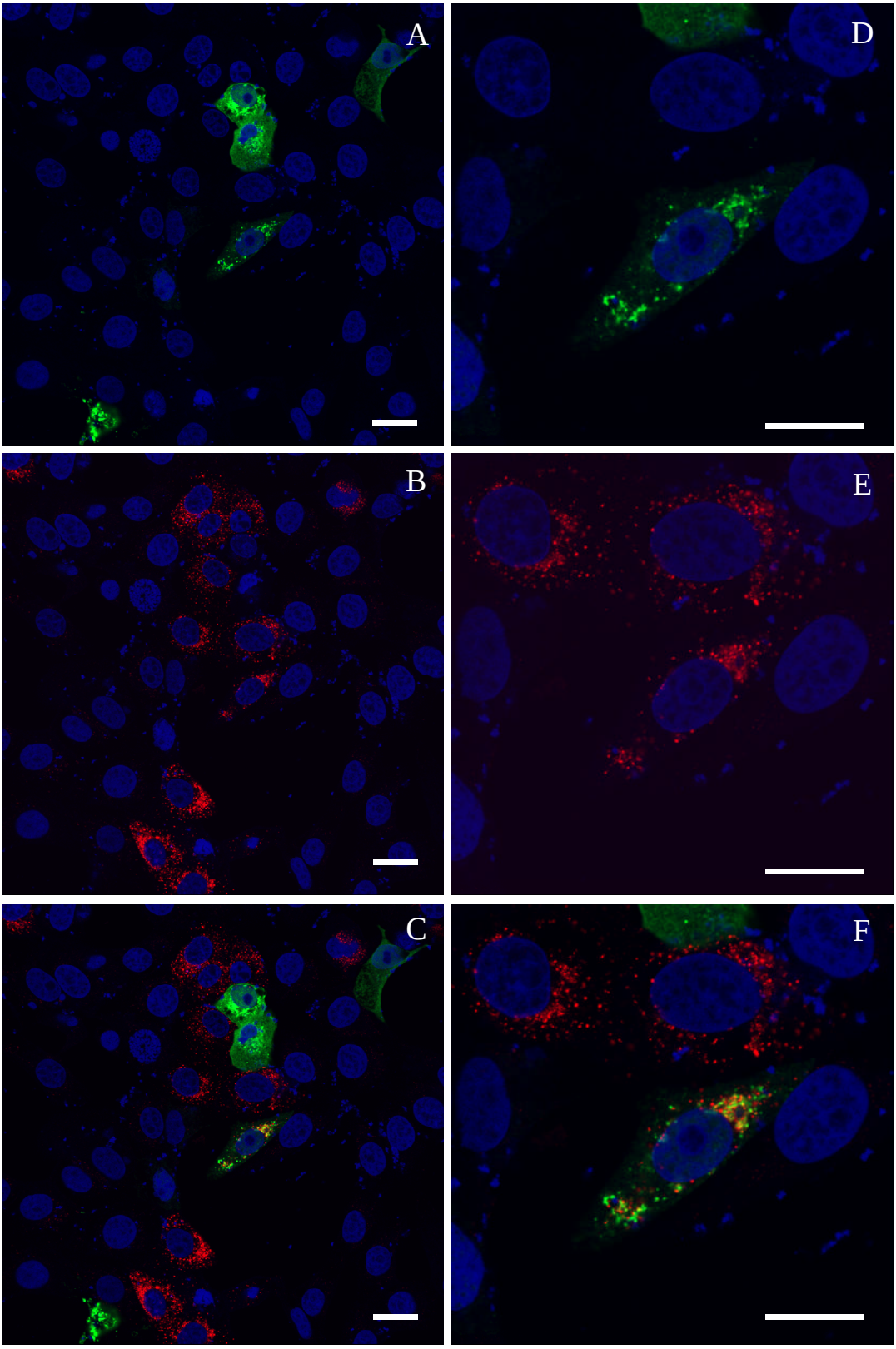
A
D
B
E
C
F

Expression of 3a in infected CK cells

In addition to the subcellular distribution expression of the 3a protein was analysed during the course of a single replication cycle. Western blot analysis of a time-course of Beau-R infection in CK cells demonstrated that the 3a protein was first detected at 6 h p.i (Fig. 3.16). The detection of alpha tubulin was used as a loading control for each sample. These data were in agreement with the 5 h p.i. detection of the 5b protein (Chapter 4, Fig. 4.13) and indicated that the Beau-R accessory proteins were first detected by Western blot by 5-6 h p.i. Detection of the IBV structural proteins occurs at approximately 4 h p.i. Observation of the image produced as a result of the Western blot to detect the 3a protein also revealed two bands potentially indicating two types of 3a protein with one possessing a higher molecular weight. These two types of possible 3a protein were observed from the earliest point of 3a protein detection. This could indicate the presence of a dimer of the 3a protein.

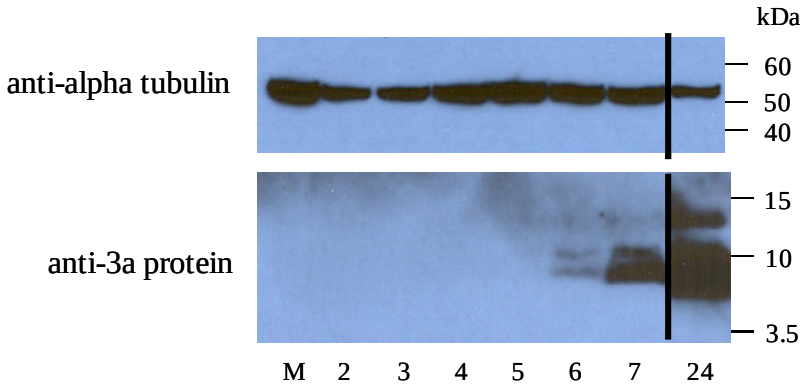

Figure 3.16. Time course of 3a expression during Beau-R infection. Subconfluent CK cells were infected with Beau-R for the indicated h p.i. Cells were lysed and clarified by centrifugation. The protein samples were separated by PAGE and transferred to PVDF membrane. The membrane was probed with either mouse anti-alpha tubulin (Sigma) (top panel) or rabbit anti-3a antibody 3480 (bottom panel). Primary antibodies were detected with HRP-conjugated anti-mouse or anti-rabbit antibody and the Immobilon Western detection system. Time in h p.i. along the bottom and molecular weight markers along the side. M = mock infected CK cells.

Generation of SUMO/3b, SUMO/ADRP and nsp8HN

Identification of the subcellular location of the accessory proteins expressed by IBV was most suitably performed by indirect immunofluorescence using IBV-infected cells. The viral proteins would accumulate at their specific subcellular location

without the possible interference from additional tag sequence and they would be expressed in quantities directed by the virus. This also applied to other viral proteins. In order to accomplish these experiments antibodies were required which could detect the IBV 3b protein as well as those which could detect individual replicase proteins. The ADRP domain of nsp3 and nsp8 were chosen to raise antibodies against because they have been shown to represent the site of viral RNA replication/transcription (Knoops *et al.*, 2008; Snijder *et al.*, 2006).

The 3b protein and the ADRP domain of nsp3 were expressed as part of a SUMO fusion protein. Expression of the SUMO with a protein of interest has been shown to increase the expression and solubility of the entire protein (Malakhov *et al.*, 2004). The nsp8 was expressed as a complete protein with a N-terminal His-tag.

Expression and purification of the SUMO/3b protein within bacteria yielded a sample which contained few contaminating proteins (SUMO/3b calculated molecular weight of 20.8 kDa) (Fig. 3.17). The recombinant protein was also soluble in a solution of Tris·HCl at neutral pH. SUMO/ADRP was soluble in Tris·HCl at neutral pH but the sample contained a visibly higher amount of contaminating protein (Appendix Fig. A.2). The SUMO/ADRP protein was further purified by separating the proteins within the sample by PAGE then removing the protein band corresponding to the expected molecular weight. Electroelution was then used to extract the protein from the gel. This further purified SUMO/ADRP protein (calculated molecular weight of 31.2 kDa) contained less contaminating protein but still retained a series of unexpected lower molecular weight proteins as shown by the stained bands at ~20, 18, 15 and 13 kDa (Fig. 3.17). Purification of nsp8HN (calculated molecular weight of 24.3 kDa) required the same further purification process as SUMO/ADRP and contained only a limited amount of detectable protein contamination (Fig. 3.15).

Samples of SUMO/3b and SUMO/ADRP were analysed by positive electrospray ionisation-mass spectrometry (ESI-MS) (Fig. 3.18). Using this method a mass accuracy of within 0.001% of the predicted molecular mass should be achieved. The results indicated that the required recombinant proteins were present in the respective samples due to the almost exact match between the calculated molecular weight and experimentally determined molecular weight (Table 3.1). (Appendix Table A.3 and A.4 for complete calculations). nsp8 was not analysed by ESI-MS due to protein solubility issues and connected incompatibility with MS examination.

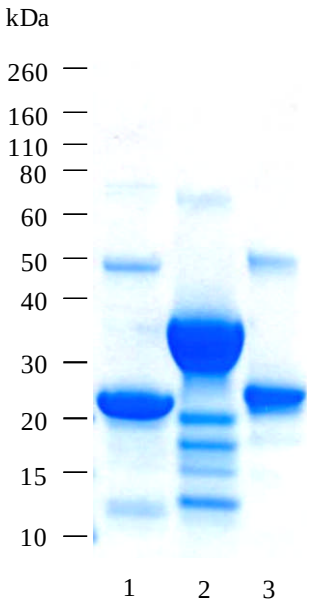

Figure 3.17. Analysis of the recombinant proteins expressed in *E. coli*. Bacteria were transformed with pET SUMO/3b, pET SUMO/ADRP or pDEST nsp8HN. After induction of protein expression the bacteria were lysed and the His-tagged proteins extracted by affinity purification. The SUMO/3b sample was not processed further. The proteins contained within the SUMO/ADRP and nsp8HN samples were separated by PAGE and the bands corresponding to the expected molecular weight for each protein were cut out and the proteins were removed from the gel by electroelution and concentrated. 7 µg total protein from each sample were separated by PAGE. The gel was fixed and the proteins stained with GelCode Blue (Coomassie-based stain). Lane 1 = SUMO/3b. Lane 2 = SUMO/ADRP. Lane 3 = nsp8HN.

Table 3.1. Comparison between the predicted and experimentally determined molecular weight of the proteins contained in the SUMO/3b and SUMO/ADRP samples.

	Calculated MW[a]	Experimental MW[b]
SUMO/3b	20839	20838
SUMO/ADRP	31267	31267

[a] Calculated molecular weight in Daltons.
[b] Experimentally determined molecular weight in Daltons.

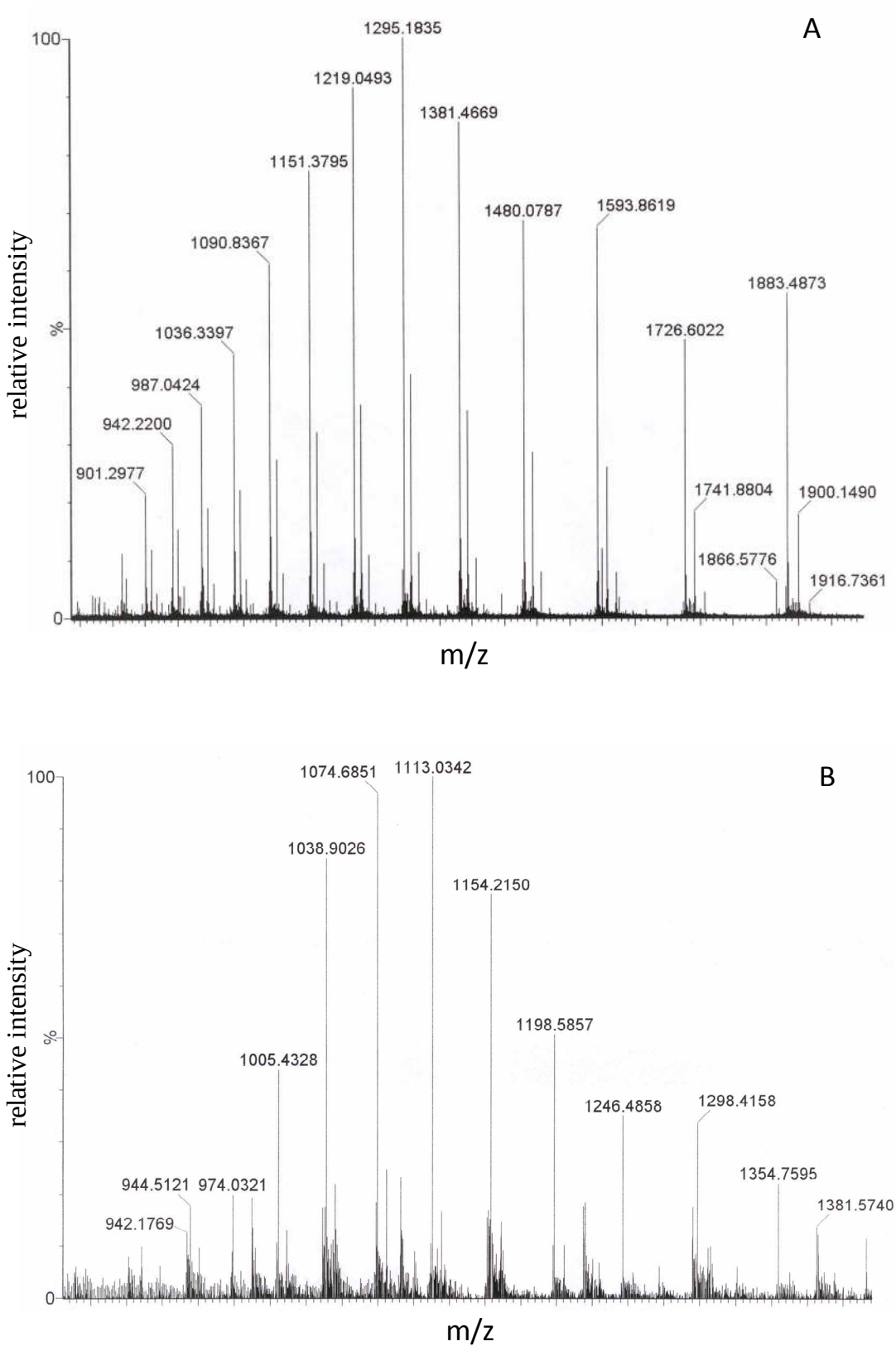

Figure 3.18. ESI mass spectra of SUMO/3b (A) and SUMO/ADRP (B). Proteins in the two samples were separated and analysed by online capillary HPLC and Q-ToF Premier mass spectrometer.

Testing the antibodies directed towards 3b, the ADRP domain and nsp8

The anti-3b, anti-ADRP and anti-nsp8 protein antibodies were used to detect the SUMO/3b, SUMO/ADRP and nsp8HN proteins to ensure that a suitable immune response had been raised. All the sera tested could be used to detect the respective proteins by Western blot analysis as proteins were detected at the calculated molecular weights for each recombinant protein (Fig. 3.19). The antibodies also detected aggregates (dimers) of the individual proteins as shown by the ~48 kDa protein for SUMO/3b, ~65 kDa protein for SUMO/ADRP and ~50 kDa protein for nsp8. Due to the same SUMO protein sequence found in the SUMO/3b and SUMO/ADRP proteins the anti-SUMO/3b protein antibodies could detect the SUMO/ADRP protein and the anti-SUMO/ADRP protein antibodies could detect the SUMO/3b protein.

Antibodies raised against the recombinant proteins were tested by indirect immunofluorescence using Beau-R-infected CK cells to assess if they could detect the virally-expressed 3b, nsp3 (containing the ADRP domain) and nsp8 proteins. A Beau-R-infected cell was identified by the presence of viral dsRNA labelling within the cell. No specific protein detection was observed within infected cells using the anti-3b (Fig. 3.20) (and mock infected cells with anti-3b - Fig. 3.21), anti-ADRP (Fig. 3.22) (and mock infected cells with anti-ADRP – Fig. 3.23) or anti-nsp8 (Fig. 3.24) (and mock infected cells with anti-nsp8 – Fig. 3.25) antibodies, although some non-specific labelling was observed due to a high background. A higher magnification would have been more appropriate to show if there was specific viral protein antibodies present in infected cells.

Figure 3.19. Testing the anti-3b protein, anti-ADRP protein and anti-nsp8 protein antibodies against the respective recombinant proteins. The SUMO/3b, SUMO/ADRP and nsp8HN proteins were separated by SDS-PAGE, transferred to PVDF membrane. The rabbit antibodies were used to probe the PVDF membrane and were detected with HRP-conjugated anti-rabbit antibody and the Immobilon Western detection system.

anti-3b 0525

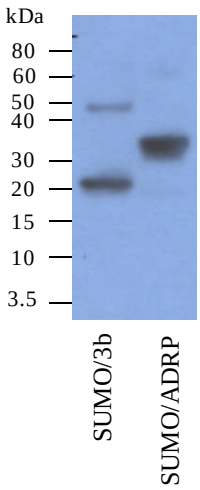

anti-3b 0526

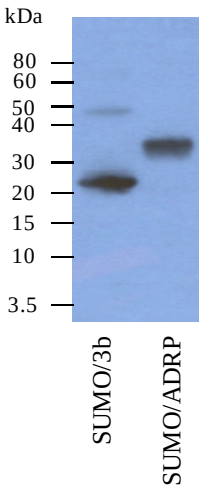

anti-ADRP 0523

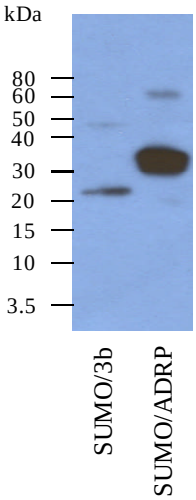

anti-ADRP 0524

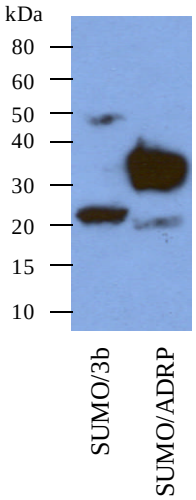

anti-nsp8 0682

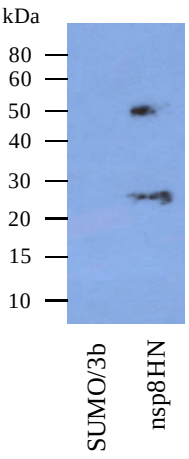

anti-nsp8 0683

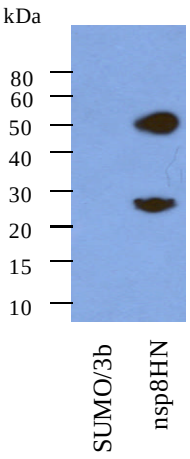

Figure 3.20. Indirect immunofluorescence analysis using the anti-3b antibodies. Subconfluent CK cells were infected with Beau-R and fixed at 10 h p.i. with paraformaldehyde. After making the cells permeable with Triton X-100 they were labelled with rabbit polyclonal anti-3b protein 525 (A,) or 526 (D,) and mouse anti-dsRNA (J2) (B and E). Secondary antibodies included Alexa Fluor 488 anti-rabbit (green) and Alexa Fluor 568 anti-mouse (red). Nuclei were labelled with DAPI. The different wavelengths (colours) were scanned independently and digitally merged (C and F). Scale bar indicates 20 μm.

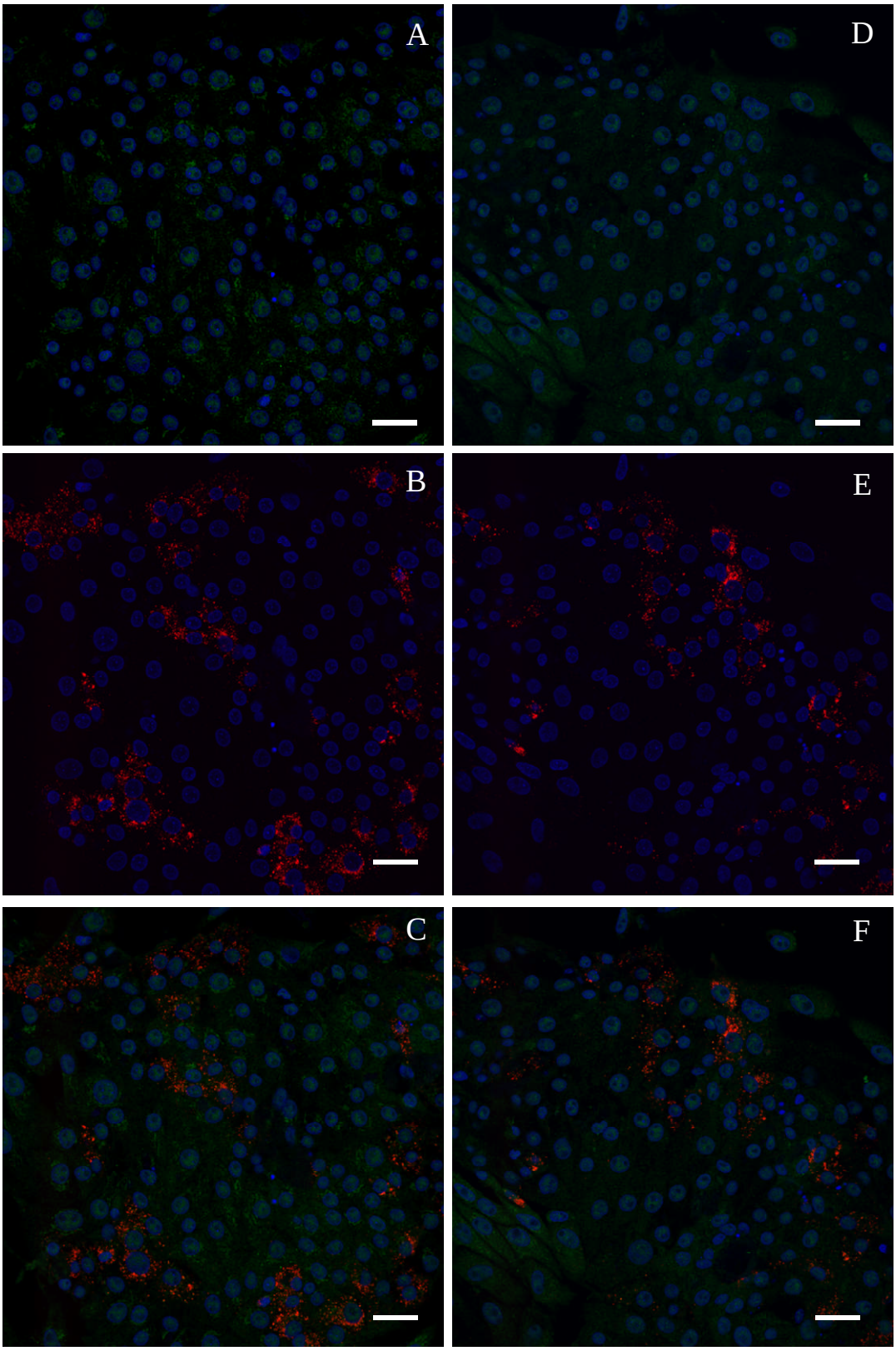
A
D
B
E
C
F

Figure 3.21. Indirect immunofluorescence analysis using the anti-3b antibodies on mock infected CK cells. Subconfluent CK cells were mock infected and fixed at 10 h p.i. with paraformaldehyde. After making the cells permeable with Triton X-100 they were labelled with rabbit polyclonal anti-3b protein 525 (A) or 526 (D) and mouse anti-dsRNA (J2) (B and E). Secondary antibodies included Alexa Fluor 488 anti-rabbit (green) and Alexa Fluor 568 anti-mouse (red). Nuclei were labelled with DAPI. The different wavelengths (colours) were scanned independently and digitally merged (C and F). Scale bar indicates 20 μm.

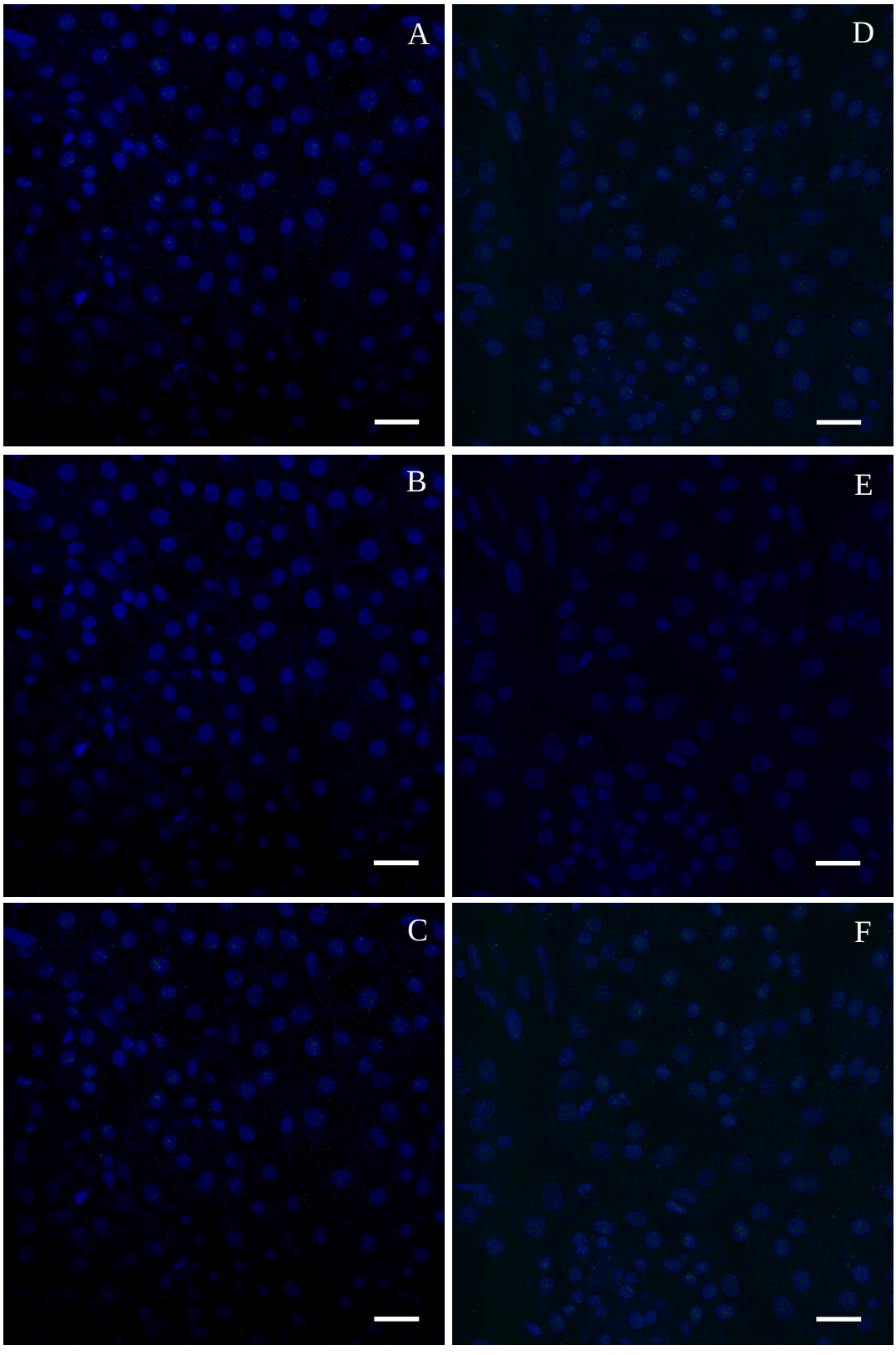
A
D
B
E
C
F

Figure 3.22. Indirect immunofluorescence analysis using the anti-ADRP antibodies. Subconfluent CK cells were infected with Beau-R and fixed at 10 h p.i. with paraformaldehyde. After making the cells permeable with Triton X-100 they were labelled with rabbit polyclonal anti-ADRP 523 (A) or 524 (D) and mouse anti-dsRNA (J2) (B and E). Secondary antibodies included Alexa Fluor 488 anti-rabbit (green) and Alexa Fluor 568 anti-mouse (red). Nuclei were labelled with DAPI. The different wavelengths (colours) were scanned independently and digitally merged (c and F). Scale bar indicates 20 μm.

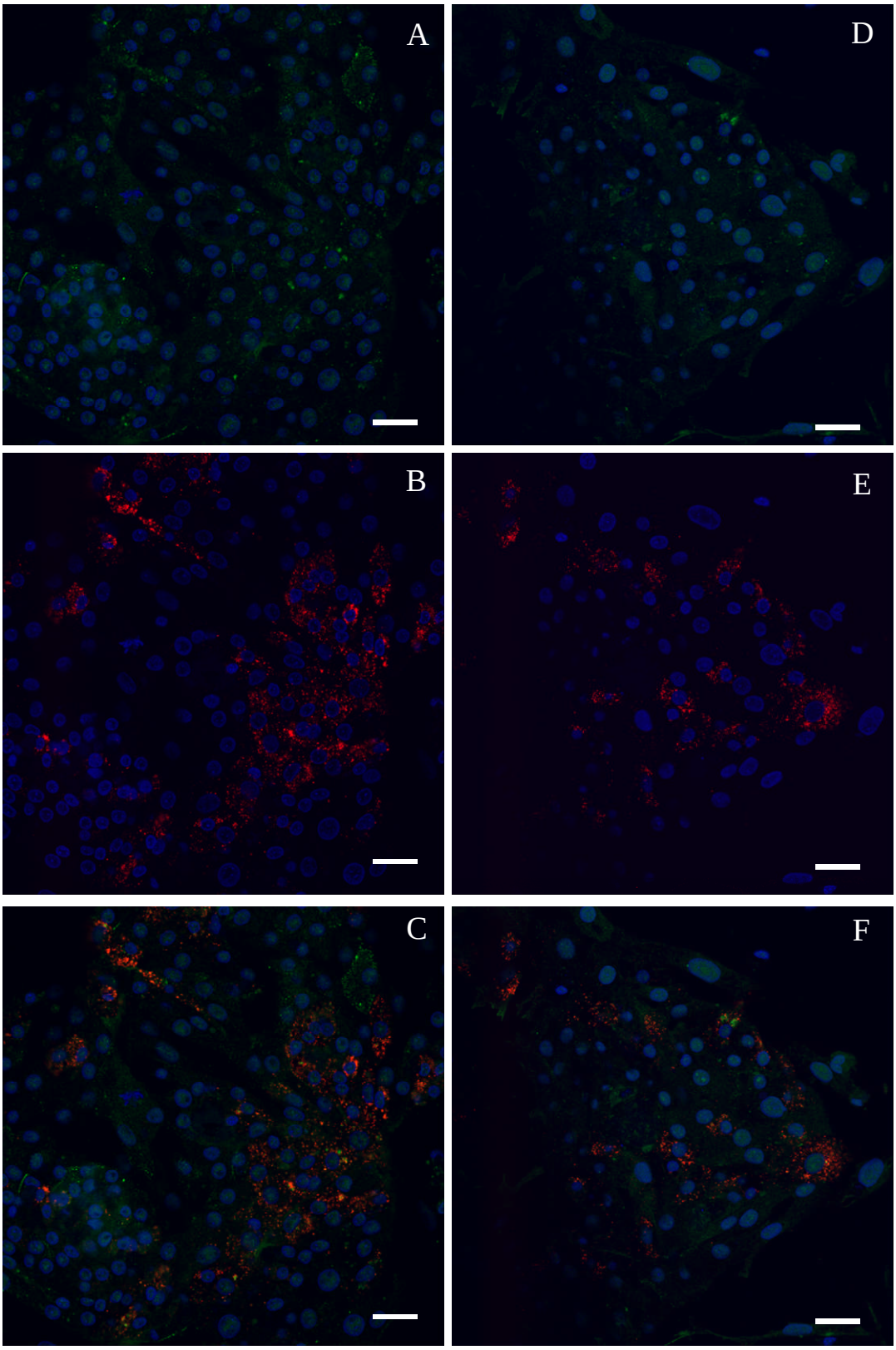
A
D
B
E
C
F

Figure 3.23. Indirect immunofluorescence analysis using the anti-ADRP antibodies on mock infected CK cells. Subconfluent CK cells were mock infected and fixed at 10 h p.i. with paraformaldehyde. After making the cells permeable with Triton X-100 they were labelled with rabbit polyclonal anti-ADRP 523 (A) or 524 (D) and mouse anti-dsRNA (J2) (B and E). Secondary antibodies included Alexa Fluor 488 anti-rabbit (green) and Alexa Fluor 568 anti-mouse (red). Nuclei were labelled with DAPI. The different wavelengths (colours) were scanned independently and digitally merged (C and F). Scale bar indicates 20 μm.

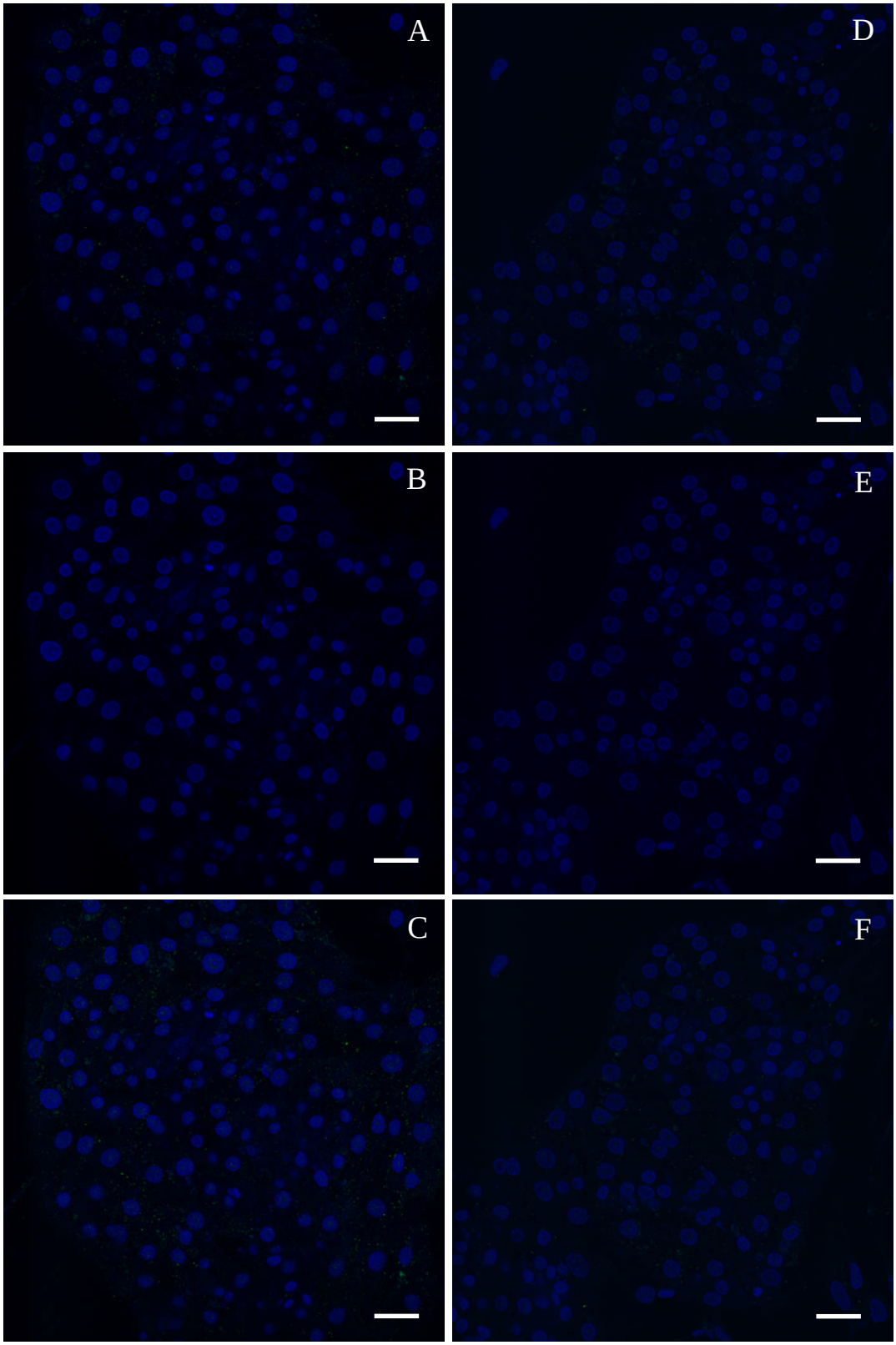
A
D
B
E
C
F

Figure 3.24. Indirect immunofluorescence analysis using the anti-nsp8. Subconfluent CK cells were infected with Beau-R and fixed at 10 h p.i. with paraformaldehyde. After making the cells permeable with Triton X-100 they were labelled with rabbit polyclonal anti-nsp8 682 (A) or 683 (D) and mouse anti-dsRNA (J2) (B and E). Secondary antibodies included Alexa Fluor 488 anti-rabbit (green) and Alexa Fluor 568 anti-mouse (red). Nuclei were labelled with DAPI. The different wavelengths (colours) were scanned independently and digitally merged (C and F). Scale bar indicates 20 μm.

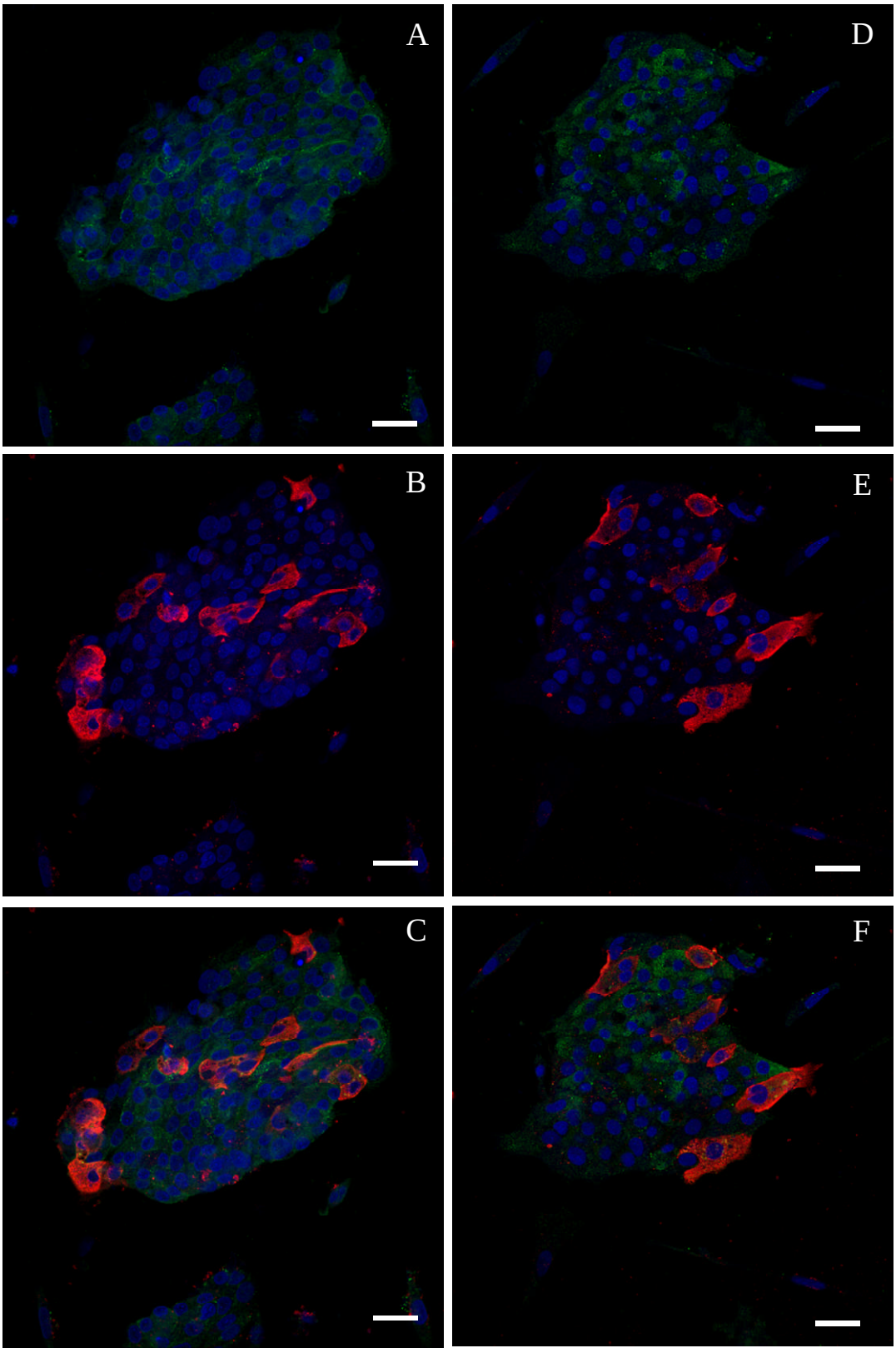
A
D
B
E
C
F

Figure 3.25. Indirect immunofluorescence analysis using the anti-nsp8 on mock infected CK cells. Subconfluent CK cells were mock infected and fixed at 10 h p.i. with paraformaldehyde. After making the cells permeable with Triton X-100 they were labelled with rabbit polyclonal anti-nsp8 682 (A) or 683 (D) and mouse anti-dsRNA (J2) (B and E). Secondary antibodies included Alexa Fluor 488 anti-rabbit (green) and Alexa Fluor 568 anti-mouse (red). Nuclei were labelled with DAPI. The different wavelengths (colours) were scanned independently and digitally merged (C and F). Scale bar indicates 20 μm.

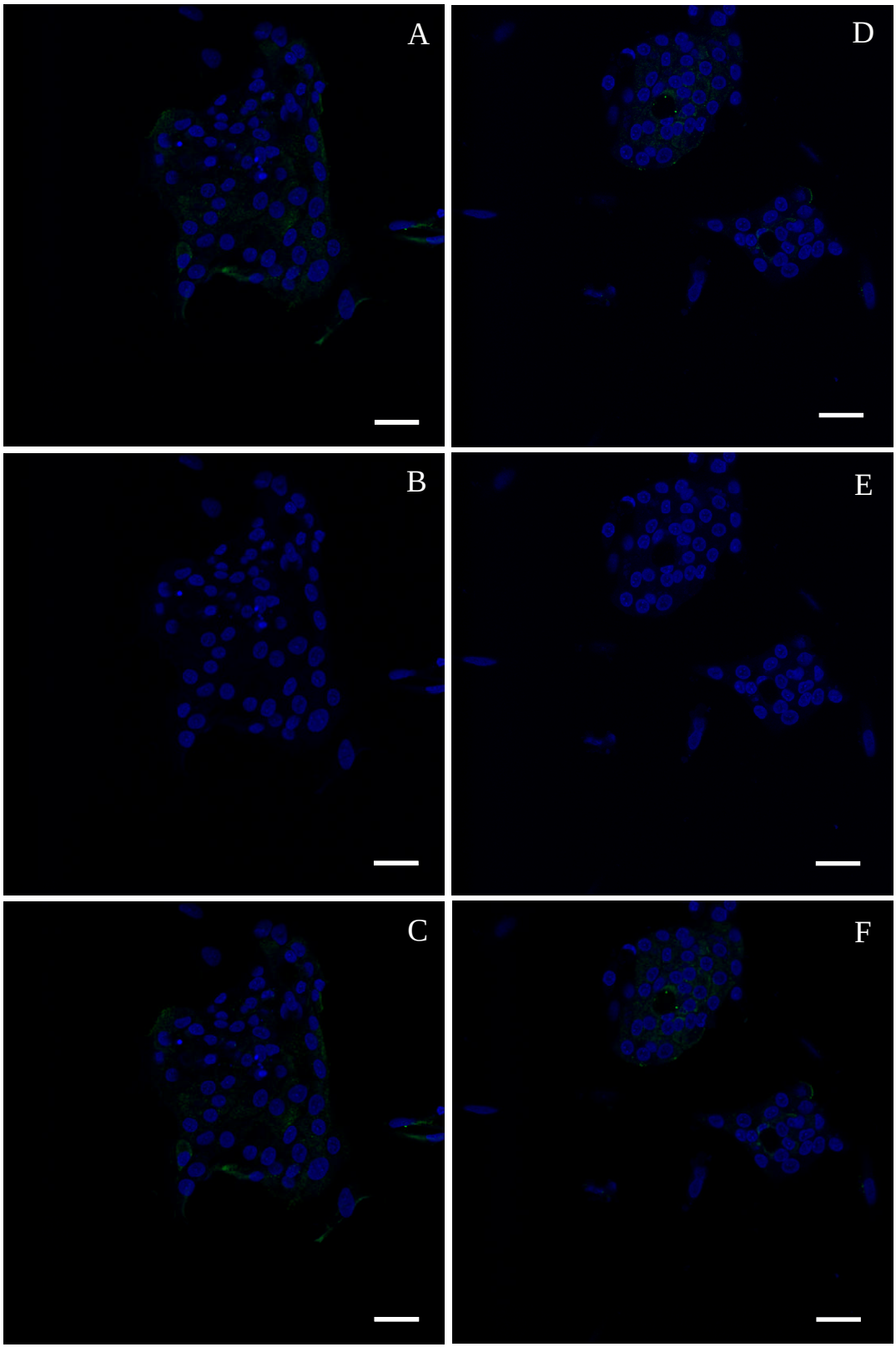
A
D
B
E
C
F

Discussion

The subcellular location of the IBV 3a protein was studied within Beau-R-infected CK and Vero cells. These experiments indicated that this viral accessory protein produced a punctate, cytoplasmic distribution pattern which didn't colocalise with protein markers for the ER, ERGIC, Golgi apparatus or with the viral structural proteins S and M. Due to the lack of antibodies which would detect the nsps, the sites of viral transcription and genome replication were labelled with an antibody which recognised dsRNA. Images of indirect immunofluorescence using the anti-dsRNA antibody indicated that dsRNA labelling occurred only within infected cells and therefore that it was probably generated as a result of viral replication and assumed to be viral in origin. Indirect immunofluorescence experiments using the anti-3a protein antibody and the anti-dsRNA antibody indicated that there was colocalisation between the two molecules.

A comparison of the subcellular location of the 3a protein with subcellular structures has previously been published for IBV-infected mammalian (Vero) cells (Pendleton and Machamer, 2005). They describe a punctate and diffuse cytoplasmic distribution pattern for the 3a protein within transfected and infected Vero cells which contrasted slightly with the images of punctate only staining presented in this chapter. This distribution pattern partially colocalised with markers for the smooth ER. The slight difference in distribution patterns observed for the 3a protein could have been a result of the antibodies used. The antibody which detected a punctate pattern only was raised against peptides corresponding to the N-terminus of the 3a protein, whereas the punctate and diffuse staining was detected using an antibody raised against the C-terminal portion of the 3a protein. The lack of 3a protein detection in the cytoplasm could suggest that the N-terminal portion of the protein was inaccessible to the antibody, possibly by association or interaction with other proteins. Pendleton and Machamer (2005) also detected the 3a protein in the lysate of IBV infected Vero cells at 24 h p.i., but not at 6 or 15 h p.i. which was in contrast to the results presented in this thesis which indicated that the 3a protein was detected by western blot at 6 h p.i. and immunofluorescence at 4 h p.i. An explanation for this difference is likely to hinge on the type of cell used and the size of the inoculum. Pendleton and Machamer (2005) used Vero cells and a m.o.i. of ~1. Beau-R can

productively replicate in Vero cells but the number of cells initially infected with the same inoculum is lower than that for CK cells (observation by immunofluorescence). As a result of the reduced number of infected cells there would be a reduced quantity of viral proteins including the 3a protein. The quantity of 3a protein in the cell lysates from the 6 and 15 h p.i. samples therefore might not have been sufficient to be detectable at these time points rather than a situation where the protein had not been expressed.

Expression of the 3a protein was detected at 6 h p.i. in the lysate of Beau-R-infected CK cells, but the 3a protein could be detected at 4 h p.i. by indirect immunofluorescence. This difference in detection could have been due to the detection limits of the two techniques. Whereas immunofluorescence can detect the presence of the 3a protein within individual cells the Western blot technique uses a small proportion of the entire cell lysate. The 3a protein would have been highly diluted in the cell lysate when first expressed and thus was only detected when more 3a protein was produced. The detection of a higher molecular weight protein at approximately double the weight of a single 3a protein indicated that a minor proportion of the 3a proteins may form a dimer. This was not observed for the 3a protein detected in the lysate of IBV-infected Vero cells (Pendleton and Machamer, 2005) and thus may be a feature of 3a protein expression in avian cells or may have been the result of incomplete sample reduction prior to SDS-PAGE.

Expression and the subcellular location of the individual accessory proteins were assessed. Plasmids which expressed N-terminally-FLAG-tagged 3a and 3b proteins were constructed. Images taken of Vero cells transfected with a plasmid expressing the FLAG/3a protein indicated that this protein had a punctate, cytoplasmic distribution similar to that of the native 3a protein in infected cells. The pattern in some cells was slightly different from that observed within infected cells displaying a punctate distribution but predominantly within the perinuclear region. The addition of the tag could have had an effect upon the subcellular location of the accessory protein by disrupting any potential signal sequences. Alternatively, overexpression of the tagged protein directed by the CMV promoter would have caused more accessory proteins to be produced than expected to be found within an infected cell. This increased level of tagged protein may have caused some of the protein to be targeted to the wrong subcellular location by overloading the correct compartment. The observed cellular location of the tagged 3a protein was not affected by

expression of the other viral proteins in most of the observed cells indicating that this accessory protein associates with pre-existing cellular structures or initiates the formation of these punctate, cytoplasmic structures independently of any other viral protein. A difference in cellular location of FLAG/3a between transfected and infected/transfected could have been the result of the time frame of infection. A later time point in infection could have resulted in the cell undergoing subcellular changes caused by infection, such as apoptosis, which was not present at the same time in transfected only cells. The absence of FLAG-tag labelling when the FLAG/3b protein was expressed within Vero cells can potentially be explained by the reported observation that there is a high turnover of the IBV 3b protein by the mammalian proteasome (Pendleton and Machamer, 2006). The factors associated with this high turnover were not disrupted by the presence of a N-terminal tag and linker sequence.

Examination of the subcellular location of the IBV accessory proteins required that antibodies were available to detect these proteins within Beau-R-infected cells. Comparison of the location of the accessory proteins to the other viral proteins also required suitable antibodies. Expression of the ADRP domain and the 3b protein was conducted using the SUMO tag expression system. The ADRP domain or 3b protein was expressed C-terminally to the SUMO protein. The recombinant protein was then purified using the N-terminal His-tag. Removal of the SUMO protein to leave an unmodified ADRP domain or 3b protein could not be achieved using the SUMO protease. Recombinant proteins were expressed and after purification the sample still retained some additional proteins. Some of these could have been multiples of the originally expressed protein as would appear possible with the ~50 kDa protein in the nsp8 sample (i.e. twice the 24.3 kDa calculated for nsp8HN). Other contaminating proteins could have been a result of their non-specific binding to the purification column or the His-tagged protein. These purified proteins were used to raise antibodies. Analysis by indirect immunofluorescence indicated that none of the sera contained anti-3b, anti-ADRP domain or anti-nsp8 protein specific antibodies which could be used with this technique. Western blot analysis using these antibodies to detect the original antigens (i.e. SUMO/3b, SUMO/ADRP and nsp8HN) were successful indicating that the recombinant proteins were immunogenic. At least with the SUMO/3a and SUMO/ADRP proteins the immunogenic part may have been the N-terminal SUMO sequence because Western blot using the anti-3b protein antibodies could detect SUMO/ADRP and visa-versa

implying that the anti-3b protein and anti-ADRP protein sera contained anti-SUMO antibodies. Antibodies directed towards the 3b protein (Pendleton and Machamer, 2006), ADRP domain of nsp3 (Snijder *et al.*, 2006) and nsp8 (Bost *et al.*, 2001; Clementz *et al.*, 2008) have been generated by other groups. The absence of suitable antibodies would appear to be a result of inappropriate antibodies being generated by the rabbits which were inoculated with the recombinant proteins, rather than with issues surrounding the actual proteins themselves.

Chapter 4: Cellular location of the gene 5 accessory proteins

Summary

The cellular location of the gene 5 accessory proteins was examined. Antibodies directed against the 5b protein indicated that the 5b protein had a diffuse, cytoplasmic distribution pattern in infected avian and mammalian cells. There were no colocalisation events seen between 5b and the S and M proteins or markers for the ER, ERGIC or Golgi apparatus. There was a limited amount of colocalisation observed between the 5b and N proteins in transfected Vero cells indicating that these two proteins share a common cellular location but this was not seen when the subcellular location of these two proteins were compared in Beau-R infected CK cells. The cellular distribution of 5b was similar in infected CK cells and transfected Vero cells. Analysis of the expression of the 5b protein within Beau-R infected CK cells indicated that it was first detected at 5 h p.i.

The expression of a FLAG epitope tagged 5a protein within transfected Vero cells revealed a punctate, cytoplasmic distribution pattern. This pattern was indicative of a protein associated with an intracellular structure/membrane.

Introduction

Determination of the intracellular location and protein interactions of the gene 5 accessory proteins would begin to elucidate the roles that these proteins play during the IBV replication cycle. The subcellular location of the gene 5 accessory proteins was explored by comparison and potential colocalisation to other cellular and viral proteins using immunofluorescence and confocal microscopy.

Where an antibody wasn't immediately available to detect a protein in immunofluorescence experiments, i.e. the 5a protein, a FLAG-tagged version was

expressed from a plasmid which had been used to transfect cells. The FLAG tag is a hydrophilic octapeptide which is recognised by commercially available antibodies. A FLAG-tagged 5b protein was also used to identify the subcellular distribution of a tagged 5b protein and compare it to the subcellular distribution of the native, virally-expressed 5b protein.

Results

Cellular location of 5b protein compared to subcellular compartments

Indirect immunofluorescence with confocal microscopy using the anti-5b protein antibody and antibodies which labelled the ER, ERGIC and Golgi apparatus were used to identify the subcellular distribution and potential subcellular location of the 5b protein. The cellular distribution pattern of the 5b protein was observed in paraformaldehyde-fixed, Beau-R-infected Vero and CK cells by indirect immunofluorescence and confocal microscopy. The 5b protein was observed to display a diffuse, cytoplasmic distribution pattern (Fig. 4.1), although some fluorescence was observed within the nucleus. This nuclear staining may have been due to the high background fluorescence when the anti-5b protein antibody was used as the levels of fluorescence within the nucleus of infected cells were less than that observed within the cytoplasm. This diffuse, cytoplasmic cellular distribution was observed in both Beau-R-infected CK (Fig.4.2) and Vero cells (Fig.4.3) and was observed very faintly at 6 h p.i. (Fig. 4.5) (with images of mock infected cells at 4 and 6 h p.i. – Fig. 4.6) and became slightly more intense by 8 h p.i. At all observable time points during the replication cycle the distribution pattern was consistent suggesting that the 5b protein does not relocate to perform a different function during the viral replication cycle.

Identification of the subcellular location to which the 5b protein accumulates was investigated. Dual labelling experiments comparing the location of the 5b protein with protein markers for subcellular structures would identify or eliminate potential sites. The IBV structural proteins S, M and E are first inserted into the ER membrane and then translocated to the ERGIC and Golgi (Klumperman *et al.*, 1994; Winter *et al.*, 2008b) When the distribution pattern of the 5b protein was compared to the

subcellular location of ER (Fig. 4.2), ERGIC (Fig. 4.3) and Golgi apparatus (Fig. 4.4) there were no colocalisation events or similarities in pattern, indicating that the IBV 5b protein does not accumulate at these particular sites within the infected cell. Due to the absence of antibodies which would label the ERGIC within avian cells the equivalent subcellular structure was identified in Vero cells.

Figure 4.1. Indirect immunofluorescence analysis of the intracellular distribution of IBV 5b protein within Beau-R-infected CK cells. Subconfluent CK cells were infected with Beau-R and fixed at 10 h p.i. with paraformaldehyde. After making the cells permeable with Triton X-100 they were labelled with rabbit polyclonal anti-5b (SK71). Secondary antibodies included Alexa Fluor 488 anti-rat (green) and nuclei were labelled with DAPI. A – Anti-3a antibody with DAPI. B – A magnified section of (A). C – The same magnified section as (B) but displaying the anti-3a antibody labelling only. D - The same magnified section as (B) but displaying the DAPI labelling only. The different wavelengths (colours) were scanned independently and digitally merged. Scale bar indicates 20 μm.

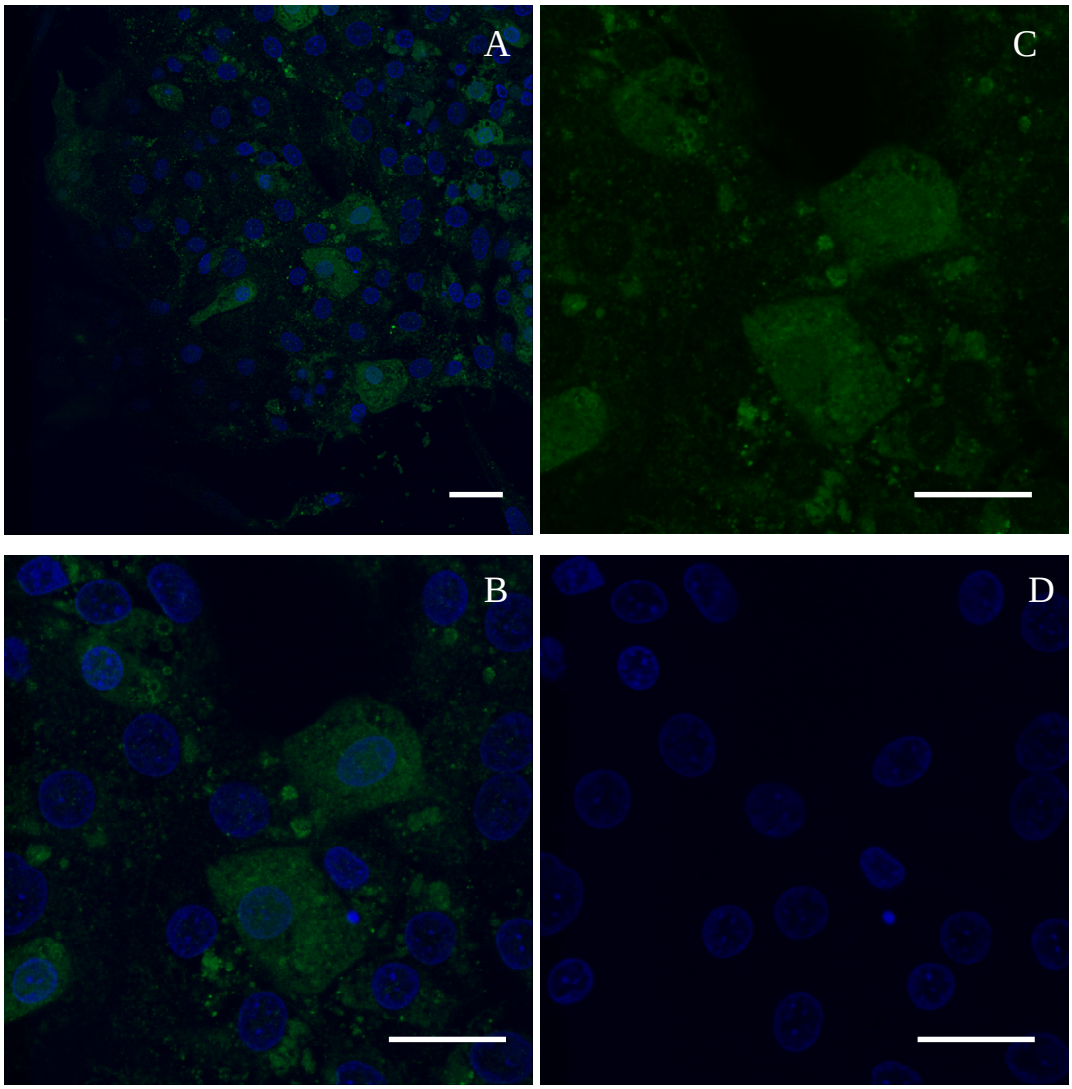
A
C
B
D

Figure 4.2. Indirect immunofluorescence analysis of the intracellular location of the 5b protein compared to ER. Subconfluent CK cells were infected with Beau-R and fixed at 10 h p.i. with paraformaldehyde. After making the cells permeable with Triton X-100 they were labelled with rat polyclonal anti-5b (SK71) (A and D) and mouse anti-PDI (ER marker) (B and E). Secondary antibodies included Alexa Fluor 488 anti-rabbit (green) and Alexa Fluor 568 anti-mouse (red). Nuclei were labelled with DAPI. The different wavelengths (colours) were scanned independently and digitally merged. Images D, E and F are a magnified section of the images A, B and C. Scale bar indicates 20 μm.

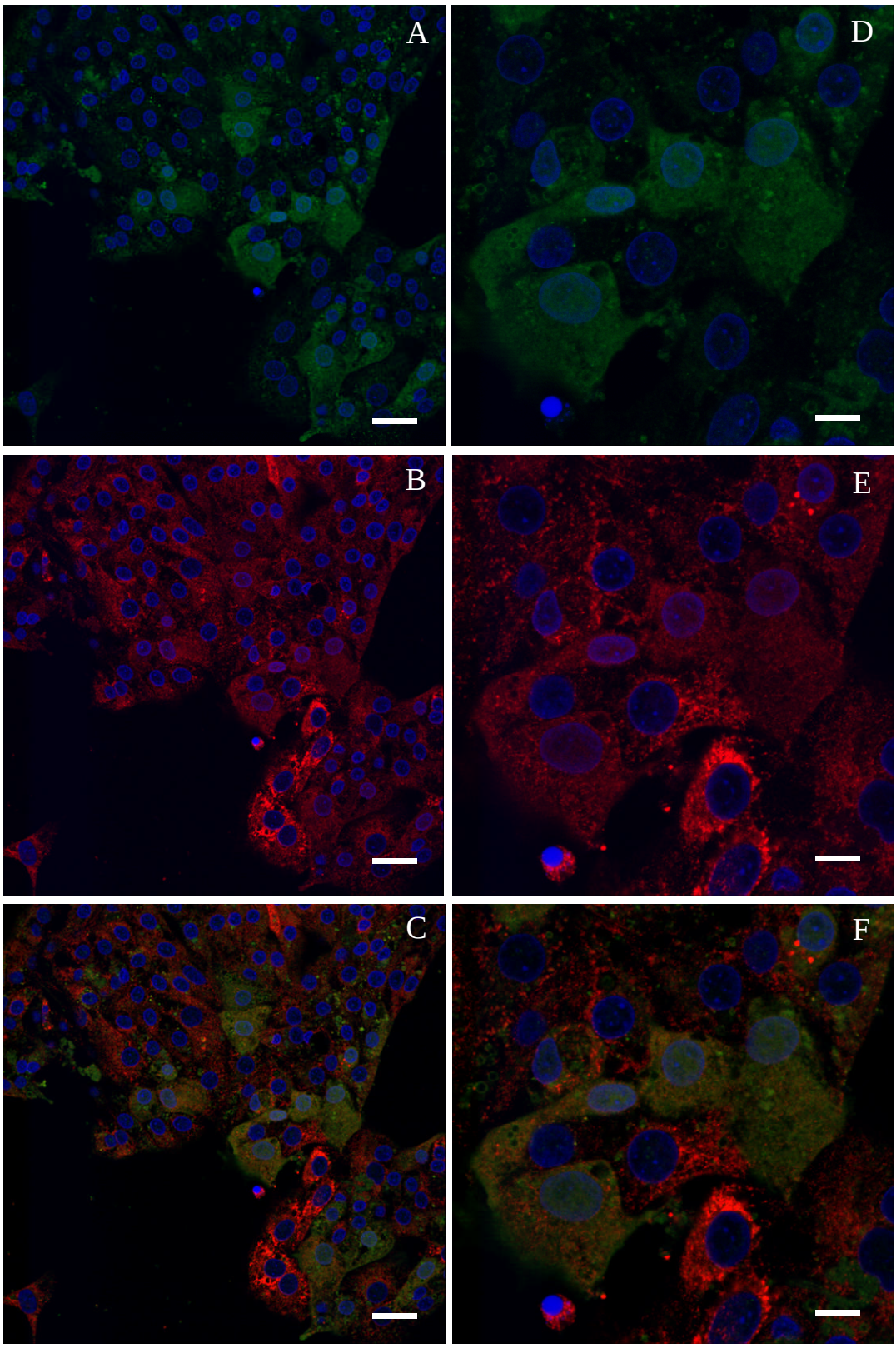
A
D
B
E
C
F

Figure 4.3. Indirect immunofluorescence analysis of the intracellular location of the 5b protein compared to ERGIC. Subconfluent Vero cells were infected with Beau-R and fixed at 20 h p.i. with paraformaldehyde. After making the cells permeable with Triton X-100 they were labelled with rat polyclonal anti-5b (SK71) (A and D) and mouse anti-ERGIC 53 (ERGIC marker) (B and E). Secondary antibodies included Alexa Fluor 488 anti-rabbit (green) and Alexa Fluor 568 anti-mouse (red). Nuclei were labelled with DAPI. The different wavelengths (colours) were scanned independently and digitally merged. Images A, B, C and D, E, F are two different fields of view of the same experiment. Scale bar indicates 20 μm.

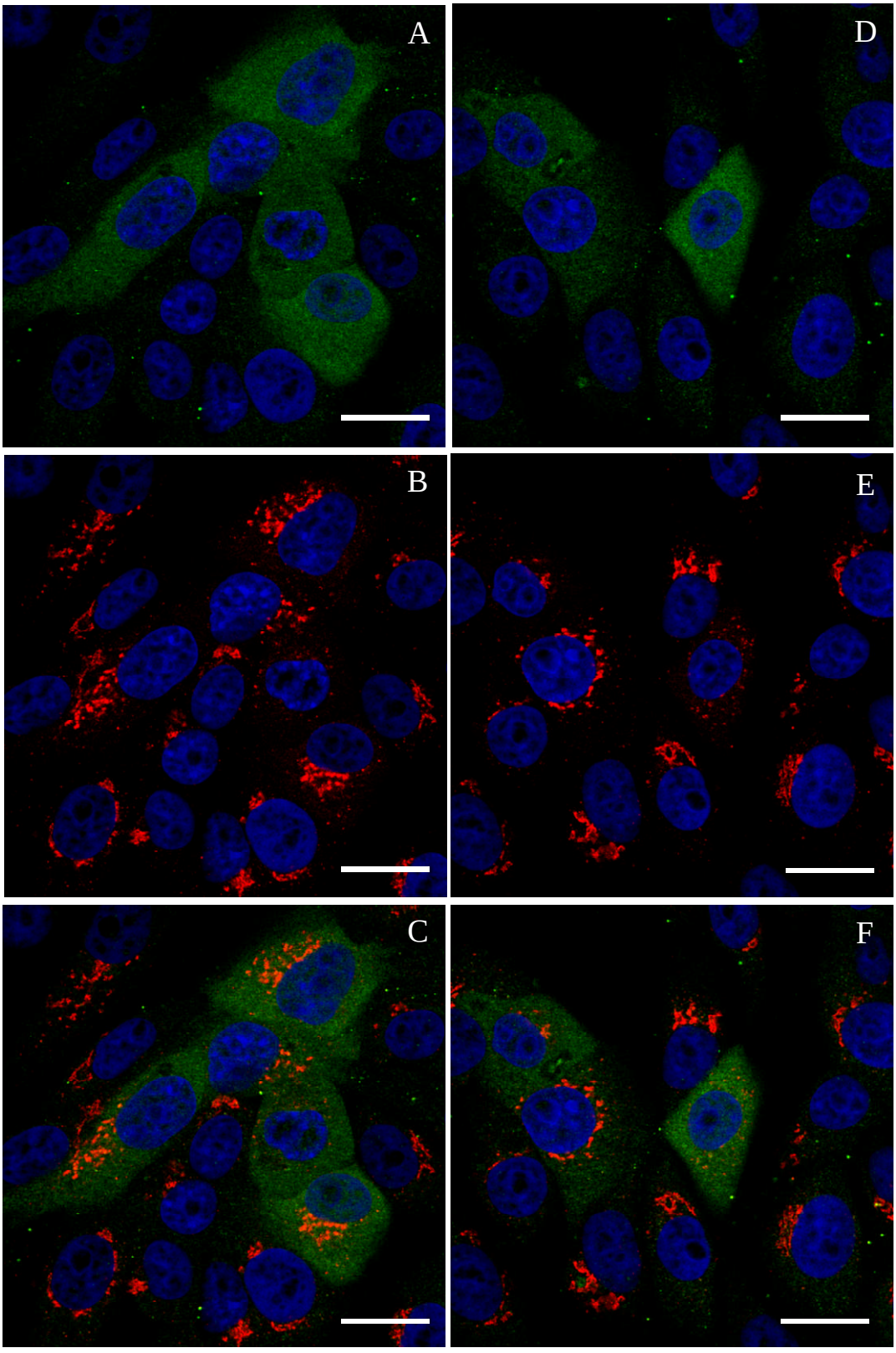
A
D
B
E
C
F

Figure 4.4. Indirect immunofluorescence analysis of the intracellular location of the 5b protein compared to Golgi apparatus. Subconfluent CK cells were infected with Beau-R and fixed at 10 h p.i. with paraformaldehyde. After making the cells permeable with Triton X-100 they were labelled with rat polyclonal anti-5b (SK71) (A and D) and mouse anti-GM130 (Golgi marker) (B and E). Secondary antibodies included Alexa Fluor 488 anti-rabbit (green) and Alexa Fluor 568 anti-mouse (red). Nuclei were labelled with DAPI. The different wavelengths (colours) were scanned independently and digitally merged. Images D, E and F are a magnified section of the images A, B and C. Scale bar indicates 20 μm.

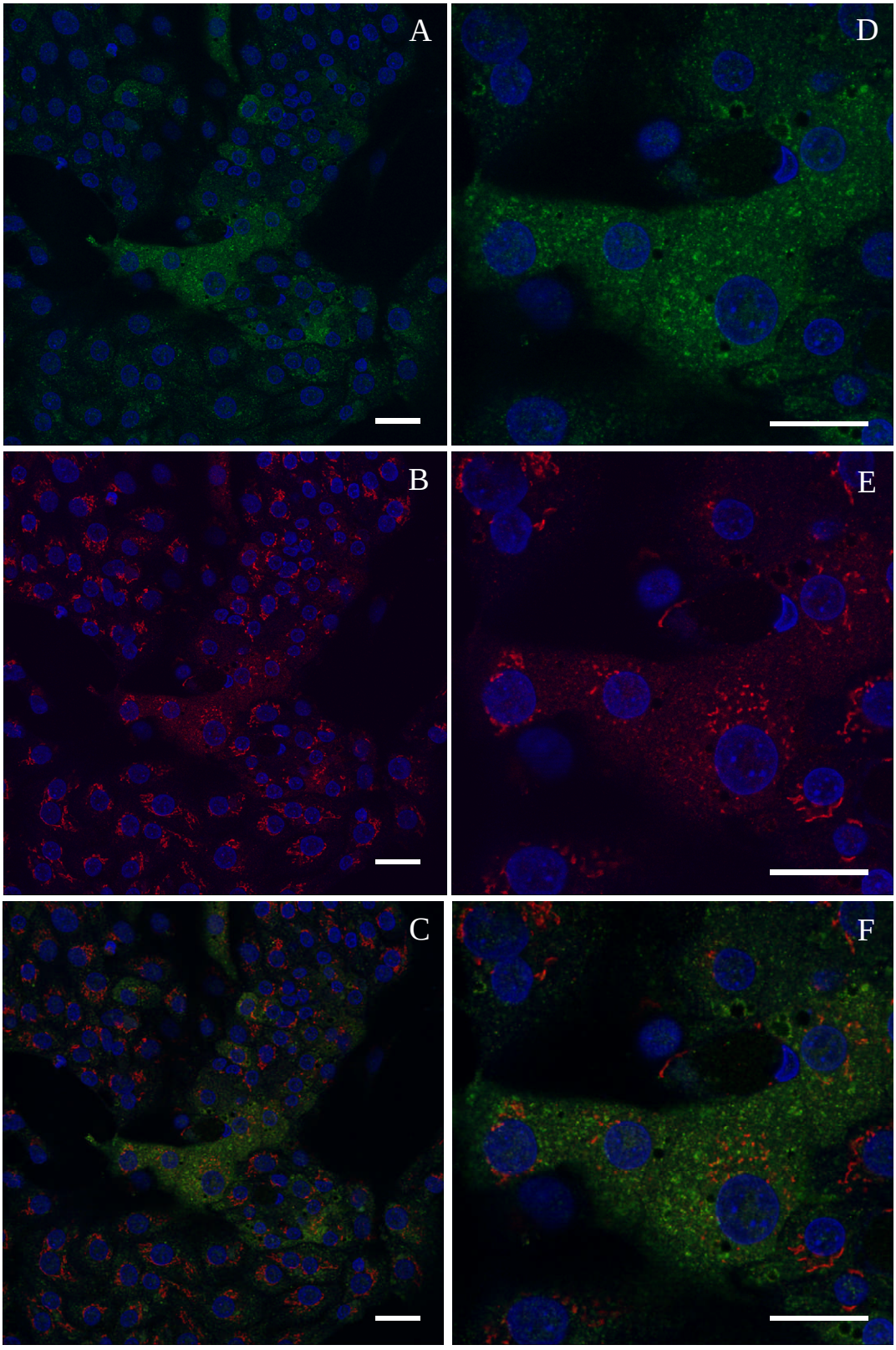
A
D
B
E
C
F

Figure 4.5. Indirect immunofluorescence analysis of the expression of the 5b protein at 4 and 6 h p.i. Subconfluent CK cells were infected with Beau-R and fixed at either 4 (A, B and C) or 6 h p.i. (D, E and F) with paraformaldehyde. After making the cells permeable with Triton X-100 they were labelled with rabbit anti-IBV (A and D) and rat anti-5b (B and E) antibodies. Secondary antibodies included Alexa Fluor 488 anti-rabbit (green) and Alexa Fluor 568 anti-rat (red). Nuclei were labelled with DAPI. The different wavelengths (colours) were scanned independently and digitally merged. Scale bar indicates 20 μm.

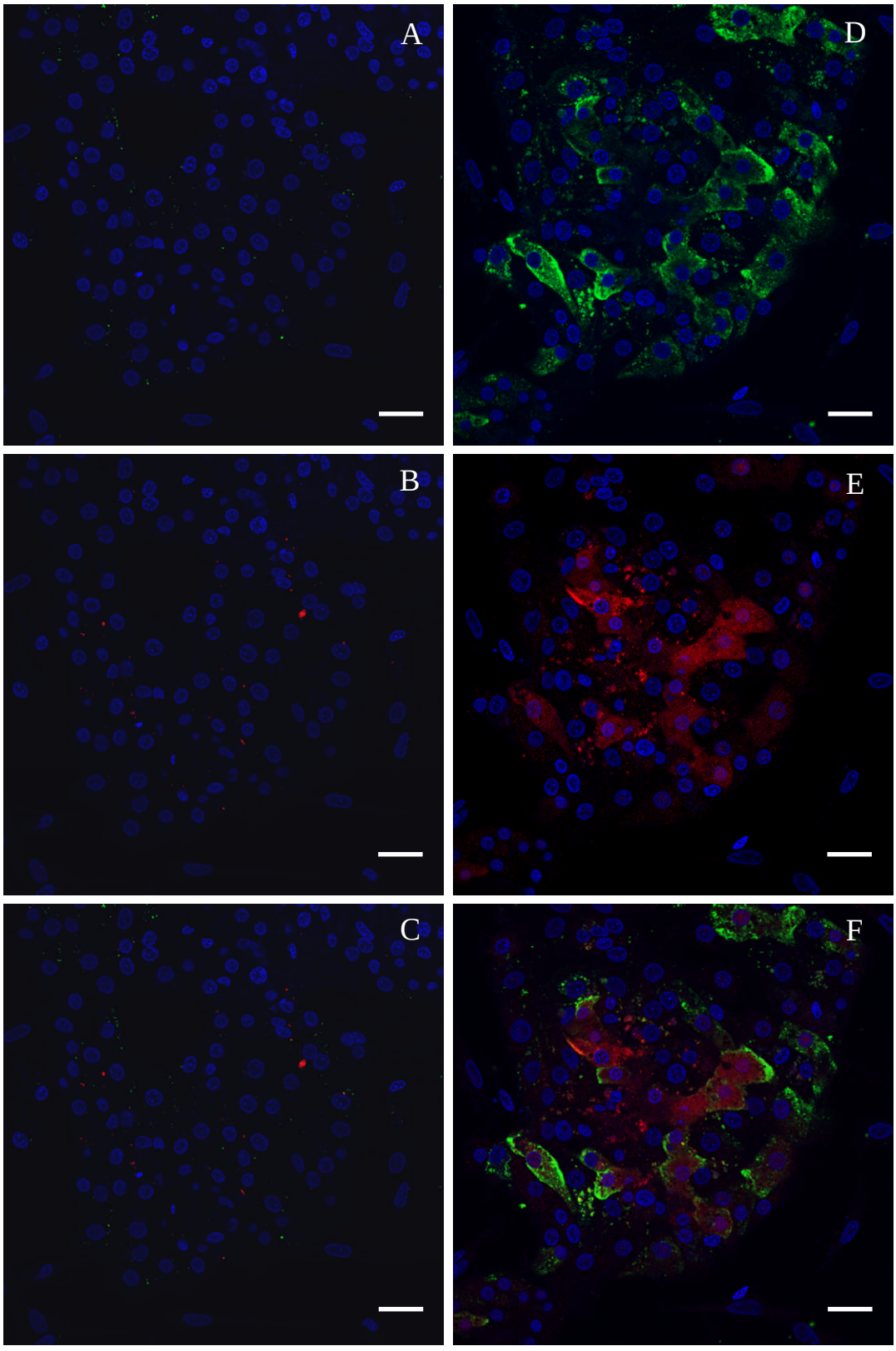
A
D
B
E
C
F

Figure 4.6. Indirect immunofluorescence analysis of the expression of the 5b protein at 4 and 6 h p.i. on mock infected CK cells. Subconfluent CK cells were mock infected and fixed at either 4 (A, B and C) or 6 h p.i. (D, E and F) with paraformaldehyde. After making the cells permeable with Triton X-100 they were labelled with rabbit anti-IBV (A and D) and rat anti-5b (B and E) antibodies. Secondary antibodies included Alexa Fluor 488 anti-rabbit (green) and Alexa Fluor 568 anti-rat (red). Nuclei were labelled with DAPI. The different wavelengths (colours) were scanned independently and digitally merged. Scale bar indicates 20 μm.

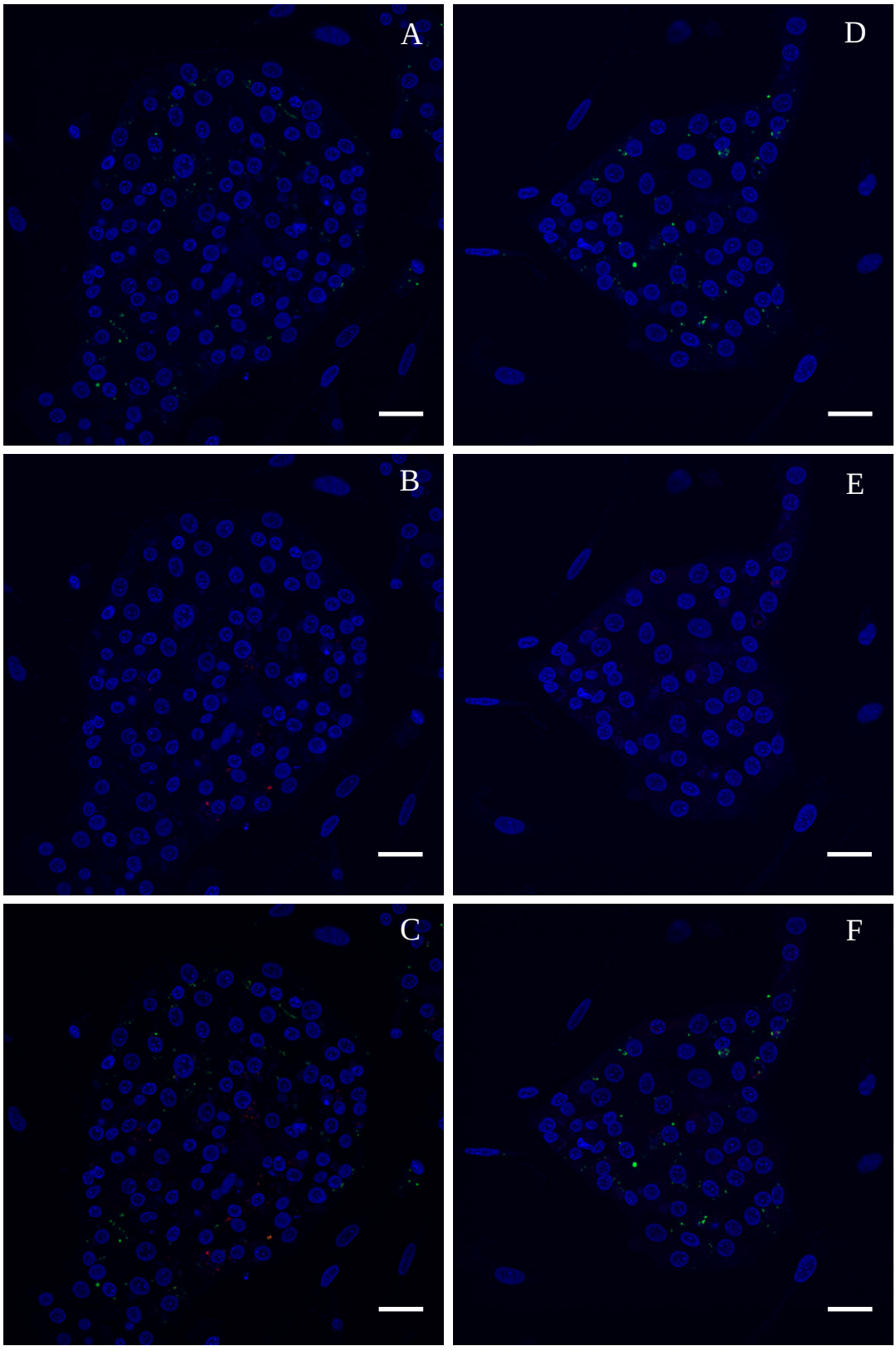
A
D
B
E
C
F

5b protein partially colocalises with a Beau-R structural protein

The 5b protein has a different cellular distribution pattern to that of the ER, ERGIC and Golgi apparatus. IBV uses these subcellular structures to produce, insert into a membrane and translocate the S, M and E proteins to the site of virion assembly. The N protein has a different cellular distribution pattern, characterised by a diffuse, cytoplasmic pattern with some punctate staining (Sims *et al.*, 2000; Wurm *et al.*, 2001). The cellular location and distribution of the 5b protein with the S or M proteins was explored with protein-specific antibodies. As expected the cellular locations were markedly different and there were no localisation events observed (Fig. 4.7) (Fig. 4.8) (with images of the respective mock infected cells – Fig. 4.9) indicating that the 5b protein does not directly function in translocation of the viral structural proteins or in virion assembly. The lack of a N protein-specific antibody meant that an anti-IBV antibody was used. The anti-IBV antibody produced a diffuse, cytoplasmic staining pattern (Fig. 4.10). The diffuse, cytoplasmic staining of the 5b protein resulted in some colocalisation with the cytoplasmic staining produced using the anti-IBV antibody (Fig. 4.10) as demonstrated by the orange hue within the infected cells, but the majority of the colour was separated indicating no colocalisation. This may indicate that the 5b protein partially colocalises with an IBV structural protein or that the concentration of the two viral proteins in the cytoplasm was enough to cause colocalisation by increased chance.

Figure 4.7. Indirect immunofluorescence analysis of the intracellular location of the 5b protein compared to S protein. Subconfluent CK cells were infected with Beau-R and fixed at 8 h p.i. with paraformaldehyde. After making the cells permeable with Triton X-100 they were labelled with rat polyclonal anti-5b (SK71) (A and D) and mouse anti-S (A13/38) (B and E). Secondary antibodies included Alexa Fluor 488 anti-rabbit (green) and Alexa Fluor 568 anti-mouse (red). Nuclei were labelled with DAPI. The different wavelengths (colours) were scanned independently and digitally merged. Images D, E and F are a magnified section of the images A, B and C. Scale bar indicates 20 μm.

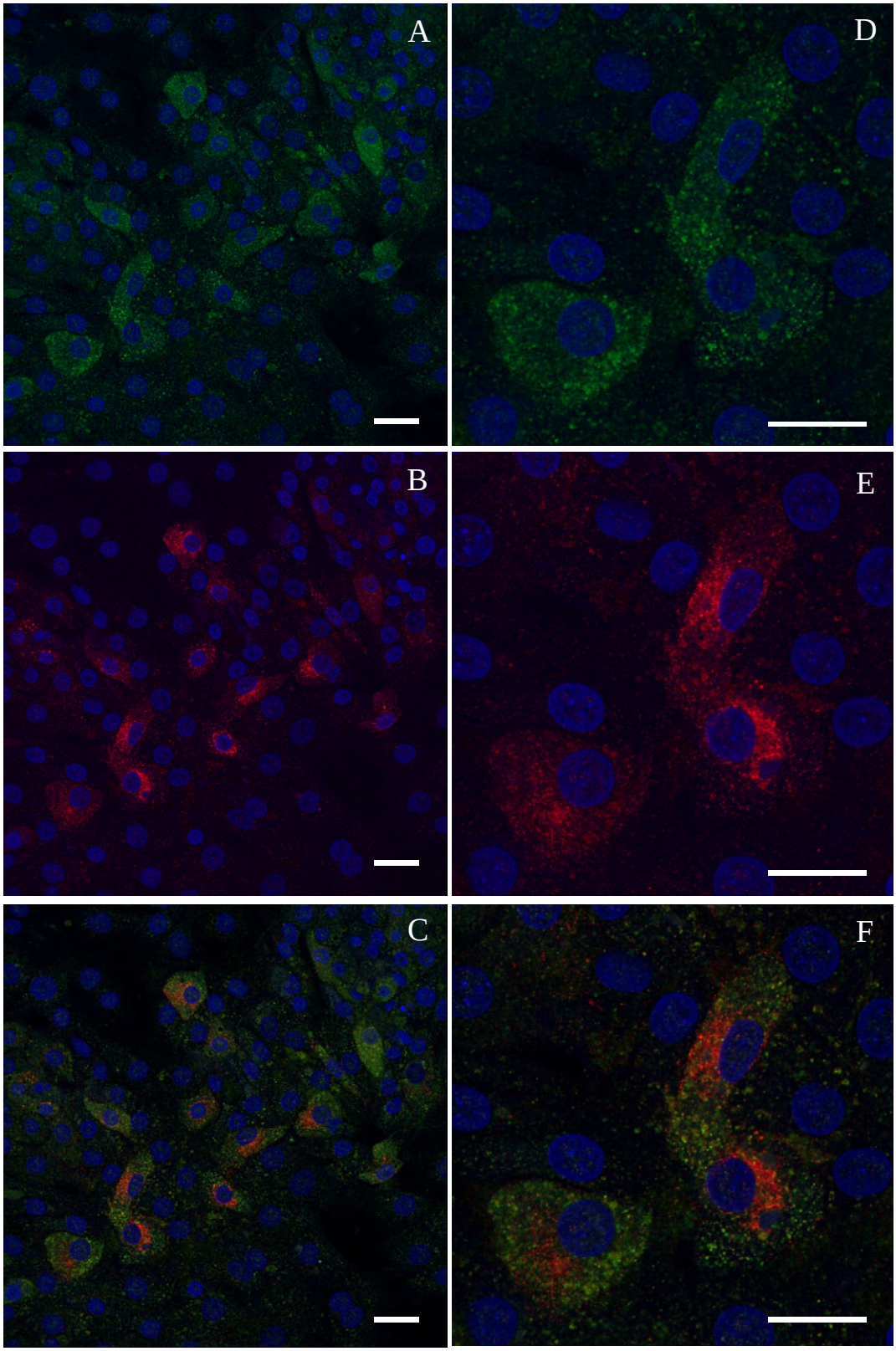
A
D
B
E
C
F

Figure 4.8. Indirect immunofluorescence analysis of the intracellular location of the 5b protein compared to M protein. Subconfluent CK cells were infected with Beau-R and fixed at 8 h p.i. with paraformaldehyde. After making the cells permeable with Triton X-100 they were labelled with rat polyclonal anti-5b (SK71) (A and D) and mouse anti-M (C5/124) (B and E). Secondary antibodies included Alexa Fluor 488 anti-rabbit (green) and Alexa Fluor 568 anti-mouse (red). Nuclei were labelled with DAPI. The different wavelengths (colours) were scanned independently and digitally merged. Images D, E and F are a magnified section of the images A, B and C. Scale bar indicates 20 μm.

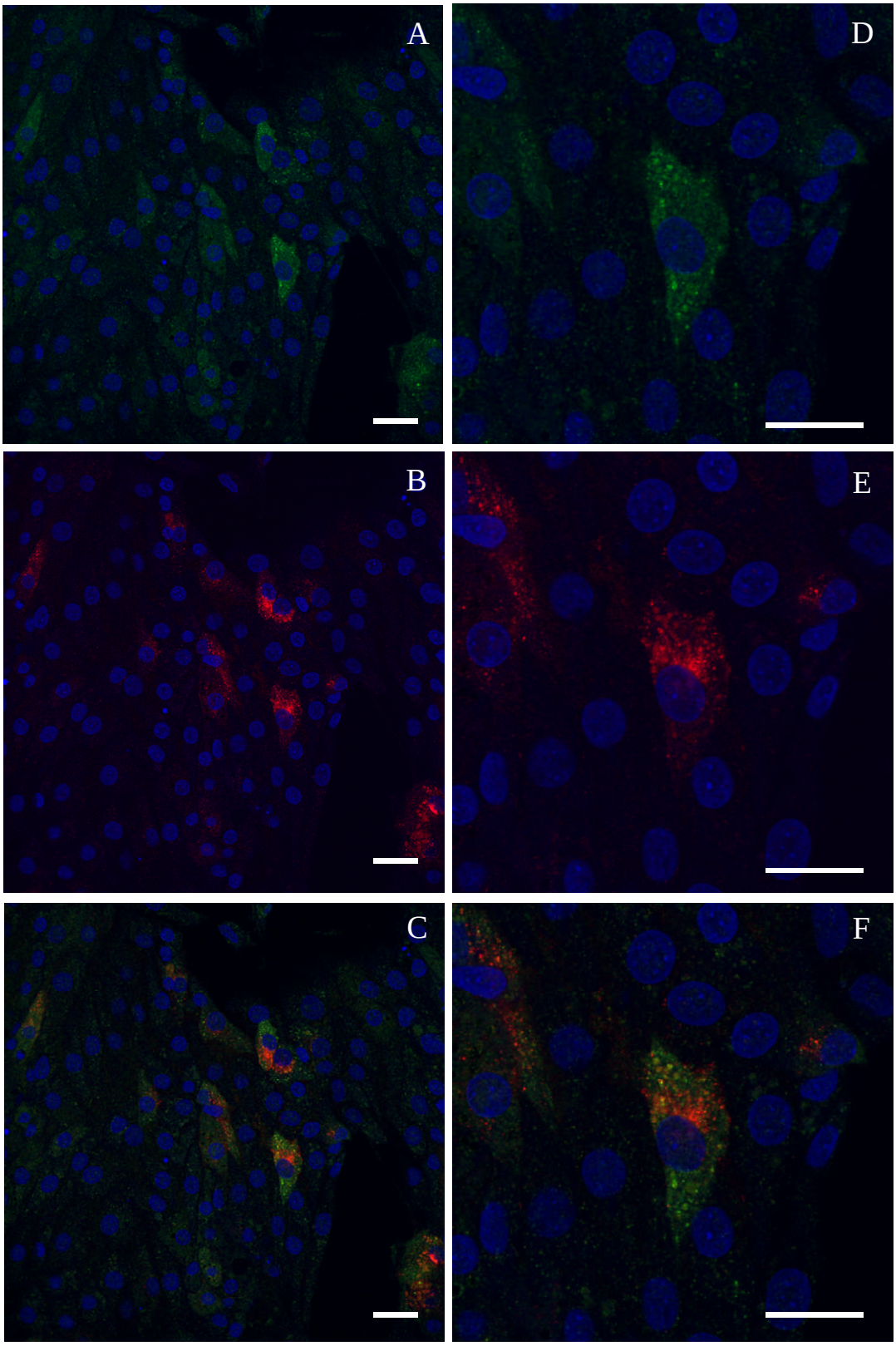
A
D
B
E
C
F

Figure 4.9. Indirect immunofluorescence analysis of the intracellular location of the 5b protein compared to the M and S proteins on mock infected cells. Subconfluent CK cells were mock infected and fixed at 8 h p.i. with paraformaldehyde. After making the cells permeable with Triton X-100 they were labelled with rat polyclonal anti-5b (SK71) (A and D) and mouse anti-M (C5/124) (B) or mouse anti-S (A13/38) (E). Secondary antibodies included Alexa Fluor 488 anti-rabbit (green) and Alexa Fluor 568 anti-mouse (red). Nuclei were labelled with DAPI. The different wavelengths (colours) were scanned independently and digitally merged (C and F). Scale bar indicates 20 μm.

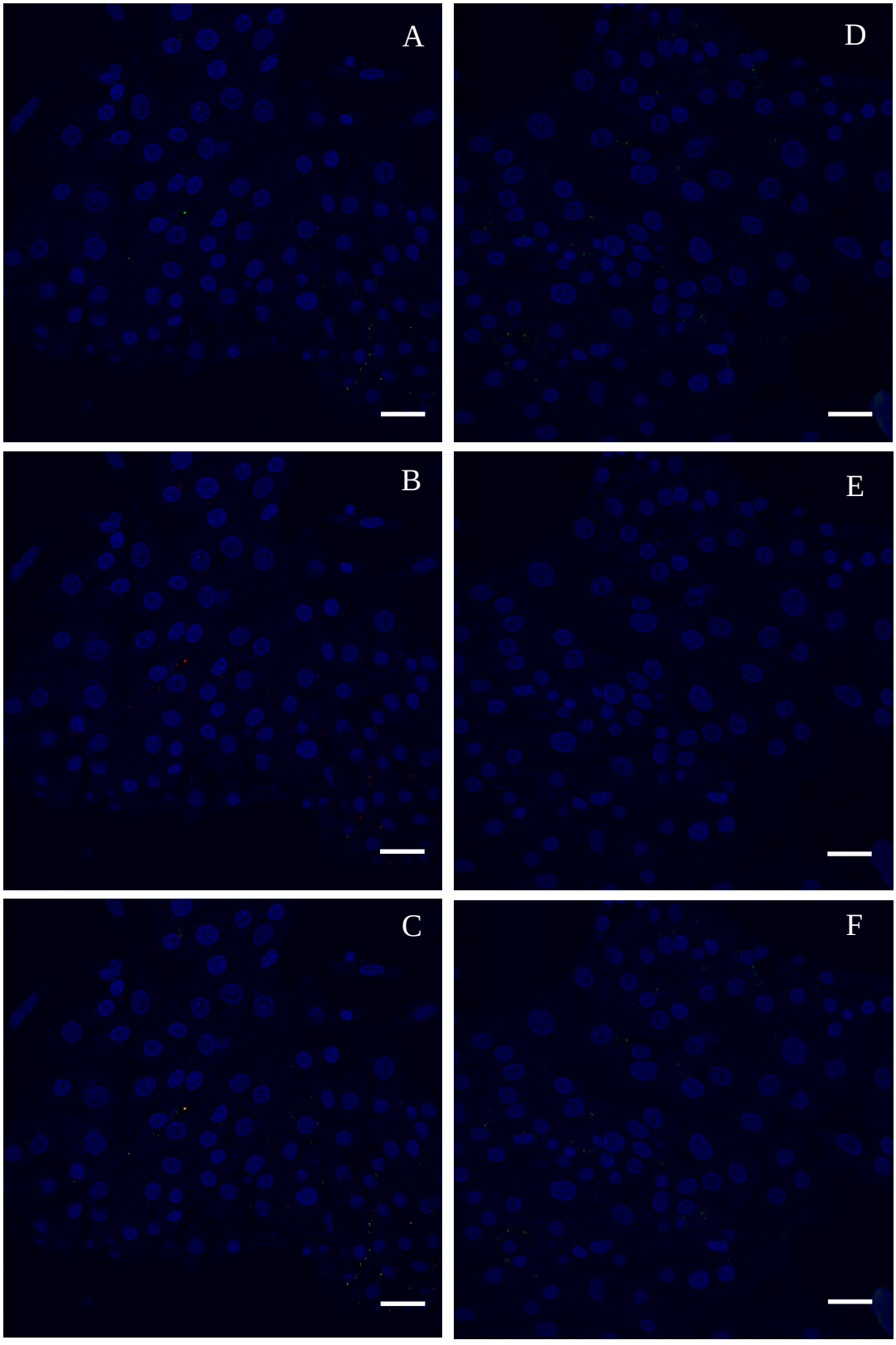
A
D
B
E
C
F

Figure 4.10. Indirect immunofluorescence analysis of the intracellular location of the 5b protein compared to IBV structural proteins. Subconfluent CK cells were infected with Beau-R and fixed at 8 h p.i. with paraformaldehyde. After making the cells permeable with Triton X-100 they were labelled with rat polyclonal anti-5b (SK71) (A and D) and chicken anti-IBV (B and E). Secondary antibodies included Alexa Fluor 488 anti-chicken (green) and Alexa Fluor 568 anti-rat (red). Nuclei were labelled with DAPI. The different wavelengths (colours) were scanned independently and digitally merged. Images D, E and F are a magnified section of the images A, B and C. Scale bar indicates 20 μm.

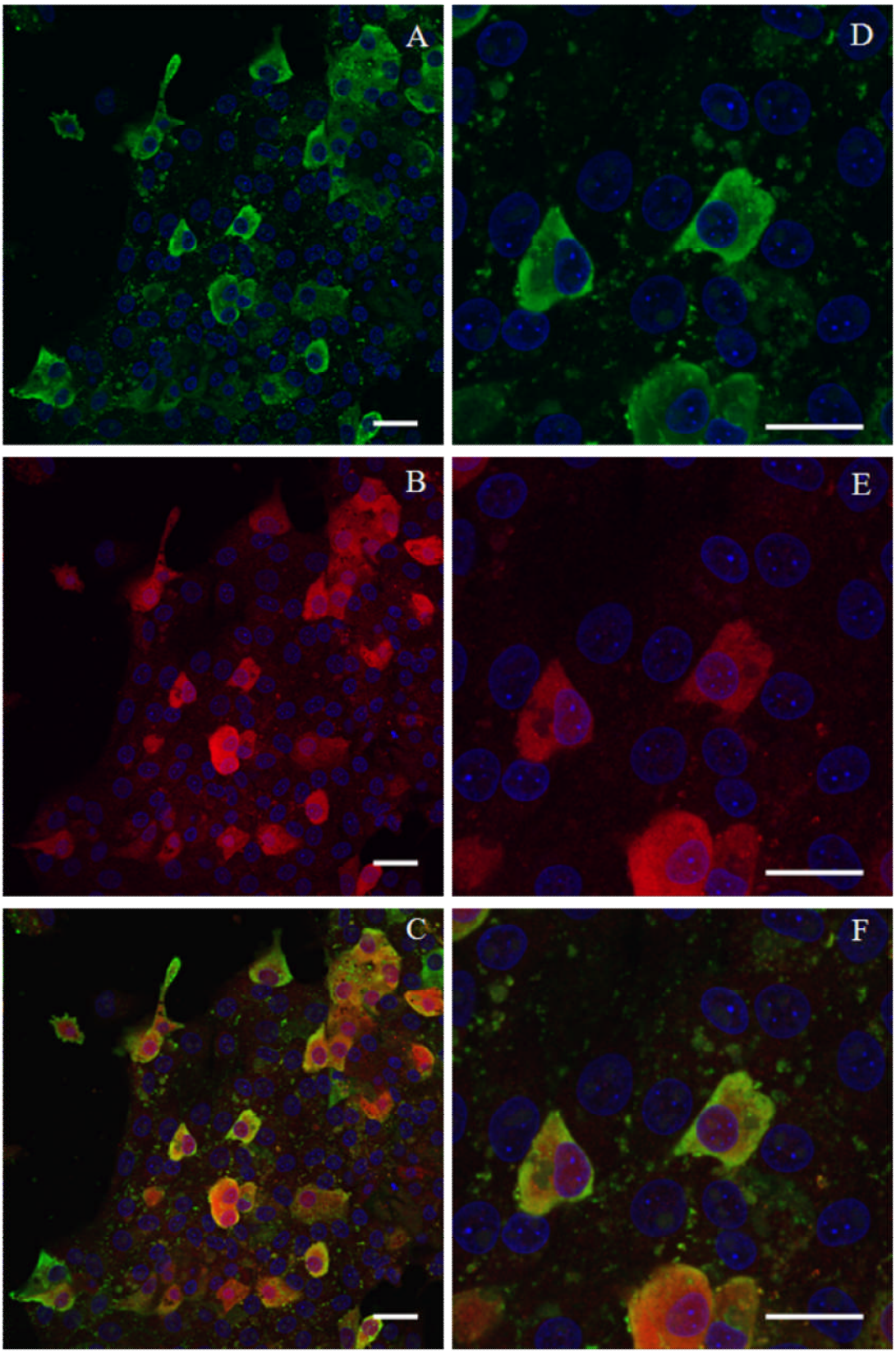
A
D
B
E
C
F

Cellular distribution of FLAG-tagged 5a and 5b in transfected Vero cells

Due to the lack of an antibody which would bind the 5a protein the cellular distribution of the 5a protein was identified by transfecting Vero cells with a plasmid which could express an epitope (FLAG) tagged version of the protein. Antibodies directed against the tag were used in indirect immunofluorescence experiments to assess the subcellular localisation.

Vero cells were transfected with a plasmid expressing a N-terminally FLAG-tagged version of the 5a protein. Images taken of these cells after indirect immunofluorescence with confocal microscopy indicated that the FLAG/5a protein displayed a punctate, cytoplasmic distribution pattern (Fig. 4.11) similar to that observed with the FLAG/3a protein (Chapter 3 Fig. 3.14). This pattern was the same in transfected only (red pattern only) or infected and transfected cells (green and red pattern) (Fig. 4.11) meaning that the cellular distribution of FLAG/5a was not reliant on other Beau-R proteins and that the FLAG/5a protein was probably membrane associated.

The subcellular distribution of the 5b protein had already been observed within Beau-R infected CK cells (Fig. 4.1). The objective of identifying the distribution of the FLAG/5b protein within transfected cells was to ensure that the tagged 5b protein targeted to the same subcellular site as the native 5b protein. This would mean that the FLAG tag was not having an adverse affect on the subcellular location of the 5b protein and consequently that any pull-down assays were more likely to identify specific interacting cellular proteins. The FLAG/5b protein expressed within transfected Vero cells displayed the same diffuse, cytoplasmic distribution pattern (Fig. 4.12) as seen in Beau-R infected Vero and CK cells. A punctate, cytoplasmic distribution was observed in a small number of cells expressing the FLAG/5b protein which could have been the result of overexpression of the recombinant protein. A similar distribution pattern within infected and transfected cells was indicative that the subcellular location of the 5b protein was independent of other viral proteins. Images of transfected/infected Vero cells dual labelled with anti-FLAG and anti-IBV antibodies suggested there were colocalisation events between the FLAG/5b and one or more IBV structural proteins (Fig. 4.12) as indicated by the yellow colour. This demonstrated that the 5b protein and at least one of the IBV structural proteins were

targeting to the same subcellular location. However the N protein has a diffuse, cytoplasmic distribution similar to the 5b protein which means that colocalisation by chance is likely and the anti-IBV serum is not N protein-specific so the limited amount of colocalisation observed in the cytoplasm may be due to another viral protein.

Figure 4.11. Indirect immunofluorescence analysis of the intracellular location of FLAG-tagged 5a protein within Beau-R infected Vero cells. Subconfluent Vero cells were infected with Beau-R and transfected with pFLAG/5a. After 24 h of infection the cells were fixed with paraformaldehyde and permeabilised with Triton X-100. Cells were labelled with chicken anti-IBV (A and D) and mouse anti-FLAG (B and E). Secondary antibodies included Alexa Fluor 488 anti-chicken (green) and Alexa Fluor 568 anti-mouse (red). Nuclei were labelled with DAPI (blue). Each wavelength (colour) was scanned separately and the images digitally merged (C and F). Two different areas of the same experiment are displayed. Images A, B, C and D, E, F are two different fields of view of the same experiment. Scale bar indicates 20 μm.

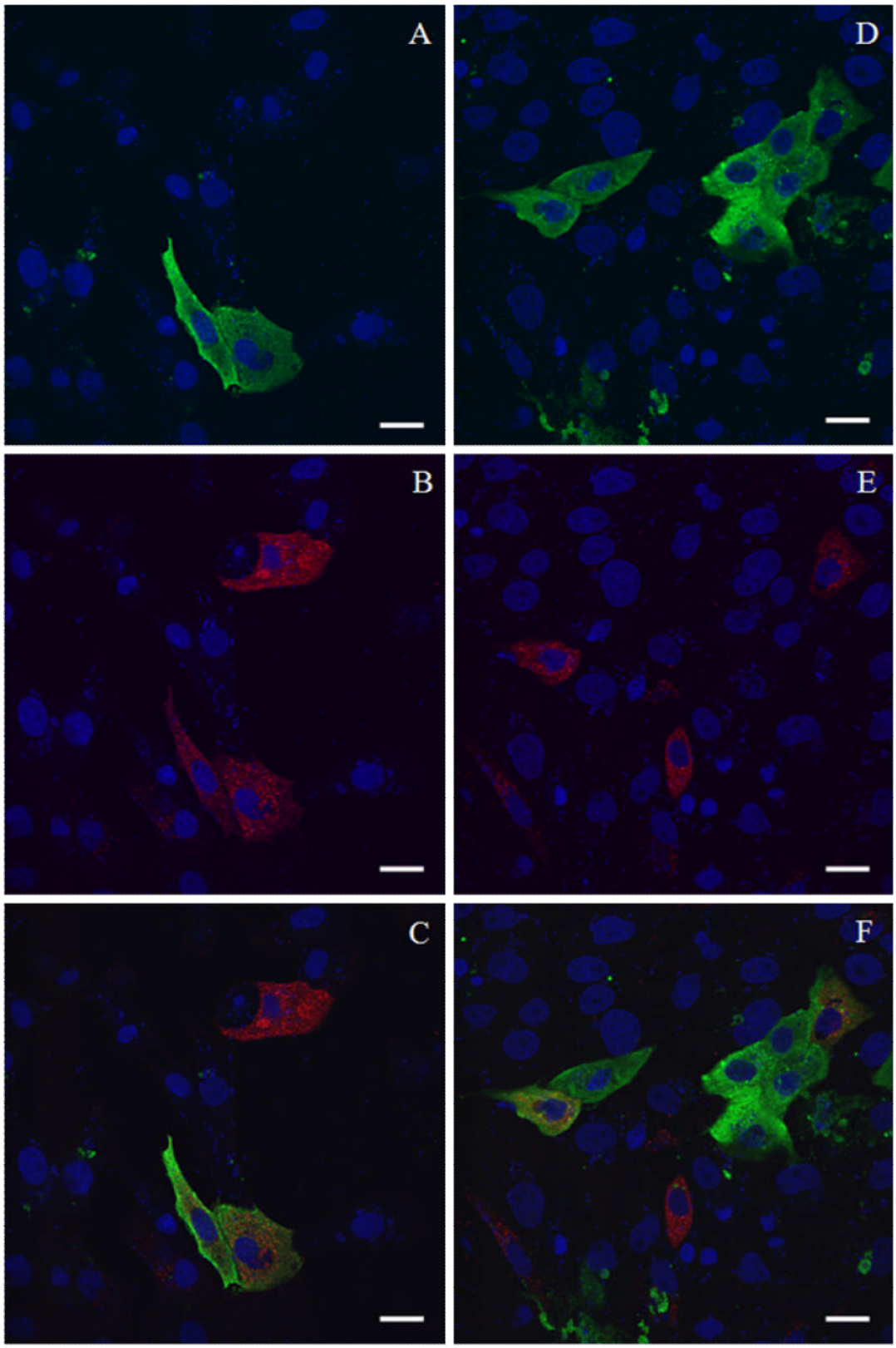
A
D
B
E
C
F

Figure 4.12. Indirect immunofluorescence analysis of the intracellular location of FLAG-tagged 5b protein within Beau-R infected Vero cells. Subconfluent Vero cells were infected with Beau-R and transfected with pFLAG/5b. After 24 h of infection the cells were fixed with paraformaldehyde and permeabilised with Triton X-100. Cells were labelled with chicken anti-IBV (A and D) and mouse anti-FLAG (B and E). Secondary antibodies included Alexa Fluor 488 anti-chicken (green) and Alexa Fluor 568 anti-mouse (red). Nuclei were labelled with DAPI (blue). Each wavelength (colour) was scanned separately and the images digitally merged (C and F). Two different areas of the same experiment are displayed. Images A, B, C and D, E, F are two different fields of view of the same experiment. Scale bar indicates 20 μm.

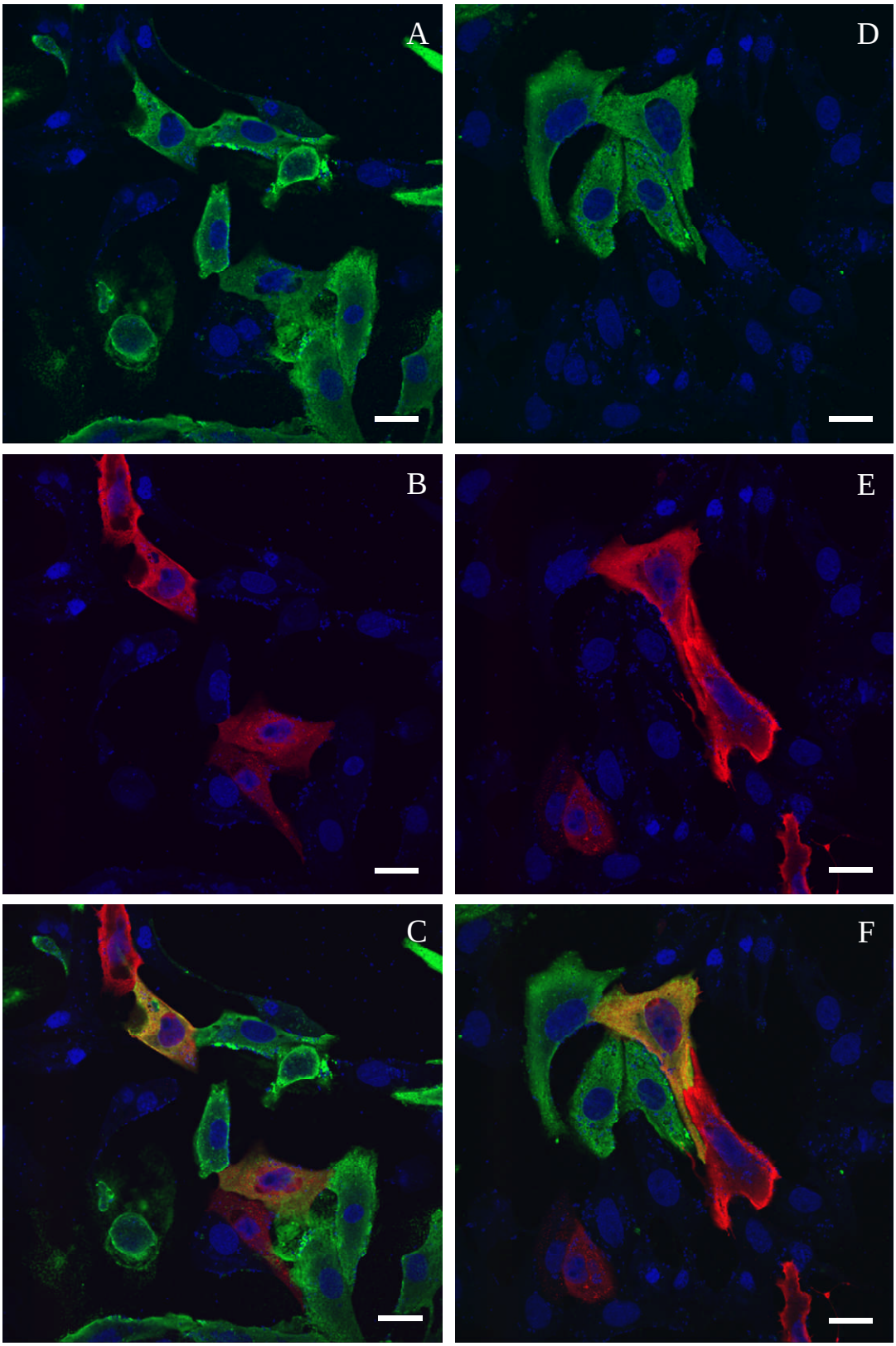
A
D
B
E
C
F

Expression of 5b in infected CK cells

In addition to the subcellular distribution the expression of the 5b protein was analysed during the course of a single replication cycle. Western blot analysis of Beau-R infected CK cell lysates demonstrated that the 5b protein was first detected at 5 h p.i. (Fig. 4.13) This was within an hour of the 6 h p.i. detection of the 3a protein (Chapter 3 Fig. 3.16) and indicated that the Beau-R accessory proteins have been produced in detectable amounts by 5-6 h p.i.

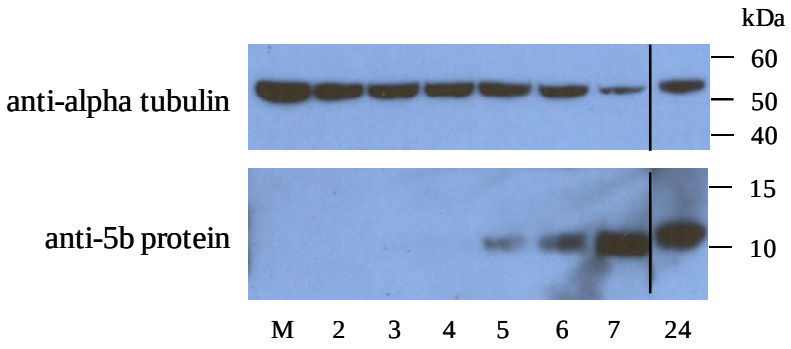

Figure 4.13. Time course of 5b expression during Beau-R infection. Subconfluent CK cells were infected with Beau-R for the indicated h p.i. Cells were lysed and clarified by centrifugation. The protein samples were separated by PAGE and the proteins were transferred to PVDF membrane. The membrane was probed with either mouse anti-alpha tubulin (Sigma) (top panel) or rat anti-5b protein antibody (bottom panel). Primary antibodies were detected with HRP-conjugated anti-mouse or anti-rat antibody and the Immobilon Western detection system. Time in h p.i. along the bottom and molecular weight markers along the side. M = mock infected CK cells.

Discussion

The objective of this study was to determine the subcellular location of the gene 5 accessory proteins. Beau-R infected Vero and CK cells were used to assess, by immunofluorescence and confocal microscopy, the distribution of the 5b protein and its cellular location as compared to markers for various subcellular structures. The diffuse cytoplasmic distribution did not colocalise with subcellular structures, such as the ER and Golgi apparatus, and considering that the viral structural proteins S

and M are translated at and targeted to these same cellular structures it was not surprising to find that there was very little colocalisation between the 5b protein and sites of S and M protein accumulation. The colocalisation observed between the FLAG/5b protein and an IBV structural protein in infected/transfected cells suggested that some of the 5b protein was targeting to sites occupied by an IBV structural protein. The N-terminal FLAG tag may have had an effect on the FLAG/5b protein to alter its cellular location towards targeting to sites of the IBV structural protein and/or the higher level of FLAG/5b protein expression from transfected cells may have simply flooded the system to increase the probability of cytoplasmic FLAG/5b protein occupying a similar spatial area to the IBV structural protein, which couldn't be differentiated by the resolution of the technique. Alternatively, lower amounts of 5b protein produced in infected cells may not have been enough to cause the colocalisation with the IBV structural protein observed in transfected/infected cells. Either way the observed distribution of the FLAG/5b protein was similar to that of the native 5b protein observed in infected cells and therefore the tagged 5b protein could be assumed to be interacting with similar cellular proteins which interact with the native 5b protein. The diffuse, cytoplasmic distribution of the 5b protein observed within infected cells was in slight contrast to that observed by Liu and Inglis (1992a) in immunofluorescence experiments. Using anti-sera raised against whole 5b protein they demonstrated that within IBV-infected Vero cells the 5b protein displayed a diffuse staining pattern which appeared punctate, particularly concentrated in the perinuclear region. The anti-5b antibody SK71 was raised against two peptides corresponding to the C-terminal 30 amino acids of the Beau-R 5b protein. The diffuse staining pattern observed was consistent between Liu and Inglis (1992a) and the images produced as part of this thesis. The punctate, perinuclear staining pattern could have been a result of antibodies binding to the N-terminal portion of the 5b protein. The same 5b protein contained within these punctate structures may have had the C-terminal portion unavailable for antibody binding due to interference by other cellular proteins and thus remained undetected by the anti-5b (C-terminal) protein antibody.

Due to the lack of an antibody directed towards the 5a protein, a FLAG-tagged protein was constructed and expressed in Vero cells. The FLAG/5a protein displayed a punctate, cytoplasmic distribution pattern. This subcellular expression profile was consistent between transfected and infected/transfected cells indicating that the

subcellular distribution of FLAG/5a was independent of other viral proteins. The similarities in subcellular distribution between the FLAG/3a, FLAG/5b proteins and their respective native proteins within an infected cell suggest that the pattern of FLAG/5a reflects the distribution of virally expressed 5a protein within a Beau-R infected cell. If the punctate pattern of FLAG/5a was an accurate representation then it suggested that the 5a protein was membrane associated, as suggested by Liu and Inglis (1992a). However, by indirect immunofluorescence they demonstrated that within IBV-infected Vero cells the 5a protein displayed a diffuse staining pattern with some apparent concentration around the nucleus. The viral dsRNA has a punctate, cytoplasmic distribution pattern within Beau-R infected cells and has already been shown to colocalise with another IBV accessory protein, the 3a protein (Chapter 3, Fig. 3.9), so the FLAG/5a may also colocalise with virus-derived dsRNA.

The expression profile of 5b protein within an infected CK cell indicated that it was first detected at 5 h p.i. This was likely to have been due to the detection limit of the technique. Detection by Western blot was reliant upon the accumulation of enough 5b protein which was only reached at 5 h p.i. An immunoprecipitation assay may have provided a more concentrated sample allowing detection of the 5b protein at earlier time points, but the anti-5b protein antibody does not work in immunoprecipitation experiments. Detection of 5b protein at 5 h p.i. was in partial agreement with the results of the immunofluorescence experiments where the 5b protein was initially detected at 6 h p.i. The diffuse nature of the 5b protein observed in infected cells by indirect immunofluorescence would have made detection at and prior to 5 h p.i. difficult to distinguish from background immunofluorescence levels.

Chapter 5: Towards discovering the protein-protein interactions by co-immunoprecipitation

Summary

Identification of the proteins which interact with the IBV accessory proteins would highlight the potential involvement of these viral proteins in virus replication. Isolation and identification of the interacting proteins could be performed using co-immunoprecipitation of the accessory proteins with the associated protein. The use of anti-IBV 3a and anti-IBV 5b protein antibodies for the immunoprecipitation of their respective antigens was assessed. Both antibodies were found to be unable to immunoprecipitate the target IBV proteins. An anti-3a protein antibody designated 3480 was acquired from another research group which could be used to immunoprecipitate the 3a protein. However, once this antibody was cross-linked to a solid support it was no longer able to immunoprecipitate the 3a protein. This would have meant that when a co-immunoprecipitation experiment, protein separation by PAGE and silver staining was performed to identify novel protein interactions the heavy and light chains of the antibody used to immunoprecipitate the 3a protein would obscure any potentially interacting proteins around 50 kDa and 25 kDa, respectively. This anti-3a protein antibody also had a high background which would have made distinguishing interacting proteins from false positives complicated and time-consuming.

These data did confirm the reports that the anti-3a protein antibody 3480 could immunoprecipitate the 3a protein from infected cell lysates (Pendleton and Machamer, 2005). Therefore this antibody could be used to confirm a protein interaction after the interaction was originally identified using other techniques.

Introduction

The role(s) which the IBV accessory proteins play during infection has not yet been identified. Discovery of the protein-protein interactions which are associated with these proteins would provide an understanding as to their function.

The experimental approach used involved the immunoprecipitation of the accessory proteins from IBV-infected cell lysates and subsequent identification of any proteins which co-precipitated (i.e. potentially interacting with the accessory protein) by mass spectrometry. The anti-3a protein antibodies and anti-5b protein antibodies were assessed for their compatibility with this approach. These polyclonal antibodies were raised against peptides generated from the N-terminal and C-terminal portions of the 3a and 5b proteins, respectively. The anti-3a protein antibodies were raised in rabbits and the anti-5b protein antibodies were raised in rats. As well as the antibodies used the immunoprecipitation procedures involved utilising a solid support to separate the protein of interest from the rest of the cell lysate. This is done by allowing an antibody to bind its respective antigen and then binding this antibody/antigen complex to a solid support or allowing the antibody to bind to the solid support first. The antibody/antigen/solid support complex is then separated from the rest of the cell lysate to isolate the protein of interest. The choice of solid support can be crucial to the success of the experiment. Two common supports are used, which are Protein G and Protein A. Both were originally cell wall components of group G *Streptocci* and *Staphylococcus aureus* respectively which bound the Fc portion of most mammalian antibodies. They have since been engineered and cross-linked to agarose or magnetic beads to provide an effective way of isolating the antibody/antigen complex from the cell lysate. Protein G and Protein A have different specificities for binding to mammalian antibodies. Both proteins have a reported strong binding to rabbit IgG. Protein G has a higher affinity for rat IgG than Protein A and was therefore used for immunoprecipitation experiments performed as part of this thesis.

Results

Immunoprecipitation experiments using the anti-3a antibodies

Identification of the potential proteins interacting with the 3a protein required that the anti-3a protein antibody could immunoprecipitate the 3a protein from cell lysate. The anti-3a protein antibody 8194 had already been used to detect 3a protein in Beau-R-infected cells by immunofluorescence (Chapter 3 Fig. 3.1). The ability of this antibody to bind and pull out the 3a protein from infected cell lysates was assessed by Western blot of an immunoprecipitation experiment. A limited amount of anti-3a protein antibody 3480 was also acquired as a gift from Dr Carolyn Machamer (John Hopkins University School of Medicine, Baltimore, USA) which had been reported to immunoprecipitate the 3a protein from infected cell lysates (Pendleton and Machamer, 2005). Immunoprecipitation experiments using both anti-3a protein antibodies indicated that the 3a protein was present in the eluted sample when the anti-3a protein antibody 3480 was used but was absent in the eluted sample when the anti-3a protein antibody 8194 was used (Fig. 5.1). This demonstrated that the anti-3a protein antibody 8194 could not be used to immunoprecipitate a detectable amount of 3a protein from Beau-R-infected cell lysates. This was in contrast to the anti-3a protein antibody 3480 which could immunoprecipitate the 3a protein from infected cell lysates. The presence of 3a protein in the cell lysate after immunoprecipitation indicated that the amount of anti-3a protein antibody used for the experiment was insufficient to immunoprecipitate all of the 3a protein. Therefore some of the 3a protein remained in the infected cell lysate and was identified within the samples.

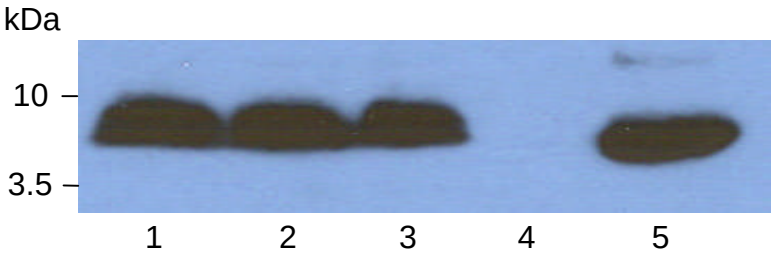

Figure 5.1. Immunoprecipitation of IBV 3a using anti-3a protein antibodies. Subconfluent CK cells were infected with Beau-R. After 36 h the cells were lysed and clarified by centrifugation. Anti-3a (8194) or anti-3a (3480) antibodies were combined with Beau-R infected CK cell lysate and incubated for 16 h. Dynabeads/Protein G were added to the cell lysate and mixed. The beads were washed with lysis buffer. Proteins were eluted and the samples were separated by PAGE. Proteins were transferred to PVDF membrane. The membrane was probed with anti-3a protein antibody 3480 and detected with HRP-conjugated anti-rabbit antibody and the Immobilon Western detection system. Lane 1 – 15 µl sample of the 550 µl total Beau-R infected cell lysate. Lane 2 – 15 µl sample of the 250 µl total infected cell lysate after immunoprecipitation using anti-3a antibody 8194. Lane 3 - 15 µl sample of the 250 µl total infected cell lysate after immunoprecipitation using anti-3a antibody 3480. Lane 4 – 15 µl sample of the 30 µl total immunoprecipitated proteins after using anti-3a antibody 8194. Lane 5 - 15 µl sample of the 30 µl total immunoprecipitated proteins after using anti-3a antibody 3480.

Due to the failure of our anti-3a protein antibody 8194 to immunoprecipitate 3a protein the anti-3a protein antibody 3480 was assessed in its ability to be used in the co-immunoprecipitation experiments. This particular technique required that the antibody be cross-linked to the Protein G beads prior to the immunoprecipitation step. If the antibody wasn't cross-linked the eluted sample would contain the antibody used for the immunoprecipitation. When the eluted proteins were separated by PAGE the heavy and light chains of the antibodies would obscure any potential interacting protein around the 50 kDa and 25 kDa positions, respectively. Western blot analysis of an immunoprecipitation experiment using the cross-linked antibody indicated that the amount of 3a protein contained within the eluted sample was far less than the amount of protein in the unprocessed cell lysate or the supernatant after immunoprecipitation. The anti-3a protein antibody was therefore not effective in precipitating the 3a protein from infected cell lysate when it was first cross-linked to Protein G (Fig. 5.2) but could be used to confirm a novel protein interaction identified using other techniques.

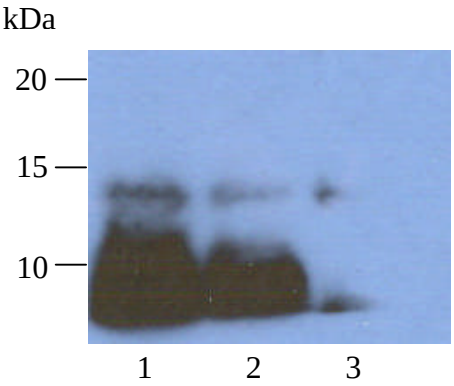

Figure 5.2. Immunoprecipitation of 3a protein using the anti-3a protein 3480 antibody cross-linked to Dynabeads Protein G. Subconfluent CK cells were infected with Beau-R. After 36 h the cells were lysed and clarified by centrifugation. Anti-3a protein antibody 3480 was bound to Dynabeads/Protein G and cross-linked. Antibody/Protein G was combined with Beau-R infected CK cell lysate and incubated. The beads were washed with lysis buffer. The eluted protein samples were separated by PAGE and transferred to PVDF membrane. The membrane was probed with anti-3a protein antibody 3480 and detected with HRP-conjugated anti-rabbit antibody and the Immobilon Western detection system. Lane 1 – 15 µl sample of the 550 µl total Beau-R infected cell lysate. Lane 2 – 15 µl sample of the 500 µl total infected cell lysate after immunoprecipitation using the anti-3a protein antibody 3480. Lane 3 – 15 µl sample of the 30 µl total immunoprecipitated proteins after using anti-3a protein antibody 3480.

Immunoprecipitation experiments using the anti-5b antibodies

An anti-5b protein antibody SK71 had previously been used to detect 5b protein in Beau-R infected cells by immunofluorescence (Chapter 4 Fig. 4.1). The capability of this antibody to be used in co-immunoprecipitation was assessed. A protein of approximately 10 kDa was identified in the lysate of Beau-R infected CK cells (Fig. 5.3, lane 2), whereas a corresponding band was not detected in the lysates of mock-infected CK cells (Fig. 5.3, lane 1). The calculated molecular weight for IBV 5b is 9.3 kDa and it would therefore appear likely that the 10 kDa protein detected by the anti-5b protein antibody SK71 was the 5b protein. Analysis of immunoprecipitation experiments indicated that the 5b protein was not detected within the immunoprecipitated proteins when using the anti-5b protein antibody SK71 was used in combination with either Dynabeads/Protein G or Sepharose/Protein G (Fig. 5.3). This indicated that the anti-5b protein antibody could not recognise the folded 5b protein and/or stay bound to the 5b protein during the immunoprecipitation

procedure. The additional proteins detected within the immunoprecipitated proteins at 25 kDa and above were due to detection of the heavy and light chains which comprised the anti-5b protein antibody used to immunoprecipitate the 5b protein. The IgG light chain has a calculated molecular weight of 25 kDa and the heavy chain has a calculated molecular weight of 50 kDa. These were observed in the eluted samples. The additional bands at 100 and 150 kDa were probably dimers of the heavy chain. Alternatively the larger molecular weight proteins could have been intact IgG antibodies from the failure to properly dissociate the antibodies into their constituent heavy and light chains.

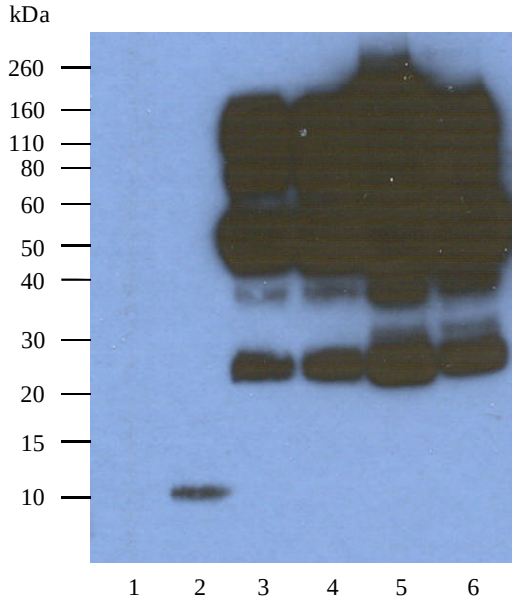

Figure 5.3. Analysis of the anti-5b protein antibody SK71 for use in immunoprecipitation experiments. Subconfluent CK cells were infected with Beau-R. After 36 h the cells were lysed and clarified by centrifugation. Rat anti-5b protein antibodies SK71 were combined with mock or Beau-R-infected CK cell lysate. Dynabeads/Protein G or Protein G/Sepharose were added to the cell lysate. After mixing, the beads or Sepharose were washed with lysis buffer. The eluted proteins were separated by PAGE and transferred to PVDF membrane. The membrane was probed with anti-5b protein antibody SK71 and detected with HRP-conjugated anti-rat antibody and the Immobilon Western detection system. Lane 1 = mock-infected CK cell lysate. Lane 2 = Beau-R-infected CK cell lysate. Lane 3 = immunoprecipitated proteins from mock-infected CK cells using Dynabeads/Protein G. Lane 4 = immunoprecipitated proteins from Beau-R-infected CK cells using Dynabeads/Protein G. Lane 5 = immunoprecipitated proteins from mock-infected CK cells using Sepharose beads. Lane 6 = immunoprecipitated proteins from Beau-R-infected CK cells using Sepharose beads.

A lack in immunoprecipitation by the anti-5b protein antibody also could have been influenced by the binding potential of Protein G for different rat IgG subclasses. The binding affinity of rat IgG_1, IgG_{2b} and IgG_{2c} for Protein G has been reported to be medium/weak (GE Healthcare / Invitrogen). An alternative to Protein G is Protein A however the binding affinity of rat IgG for Protein A has been reported to be weak or absent (GE Healthcare / Invitrogen). The anti-5b protein antibody used was a polyclonal set of antibodies contained in rat serum. The subclass of IgG which bound the 5b protein was not determined as the serum was not affinity purified to provide pure IgG with which to test. The rat IgG which bound the 5b protein in immunofluorescence and Western blot analysis could have been one that was reported to have a weak binding affinity for Protein G. This could have meant that the antibody bound the 5b protein but that the antibody/protein complex was unable to bind to the solid support and thus remained in the supernatant. To circumvent this problem rabbit anti-rat IgG antibodies were used. All subclasses of rabbit IgG bind strongly to Protein G and thus the rabbit IgG would act as an intermediate to link the rat IgG to Protein G and the solid support. Analysis of the immunoprecipitation of 5b protein from infected cell lysate using this approach indicated that 5b protein was still detected only in the cell lysate after immunoprecipitation and absent from the immunoprecipitated proteins (Fig. 5.4). The binding of anti-5b protein antibody SK71 to the 5b protein would appear to be the limiting factor when using the anti-5b protein antibody for immunoprecipitation experiments. The anti-5b protein antibody SK71 was therefore unsuitable to be used in co-immunoprecipitation experiments because it could not be used to immunoprecipitate the 5b protein from infected cell lysates.

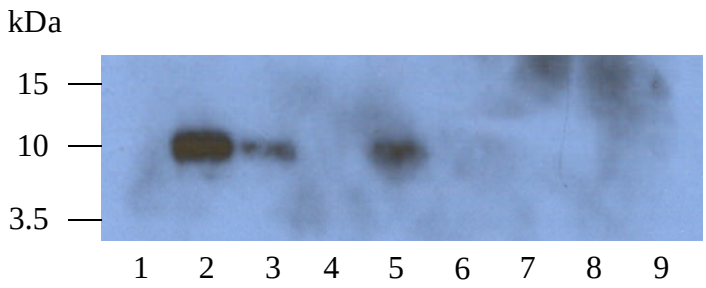

Figure 5.4. Analysis of the anti-5b protein antibody SK71 for use in immunoprecipitation experiments. Subconfluent CK cells were infected with Beau-R. After 36 h the cells were lysed and clarified by centrifugation. Rabbit anti-rat or rabbit anti-rat plus rat anti-5b protein antibodies SK71 were combined with mock or Beau-R infected CK cell lysate. Dynabeads/Protein G were added to the cell lysate. After mixing, the beads were washed with lysis buffer. The immunoprecipitated proteins were separated by PAGE and transferred to PVDF membrane. The membrane was probed with anti-5b protein antibody and detected with HRP-conjugated anti-rat antibody and the Immobilon Western detection system. Lane 1 – mock infected cell lysate. Lane 2 – Beau-R infected cell lysate. Lane 3 – Beau-R infected cell lysate after immunoprecipitation using the rabbit anti-rat IgG antibody. Lane 4 – mock infected cell lysate after immunoprecipitation using rabbit anti-rat IgG antibody plus rat anti-5b protein antibody SK71. Lane 5 – Beau-R infected cell lysate after immunoprecipitation using the rabbit anti-rat IgG antibody plus the rat anti-5b protein antibody. Lane 6 – immunoprecipitated proteins after using the rabbit anti-rat IgG antibody with mock infected cell lysate. Lane 7 – immunoprecipitated proteins after using the rabbit anti-rat antibody with Beau-R infected cell lysate. Lane 8 – immunoprecipitated proteins after using the anti-rat IgG plus rat anti-5b protein antibody with mock infected cell lysate. Lane 9 – eluted proteins from the immunoprecipitation using rabbit anti-rat IgG plus anti-5b protein antibody with Beau-R infected cell lysate.

Discussion

Experimental procedures designed to discover proteins-protein interactions include the immunoprecipitation of a target protein from a cell lysate and identification of the co-precipitating proteins. To facilitate this process an antibody is required which not only recognises the target protein but stays bound to that target protein during the wash steps of the immunoprecipitation required to remove any contaminating proteins. Antibodies were available which recognised the 3a and 5b proteins by indirect immunofluorescence within infected cells and in infected cell lysates by Western blot. The use of these antibodies for co-immunoprecipitation experiments

was evaluated. Neither of the anti-3a protein antibodies nor the anti-5b protein antibody could be used or were suitable for use in the co-immunoprecipitation experiments to identify novel protein interactions. Only the anti-3a protein antibody 3480 could be used to immunoprecipitate its target antigen.

Two factors are involved when considering the characteristics of antibodies: the binding affinity of the antibody and the epitope which the antibody recognises. An antibody could have enough affinity to bind its target under gentle conditions but not enough to bind or stay bound under stringent conditions. Alternatively, the epitope which is recognised may be inaccessible or unrecognisable under certain conditions. The anti-5b protein antibody had enough affinity for its target protein to bind and allow detection (by Western blot and immunofluorescence) but may not have had enough to bind or stay bound during the immunoprecipitation steps. The epitope which was recognised by the anti-5b protein antibody would have also determined its usefulness. The anti-5b protein antibody was raised against two peptides corresponding to the C-terminal portion of the 5b protein. The denatured form of the 5b protein found in Western blot and immunofluorescence experiments was likely to have a similar configuration. However, due to the non-denaturing conditions of the cell lysis buffer the 5b protein would have retained a folded state in the infected cell lysate used for the immunoprecipitation experiments. This protein conformation may have made the antibody binding site inaccessible or unrecognisable. The anti-3a protein antibody 8194 only bound to 3a protein during immunofluorescence. As with the anti-5b protein antibody epitope recognition and binding affinity caused the antibody to be suitable for only some experiments.

An anti-3a protein antibody was received from Dr Carolyn Machamer. This antibody had been used to immunoprecipitate the 3a protein (Pendleton and Machamer, 2005) and was used as a positive control during the experiments to show whether the anti-3a antibody 8194 could be used for immunoprecipitation. The anti-3a protein antibody 8194 couldn't be used to immunoprecipitate the 3a protein, so the anti-3a antibody 3480 was tested for its potential use in the co-immunoprecipitation experiments. When cross-linked to Protein G this antibody could only precipitate a small amount of the original input 3a protein. Without cross-linking the antibody the heavy and light chains that make up the antibody would produce strong bands at 50 and 25 kDa (and probably higher due to the formation of dimers), thereby interfering with the identification of potentially interacting proteins around these molecular

weights. It would also mean that the antibody couldn't be re-used. This was particularly important for the anti-3a protein antibody 3480 as there was only a limited amount received. The difference in success between the two approaches to the immunoprecipitation of the 3a protein could have been due to the state of the antibody involved. Free antibody was used when the experiment was successful and cross-linked antibody was used when this success was extremely limited. Free antibody would have been able to diffuse through the cell lysate more effectively than antibody bound to a solid support, such as the magnetic beads. This would have meant that more of the stable antibody/antigen complexes would have formed allowing additional antigen to be separated from the other non-specific proteins.

Chapter 6: Protein-protein interactions of the accessory proteins using pull-down assays

Summary

IBV encodes for four accessory proteins, 3a, 3b, 5a and 5b, ranging between 57 and 82 amino acids in length. The functions of these proteins are presently unknown. To begin to understand their role in the virus replication cycle the proteins to which they interact have been investigated. Using FLAG-tagged recombinant accessory proteins the potential protein interactions of the IBV 3a protein have been identified. Potential interactions include GCN1 which could affect host cell protein synthesis, protein phosphatase 2A which may lead to inhibition of IFN-α signalling, arrest of the cell cycle and/or apoptosis and Exportin-1 the inhibition of which may attenuate the nuclear export of a specific subset of cellular mRNAs.

Introduction

When specific antibodies to a protein are not available the protein can be purified from a complex mixture through the use of a tag. These tags are additional specific amino acids which allow binding to tag-specific antibodies or solid supports. However the addition of a tag sequence to a protein of interest can interfere with the folding and interactions of that protein. Minimisation of these potential shortcomings can be accomplished by using tags with short sequences composed of neutral amino acids and by inserting them either N- or C-terminally. For example the His-tag is composed of six histidine amino acids ensuring a short sequence, but does result in a highly basic charge wherever it is inserted within the protein sequence. Purification of His-tagged proteins can be performed at a high capacity (5-10 mg His-tagged protein per ml of His-tag binding solid support) and the process is cheap to purify a

set amount of tagged protein compared to other techniques (Lichty *et al.*, 2005). Alternatively, the FLAG-tag is eight amino acids in length with a more neutral charge than the His-tag. It contains five acidic residues balanced by one neutral and two basic residues. Purification of FLAG-tagged proteins has been shown to result in a low background but has a limited capacity (0.6 mg of FLAG-tagged protein per ml of anti-FLAG antibody linked to agarose) and is expensive compared to His-tag purification (Lichty *et al.*, 2005).

Expression and purification of a tagged protein from cell lysates can be used to identify novel protein interactions. The tagged protein is precipitated and the proteins which coprecipitate can be identified by mass spectrometry. Confirmation of the protein interactions within the context of an IBV-infected cell would be performed to provide further evidence for the interaction. The use of recombinant IBVs (rIBV) which lacked the expression of individual accessory proteins would enable additional control experiments. These rIBVs have been constructed and the lack of accessory protein expression confirmed (Casais *et al.*, 2005; Hodgson *et al.*, 2006), such as rIBV ScAUG3a which does not express detectable quantities of the 3a protein.

Host cell translation and GCN1

Virus infection can result in the attenuation of host cell translation. Eukaryotic protein translation initiation involves the assembly of eukaryotic initiation factors (eIF) with the 40S and 60S ribosomal subunits and mRNA to identify the start codon and proceed with translation. The eIF4F complex consists of three subunits. eIF4G acts as the scaffolding protein, eIF4E binds to the 5' cap structure of mRNAs and eIF4A possesses ATP-dependent RNA helicase activity. eIF3 binds to the small (40s) ribosomal subunit and also interacts with eIF4G to bring the complexes together. The translation process is initiated by a methionine-charged tRNA binding to eIF2 and translocation to the P site of the ribosome. eIF2 hydrolyses GTP to GDP which allows the release of several factors and association of the large (60s) ribosomal subunit to form the complete 80s ribosomal complex. This begins translation elongation. Initiation of protein translation requires that the GDP attached to eIF2 is converted back to GTP. The guanine nucleotide exchange factor eIF2B is required for this conversion. The eIF2 complex consists of three subunits, α, β and γ. Phosphorylation of the eIF2α subunit causes an inhibition to the activity of eIF2B and the cessation of translation initiation.

Phosphorylation of the eIF2α subunit can be performed from the action of four proteins in mammalian cells: 1) PKR is activated by dsRNA which is commonly found in virus infected cells. 2) PKR-like ER kinase (PERK) is activated in response to misfolded proteins in the ER. 3) Haem-regulated inhibitor is activated by haem deprivation and stress caused by oxidation and heat. 4) general control non-derepressible (GCN) 2 activated during amino acid deprivation, UV irradiation and proteasome inhibition. GCN1 is a large (297 kDa) protein which interacts with GCN20 (Vazquez de Aldana *et al.*, 1995) to activate GCN2 (Garcia-Barrio *et al.*, 2000; Marton *et al.*, 1993). The GCN1/GCN20 complex interacts with polyribosomes to promote GCN2 activation by uncharged tRNAs (Marton *et al.*, 1997; Sattlegger and Hinnebusch, 2000). Indirect immunofluorescence using ani-GCN1 antibody with yeast cells indicated a diffuse, cytoplasmic distribution pattern was observed for GCN1 (Marton *et al.*, 1997). Using SARS-CoV-infected cells PKR and PERK were both shown to be activated but GCN2 was not activated (Krahling *et al.*, 2009). The suppression of PKR expression in SARS-CoV-infected cells did not affect viral replication (Krahling *et al.*, 2009). MHV replication has been shown to be increased from 8 h p.i. in cells which could only express the mutant non-phosphorylatable eIF2α (Raaben *et al.*, 2007) which suggested that host cell protein translation inhibition was not directly beneficial to MHV replication but may contribute to the downregulation of components of the anti-viral response.

Protein phosphatase 2A (PP2A)

The core subunits for PP2A comprise a scaffolding A subunit, a catalytic C subunit and a variety of different regulatory B subunits. The B subunit regulates the activity of the heterotrimeric enzyme (Kamibayashi *et al.*, 1994). PP2A is primarily a serine/threonine phosphatase involved in the dephosphorylation, and thus inactivation, of many protein kinases which affect the cell cycle (Voorhoeve *et al.*, 1999), signal transduction (Westphal *et al.*, 1998) and apoptosis (Shtrichman *et al.*, 1999). PP2A can also affect transcription by negatively regulating the transcription factors NF-κB (Sontag *et al.*, 1997), AP1/SRE (Frost *et al.*, 1994), Sp1 (Vlach *et al.*, 1995) and CREB (Wheat *et al.*, 1994). The subcellular location of PP2A, which can be cytoplasmic or nuclear, is dependent upon the specific B subunit which completes the heterotrimeric complex (McCright *et al.*, 1996). PP2A can translocate and

become active within a cell due to a signal-mediated process (Ludowyke *et al.*, 2000).

Exportin-1

Exportin-1 is a nuclear protein which shuttles between the nucleus and the cytoplasm (Stade *et al.*, 1997). It facilitates the nuclear export of proteins containing a nuclear export signal (Fornerod *et al.*, 1997). As well as proteins, Exportin-1 has also been implicated in facilitating the nuclear export of ribosomal RNA (Thomas and Kutay, 2003) and specific subsets of mRNA (Schutz *et al*. 2006).

Results

Using the expression of tagged accessory proteins to identify protein interactions

The identification of protein interactions using tagged proteins required the consideration of several different issues which can arise. Expression of the tagged protein may result in a different subcellular localisation pattern to that which the native protein would display, the tag may cause the mis-folding of the protein and if the protein does fold correctly the tag may interfere with protein interactions at the specific termini to which it is attached. To counter these possible scenarios plasmids which would express the IBV accessory proteins with a C-terminal His-tag or N-terminal FLAG-tag were constructed. The subcellular location of each tagged protein was also examined by observation of the colour distribution present in images obtained of transfected Vero cells after indirect immunofluorescence and confocal microscopy to ensure that the tags were not adversely affecting the distribution pattern. Expression of the C-terminally His-tagged accessory proteins using anti-His tag antibody in indirect immunofluorescence experiments could not be detected after transfection of Vero and CK cells and was not taken forward. Expression of the N-terminally FLAG-tagged 3a, 5a and 5b proteins could be detected as shown by the red colour representing the location of FLAG-tagged protein in images of transfected Vero cells labelled with an anti-FLAG antibody (Chapter 3 Fig. 3.14 and Chapter 4

Fig. 4.11 and 4.12 and shown here for clarity, Fig. 6.1 – FLAG/3a, Fig. 6.2 – FLAG/5a, Fig. 6.3 – FLAG/5b). The cellular distribution of the fluorescence, which indicated the location of the FLAG-tagged protein, was the same whether the other viral proteins were present or absent in most of the images. This was interpreted to suggest that the subcellular locations of the FLAG-tagged IBV accessory proteins were independent of the other viral proteins and that because of this independence the FLAG-tagged accessory proteins would also interact with the same cellular proteins which they would if the cell had been infected with Beau-R expressing native accessory proteins.

Figure 6.1. Indirect immunofluorescence analysis of the intracellular location of FLAG-tagged 3a protein within Beau-R infected Vero cells. Subconfluent Vero cells were infected with Beau-R and transfected with pFLAG/3a. After 24 h of infection the cells were fixed with paraformaldehyde and permeabilised with Triton X-100. Cells were labelled with chicken anti-IBV (A and D showing infected cells) and mouse anti-FLAG (B and E showing transfected cells). Secondary antibodies included Alexa Fluor 488 anti-chicken (green) and Alexa Fluor 568 anti-mouse (red). Nuclei were labelled with DAPI (blue). Each wavelength (colour) was scanned separately and the images digitally merged (C and F). Two different areas of the same experiment are displayed. Images A, B, C and D, E, F are two different fields of view of the same experiment. Scale bar indicates 20 μm.

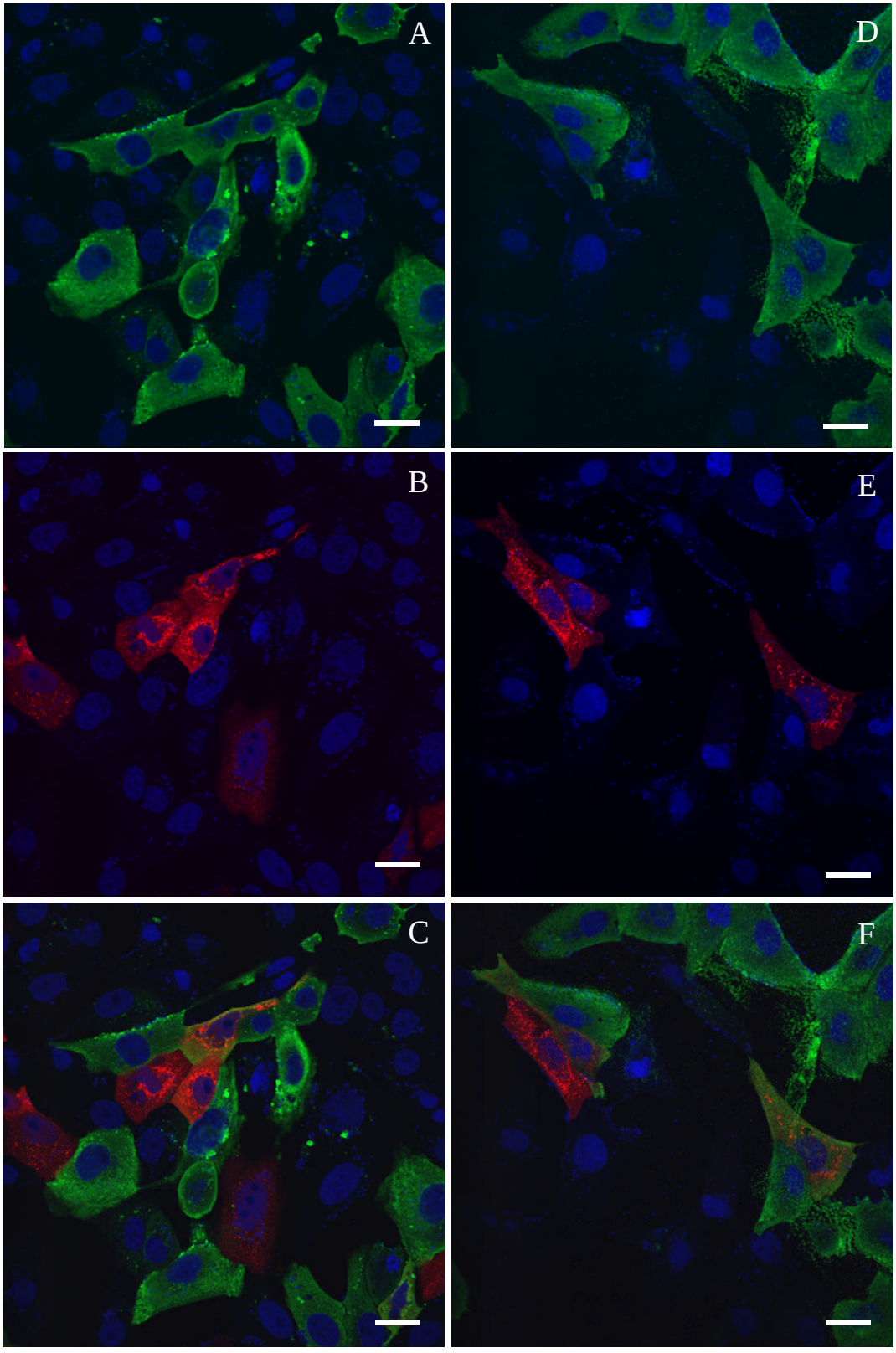
A
D
B
E
C
F

Figure 6.2. Indirect immunofluorescence analysis of the intracellular location of FLAG-tagged 5a protein within Beau-R infected Vero cells. Subconfluent Vero cells were infected with Beau-R and transfected with pFLAG/5a. After 24 h of infection the cells were fixed with paraformaldehyde and permeabilised with Triton X-100. Cells were labelled with chicken anti-IBV (A and D showing infected cells) and mouse anti-FLAG (B and E showing transfected cells). Secondary antibodies included Alexa Fluor 488 anti-chicken (green) and Alexa Fluor 568 anti-mouse (red). Nuclei were labelled with DAPI (blue). Each wavelength (colour) was scanned separately and the images digitally merged (C and F). Two different areas of the same experiment are displayed. Images A, B, C and D, E, F are two different fields of view of the same experiment. Scale bar indicates 20 μm.

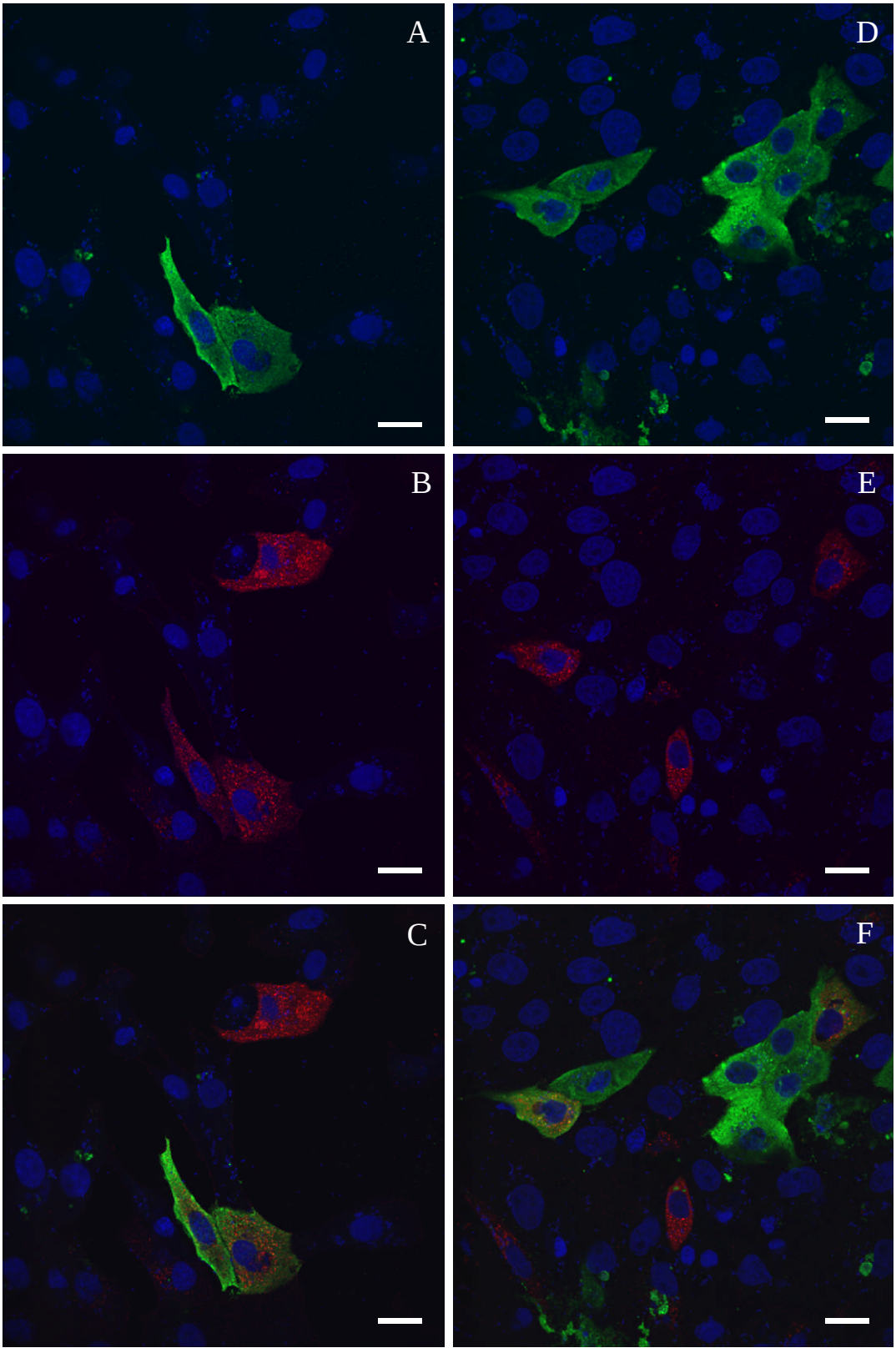
A
D
B
E
C
F

Figure 6.3. Indirect immunofluorescence analysis of the intracellular location of FLAG-tagged 5b protein within Beau-R infected Vero cells. Subconfluent Vero cells were infected with Beau-R and transfected with pFLAG/5b. After 24 h of infection the cells were fixed with paraformaldehyde and permeabilised with Triton X-100. Cells were labelled with chicken anti-IBV (A and D showing infected cells) and mouse anti-FLAG (B and E showing transfected cells). Secondary antibodies included Alexa Fluor 488 anti-chicken (green) and Alexa Fluor 568 anti-mouse (red). Nuclei were labelled with DAPI (blue). Each wavelength (colour) was scanned separately and the images digitally merged (C and F). Two different areas of the same experiment are displayed. Images A, B, C and D, E, F are two different fields of view of the same experiment. Scale bar indicates 20 μm.

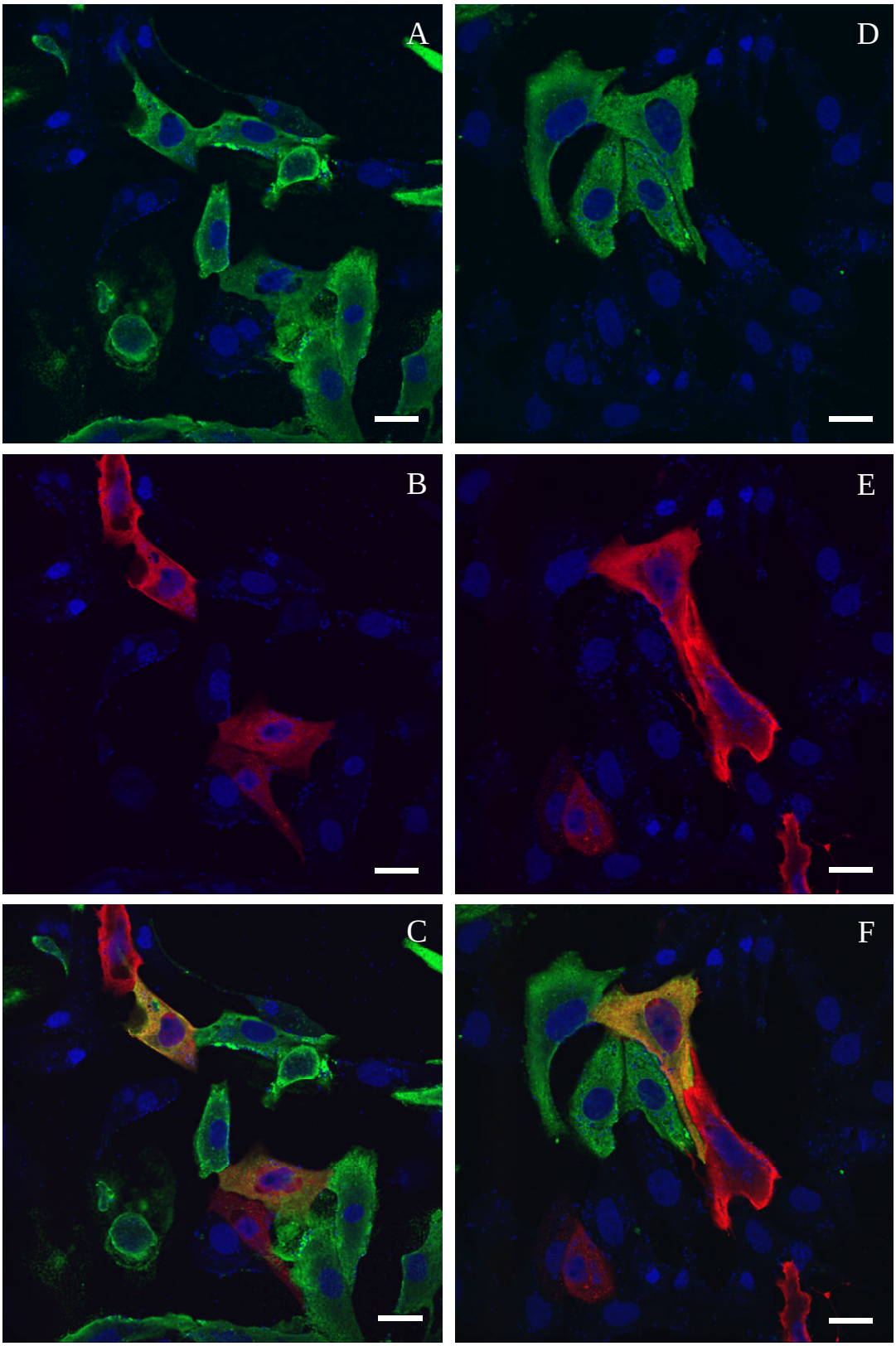
A
D
B
E
C
F

Expression of FLAG-tagged accessory proteins

Elucidation of the cellular proteins to which the IBV accessory proteins interact was conducted by immunoprecipitating the FLAG-tagged accessory proteins from transfected Vero cells and identifying any potential interacting proteins by mass spectrometry. The N-terminal FLAG-tagged accessory proteins were expressed in Vero cells and the lysates tested for the presence of the FLAG tag. Expression of the FLAG/3a protein was detected at the calculated molecular weight of 8.3 kDa (Fig. 6.4). Expression of the control protein, FLAG/BAP, was also detected at a calculated molecular weight of 55 kDa (Fig. 6.4). The anti-FLAG antibody could immunoprecipitate the FLAG-tagged 3a and BAP proteins from a lysate of transfected Vero cells (Fig. 6.4) as the FLAG-tagged proteins were partially removed from the cell lysate and were more concentrated in the immunoprecipitated sample. Expression of the FLAG/5a or FLAG/5b proteins could not be detected by Western blot using the anti-FLAG antibody at the calculated molecular weights of 9.1 and 10.9 kDa respectively (Fig. 6.5). Expression of the FLAG/5a and FLAG/5b proteins in transfected Vero cells had previously been confirmed by a strong signal in immunofluorescence experiments (Fig. 6.2 – FLAG/5a, Fig. 6.3 – FLAG/5b). Part of the procedure to perform the immunoprecipitation experiments involved centrifugation of the insoluble material after lysis of the cells. This would remove the proteins and other cell matter that could not be solubilised by the lysis buffer. The insoluble fraction of the cell lysate was analysed for the presence of the FLAG/5a and FLAG/5b proteins by lysing the transfected Vero cells and not performing the centrifugation step.

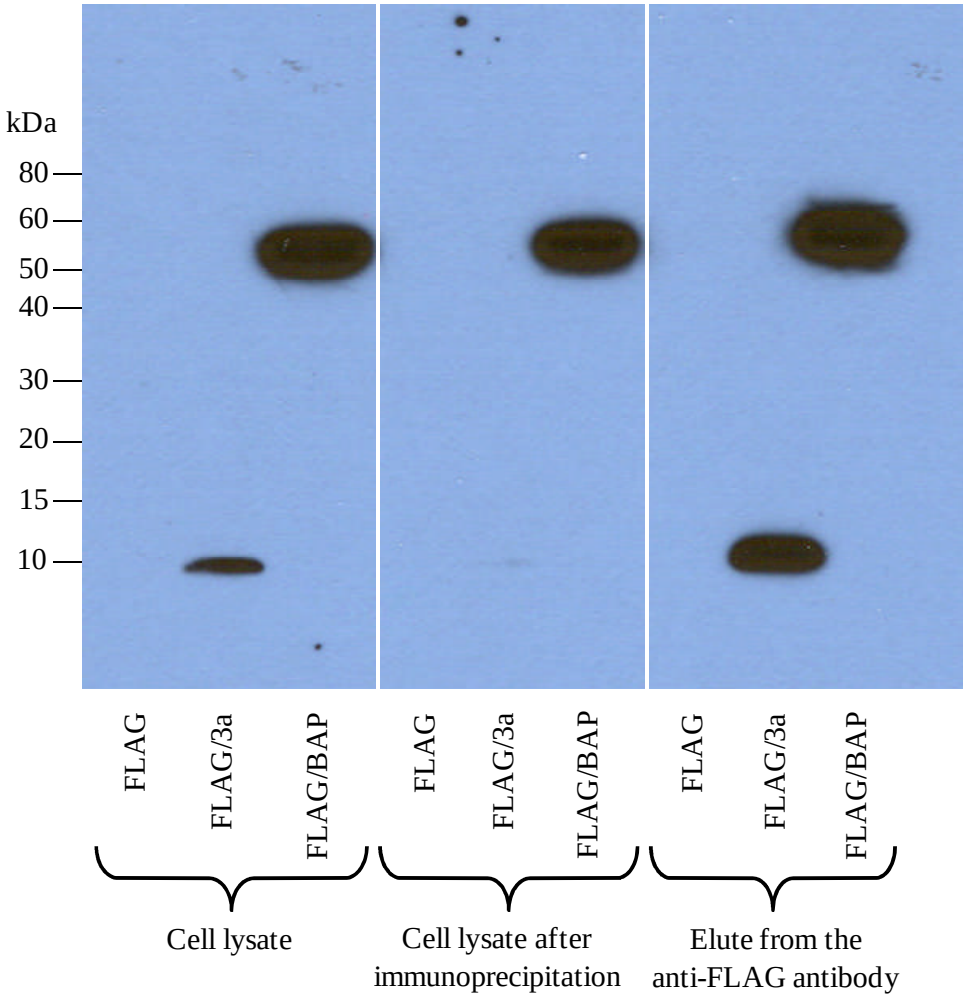

Figure 6.4. Western blot analysis to detect the presence of FLAG-tagged proteins during a pull-down assay. Subconfluent Vero cells were transfected with pFLAG, pFLAG/3a or pFLAG/BAP for 24 h. Cells were lysed and clarified by centrifugation. Clarified lysate was incubated with anti-FLAG M2 antibody which had been cross-linked to Dynabeads/Protein G. Beads were washed with cell lysis buffer. Proteins were eluted using a low pH buffer. Proteins were separated by PAGE and transferred to PVDF membrane. The membrane was probed with anti-FLAG M2 antibody and detected with HRP-conjugated anti-mouse antibody and the Immobilon Western detection system.

Non-clarified cell lysate was separated by PAGE and examined by Western blot using the anti-FLAG antibody. Expression of the FLAG/5a and FLAG/5b proteins could not be detected as shown by the lack of protein bands at the respective calculated molecular weights (Fig. 6.5).

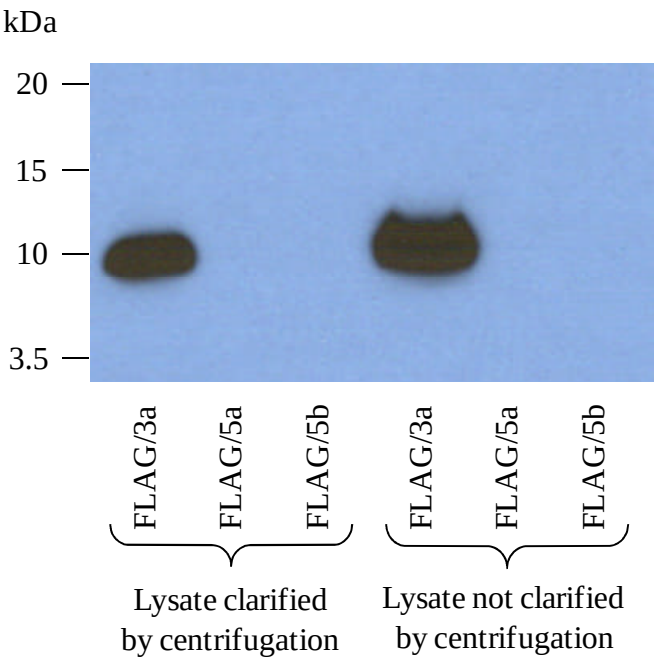

Figure 6.5. Detection of FLAG-tagged proteins after expression in Vero cells. Subconfluent Vero cells were transfected with plasmids expressing FLAG/3a, FLAG/5a or FLAG/5b. Cells were lysed and clarified or not by centrifugation (as indicated). Proteins were separated by PAGE and transferred to PVDF membrane. The membrane was probed with anti-FLAG M2 antibody and detected with HRP-conjugated anti-mouse antibody and the Immobilon Western detection system.

FLAG/3a interacts with different proteins compared to FLAG/BAP

A comparison was made between the proteins which interacted with the FLAG/3a protein and the FLAG/BAP protein. This was to identify any differences which may indicate that cellular proteins were specifically interacting with the IBV 3a sequence. The eluted samples from several immunoprecipitation experiments were combined and concentrated to provide enough protein to visualise by silver stain. Analysis of the eluted proteins by PAGE and silver staining highlighted several proteins which were present in the FLAG/3a immunoprecipitated sample and absent from the FLAG/BAP immunoprecipitated sample indicating they were specifically interacting with FLAG/3a protein (Fig. 6.6). This experiment was repeated and the same proteins were observed. Also identified were proteins present within both samples indicating they were interacting with factors common to both samples such as the anti-FLAG antibody or the FLAG sequence. A reduction in the amount of contaminating protein was performed by cross-linking the anti-FLAG tag antibody to the Protein G solid support. This ensured that only a minimal amount of the heavy

and light chains of the anti-FLAG antibody used to immunoprecipitate the FLAG-tagged protein were contained in the eluted fractions and available to interfere with the analysis of the proteins which interacted with the FLAG/3a protein.

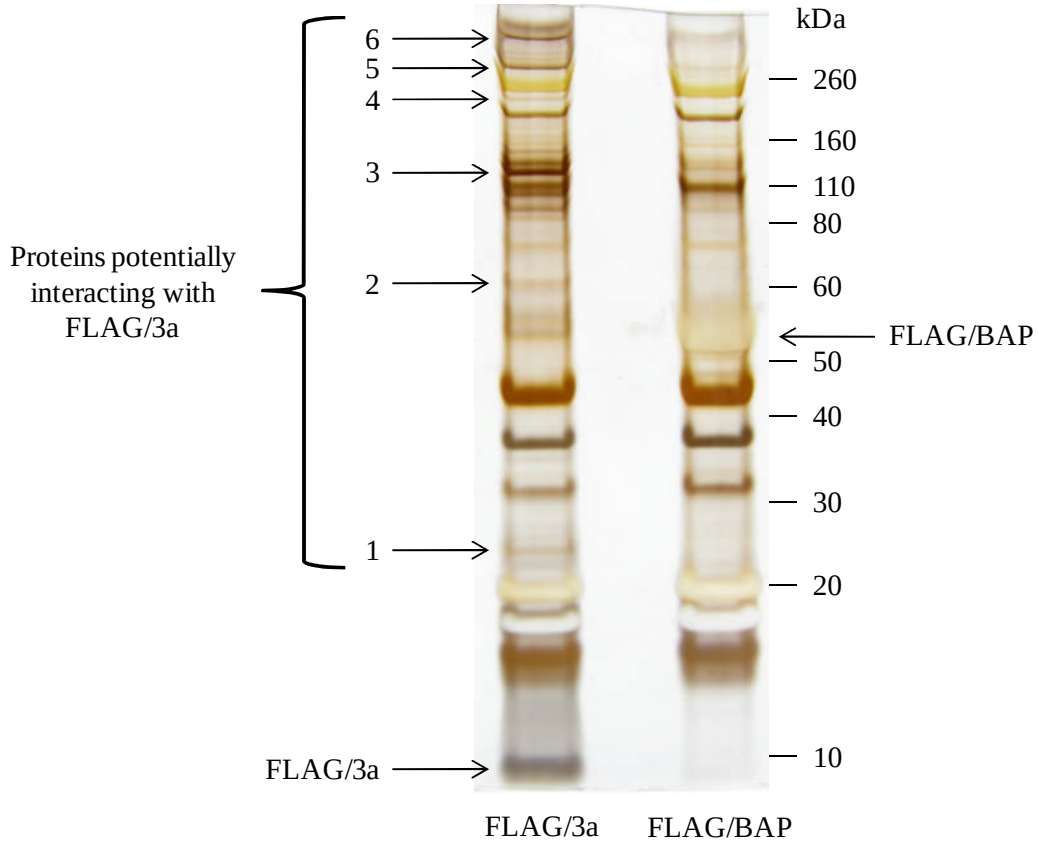

Figure 6.6. Analysis of the pull-down assay using FLAG/3a and FLAG/BAP. Subconfluent Vero cells were transfected with pFLAG/3a or pFLAG/BAP for 24 h. Cells were lysed and clarified by centrifugation. Clarified lysates were incubated with Dynabeads cross-linked to anti-FLAG M2 antibody. The beads were washed with cell lysis buffer. Proteins were eluted with a low pH buffer, concentrated by acetone precipitation and resuspended in dH_2O. The protein samples were separated by PAGE and detected using mass spectrometry-compatible silver staining. Numbers refer to the cellular proteins identified as potentially interacting with the FLAG/3a protein and not the FLAG/BAP protein.

To ensure that the protein bands detected after analysis of the immunoprecipitation of the FLAG/3a protein were not due to non-specific binding control experiments were performed. Analysis of immunoprecipitation experiments using Dynabeads only or an unrelated IgG_1 antibody (anti-FLAG was an IgG_1 isotype antibody) bound

to Protein G/Dynabeads indicated that the majority of the proteins contained in the FLAG/3a protein immunoprecipitated sample were not present in the other two control samples (Fig. 6.7). This suggested that the proteins contained in the FLAG/3a protein immunoprecipitated sample were specifically interacting with the FLAG/3a protein and were not a result of non-specific binding to the antibody or the solid support. The potentially interacting proteins at >260 kDa and 230 kDa (protein numbers 6 and 4, respectively, compared between Fig. 6.6 and 6.7) are absent possibly due to a low amount of protein which was below detection. The protein at 63 kDa (protein number 2) appeared to have corresponding proteins in the control lanes but these proteins in the control lanes displayed a slightly slower migration indicating they were of a higher molecular weight than the 63 kDa protein.

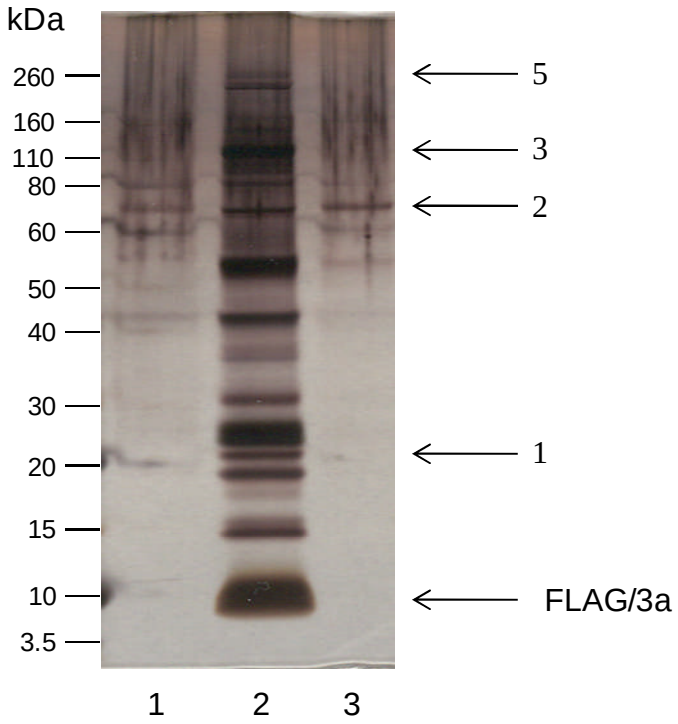

Figure 6.7. Analysis of the controls for the pull-down assay using FLAG/3a. Subconfluent Vero cells were transfected with pFLAG/3a for 24 h. Cells were lysed clarified by centrifugation. Clarified lysate was incubated with either Dynabeads Protein G only (lane 1), mouse IgG_1 anti-FLAG M2 antibody bound to Dynabeads Protein G (lane 2) or Dynabeads Protein G cross-linked to an unrelated mouse IgG_1 antibody (AV20 – I.A.H.) (lane 3). The beads were washed with lysis buffer. Proteins were eluted with a low pH buffer, concentrated by acetone precipitation and resuspended in dH_2O. The protein samples were separated by PAGE and detected using silver staining. The position of the FLAG/3a protein is indicated along with numbers corresponding to the same proteins display in Fig. 6.6.

Identification of the proteins interacting with FLAG/3a

A comparison between the proteins precipitating with the FLAG/3a and FLAG/BAP proteins suggested that there were six readily distinguishable proteins between the two samples (Fig. 6.6). The presence of these proteins suggested that the FLAG/3a protein was interacting with different cellular proteins than identified for the FLAG/BAP protein. These proteins were the ones most likely to be specifically interacting with the 3a section of the tagged protein. Identification of these proteins was performed by tandem mass spectrometry. Analysis of the generated data provided a list of proteins most likely to be present in each band (Fig. 6.8). Each protein was identified using more than two unique peptides. The number of unique peptides and the total peptide coverage for each protein are indicated in Table 6.1.

A combination of data generated by tandem mass spectrometry and a subsequent Mascot search revealed a list of proteins which were potentially contained within the originally protein sample. Each protein was identified as a result of a search which used a list of peptides, the sequences of which were obtained from the MS/MS data. The GCN1 protein sequence was covered by eight different peptides identified by mass spectrometry (Fig. 6.9). Examples of the fragmentation ion spectra for two of these peptides are shown (Fig. 6.11). PP2A was identified by the coverage of three different peptides (Fig. 6.10) and examples of the fragmentation ion spectra used to identify two of these peptides are shown (Fig. 6.12).

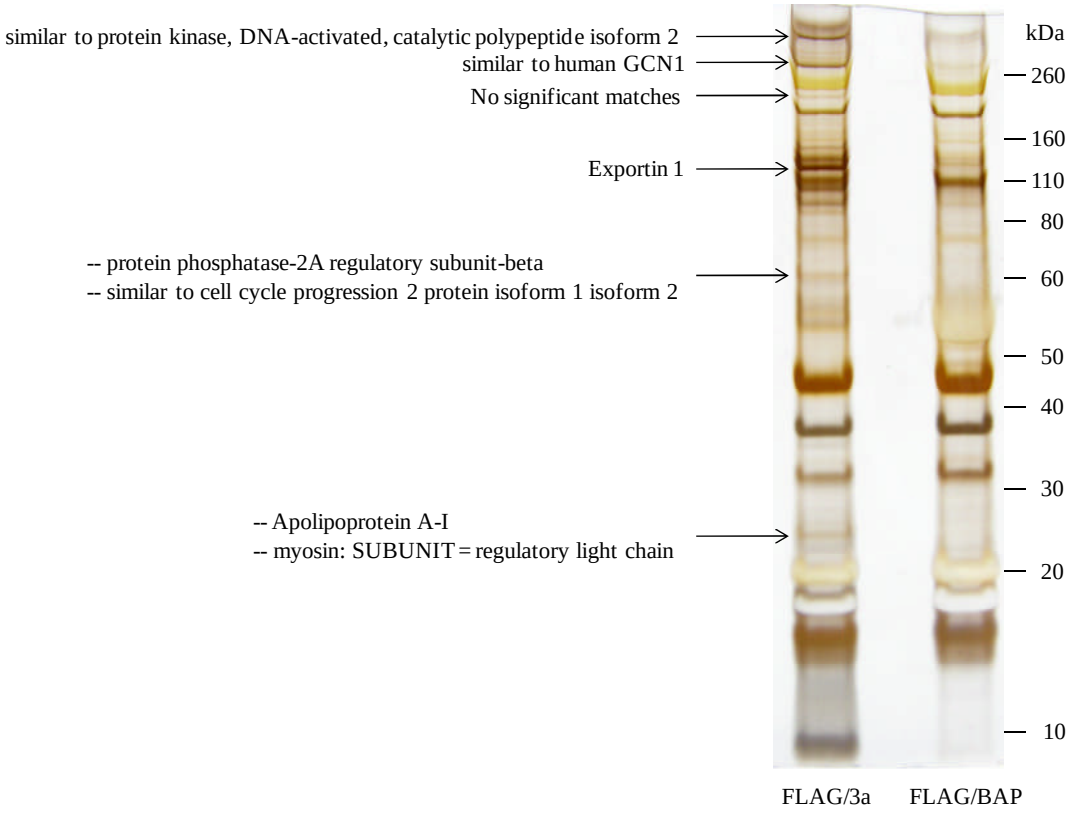

Figure 6.8. Identification of the proteins interacting with FLAG/3a. The six indicated protein bands were cut out of the gel from the FLAG/3a sample, digested with trypsin and analysed by LC-MS/MS. The peptide data was examined using the MASCOT search engine and the proteins with the highest probability of being present (excluding trypsin which was used to digest the original proteins) are indicated.

Table 6.1. The number of unique peptides and peptide coverage for each of the proteins identified by mass spectrometry and MASCOT.

Protein name	Number unique peptides	Peptide coverage (%)
Protein kinase, DNA-activated	4	1.4
GCN1	8	4.4
Exportin 1	7	7.5
PP2A	3	6.4
Cell cycle progression 2 protein	4	9.7
Apolipoprotein A-I	8	40
Myosin: regulatory light chain	4	30

dscapllrylshsefkdlilptiqksllrspenvietissllasvtldlsqyamdivkglaghlksnsprlmdeavlalrnla
rqcsdssamesltkhlfailggsegkltvvaqkmsvlsgigsvshhvvsgpssqvlngivaelfipflqqevhegtlvh
avsvlalwcnrftmevpkkltewfkkafslktstsavrhaylqcmlasyrgdtllqaldllplliqtvekaasqstqvptit
egvaaallllklsvadsqaeaklssfwqlivdekkqvftsekflvmasedalctvlhlterlfldhphrltgnkvqqyhra
lvavllsrtwhvrrqaqqtvrkllsslggfklahglleelktvlsshkvlplealvtdagevteagkayvpprvlqealcvi
sgvpglkgdvtdteqlaqemliishhpslgpwlrwssmnamgslsvlspdrvlpqlistitasvqnpalrlvtreefai
mqtpagelydksiiqsaqqdsikkanmkrenkaysfkeqiielelkeeikkkkgikeevqltskqkemlqaqldrea
qvrrrlqeldgeleaalglldiilaknpsgltqyipvlvdsflpllksplaapriknpflslaacvmpsrlkalgtlvshvtlrl
lkpecvldkswcqeelsvavkravmllhthtitsrvgkgepgaaplsapafslvfpflkmvltemphhseeeeewm
aqilqiltvqaqlraspntppgrvdengpellprvamlrlltwvigtgsprlqvlasdtlttlcasssgddgcafaeqeevd
vllcalqspcasvretvlrglmelhmvlpapdtdeknglnllrrlwvvkfdkeeeirklaerlwsmmgldlqpdlcsll
iddviyheaavrqagaealsqavaryqrqaaevmgrlmeiyqeklyrpppvldalgrvisesppdqwearcglalal
nklsqyldssqvkplfqffvpdalndrhpdvrkcmldaalatlnthgkenvnsllpvfeeflknapndasydavrqsv
vvlmgslakhldksdpkvkpivakliaalstpsqqvqesvasclpplvpaikedaggmiqrlmqqllesdkyaerk
gaayglaglvkglgilslkqqemmaaltdaiqdkknfrrregalfafemlctmlgklfepyvvhvlphlllcfgdgnq
yvreaaddcakavmsnlsahgvklvlpsllaaleeeswrtkagsvellgamaycapkqlssclpnivpkltevltdsh
vkvqkagqqalrqigsvirnpeilaiapvlldaltdpsrktqkclqtlldtkfvhfidapslalimpivqrafqdrstdtrk
maaqiignmysltdqkdlapylpsvtpglkaslldpvpevrtvsakalgamvkgmgescfedllpwlmetltyeqs
svdrsgaaqglaevmaglgvekleklmpeivataskvdiaphvrdgyimmfnylpitfgdkftpyvgpiipcilkal
adenefvrdtalragqrvismyaetaialllpqleqglfddlwrirfssvqllgdllfhisgvtgkmttetaseddnfgtaq
snkaiitalgverrnrvlaglymgrsdtqlvvrqaslhvwkivvsntprtlreilptlfglllgflastcadkrtiaartlgdlv
rklgekilpeiipileeglrsqksderqgvciglseimkstsrdavlyfseslvptarkalcdpleevreaaaktfeqlhsti
ghqaledilpfllkqlddeevsefaldglkqvmaiksrvvlpylvpklttppvntrvlaflssvagdaltrhlgvilpavm
lalkeklgtpdeqlemancqavilsveddtghriiieylleatrspevgmrqaaaiilniycsrskadytshlrslvsglirl
fndsspvvleeswdalnaitkkldagnqlalieelhkeirligneskgehvpgfclpkkgvtsilpvlregvltgspeqk
eeaakalglvirltsadalrpsvvsitgplirilgdrfswnvkaalletlslllakvgialkpflpqlqttftkalqdsnrgvrlk
aadalgklisihikvdplftellngiramedpgvrdtmlqalrfviqgagakvdavirknivslllsmlghdedntrissa
gclgelcaflteeelsavlqqclladvsgidwmvrhgrslalsvavnvapgrlcagryssdvqemilssatadripiavs
gvrgmgflmrhhietgggqlpaklsslfvkclqnpssdirlvaekmiwwankdplppldpqaikpilkalldntkdk
ntvvraysdqaivnllkmrqgeevfqslskildvaslevlnevnrrslkklasqadsteqvddtilt

Figure 6.9. Peptide coverage of the GCN1 protein sequence. MS/MS identified peptides are shown in red. There was 4.4% sequence coverage by the eight identified peptides. This was the human GCN1 sequence from accession number AAC83183.

Efrpelrnedvqlrlnsikklstialalgvertrsellpfltdtiydvdevllalaeqlgnftglvggpdfahcllpplenlatv
eetvvrdkaveslrqisqehtpvaleayfvplvkrlasgdwftsrtsacglfsvcyprasnavkaetrqqfrslcsddtp
mvrraaasklgefakvleldsvkseivplftslasdeqdsvrllaveacvsiaqllsqddletlvmptlrqaaedkswrvr
ymvadrfselqkamgpkitlndlipafqnllkdceaevraaaahkvkelgenlpiedretiimnqilpyikelvsdtnq
hvksalasvimglstilgkentiehllplflaqlkdecpdvrlniisnldcvnevigirrlsqsllpaivelaedakwrvrla
iieympllagqlgveffdeklnslcmawlvdhvyaireaatnnlmklvqkfgtewaqntivpkvlvmandpnylhr
mttlfcinalseacgqeittkqmlpivlkmagdqvanvrfnvakslqkigpildtnalqgevkpvlqklgqdedmdv
kyfaqeaisvlala

Figure 6.10. Peptide coverage of the PP2A protein sequence. MS/MS identified peptides are shown in red. There was 6.4% sequence coverage by the three identified peptides. This was the human PP2A sequence from accession number AAA59983.

Figure 6.11. Fragment ion spectra and accompanying table of fragment ions for two of the peptides identified from MS/MS analysis of the ~260 kDa protein. The raw data generated by tandem MS for the protein of interest was analysed with the Mascot program. The fragment ion spectra for the deduced peptides are displayed along with an indication of which peak correspond to which fragment ion. The peptide sequence is in the top right corner. The table below includes the m/z for the fragment ions which were used to deduce the peptide sequence (red and bold).

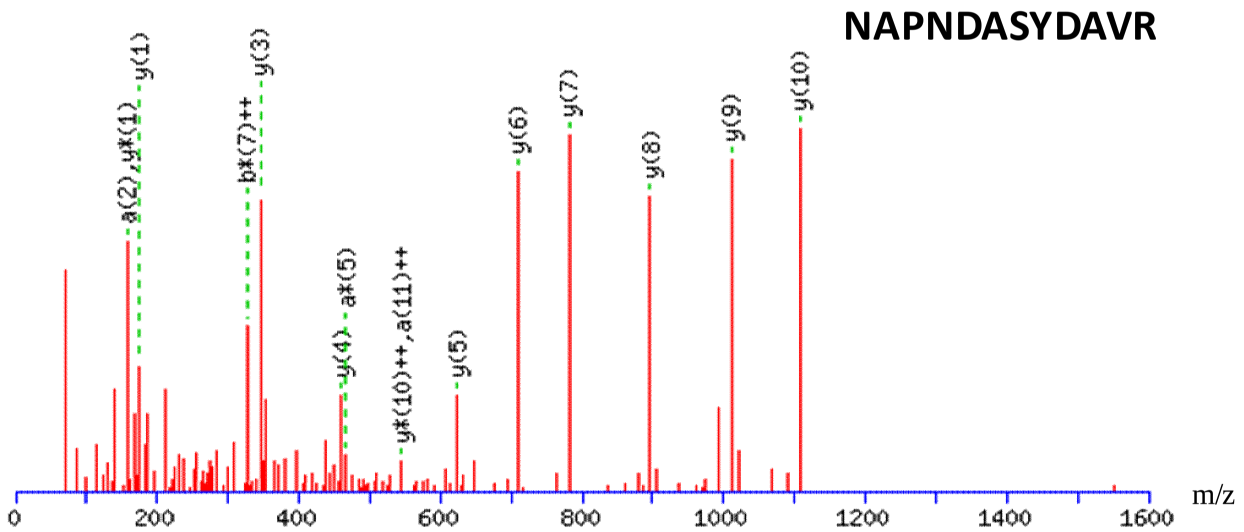

#	a	a^{++}	a*	a*$^{++}$	b	b^{++}	b*	b*$^{++}$	Seq.	y	y^{++}	y*	y*$^{++}$	#
1	87.0553	44.0313	70.0287	35.5180	115.0502	58.0287	98.0237	49.5155	N					12
2	158.0924	79.5498	141.0659	71.0366	186.0873	93.5473	169.0608	85.0340	A	1178.5436	589.7755	1161.5171	581.2622	11
3	255.1452	128.0762	238.1186	119.5629	283.1401	142.0737	266.1135	133.5604	P	1107.5065	554.2569	1090.4800	545.7436	10
4	369.1881	185.0977	352.1615	176.5844	397.1830	199.0951	380.1565	190.5819	N	1010.4538	505.7305	993.4272	497.2172	9
5	484.2150	242.6112	467.1885	234.0979	512.2100	256.6086	495.1834	248.0953	D	896.4108	448.7091	879.3843	440.1958	8
6	555.2522	278.1297	538.2256	269.6164	583.2471	292.1272	566.2205	283.6139	A	781.3839	391.1956	764.3573	382.6823	7
7	642.2842	321.6457	625.2576	313.1325	670.2791	335.6432	653.2525	327.1299	S	710.3468	355.6770	693.3202	347.1638	6
8	805.3475	403.1774	788.3210	394.6641	833.3424	417.1748	816.3159	408.6616	Y	623.3148	312.1610	606.2882	303.6477	5
9	920.3744	460.6909	903.3479	452.1776	948.3694	474.6883	931.3428	466.1750	D	460.2514	230.6293	443.2249	222.1161	4
10	991.4116	496.2094	974.3850	487.6961	1019.4065	510.2069	1002.3799	501.6936	A	345.2245	173.1159	328.1979	164.6026	3
11	1090.4800	545.7436	1073.4534	537.2304	1118.4749	559.7411	1101.4483	551.2278	V	274.1874	137.5973	257.1608	129.0840	2
12									R	175.1190	88.0631	158.0924	79.5498	1

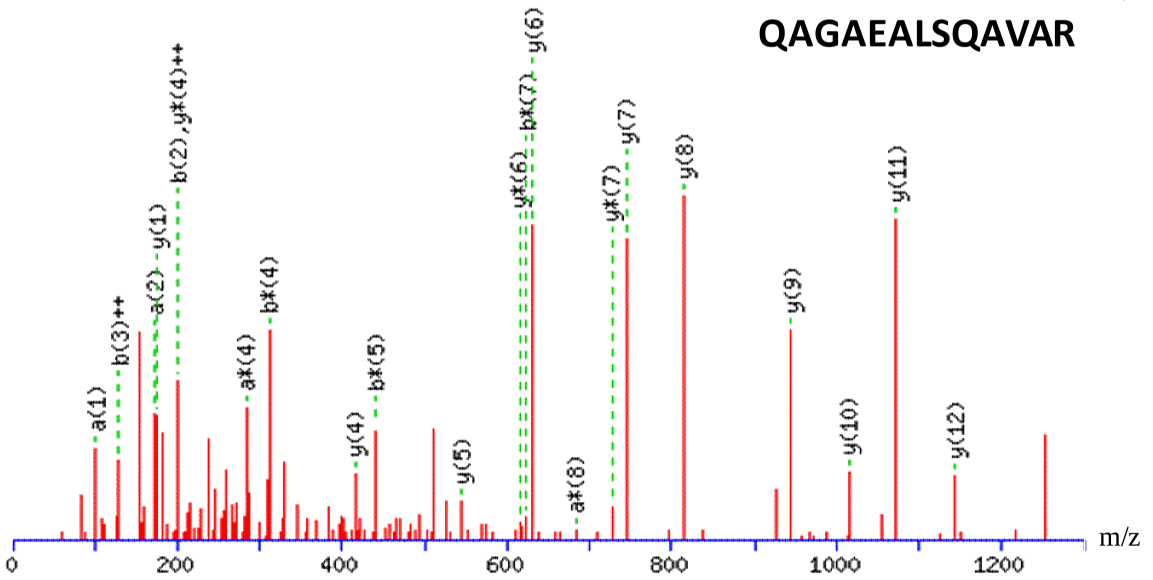

#	a	a++	a*	a*++	b	b++	b*	b*++	Seq.	y	y++	y*	y*++	#
1	101.0709	51.0391	84.0444	42.5258	129.0659	65.0366	112.0393	56.5233	Q					13
2	172.1081	86.5577	155.0815	78.0444	200.1030	100.5551	183.0764	92.0418	A	1143.6117	572.3095	1126.5851	563.7962	12
3	229.1295	115.0684	212.1030	106.5551	257.1244	129.0659	240.0979	120.5526	G	1072.5745	536.7909	1055.5480	528.2776	11
4	300.1666	150.5870	283.1401	142.0737	328.1615	164.5844	311.1350	156.0711	A	1015.5531	508.2802	998.5265	499.7669	10
5	429.2092	215.1083	412.1827	206.5950	457.2041	229.1057	440.1776	220.5924	E	944.5160	472.7616	927.4894	464.2483	9
6	500.2463	250.6268	483.2198	242.1135	528.2413	264.6243	511.2147	256.1110	A	815.4734	408.2403	798.4468	399.7271	8
7	613.3304	307.1688	596.3039	298.6556	641.3253	321.1663	624.2988	312.6530	L	744.4363	372.7218	727.4097	364.2085	7
8	700.3624	350.6849	683.3359	342.1716	728.3573	364.6823	711.3308	356.1690	S	631.3522	316.1797	614.3257	307.6665	6
9	828.4210	414.7141	811.3945	406.2009	856.4159	428.7116	839.3894	420.1983	Q	544.3202	272.6637	527.2936	264.1504	5
10	899.4581	450.2327	882.4316	441.7194	927.4530	464.2302	910.4265	455.7169	A	416.2616	208.6344	399.2350	200.1212	4
11	998.5265	499.7669	981.5000	491.2536	1026.5215	513.7644	1009.4949	505.2511	V	345.2245	173.1159	328.1979	164.6026	3
12	1069.5637	535.2855	1052.5371	526.7722	1097.5586	549.2829	1080.5320	540.7696	A	246.1561	123.5817	229.1295	115.0684	2
13									R	175.1190	88.0631	158.0924	79.5498	1

Figure 6.12. Fragment ion spectra and accompanying table of fragment ions for two of the peptides identified from MS/MS analysis of the ~60 kDa protein. The raw data generated by tandem MS for the protein of interest was analysed with the Mascot program. The fragment ion spectra for the deduced peptides are displayed along with an indication of which peak correspond to which fragment ion. The peptide sequence is in the top right corner. The table below includes the m/z for the fragment ions which were used to deduce the peptide sequence (red and bold).

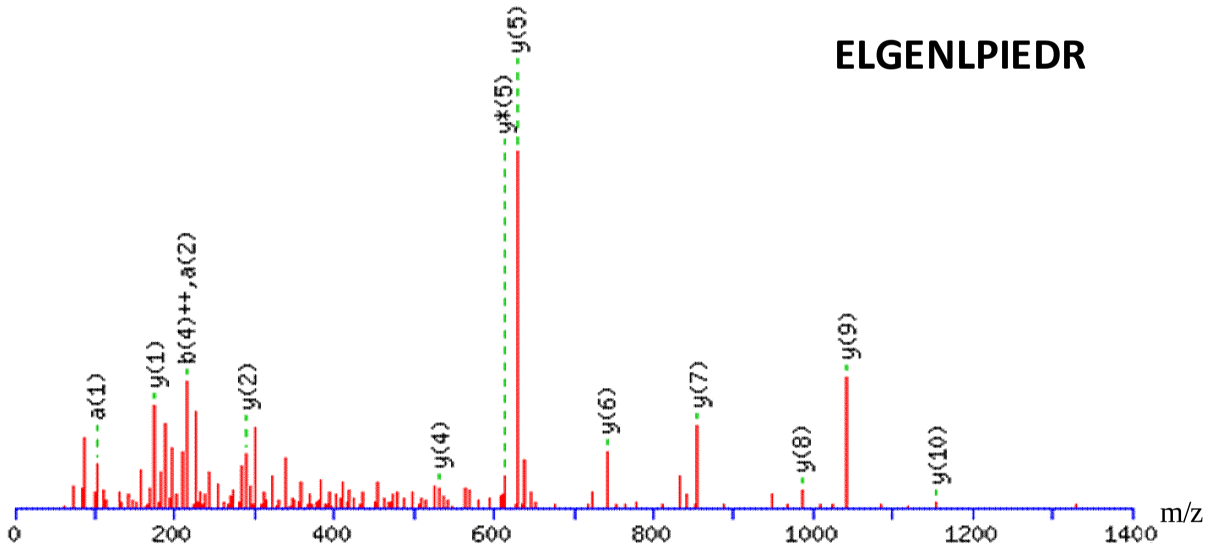

#	a	a^{++}	a*	a*$^{++}$	b	b^{++}	b*	b*$^{++}$	Seq.	y	y^{++}	y*	y*$^{++}$	#
1	102.0550	51.5311			130.0499	65.5286			E					11
2	215.1390	108.0731			243.1339	122.0706			L	1155.6004	578.3039	1138.5739	569.7906	10
3	272.1605	136.5839			300.1554	150.5813			G	1042.5164	521.7618	1025.4898	513.2485	9
4	401.2031	201.1052			429.1980	215.1026			E	985.4949	493.2511	968.4684	484.7378	8
5	515.2460	258.1266	498.2195	249.6134	543.2409	272.1241	526.2144	263.6108	N	856.4523	428.7298	839.4258	420.2165	7
6	628.3301	314.6687	611.3035	306.1554	656.3250	328.6661	639.2984	320.1529	L	742.4094	371.7083	725.3828	363.1951	6
7	725.3828	363.1951	708.3563	354.6818	753.3777	377.1925	736.3512	368.6792	P	629.3253	315.1663	612.2988	306.6530	5
8	838.4669	419.7371	821.4403	411.2238	866.4618	433.7345	849.4353	425.2213	I	532.2726	266.6399	515.2460	258.1266	4
9	967.5095	484.2584	950.4829	475.7451	995.5044	498.2558	978.4779	489.7426	E	419.1885	210.0979	402.1619	201.5846	3
10	1082.5364	541.7719	1065.5099	533.2586	1110.5313	555.7693	1093.5048	547.2560	D	290.1459	145.5766	273.1193	137.0633	2
11									R	175.1190	88.0631	158.0924	79.5498	1

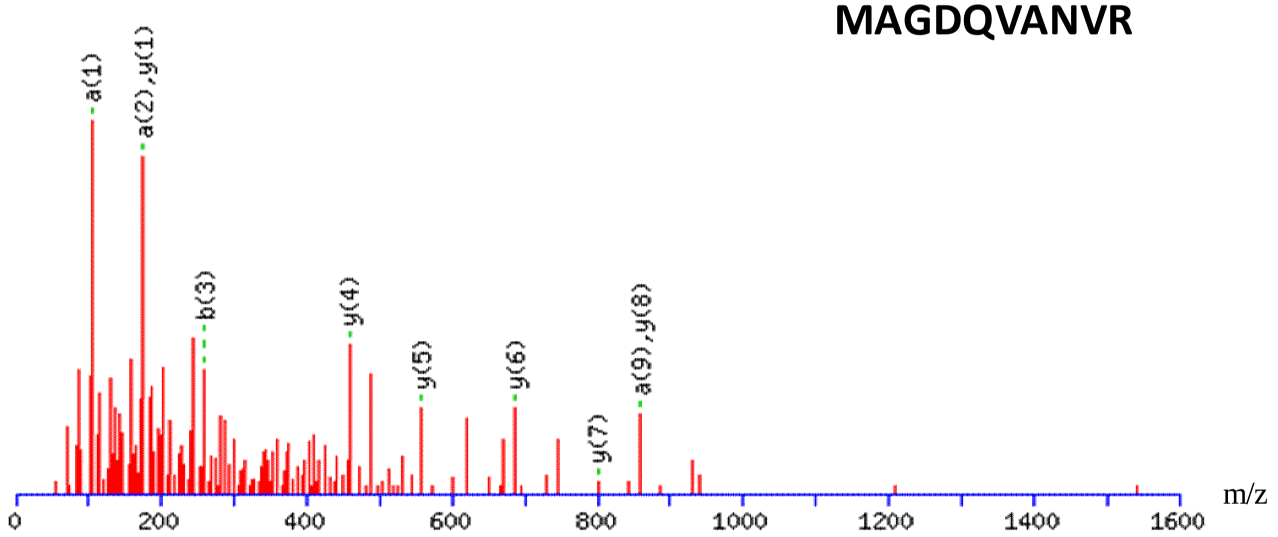

#	a	a^{++}	a*	a*$^{++}$	b	b^{++}	b*	b*$^{++}$	Seq.	y	y^{++}	y*	y*$^{++}$	#
1	104.0528	52.5301			132.0478	66.5275			M					10
2	175.0900	88.0486			203.0849	102.0461			A	929.4799	465.2436	912.4534	456.7303	9
3	232.1114	116.5594			260.1063	130.5568			G	858.4428	429.7250	841.4163	421.2118	8
4	347.1384	174.0728			375.1333	188.0703			D	801.4213	401.2143	784.3948	392.7010	7
5	475.1969	238.1021	458.1704	229.5888	503.1919	252.0996	486.1653	243.5863	Q	686.3944	343.7008	669.3678	335.1876	6
6	574.2654	287.6363	557.2388	279.1230	602.2603	301.6338	585.2337	293.1205	V	558.3358	279.6715	541.3093	271.1583	5
7	645.3025	323.1549	628.2759	314.6416	673.2974	337.1523	656.2708	328.6391	A	459.2674	230.1373	442.2409	221.6241	4
8	759.3454	380.1763	742.3189	371.6631	787.3403	394.1738	770.3138	385.6605	N	388.2303	194.6188	371.2037	186.1055	3
9	858.4138	429.7105	841.3873	421.1973	886.4087	443.7080	869.3822	435.1947	V	274.1874	137.5973	257.1608	129.0840	2
10									R	175.1190	88.0631	158.0924	79.5498	1

Confirmation of the protein interactions in Vero cells

Each of the identified proteins were assessed for their known biological functions and potential relevance in the cellular replication cycle of IBV. GCN1 was recognised as potentially involved in IBV-infected cells by indirectly causing the phosphorylation of the eIF2α subunit of the eukaryotic translation initiation complex, thereby attenuating host cell protein translation. Infection of cells with the coronaviruses MHV and SARS result in the phosphorylation of the eIF2α subunit (Bechill *et al.*, 2008; Krahling *et al.*, 2009; Raaben *et al.*, 2007) resulting in the attenuation of host cell protein translation (Hilton *et al.*, 1986; Rottier *et al.*, 1981).

Confirmation of the presence of GCN1 was conducted by immunoprecipitation of the FLAG/3a and FLAG/BAP proteins from transfected and lysed cells and analysis of the eluted fraction by Western blot with an anti-FLAG antibody and anti-GCN1 antibody. A protein band at 260 kDa was detected in the eluted sample from the FLAG/3a immunoprecipitation but not in the eluted sample from the FLAG/BAP immunoprecipitation (Fig. 6.13a) indicating that the FLAG/3a protein specifically interacted with the GCN1 protein. To further confirm this interaction the GCN1 protein was immunoprecipitated with the anti-GCN1 antibody and the anti-FLAG antibody was used to detect the FLAG/3a or FLAG/BAP proteins in the eluted sample (Fig. 6.13b). The absence of protein bands detected at the calculated molecular weight for the FLAG/3a and FLAG/BAP proteins indicated that neither protein were immunoprecipitated with GCN1. This could have indicated that the amount of GCN1 immunoprecipitated was not sufficient to provide a detectable quantity of FLAG/3a protein or that the anti-GCN1 epitope recognised by the antibody was not available when GCN1 was complexed with the 3a protein.

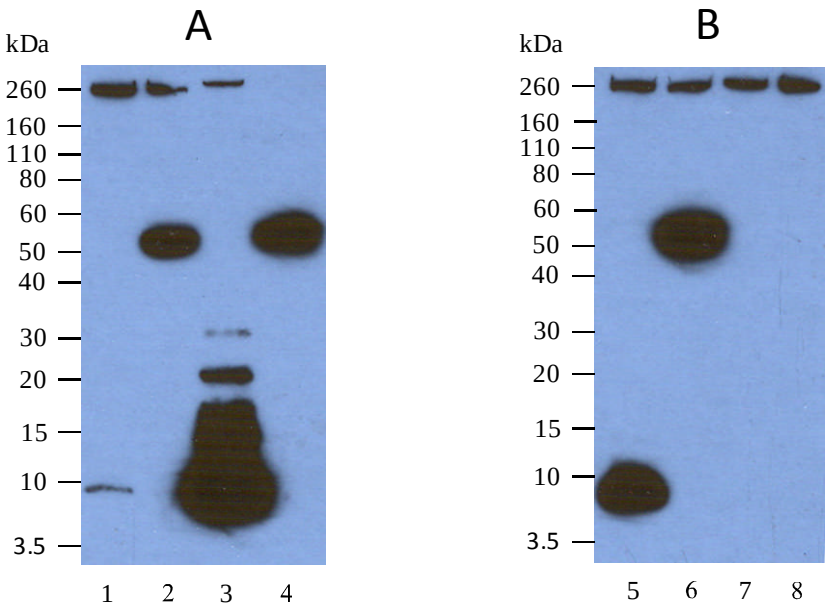

Figure 6.13. Confirmation of the interaction between FLAG/3a and GCN1. Subconfluent Vero cells were transfected with pFLAG, pFLAG/3a or pFLAG/BAP for 24 h. Cells were lysed and clarified by centrifugation. Clarified lysate was incubated with anti-FLAG M2 antibody (A) or anti-GCN1 antibody (B). Dynabeads/Protein G were added to bind the antibodies. Beads were washed with cell lysis buffer. Eluted proteins were separated by PAGE and transferred to PVDF membranes. The membranes were probed with anti-FLAG M2 antibody and anti-GCN1L1 antibody and detected with HRP-conjugated anti-mouse antibody, HRP-conjugated anti-rabbit antibody and the Immobilon Western detection system. Lane 1 – lysate of FLAG/3a expressing cells after immunoprecipitation using the anti-FLAG antibody. Lane 2 - lysate of FLAG/BAP expressing cells after immunoprecipitation using the anti-FLAG antibody. Lane 3 – proteins eluted from the anti-FLAG antibody after addition to the FLAG/3a cell lysate. Lane 4 - proteins eluted from the anti-FLAG antibody after addition to the FLAG/BAP cell lysate. Lane 5 – lysate of FLAG/3a expressing cells after immunoprecipitation using the anti-GCN1 antibody. Lane 6 - lysate of FLAG/BAP expressing cells after immunoprecipitation using the anti-GCN1 antibody. Lane 7 – proteins eluted from the anti-GCN1 antibody after addition to the FLAG/3a cell lysate. Lane 8 - proteins eluted from the anti-GCN1 antibody after addition to the FLAG/BAP cell lysate.

Towards the confirmation of the protein interactions in avian cells

The three proteins potentially interacting with the FLAG/3a protein in Vero cells were assessed for the similarity in sequence between mammalian and avian cells. A conserved sequence between the two cell types would indicate that the 3a protein has the potential to interact with the same cellular protein and thus a protein-protein interaction in mammalian cells may also reflect a similar situation during IBV

infection of avian cells. Where the protein sequence is not currently available for the avian protein the same protein from other species is given as an example to highlight conservation. The GCN1 sequence has been characterised for several species and has an 85% amino acid sequence identity between human and Zebra finch (human GCN1L1 sequence accession number NP_006827.1 and Zebra finch GCN1L1 sequence accession number XP_002196360) indicating a high level of conservation between mammalian and avian species. The PP2A regulatory subunit ß isoform also exhibits a high level of conservation with an 88-89% amino acid sequence identity between human and *Xenopus laevis* (human accession number NP_002707.3 and the *Xenopus laevis* accession number CAJ82271) as does Exportin-1 which has a 98% sequence identity between mammalian and avian proteins (human accession number NP_003391.1 and chicken accession number XP_001231648.1).

An assessment of the potential interaction between the IBV 3a protein and GCN1 was conducted using the lysate of IBV infected CK cells to identify whether native 3a protein interacts with GCN1 in the context of IBV infection. The anti-3a protein antibody 3480 was used to immunoprecipitate the IBV 3a protein from infected cell lysate. Western blot analysis of the eluted proteins from the immunoprecipitation demonstrated that the 3a protein was detected in the original infected cell lysate and the eluted protein samples indicating that the 3a protein was purified from the total cell lysate (Fig. 6.14). GCN1 was detected in the samples from the unprocessed cell lysate and the supernatant from which the 3a protein has been removed. Detection of GCN1 in the eluted protein samples was inhibited by the presence of the heavy chain of the anti-3a protein antibody.

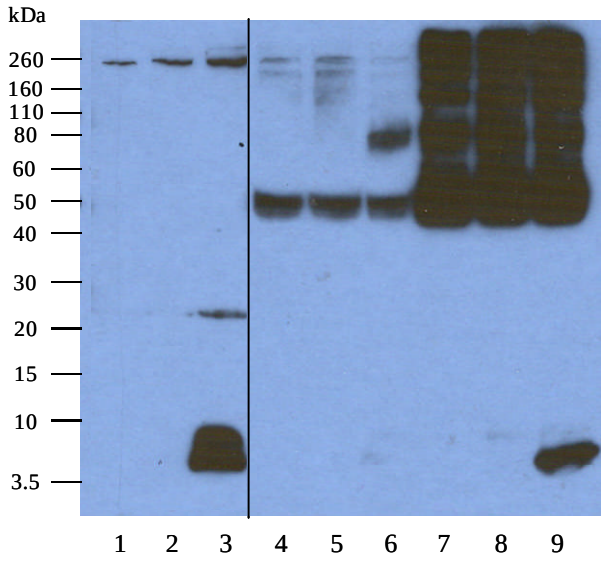

Figure 6.14. Detecting GCN1 after immunoprecipitating the 3a protein from IBV-infected cell lysate. CK cells were infected with Beau-R for 10 h p.i. The cells were lysed with cell lysis buffer and clarified by centrifugation. Anti-3a protein (3480) antibody was combined with mock-, IBV ScAUG3a- or Beau-R infected CK cell lysate and incubated overnight. Dynabeads/Protein G were added to the cell lysate and mixed. The beads were washed with cell lysis buffer. Proteins were eluted with a low pH buffer and the samples were separated by PAGE. Proteins were transferred to PVDF membrane. The membrane was probed with anti-3a protein antibody Machamer and anti-GCN1 antibody and detected with HRP-conjugated anti-rabbit antibody and the Immobilon Western detection system. Lane 1 – Mock-infected cell lysate. Lane 2 – rIBV ScAUG3a-infected cell lysate. Lane 3 – Beau-R-infected cell lysate. Lane 4 – Mock cell lysate after immunoprecipitation using the anti-3a protein antibody. Lane 5 – rIBV ScAUG3a cell lysate after immunoprecipitation using the anti-3a protein antibody. Lane 6 – Beau-R cell lysate after immunoprecipitation using the anti-3a protein antibody. Lane 7 – eluted proteins from the immunoprecipitation using mock-infected cell lysate. Lane 8 – eluted proteins from the immunoprecipitation using rIBV ScAUG3a-infected cell lysate. Lane 9 – eluted proteins from the immunoprecipitation using Beau-R-infected cell lysate. Lanes 1, 2 and 3 are shown with increased exposure compared to the rest of the image to visualise GCN1 at 260 kDa.

The heavy chain of antibodies has been calculated to have a molecular weight of ~50 kDa and this would explain the protein bands at ~50 kDa displayed on the Western blot. The additional higher molecular weight protein bands were aggregates of the heavy chain that obscured the region of the Western blot potentially occupied by the GCN1 protein at ~250 kDa.

If the IBV 3a protein interaction with GCN1 a determination of the consequences of this interact is required. The total amount of GCN1 present within infected cells was assessed by Western blot analysis. A 12 h time course of IBV infection in CK cells

was used to assess any variation in the total amounts of GCN1 between mock-infected, Beau-R-infected and rIBV ScAUG3a-infected CK cell lysates (Fig. 6.15). Alpha-tubulin was used as a loading control. Due to the relatively constant size and shape of the protein bands detected by the anti-alpha tubulin antibody the amount of alpha-tubulin loaded from each sample was assumed to be constant and therefore the amount of total protein was constant. The IBV 3a protein was detected in the Beau-R infected cell lysates from 8 h p.i. onwards, although a faint band could be detected at 6 h p.i. with a longer exposure. The levels of GCN1 detection did not change throughout the time-course of infection within the mock, Beau-R or IBV ScAUG3a cell lysates as shown by the constant size, shape and exposure of the bands indicating that the potential interaction of the 3a protein with GCN1 did not affect the amount of GCN1 in IBV-infected CK cells.

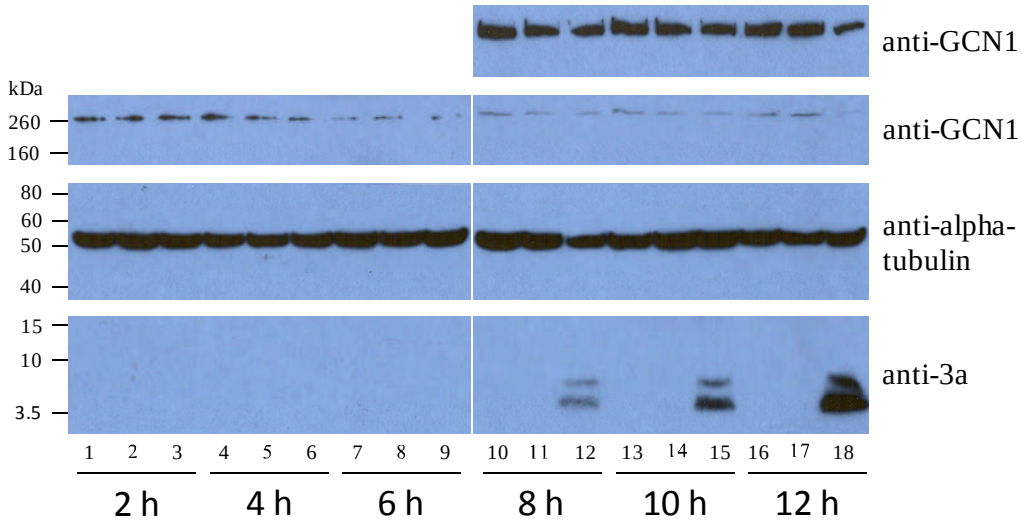

Figure 6.15. The total amount of GCN1 does not change in cells infected with IBV. Subconfluent CK cells were infected with either mock, rIBV ScAUG3a or Beau-R. Upon the required time post infection the CK cells were lysed and clarified by centrifugation. Samples of each supernatant were separated by PAGE. Proteins were transferred to PVDF membranes. The membranes were probed with anti-GCN1 antibody, anti-alpha-tubulin antibody and anti-3a protein antibody (3480) and detected with HRP-conjugated anti-mouse antibody, HRP-conjugated anti-rabbit antibody and the Immobilon Western detection system. Lanes 1, 4, 7, 10, 13 and 16 – lysates of mock infected CK cells at the indicated time-points. Lanes 2, 5, 8, 11, 14 and 17 – lysates of rIBV ScAUG3a infected CK cells at the indicated time-points. Lanes 3, 6, 9, 12, 15 and 18 – lysates of Beau-R infected CK cells at the indicated. The top anti-GCN1 panel represents a longer exposure than the bottom anti-GCN1 panel.

Discussion

Experiments designed to identify the protein interactions of the IBV accessory protein were conducted using N-terminally tagged FLAG-tagged proteins. Expression of the N-terminal FLAG-tag accessory proteins within Vero cells was achieved. Western blot analysis of the lysates from these transfected cells indicated that the FLAG/3a protein was present in the samples. After confirmation that the FLAG/3a protein could be immunoprecipitated from transfected cells using the anti-FLAG antibody experiments to identify the cellular proteins to which the FLAG/3a interacted were performed. Analysis of the resulting experiments indicated that there were several proteins specifically interacting with the FLAG/3a protein and of these seven proteins were identified by mass spectrometry.

The protein interaction of the FLAG/3a protein with GCN1 was detected using a tagged 3a protein where the tag was expressed at the N-terminal end of the 3a protein. Depending upon the effect of this tag on the folding of the 3a protein various outcomes can be predicted. The tag could have no effect upon the conformation of the 3a protein so that the 3a protein interacts with the same proteins that interact with the natively folded 3a protein. The interaction of GCN1 with the 3a protein would therefore have biological relevance and warrant further investigation. If the presence of the tag interfered with the folding of the recombinant 3a protein then protein interactions may be blocked or the incorrectly folded 3a protein may enable protein interactions that would not normally occur during the infection of cells by IBV. The interaction of the 3a protein with GCN1 would not be relevant in the context of an IBV infection and result from the overexpression of an altered protein within transfected cells. The same caution can be applied to all the proteins identified as potentially interacting with the FLAG/3a protein. Biologically relevant protein interactions would also depend upon the subcellular location to which the tagged protein targeted. Immunofluorescence experiments indicated that the FLAG/3a protein localised in the same punctate, cytoplasmic pattern observed within Beau-R infected cells. The FLAG/3a protein was therefore likely to interact with the same proteins with which the native protein interacted. Images of some of the transfected cells also indicated that the FLAG/3a could be localised in a perinuclear pattern. This different subcellular location may have resulted in the FLAG/3a protein interacting with cellular proteins not normally meant to interact with the natively folded IBV 3a

protein during infection. The identification of Exportin 1 as a protein interacting with the FLAG/3a protein may have been a consequence of the different subcellular distribution pattern of the FLAG/3a protein compared to native 3a protein. Images of the subcellular localisation of Exportin 1 within cells have displayed fluorescence in the nuclear rim (Van Neck *et al.*, 2008) which was different from the punctate, cytoplasmic distribution of the majority of the fluorescence displayed by the FLAG/3a protein. This potential interaction cannot be dismissed without further consideration because the 3a protein may have caused the relocation of this cellular protein similar to a report that the Meq protein of Marek's disease virus relocated the subcellular distribution of the cellular protein hsp70 (Zhao *et al.*, 2009b).

Identification of proteins by tandem mass spectrometry involved the assembly of fragmented ion peaks into a predicted peptide sequence and two or more peptides were used to predict the protein from which they originated. The exact reconstruction of a peptide sequence from the MS/MS spectrum is not always possible due a low signal to noise ratio and/or an incomplete set of ion peaks. Under these circumstances a set of possible peptides can be assigned to one particular spectrum. This process can therefore lead to the identification of more than one protein. Additionally the protein database which was used to search for matches to the peptide sequences generated by mass spectrometry will not contain all the possible proteins and their variations needed to make a complete list. In this way identification of proteins may be erroneous or there may be no matches possible. This may have been the reason for the absence of any matches to the peptides generated from third highest molecular weight protein (Number 4, Fig. 6.8). Alternatively there may not have been enough original protein present to produce adequate data. The proteins identified within each of the gel slices may not necessarily represent the major species within the precipitation. If there was a low amount of total protein originally in the gel slice and a suitable number of peptides were not removed from the gel slice then the major species of protein contained within that gel slice may only be represented by a relatively small number of peptides. To counter this possibility the equivalent gel slice from the control experiment could be analysed by mass spectrometry and a MASCOT search. Those proteins identified in both samples would be discounted and the proteins specific to the FLAG/3a precipitation would be taken forward.

Confirmation of the presence of GCN1 in the eluted sample after immunoprecipitation of the FLAG/3a protein was obtained by Western blot using an anti-GCN1 antibody. The FLAG/BAP protein did not interact with GCN1 as the anti-GCN1 antibody did not detect a protein at the calculated molecular weight for GCN1 in the eluted sample. The immunoprecipitation of GCN1 from cells also containing the FLAG/3a protein did not confirm the interaction of GCN1 with the FLAG/3a protein. An explanation for this could involve the efficiency of transfection using the pFLAG/3a plasmid. Immunofluorescence with confocal microscopy indicated that approximately 10-20% of cells were transfected and expressing FLAG-tagged protein. Therefore 80-90% of cells were not expressing FLAG-tagged protein and the GCN1 within these cells would not bind the FLAG/3a protein. The majority of anti-GCN1 antibody would bind GCN1 not interacting with the FLAG/3a protein and the FLAG/3a protein would not be detected when GCN1 was immunoprecipitated from cell lysate. Alternatively only a small percentage of FLAG/3a protein may be interacting with GCN1. The rationale for this involved the difference in detection of FLAG/3a protein and GCN1 between the cell lysate after immunoprecipitation and that in the eluted fraction. The FLAG/3a protein was concentrated as shown by the large signal detected for the FLAG/3a protein in the eluted fraction but the signal of GCN1 hardly changed. If this was the case the amount of FLAG/3a protein interacting with GCN1 would be low and possibly below the detection limit of the anti-FLAG antibody used in the Western blot when the anti-GCN1 antibody was used to immunoprecipitate GCN1. Confirming the interaction of GCN1 with the 3a protein within Beau-R infected cells was hampered by the cross-reactivity between the antibodies used to immunoprecipitate the 3a protein or GCN1 and the antibodies used to perform the Western blot. The rabbit anti-3a protein antibody 3480 could not be cross-linked to the solid support meaning that the antibody was present in the eluted sample after the immunoprecipitation of the 3a protein and any interacting proteins. The eluted sample was reduced and denatured so that the antibodies were divided into the heavy and light chains. These components of the rabbit antibodies were detected by the anti-rabbit secondary antibodies used to detect the anti-GCN1 and anti-3a protein primary antibodies. The presence of a band at 50 kDa indicated the location of the antibody heavy chains. The occurrence of additional bands at multiples of 50, i.e. 100, 150, etc, indicated the

location of aggregates of the heavy chain in the form of dimers but also possibly the incomplete dissociation of the antibodies into the constituent heavy and light chains.

Expression of the FLAG/5a and FLAG/5b proteins within Vero cells transfected with pFLAG/5a and pFLAG/5b had already been confirmed by immunofluorescence. Detection of the FLAG/5a and FLAG/5b proteins in the lysates of transfected Vero cells by Western blot was unsuccessful. The anti-FLAG antibody was suitable for detection of the FLAG-tag in Western blots because the FLAG/3a protein could be visualised using this technique. A similar situation encompassing protein detection by immunofluorescence but not by Western blot has been reported for the expression of some of the SARS-CoV accessory proteins (Pewe *et al.*, 2005). The ORFs encoding six of the SARS-CoV accessory proteins with C-terminal tags were inserted into the ORF4 site of MHV. All six tagged proteins could be detected by immunofluorescence but only three could be detected by Western blot. An explanation for this observation could involve the aggregation of the FLAG/5a protein or FLAG/5b protein during cell lysis or during the preparation for PAGE. If this occurred the aggregated protein would either not be loaded onto the gel because it would have formed a pellet during clarification of the cell lysate or not been able to be dispensed using the pipette tips used or the protein would not have migrated into the gel and stayed in the well.

Due to the absence of FLAG/3b expression as determined by a lack of fluorescence in cells transfected with pFLAG/3b and a report that the IBV 3b protein is rapidly degraded in mammalian cells (Pendleton and Machamer, 2006) experiments to detect FLAG/3b in the cell lysates of transfected Vero cells were not performed.

The construction of 5a and 5b proteins with different tags and expression of the FLAG/3b protein in avian cells would facilitate the same successful determination of the cellular protein interactions as performed for the FLAG/3a protein.

Chapter 7: General discussion and future work

General discussion

The aims of this project were to elucidate the target compartment and protein interactions of the IBV gene 3 and 5 accessory proteins. Immunofluorescence with confocal microscopy was used to identify the subcellular distribution of three of the four accessory proteins that have allowed a more tailored research approach to the study of these proteins. This was important not only to identify compartments of the cell where the accessory protein localise but also to eliminate potential functions of these proteins in the replication cycle of IBV. An example of this included the observation that neither the 3a or 5b proteins within infected cells localised to sites of S and M accumulation. A direct function for these two proteins in virion assembly was therefore unlikely and other lines of investigation were followed. Defining the protein-protein interactions of the IBV accessory proteins would assist in assigning a role these proteins play in the viral replication cycle. Immunoprecipitation experiments were used to distinguish the cellular proteins interacting with the 3a protein from the multitude of proteins expressed in a cell. Mass spectrometry was used to identify these interacting proteins and led to a modified pathway of research towards identifying the function of the 3a protein.

The IBV 3a protein

Subcellular location

Images of Beau-R infected CK and Vero cells produced by immunofluorescence and confocal microscopy displayed a punctate, cytoplasmic distribution pattern for the 3a protein. These puncta, as shown by the lack of colocalisation and even a similar distribution pattern, were distinct from the cellular structures of the ER, ERGIC and Golgi apparatus and from the viral proteins S and M. These were the subcellular sites of, and viral protein involved in, the assembly of virions and therefore the 3a protein would appear to play no direct part in this process. The formation of the punctate

fluorescence was interpreted to suggest that the 3a protein was associated with or inserted into a membrane which formed these structures. Pendleton and Machamer (2005) described a punctate cytoplasmic distribution pattern for the 3a protein, but a diffuse cytoplasmic distribution was also observed within infected and transfected Vero cells. This observation was accompanied by data suggesting that 60% of the 3a protein expressed *in vitro* was cytoplasmic and 40% was membrane associated. The detection of a diffuse, cytoplasmic species of the 3a protein could simply have been due to the antibody used, in so much as the antibody used to label the 3a protein for the images in this thesis was directed against the N-terminal section of the 3a protein and the C-terminal section of the 3a protein was detected with the antibody used for the Pendleton and Machamer (2005) images suggesting that the N-terminal portion of the diffuse 3a protein was unavailable for antibody binding. This may indicate that there were two species of 3a protein within an IBV-infected cell leading to the possibility of two or more different functions. Pendleton and Machamer (2005) showed that the punctate 3a protein colocalised with the MxA protein in transfected HeLa cells expressing a GFP tagged 3a protein which were induced to express the MxA protein by treatment with IFN-β were used. This colocalisation was only partial and may not suggest a protein interaction. Also MxA expression is induced by IFN signalling and the subsequent upregulation in IFN-inducible gene expression (Horisberger *et al.*, 1983; Staeheli and Haller, 1985) and coronaviruses have been demonstrated to induce undetectable amounts of IFN in cell culture (Frieman *et al.*, 2007; Roth-Cross *et al.*, 2007). The partial localisation of the 3a protein with MxA may only represent a situation produced by artificial manipulation of the cells. However, the work did show that the 3a protein localised to areas of the smooth ER where MxA can accumulate (Reichelt *et al.*, 2004).

Results from this thesis demonstrated that the punctate distribution of the 3a protein colocalised with an antibody which recognised dsRNA. This dsRNA was assumed to be generated by viral genome replication and transcription and as such was a marker for coronavirus RTCs present in the vicinity of virally induced DMVs. The source of membrane for the construction of these DMVs has been proposed to be the ER (Knoops *et al.*, 2008; Snijder *et al.*, 2006). If this is the case then the observations that the 3a protein localised to the smooth ER, colocalised with virally produced dsRNA and the ER being the source of the DMVs all fit the same scenario: 1) The ER was the source of the coronavirus DMVs which facilitated or, more likely, were a

product of the assembly of the RTCs. 2) The RTCs generated viral genomes and subgenomic RNAs, which also led to the formation of dsRNA. 3) These dsRNA molecules colocalised with the 3a protein where the activity of the 3a protein was conducted. This situation was interpreted to suggest that the role of the 3a protein in the replication cycle of IBV was to facilitate a process directly or indirectly involved in the replication and/or transcription of the RNAs generated by IBV. Certain caveats to this situation include the suggestion that the rough ER was the source of the DMVs, at least in SARS-CoV-infected Vero cells (Knoops *et al.*, 2008) and that the subcellular location of the dsRNA generated by coronavirus replication was distinct from the active RTCs. The fluorescence of two different nsps of SARS-CoV has been shown to colocalise within infected cells, but labelling of individual nsps with dsRNA did not produce any colocalisation. However, a very similar distribution pattern where the fluorescence from the two fluorophores surrounded each other was observed (Knoops *et al.*, 2008). The authors suggest that this discrepancy could result from the possible production of a huge excess of nsps of which only a small percentage would be active. Only those nsps which were actively involved in viral RNA synthesis would produce dsRNA and cause colocalisation between the nsp and dsRNA. The excess of inactive nsps would bind the majority of the anti-nsp antibody causing a separate fluorescence pattern from the anti-dsRNA antibody. Alternatively the majority of the dsRNA labelled by antibody may represent inactive complexes which were separate from the active RTCs containing the nsps. Either way the lack of colocalisation between the nsps and dsRNA may be a feature unique to SARS-CoV infection of Vero cells and may not apply to IBV infection of CK cells. But if it does this situation would imply that the IBV 3a protein is not directly or indirectly involved in the replication and/or transcription of the RNAs generated by IBV but rather with processing of the viral dsRNA to hide it from the host cell's innate immune defence system (Zhou and Perlman, 2007) or interacting with cellular proteins that were in the vicinity of the viral dsRNA.

The apparent localisation of the 3a protein with IBV-induced dsRNA was not influenced by the expression of other viral proteins as the subcellular distribution of a tagged 3a protein within transfected cells without any other IBV protein was the same as the distribution of native 3a protein in images of IBV-infected cells. This would indicate that the 3a protein alone can induce its accumulation to these punctate, presumably membranous structures to which it was inserted (Pendleton and

Machamer, 2005). An association of these 3a protein-containing membranes with the sites of dsRNA accumulation and thus the potential sites of IBV genome replication and transcription implied that the 3a protein performed one or more of its functions within the vicinity of the DMVs or surrounding convoluted membrane once they had been formed by the nsps. This action would have been later in the infection cycle as the 3a protein was first detected by immunofluorescence at 4 h p.i. in IBV infected CK cells while the DMVs can be observed at 2 h p.i. along with the first indications of dsRNA (Knoops *et al.*, 2008). The SARS ORF6 protein has been shown by immunofluorescence to colocalise with newly synthesised viral RNA (Tangudu *et al.*, 2007) and to enhance viral replication (Pewe *et al.*, 2005; Tangudu *et al.*, 2007; Zhao *et al.*, 2009a), with the enhancement observed to begin between 7 and 12 h p.i. The suggested mode of enhancement involved the viral RNA replication machinery as cells infected with MHV expressing the ORF6 protein contained five to eight fold more viral RNA than MHV not expressing the ORF6 protein (Tangudu *et al.*, 2007). The similarity in colocalisation with viral RNA for the SARS-CoV ORF6 protein and IBV 3a protein and the reduction in virus titres from SARS-CoV lacking the expression of the ORF6 protein and IBV lacking expression of the 3a protein (Hodgson *et al.*, 2006) suggest that the IBV 3a protein may also act to enhance viral RNA replication. The method of enhancement may not be identical to the direct action of the ORF6 protein as a reduction in virus titres of the recombinant IBV lacking the ability to express the 3a protein was only observed after 25 h p.i. in TOCs (Hodgson *et al.*, 2006) whereas SARS-CoV titres were increased after 6 h p.i. in Vero cells (Zhao *et al.*, 2009a). No reduction in virus titres for the rIBV ScAUG3a compared to Beau-R was observed in CK cells up to 90 h p.i. and therefore the activity of the Beau-R 3a protein may only manifest in epithelial cells of the respiratory tract rather than kidney-derived cells. This potential for an accessory protein to affect cell tropism has been described previously for the 3b accessory protein of TGEV (Zhang *et al.*, 2007), although the S protein sequence, which is a determinant of cell tropism (Casais *et al.*, 2003; Navas *et al.*, 2001; Sanchez *et al.*, 1999) contained deletions and there were amino acid changes to other viral proteins which may have contributed to this altered phenotype.

Protein interactions

Identification of the proteins interacting with the FLAG/3a protein revealed seven potential candidates. One of these was GCN1, the known function of which, in concert with GCN20 (Garcia-Barrio *et al.*, 2000; Vazquez de Aldana *et al.*, 1995), is to activate GCN2 (Pereira *et al.*, 2005) which phosphorylates the eIF2α subunit thereby attenuating host cell protein translation (Sood *et al.*, 2000). MHV and SARS-CoV have been shown to attenuate host cell protein translation (Bechill *et al.*, 2008; Krahling *et al.*, 2009; Raaben *et al.*, 2007) through the activation of PKR and PERK but not GCN2 (Krahling *et al.*, 2009) indicating that the eIF2α kinase activity of GCN2 was not required for translational inhibition in SARS-CoV infected human 293/ACE2 cells. A non-eIF2α kinase activity for GCN2 has been implicated in restricting the replication of several positive-sense RNA viruses, including Sindbis virus (Berlanga *et al.*, 2006) and VSV (Krishnamoorthy *et al.*, 2008). This hypothesis was based upon data demonstrating that production of VSV and Sindbis virus proteins increased in cells which did not express GCN2 or PERK indicating that there was a reduced host cell antiviral activity but that the level of viral protein production was unaffected by the presence or absence of high levels of phosphorylated eIF2α (Berlanga *et al.*, 2006; Krishnamoorthy *et al.*, 2008; Tesfay *et al.*, 2008). The potential interaction of the IBV 3a protein with GCN1 implies that, unlike Sindbis virus, the IBV genome is not detected by GCN2 immediately upon infection to initiate an antiviral activity but that like VSV and Sindbis virus GCN2 eventually detects the coronavirus genome, possibly during the large increase in viral RNA and protein levels between 4-6 h p.i. (Raaben *et al.*, 2007) at which time the expression of the 3a protein was first detected. At this time in the viral replication cycle GCN2 would exert an antiviral influence except that the 3a protein may bind to GCN1 thereby inhibiting the activation of GCN2. The antiviral activity of GCN2 has only recently been reported and many of the details remain to be determined. One of these finer points important in the hypothesis that the 3a protein binds to GCN1 thereby inactivating GCN2 is whether or not the antiviral activity of GCN2, as opposed to the eIF2α kinase activity, requires activation by GCN1. GCN1 has been shown to bind ribosomes where it interacts and promotes the activity of GCN2 to phosphorylate eIF2α by recognition of uncharged tRNAs during amino acid starvation (Sattlegger and Hinnebusch, 2000; 2005). This provides a reason for the GCN1-GCN2 interaction for the inhibition of host cell protein translation but also

suggests that if the antiviral activity of GCN2 is distinct from ribosomes then GCN1 may not be needed for GCN2 activation. If GCN1 is not required for the antiviral response of GCN2 then other functions for GCN1 in the context of an IBV-infected cell will have to be examined.

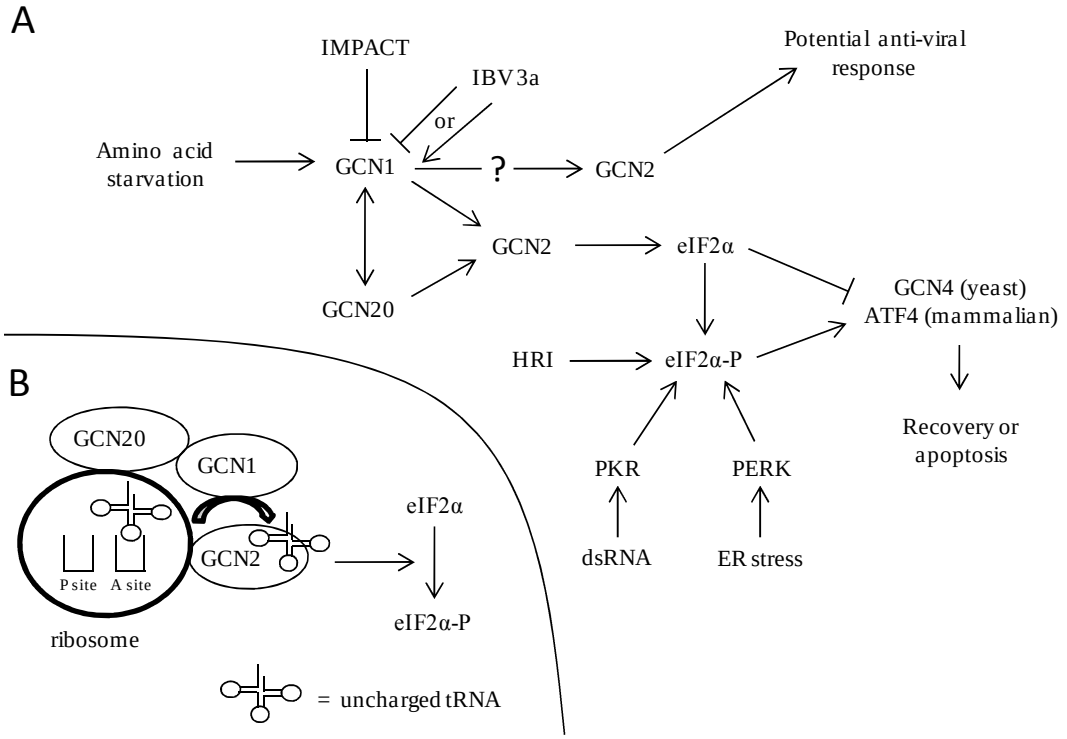

Figure 7.1. Model of GCN1 function in activating GCN2. (A) Amino acid starvation within a cell is detected by GCN1 which activates, in conjunction with GCN20, GCN2. GCN2 phosphorylates the eIF2α subunit of the eukaryotic translation initiation factor eIF2. Attenuation of host cell translation leads to an increase in the translation of ATF4 resulting in the activation of downstream factors which can either lead to the cell recovering from temporary stress or apoptosis. The other pathways culminating in phosphorylation of the eIF2α subunit are shown as well as IMPACT, a competitive inhibitor of GCN1 binding to GCN2. The potential interaction of the IBV 3a protein may inhibit or activate GCN1 to manipulate the protein kinase or anti-viral activity of GCN2. (B) Model of the process whereby uncharged tRNAs activate GCN2 to phosphorylate the eIF2α subunit. Upon binding of uncharged tRNAs to the A site within ribosomes the GCN1/GCN20 complex activates the translocation of the uncharged tRNA to GCN2 which facilitates the initiation of the protein kinase function of GCN2. The eIF2α subunit is then phosphorylated attenuating cellular translation.

The other main candidate protein identified as potentially interacting with the FLAG/3a protein was PP2A. Cell cycle regulation, signal transduction, apoptosis

and the stress response have all been attributed to the multifunctional PP2A. Confirmation of the protein interaction between PP2A and the IBV 3a protein would be worth investigating further as PP2A is influenced during infection by many viruses. An increased expression of PP2A was found in cells infected with Hepatitis B virus as a consequence of an activated ER stress response (Christen *et al.*, 2007b). The upregulation of which led indirectly to an inhibition of IFN-α signalling (Christen *et al.*, 2007a). Coronaviruses have been shown to induce ER stress (Bechill *et al.*, 2008; Chan *et al.*, 2006; Versteeg *et al.*, 2007b) although no observations concerning the state of PP2A have been presented. The coronavirus S protein has been demonstrated to cause ER stress followed by activation of the UPR (Chan *et al.*, 2006) and presumably an upregulation in PP2A activity but the 3a protein may also influence PP2A to inhibit interferon signalling. The small t antigen of simian virus 40 was found to downregulate the phosphatase activity of PP2A (Yang *et al.*, 1991) which resulted in the potential for cell transformation (Hahn *et al.*, 2002) but in contrast arrest of the cell cycle by upregulation of PP2A has been described for the HIV Vpr protein (Elder *et al.*, 2001), the Adenovirus E4orf4 protein (Li *et al.*, 2009) and implied for the HTLV Tax protein (Fu *et al.*, 2003; Haoudi *et al.*, 2003). Manipulation of the cell cycle has been described for several coronaviruses and may be influenced by regulation of PP2A. MHV induced G0/G1 phase arrest from the accumulation of non-phosphorylated pRb (Chen and Makino, 2004) but this was demonstrated to be a consequence of nsp1 protein expression (Chen *et al.*, 2004). IBV does not express the equivalent of an nsp1 protein and so the function of causing arrest of the cell cycle may reside in another viral protein. Several different non-gene 1 accessory proteins of the SARS-CoV have been implicated in inducing G0/G1 phase arrest via the cyclin D3/pRb pathway (Yuan *et al.*, 2005b; Yuan *et al.*, 2006b; Yuan *et al.*, 2007). In contrast to these two Group 2 coronaviruses the Group 3 coronavirus IBV was demonstrated to induce G2/M phase arrest (Dove *et al.*, 2006) as a result of reduced amounts of cyclin D1 (Harrison *et al.*, 2007). Transcriptional expression of cyclin D1 is facilitated by transcription factors including NF-κB (Guttridge *et al.*, 1999), AP-1 (Albanese *et al.*, 1999) and GLI3 (Hu *et al.*, 2006). PP2A has been shown to reduce transcriptional expression of the cyclin D1 gene by negatively regulating these transcription factors (Frost *et al.*, 1994; Krauss *et al.*, 2008; Sontag *et al.*, 1997). Therefore the manipulation of the cell

cycle, along with the potential control of the UPR and other cellular functions may occur via the interaction of the IBV 3a protein with PP2A.

GCN1 and the regulatory subunit of PP2A were both identified as cellular proteins which associate with the SARS-CoV virion (Neuman *et al.*, 2008). The SARS-CoV virion also includes some of the accessory proteins (Huang *et al.*, 2006; Huang *et al.*, 2007; Ito *et al.*, 2005). Given that the IBV 3a protein potentially interacts with these cellular proteins one or more of the SARS-CoV –associated accessory proteins may also interact with these cellular proteins providing an explanation for their association with virions.

The potential interaction with Exportin 1 may also be worth investigating even though the subcellular distribution of Exportin 1 does not match that of the 3a protein. Exportin 1, also known as CRM1, is a karyopherin β protein which exports proteins possessing a leucine-rich nuclear export signal (NES) from the nucleus into the cytoplasm. This nuclear export protein facilitates the shuttling of many proteins including STAT1 (Begitt *et al.*, 2000). The binding of type I interferon (IFN-α/β) to the IFN receptor leads to the phosphorylation of cytoplasmic STAT1 and subsequent translocation to the nucleus via karyopherin alpha 1 and beta 1. Within the nucleus the protein complex interferon-stimulated gene factor 3, which includes STAT1, initiates transcription of IFN-α/β-inducible genes that establish an antiviral response. STAT1 accumulation in the nucleus is transient and translocates back to the cytoplasm when Exportin 1 recognises the leucine-rich NES within STAT1 and binds to RanGTP. The IBV 3a protein could sequester Exportin 1 in the cytoplasm so that it cannot be used to export STAT1 back out of the nucleus and initiate additional rounds of transcription. This scenario would not inhibit an opening round of IFN-α/β-inducible gene expression and therefore would appear of questionable importance. Alternatively the cytoplasmic accumulation of Exportin 1 may inhibit the nuclear export of certain mRNAs. Exportin 1 has been shown to be dispensable for the export of tRNA (Fornerod *et al.*, 1997) and most cellular mRNAs (Herold *et al.*, 2003) but a subset of mRNAs have been demonstrated to require Exportin 1 for nuclear export. Several mRNAs from Jurkat T cells were shown to be dependent upon export by Exportin 1 including tumour necrosis factor alpha and the interleukin 2 receptor alpha (Schutz *et al.*, 2006) and the cytoplasmic accumulation of IFN-α1 mRNA was arrested by the inhibition of Exportin 1 in HeLa cells (Kimura *et al.*,

2004). The sequestering of Exportin 1 in the cytoplasm by the X protein of Hepatitis B virus has been reported (Forgues *et al.*, 2001) so the IBV 3a protein may bind and cause the cytoplasmic accumulation of Exportin 1 so that certain mRNAs involved in generating an antiviral response are inhibited from leaving the nucleus and being used to generate protein. Analysis of the amino acid sequence of the 3a accessory protein of IBV Beaudette highlighted a high percentage of leucines. 25% of the amino acids which constitute the 3a protein are leucines compared to 6% and 10% for the 3b and 5b accessory proteins respectively. The IBV 5a protein also contains a large percentage of leucines at 26%. The current consensus for a leucine-rich NES is $\Phi-X_{2-3}-\Phi-X_{2-3}-\Phi-X-\Phi$ (Φ: L, I, F, V, M; X: any amino acid) (Engelsma *et al.*, 2004) with the 3a protein containing the sequence INSNLQSRLTL at the C-terminal end. This site could bind Exportin 1 to sequester it in the cytoplasm although the interaction between Exportin 1 and the 3a protein may not occur via a leucine-rich NES and the high leucine content may have another function.

The interaction of a coronavirus accessory protein with a member of the cellular karyopherin family has been described previously. Frieman *et al*. (2007) demonstrated that the SARS-CoV ORF6 protein could interact with karyopherin alpha 2 (KPNA2) to cause an indirect arrest in the nuclear import of activated STAT1. This effect was caused by tethering of KPNA2, via the ORF6 protein, to the rough ER/Golgi membrane. The ORF6 protein consists of a N-terminal hydrophobic region and a C-terminal hydrophilic region. The N-terminal domain has been implicated in membrane association/insertion (Netland *et al.*, 2007) whereas the C-terminal ten amino acids were involved in binding to KPNA2 and predicted to protrude into the cytoplasm (Frieman *et al.*, 2007). The IBV 3a protein has a similar hydrophobicity profile (Fig. 7.2) with a N-terminal hydrophobic region and C-terminal hydrophilic domain and shown to have a C-terminal tail located in the cytoplasm (Pendleton and Machamer, 2005). These data were interpreted to indicate that both the 3a protein and the ORF6 protein have similar topologies and potentially bind karyopherin proteins at their C-termini to inhibit nucleocytoplasmic shuttling.

Figure 7.2. Hydrophobicity plots of the IBV accessory proteins compared to the SARS-CoV ORF6 protein. The amino acid sequences for the IBV accessory proteins and the SARS-CoV ORF6 protein were compared using the Kyte and Doolittle scale mean hydrophobicity scale.

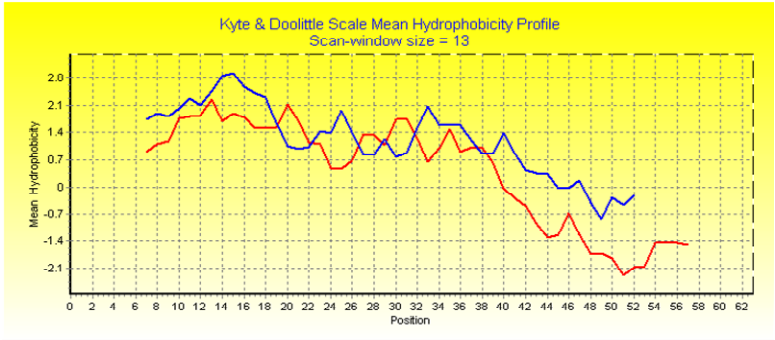

SARS ORF6

IBV 3a

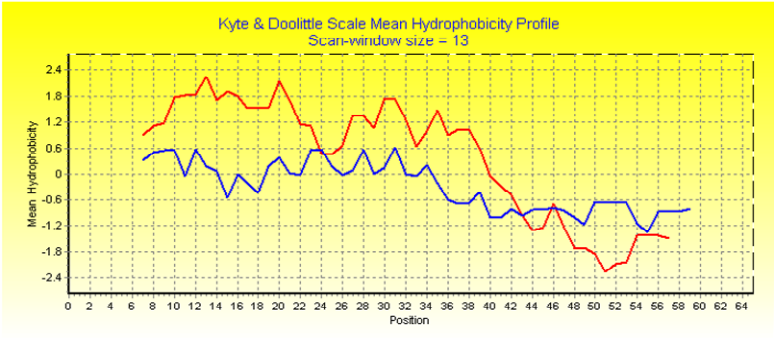

SARS ORF6

IBV 3b

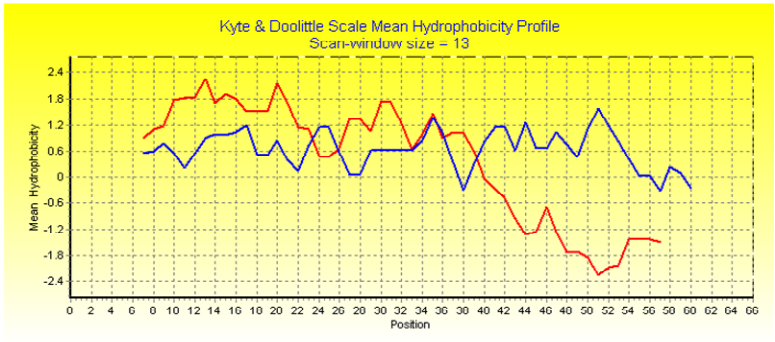

SARS ORF6

IBV 5a

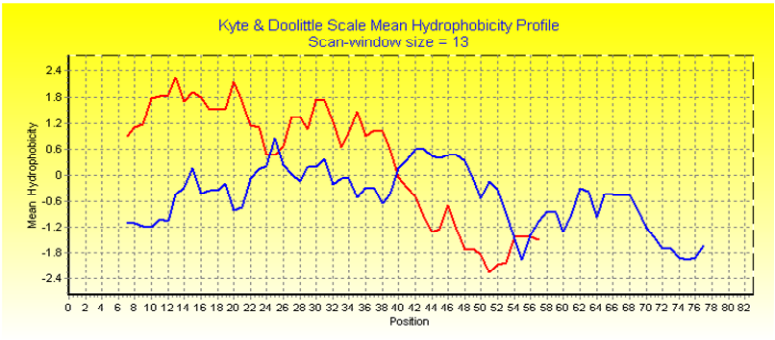

SARS ORF6

IBV 5b

The IBV 3b protein

Identification of the subcellular location and protein interactions of the IBV 3b protein was unsuccessful. This was due to the lack of an antiserum directed towards the 3b sequence to perform immunofluorescence with confocal microscopy using cells infected with Beau-R and the high turn-over of the IBV 3b protein in Vero cells. Protein interactions for the IBV 3a protein were identified using a FLAG-tagged version of the 3a protein. Expression of a FLAG-tagged 3b protein could not be detected in transfected Vero cells using an anti-FLAG antibody when expression of FLAG/3a, FLAG/5a and FLAG/5b could be detected. This may have been due to the short half-life of the 3b protein demonstrated to occur in mammalian cells (Pendleton and Machamer, 2006). Expression of the FLAG/3b protein could not be detected in transfected CK cells which was possibly due to a reduced efficiency in transfection of these cells.

The IBV 5a protein

The subcellular localisation of the IBV 5a protein was examined by expressing a FLAG-tagged 5a protein in Vero cells and performing indirect immunofluorescence with confocal microscopy to generate images of the resulting fluorescence. These images of transfected cells indicated that the FLAG/5a protein localised in a punctate, cytoplasmic distribution pattern which was not dependent on the presence of other viral proteins. Colocalisation between the FLAG/5a protein and markers for the ER, ERGIC and Golgi apparatus would not be expected due to the different distribution patterns observed within IBV infected cells. This would also suggest that the FLAG/5a would not colocalise with the M and S proteins indicating that the FLAG/5a protein does not have a function in virion assembly. There was also no colocalisation observed between the diffuse, cytoplasmic N protein and the FLAG/5a protein. The punctate cytoplasmic pattern was reminiscent of the distribution of dsRNA labelling and therefore also of the 3a protein within IBV infected Vero and CK cells. If this was correct then a similar scenario as to the function of the 3a protein can be envisioned where the 3a protein provides a direct or indirect function to the DMVs or RTCs which ensures efficient generation of viral RNA at later time points of infection (i.e. after 5-6 h p.i. when the accessory proteins are first detected).

However a reduction in virus titres observed for the rIBV ScAUG3a after 25 h p.i. in TOCs (Hodgson *et al.*, 2006) was not observed for rIBV ScAUG5a (Casais *et al.*, 2005) possibly negating the potential activity of the 5a protein in viral RNA synthesis. The absence of variations in virus titres between Beau-R and rIBV ScAUG5a in CK cells and TOCs would suggest that a function for the 5a protein in evading the innate immune response is unlikely as CK cells and TOCs are assumed to be innate immune competent as they are obtained directly from immune competent chicks.

The IBV 5b protein

Images of the subcellular distribution of the IBV 5b protein indicated a diffuse, cytoplasmic distribution. This pattern was the same in cells transfected with a plasmid which expressed the FLAG/5b protein. As with the IBV 3a protein, the subcellular distribution of the 5b protein was not dependent upon the expression of other IBV proteins. The diffuse cytoplasmic distribution did not colocalise with any subcellular markers used or other viral proteins indicating that the 5b protein was not directly involved in virion assembly. This distribution pattern was very similar to the distribution of a combination of IBV structural proteins within Beau-R infected cells. The fluorescence obtained by labelling the FLAG/5b protein and the IBV structural proteins within transfected and infected Vero cells partially overlapped indicating a close spatial relationship for a minor proportion of these two proteins. The majority of the fluorescence was separate however and suggested that the two proteins were spatially distinct indicating no direct role of the 5b protein in regulating or influencing these IBV structural proteins. The IBV 5b protein was not detected in purified IBV virions (Liu and Inglis, 1991) and thus is a non-structural protein thereby also discounting the possibility of the 5b protein interacting with an IBV structural protein. If the small amount of colocalisation of the 5b protein with one or more of the structural proteins indicates an interaction this would appear to not lead to the incorporation of the protein in the virion.

Overview

The current literature concerned with the non-gene 1 accessory proteins of coronaviruses suggest that their loss is well tolerated by the recombinant virus in cell culture (Casais *et al.*, 2005; de Haan *et al.*, 2002; Haijema *et al.*, 2004; Hodgson *et al.*, 2006; Sola *et al.*, 2003; Yount *et al.*, 2005). However there are conflicting results as to the effect these accessory proteins have in causing clinical signs of disease. Some recombinant coronaviruses not expressing one or more of the accessory proteins result in reduced morbidity and mortality (de Haan *et al.*, 2002; Haijema *et al.*, 2004) whereas for other coronaviruses there would appear to be little or no change in the virus's ability to cause disease (Dediego *et al.*, 2008; Mardani *et al.*, 2008; Yount *et al.*, 2005). The accessory proteins of other viruses have a wide variation in functions which includes inhibition of the innate immune response. If any of the IBV accessory proteins perform a similar role it would appear likely to be the 3a protein. The reduction in rIBV ScAUG3a titres after 25 h p.i. could suggest that the viral replication is being inhibited by an induced antiviral state. Results from this thesis indicating that the 3a protein colocalises with viral dsRNA and potentially interacts with GCN1, PP2A and Exportin 1 suggest that the potential role of this accessory protein is not countering a direct innate immune response but manipulating the cellular environment for the benefit of virus replication which also affects the antiviral state. The discovery of novel IBVs lacking three of the four accessory proteins circulating in Australian chicken flocks indicated that IBV can replicate *in vivo* without these proteins and still cause a similar level of pathology although with reduced titres (Mardani *et al.*, 2008). This could imply that there is more redundancy in the rest of the IBV genome for the functions of the accessory proteins than there is in the MHV or FIPV genomes where absence of the accessory proteins resulted in the appearance of markedly less severe clinical signs.

An effective vaccine would generate adequate levels of neutralising antibody to provide protection against infection. Data obtained from kittens infected with recombinant FIPV indicated that levels of neutralising antibody were high when infected with viruses lacking expression of either the gene 3 or 7 accessory proteins but were reduced when infected with a virus lacking the expression of both (Haijema *et al.*, 2004). The same situation occurred with the novel IBVs where high titres of neutralising antibody were found in chickens infected with IBVs expressing a full

complement of accessory proteins but much lower titres were induced upon infection with the novel IBVs (Mardani *et al.*, 2008). It would seem appropriate to suggest that a candidate IBV vaccine should include two or more of the accessory proteins to facilitate a good neutralising antibody response but that expression of the 3a protein be removed because of its potential to upregulate the amount of viral RNA and to inhibit an antiviral state within the infected cell thereby generating more viral progeny and causing unacceptable levels of morbidity.

Future work

The 3a protein colocalises with viral dsRNA, but is this newly replicated viral RNA found at active RTCs or the location of a non-functional by-product of replication?

To answer this question newly transcribed RNA can be monitored by the inclusion of 5-Bromouridine 5′-triphosphate (BrUTP) and indirect immunofluorescence with confocal microscopy using an anti-BrUTP antibody to detect this compound. Colocalisation between the 3a protein and newly synthesised viral RNA would suggest that this accessory protein could affect the generation of viral RNA. The absence of colocalisation would suggest that the dsRNA detected within coronavirus infected cells is inactive and possibly sequestered away from the RTCs for processing.

Is the 3a protein affecting the levels of viral RNA and protein?

Quantitative real-time PCR can be used to compare the levels of viral RNA generated in cells infected with Beau-R and rIBV ScAUG3a against a cellular house-keeping gene. A time-course of infection could also be performed to compare when the levels of viral RNA rise in IBV infected cells to when the 3a protein is first expressed. Analysis of the levels of viral protein production in cells infected with Beau-R and rIBV ScAUG3a can be performed by Western blot using anti-viral protein antibodies.

What effect is the 3a protein having on the cell by interacting with GCN1, PP2A and Exportin 1?

Presently the GCN1 protein has two functions, one of which involves activation of GCN2 to phosphorylate the eIF2α subunit and the other is an undefined antiviral activity not related to the inhibition of host cell protein translation. The degree of GCN2 activation by phosphorylation could be studied along with the amount of eIF2α phosphorylation in cells infected with Beau-R or rIBV ScAUG 3a to determine whether the interaction between the 3a protein and GCN1 changes the phosphorylation states of both GCN2 and the eIF2α subunit. If these are unaffected then the undefined antiviral activity of GCN2 may be playing a part.

What do the 3b, 5a and 5b proteins interact with?

The 3b, 5a and 5b accessory proteins have yet to be assigned a function during the replication cycle of IBV. A modification to the tagged protein pull-down assays used in Chapter 6 could be used to identify the protein-protein interactions. The use of a different tag or the FLAG tag at the C-terminal end of the protein may facilitate the detection by Western blot of the 5a and 5b proteins which had been expressed in Vero cells. Once detected in the cell lysate by Western blot the tagged proteins could be precipitated from the lysate and the cellular proteins interacting identified by tandem mass spectrometry.

Ultimately, using a pathogenic clone of IBV, does knocking-out one or more of the accessory proteins make the virus less pathogenic and a good vaccine candidate?

A pathogenic clone of IBV which could not express one or more of the accessory proteins would demonstrate whether these proteins are involved in the pathogenicity of IBV or whether they have another function. Data from these experiments combined with the identification of protein interactions will facilitate the generation of a rationally attenuated vaccine for IBV.

Appendix

List of oligonucleotides

SUMO plasmids

Table A.1. Oligonucleotides used to amplify the IBV 3b and ADRP sequences

			Position in IBV genome	
Name	Sequence	Sense	5'end	3' end
3b-forward	ATGTTAAACTTAGAAGTAATTATTG	+	24029	24053
3b-reverse	TTATTCAATAAATTCATCATCACC	–	24223	24200
ADRP-forward	GAGTATAAAACATGTGTGGGTG	+	3571	3592
ADRP-reverse	ATCGAAATAATCGATGTGTTCTTG	–	4044	4021

Table A.2. List of oligonucleotides used to amplify the IBV accessory protein ORFs and construct the pFLAG plasmids.

			Position in IBV genome[b]	
Name	Sequence[a]	Sense	5' end	3' end
3a-forward EcoRI	GCCGCGAATTCGATGATCCAAAGTCCCACG	+	23856	23873
3a-reverse EcoRI	TATCGATGAATTCGCTTAGTCTAGACTGTGCCAAAGG	–	24029	24006
3b-forward EcoRI	GCCGCGAATTCAATGTTAAACTTAGAAGTAATTATTGAAACTG	+	24029	24059
3b-reverse EcoRI	TATCGATGAATTCGCTTATTCAATAAATTCATCATCACC	–	24223	24200
5a-forward EcoRI	GCCGCGAATTCAATGAAATGGCTGACTAGTTTTG	+	25488	25509
5a-reverse EcoRI	TATCGATGAATTCGCTCATGCCAGCGATTGGGTGG	–	25685	25666
5b-forward EcoRI	GCCGCGAATTCAATGAATAATAGTAAAGATAATCCTTTTCG	+	25682	25710
5b-reverse EcoRI	TATCGATGAATTCGCCTAGTTTAATGACTGGCGCTG	–	25930	25910

[a] Restriction site sequences are highlighted in red. Start codons are highlighted in blue. Stop codons are highlighted in green.
[b] Position in IBV genome starting from the start or stop codon.

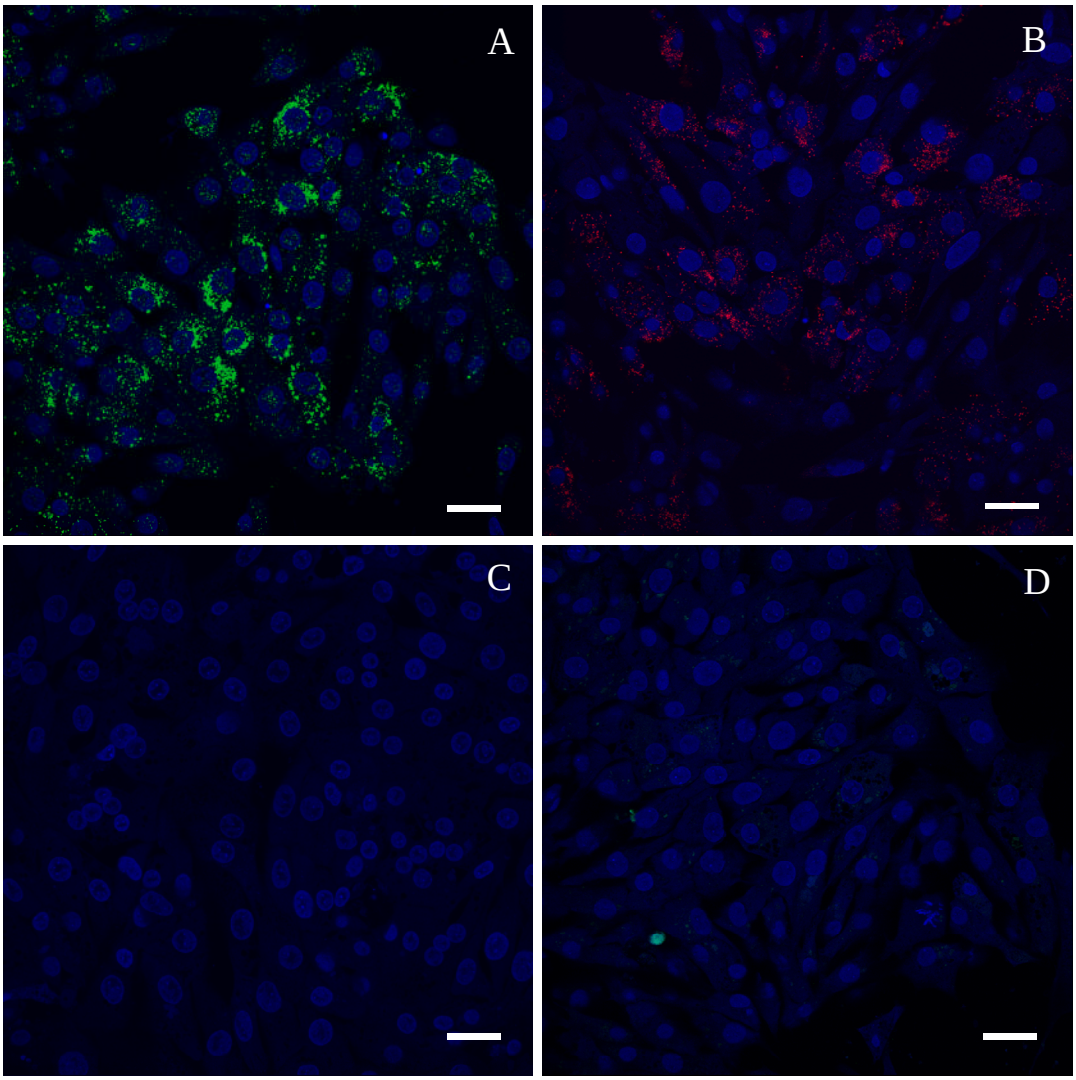

Figure A.1. Indirect immunofluorescence analysis of the antibody cross-reactivity controls for the immunofluorescence experiments. Subconfluent CK cells were infected with Beau-R and fixed at 14 h p.i. with paraformaldehyde. After making the cells permeable they were labelled with (A) rabbit anti-3a protein 8194 + Alexa Fluor 488 anti-rabbit IgG (green); (B) mouse anti-dsRNA J2 + Alexa Fluor 568 anti-mouse IgG (red); (C) rabbit anti-3a protein 8194 + Alexa Fluor 568 anti-mouse IgG (red); and (D) mouse anti-dsRNA J2 + Alexa Fluor 488 anti-rabbit IgG (green). Nuclei were labelled with DAPI. The different wavelengths (colours) were scanned independently and digitally merged.

Figure A.1a. Indirect immunofluorescence analysis of the intracellular location of the 3a protein compared to dsRNA in mock infected cells. Subconfluent CK cells were infected with Beau-R and fixed at 10 h p.i. with paraformaldehyde. After making the cells permeable with Triton X-100 they were labelled with rabbit polyclonal anti-3a (8194) (A) and mouse anti-dsRNA J2 (B). Secondary antibodies included Alexa Fluor 488 anti-rabbit (green) and Alexa Fluor 568 anti-mouse (red). Nuclei were labelled with DAPI. The different wavelengths (colours) were scanned independently and digitally merged (C). Scale bar indicates 20 μm.

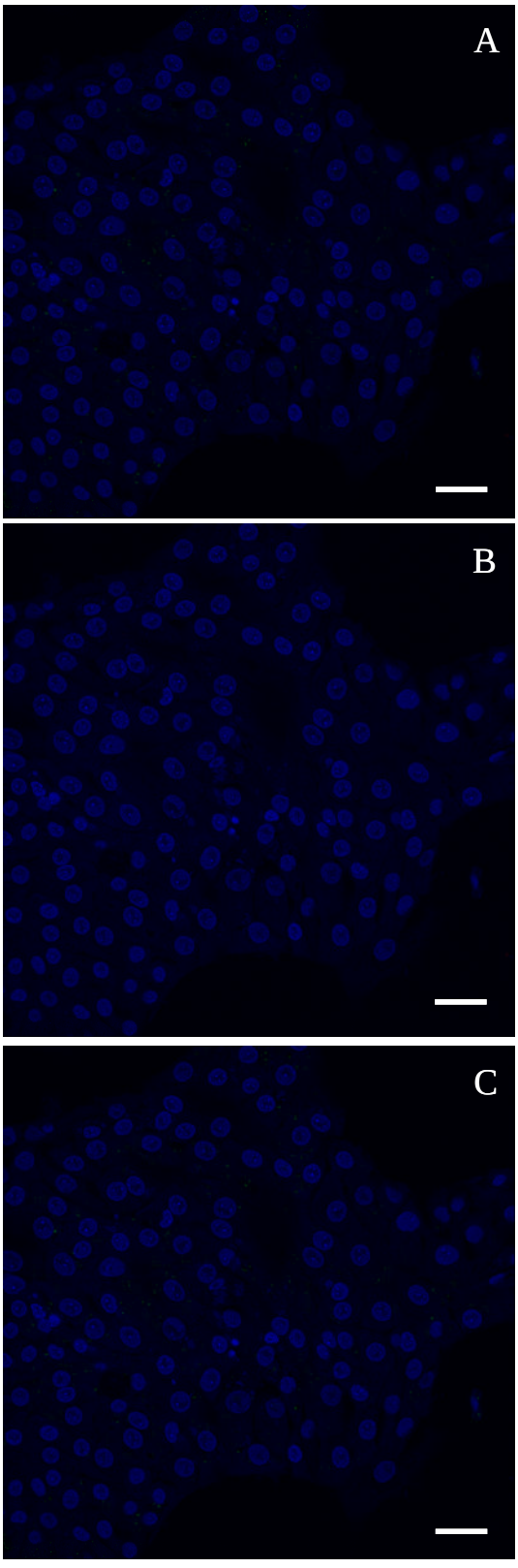
A
B
C

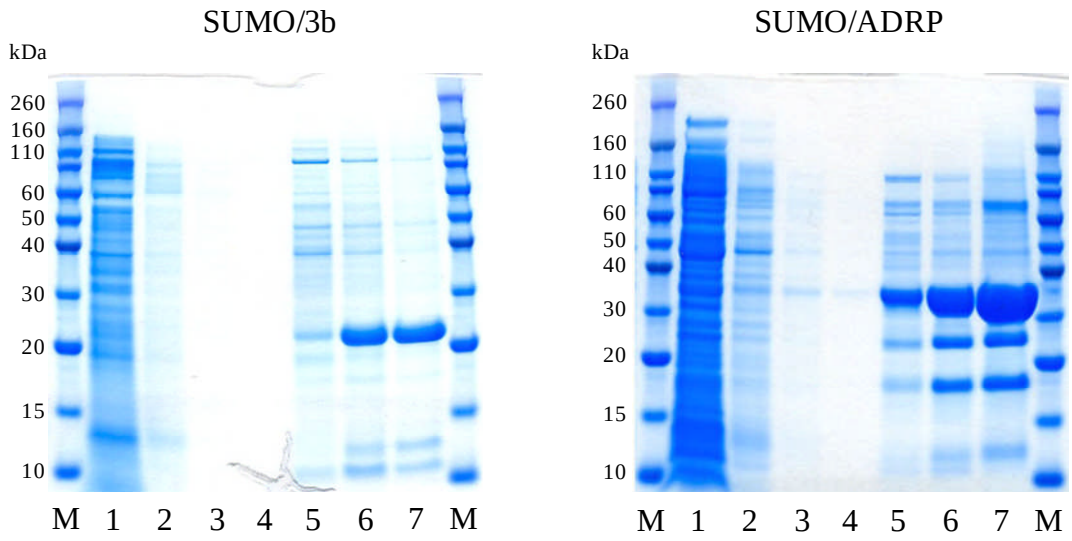

Figure A.2. Purification of the recombinant SUMO/3b and SUMO/ADRP proteins. pET SUMO/3b and pET SUMO/ADRP were used to transform E. coli. After bacterial growth and expression of the recombinant proteins the cells were lysed and the His-tagged SUMO proteins were purified using the His-select gel. Protein samples were separated by PAGE and the proteins were visualised with the total protein stain GelCode Blue. M = molecular weight marker. Lane 1 = cell lysate. Lane 2 = supernatant after the first wash. Lane 3 = supernatant after the second wash. Lane 4 = supernatant after the third wash. Lane 5 = eluted proteins after elution with 20 mM Imidazole. Lane 6 = eluted proteins after elution with 60 mM Imidazole. Lane 7 = eluted proteins after elution with 250 mM Imidazole.

Table A.3. Confirmation of the expression of the SUMO/3b protein.

SUMO/3b ESI mass spectrometry analysis

m/z	Number of charges	m/z x charges	mass - protons	+ methionine
901.29	23	20729.67	20706.486	20837.486
942.22	22	20728.84	20706.664	20837.664
987.04	21	20727.84	20706.672	20837.672
1036.33	20	20726.6	20706.44	20837.44
1090.83	19	20725.77	20706.618	20837.618
1151.37	18	20724.66	20706.516	20837.516
1219.04	17	20723.68	20706.544	20837.544
1295.18	16	20722.88	20706.752	20837.752
1381.46	15	20721.9	20706.78	20837.78
1480.07	14	20720.98	20706.868	20837.868
1593.86	13	20720.18	20707.076	20838.076
1726.6	12	20719.2	20707.104	20838.104
1883.48	11	20718.28	20707.192	20838.192

SUMO/3b average mass predicted	20839
SUMO/3b average mass experimental	20837.75
SUMO/3b standard deviation experimental	0.25

Table A.4. Confirmation of the expression of the SUMO/ADRP protein.

SUMO/ADRP ESI mass spectrometry analysis

m/z	Number of charges	m/z * charges	mass - protons	+ methionine
944.51	33	31168.83	31135.566	31266.566
974.03	32	31168.96	31136.704	31267.704
1005.43	31	31168.33	31137.082	31268.082
1038.9	30	31167	31136.76	31267.76
1074.68	29	31165.72	31136.488	31267.488
1113.03	28	31164.84	31136.616	31267.616
1154.21	27	31163.67	31136.454	31267.454
1198.58	26	31163.08	31136.872	31267.872
1246.48	25	31162	31136.8	31267.8
1298.41	24	31161.84	31137.648	31268.648
1354.75	23	31159.25	31136.066	31267.066

SUMO/ADRP average mass predicted	31267
SUMO/ADRP average mass experimental	31267.64
SUMO/ADRP standard deviation experimental	0.53

Bibliography

Aiken, C. and Trono, D. (1995)**.** Nef stimulates human immunodeficiency virus type 1 proviral DNA synthesis. *J Virol* **69**, 5048-5056.

Albanese, C., D'Amico, M., Reutens, A. T., Fu, M., Watanabe, G., Lee, R. J., Kitsis, R. N., Henglein, B., Avantaggiati, M., Somasundaram, K., Thimmapaya, B. and Pestell, R. G. (1999)**.** Activation of the cyclin D1 gene by the E1A-associated protein p300 through AP-1 inhibits cellular apoptosis. *J Biol Chem* **274**, 34186-34195.

Alvarado, I. R., Villegas, P., Mossos, N. and Jackwood, M. W. (2005)**.** Molecular characterization of avian infectious bronchitis virus strains isolated in Colombia during 2003. *Avian Dis* **49**, 494-499.

Ammayappan, A., Upadhyay, C., Gelb, J., Jr. and Vakharia, V. N. (2009)**.** Identification of sequence changes responsible for the attenuation of avian infectious bronchitis virus strain Arkansas DPI. *Arch Virol*. **154**, 495-499.

Armesto, M., Cavanagh, D. and Britton, P. (2009). The replicase gene of avian coronavirus infectious bronchitis virus is a determinant of pathogenicity. *PLoS One* 4: e7384.

Baric, R. S., Nelson, G. W., Fleming, J. O., Deans, R. J., Keck, J. G., Casteel, N. and Stohlman, S. A. (1988)**.** Interactions between coronavirus nucleocapsid protein and viral RNAs: implications for viral transcription. *J Virol* **62**, 4280-4287.

Bechill, J., Chen, Z., Brewer, J. W. and Baker, S. C. (2008)**.** Coronavirus infection modulates the unfolded protein response and mediates sustained translational repression. *J Virol* **82**, 4492-4501.

Begitt, A., Meyer, T., van Rossum, M. and Vinkemeier, U. (2000)**.** Nucleocytoplasmic translocation of Stat1 is regulated by a leucine-rich export signal in the coiled-coil domain. *Proc Natl Acad Sci U S A* **97**, 10418-10423.

Bell, I., Schaefer, T. M., Trible, R. P., Amedee, A. and Reinhart, T. A. (2001)**.** Down-modulation of the costimulatory molecule, CD28, is a conserved activity of multiple SIV Nefs and is dependent on histidine 196 of Nef. *Virology* **283**, 148-158.

Benson, R. E., Sanfridson, A., Ottinger, J. S., Doyle, C. and Cullen, B. R. (1993)**.** Downregulation of cell-surface CD4 expression by simian immunodeficiency virus Nef prevents viral super infection. *J Exp Med* **177**, 1561-1566.

Berlanga, J. J., Ventoso, I., Harding, H. P., Deng, J., Ron, D., Sonenberg, N., Carrasco, L. and de Haro, C. (2006)**.** Antiviral effect of the mammalian translation initiation factor 2alpha kinase GCN2 against RNA viruses. *EMBO J* **25**, 1730-1740.

Bermingham, A. and Collins, P. L. (1999)**.** The M2-2 protein of human respiratory syncytial virus is a regulatory factor involved in the balance between RNA replication and transcription. *Proc Natl Acad Sci U S A* **96**, 11259-11264.

Bhardwaj, K., Guarino, L. and Kao, C. C. (2004)**.** The severe acute respiratory syndrome coronavirus Nsp15 protein is an endoribonuclease that prefers manganese as a cofactor. *J Virol* **78**, 12218-12224.

Bossert, B. and Conzelmann, K. K. (2002)**.** Respiratory syncytial virus (RSV) nonstructural (NS) proteins as host range determinants: a chimeric bovine RSV with NS genes from human RSV is attenuated in interferon-competent bovine cells. *J Virol* **76**, 4287-4293.

Bost, A. G., Prentice, E. and Denison, M. R. (2001)**.** Mouse hepatitis virus replicase protein complexes are translocated to sites of M protein accumulation in the ERGIC at late times of infection. *Virology* **285**, 21-29.

Brayton, P. R., Ganges, R. G. and Stohlman, S. A. (1981)**.** Host cell nuclear function and murine hepatitis virus replication. *J Gen Virol* **56**, 457-460.

Bredenbeek, P. J., Noten, A. F., Horzinek, M. C. and Spaan, W. J. (1990)**.** Identification and stability of a 30-kDa nonstructural protein encoded by mRNA 2 of mouse hepatitis virus in infected cells. *Virology* **175**, 303-306.

Bridgen, A., Weber, F., Fazakerley, J. K. and Elliott, R. M. (2001)**.** Bunyamwera bunyavirus nonstructural protein NSs is a nonessential gene product that contributes to viral pathogenesis. *Proc Natl Acad Sci U S A* **98**, 664-669.

Brierley, I., Boursnell, M. E., Binns, M. M., Bilimoria, B., Blok, V. C., Brown, T. D. and Inglis, S. C. (1987)**.** An efficient ribosomal frame-shifting signal in the polymerase-encoding region of the coronavirus IBV. *EMBO J* **6**, 3779-3785.

Brierley, I., Digard, P. and Inglis, S. C. (1989)**.** Characterization of an efficient coronavirus ribosomal frameshifting signal: requirement for an RNA pseudoknot. *Cell* **57**, 537-547.

Brierley, I., Jenner, A. J. and Inglis, S. C. (1992)**.** Mutational analysis of the "slippery-sequence" component of a coronavirus ribosomal frameshifting signal. *J Mol Biol* **227**, 463-479.

Bussmann, B. M., Reiche, S., Jacob, L. H., Braun, J. M. and Jassoy, C. (2006)**.** Antigenic and cellular localisation analysis of the severe acute respiratory syndrome coronavirus nucleocapsid protein using monoclonal antibodies. *Virus Res* **122**, 119-126.

Butcher, G. D., Winterfield, R. W. and Shapiro, D. P. (1990)**.** Pathogenesis of H13 nephropathogenic infectious bronchitis virus. *Avian Dis* **34**, 916-921.

Calenoff, M. A., Badshah, C. S., Dal Canto, M. C., Lipton, H. L. and Rundell, M. K. (1995)**.** The leader polypeptide of Theiler's virus is essential for neurovirulence but not for virus growth in BHK cells. *J Virol* **69**, 5544-5549.

Casais, R., Davies, M., Cavanagh, D. and Britton, P. (2005)**.** Gene 5 of the avian coronavirus infectious bronchitis virus is not essential for replication. *J Virol* **79**, 8065-8078.

Casais, R., Dove, B., Cavanagh, D. and Britton, P. (2003)**.** Recombinant avian infectious bronchitis virus expressing a heterologous spike gene demonstrates that the spike protein is a determinant of cell tropism. *J Virol* **77**, 9084-9089.

Casais, R., Thiel, V., Siddell, S. G., Cavanagh, D. and Britton, P. (2001)**.** Reverse genetics system for the avian coronavirus infectious bronchitis virus. *J Virol* **75**, 12359-12369.

Cavanagh, D., Darbyshire, J. H., Davis, P. and Peters, R. W. (1984)**.** Induction of humoral neutralising and haemagglutination-inhibiting antibody by the spike protein of avian infectious bronchitis virus. *Avian Pathol* **13**, 573-583.

Cavanagh, D., Davis, P. J. and Cook, J. K. (1992)**.** Infectious bronchitis virus: evidence for recombination within the Massachusetts serotype. *Avian Pathol* **21**, 401-408.

Cavanagh, D., Davis, P. J. and Mockett, A. P. (1988)**.** Amino acids within hypervariable region 1 of avian coronavirus IBV (Massachusetts serotype) spike glycoprotein are associated with neutralization epitopes. *Virus Res* **11**, 141-150.

Cavanagh, D., Mawditt, K., Sharma, M., Drury, S. E., Ainsworth, H. L., Britton, P. and Gough, R. E. (2001)**.** Detection of a coronavirus from turkey poults in Europe genetically related to infectious bronchitis virus of chickens. *Avian Pathol* **30**, 355-368.

Cavanagh, D., Mawditt, K., Welchman Dde, B., Britton, P. and Gough, R. E. (2002)**.** Coronaviruses from pheasants (Phasianus colchicus) are genetically closely related to coronaviruses of domestic fowl (infectious bronchitis virus) and turkeys. *Avian Pathol* **31**, 81-93.

Chan, C. M., Tsoi, H., Chan, W. M., Zhai, S., Wong, C. O., Yao, X., Chan, W. Y., Tsui, S. K. and Chan, H. Y. (2009)**.** The ion channel activity of the SARS-coronavirus 3a protein is linked to its pro-apoptotic function. *Int J Biochem Cell Biol*.

Chan, C. P., Siu, K. L., Chin, K. T., Yuen, K. Y., Zheng, B. and Jin, D. Y. (2006)**.** Modulation of the unfolded protein response by the severe acute respiratory syndrome coronavirus spike protein. *J Virol* **80**, 9279-9287.

Chan, W. S., Wu, C., Chow, S. C., Cheung, T., To, K. F., Leung, W. K., Chan, P. K., Lee, K. C., Ng, H. K., Au, D. M. and Lo, A. W. (2005)**.** Coronaviral hypothetical and structural proteins were found in the intestinal surface enterocytes and pneumocytes of severe acute respiratory syndrome (SARS). *Mod Pathol* **18**, 1432-1439.

Chen, B. Y., Hosi, S., Nunoya, T. and Itakura, C. (1996)**.** Histopathology and immunohistochemistry of renal lesions due to infectious bronchitis virus in chicks. *Avian Pathol* **25**, 269-283.

Chen, C. J. and Makino, S. (2004)**.** Murine coronavirus replication induces cell cycle arrest in G0/G1 phase. *J Virol* **78**, 5658-5669.

Chen, C. J., Sugiyama, K., Kubo, H., Huang, C. and Makino, S. (2004)**.** Murine coronavirus nonstructural protein p28 arrests cell cycle in G0/G1 phase. *J Virol* **78**, 10410-10419.

Chen, C. Y., Ping, Y. H., Lee, H. C., Chen, K. H., Lee, Y. M., Chan, Y. J., Lien, T. C., Jap, T. S., Lin, C. H., Kao, L. S. and Chen, Y. M. (2007)**.** Open reading frame 8a of the human severe acute respiratory syndrome coronavirus not only promotes viral replication but also induces apoptosis. *J Infect Dis* **196**, 405-415.

Chen, Y., Cai, H., Pan, J., Xiang, N., Tien, P., Ahola, T. and Guo, D. (2009)**.** Functional screen reveals SARS coronavirus nonstructural protein nsp14 as a novel cap N7 methyltransferase. *Proc Natl Acad Sci U S A* **106**, 3484-3489.

Chinese, S. M. E. C. (2004)**.** Molecular evolution of the SARS coronavirus during the course of the SARS epidemic in China. *Science* **303**, 1666-1669.

Chowers, M. Y., Spina, C. A., Kwoh, T. J., Fitch, N. J., Richman, D. D. and Guatelli, J. C. (1994)**.** Optimal infectivity in vitro of human immunodeficiency virus type 1 requires an intact nef gene. *J Virol* **68**, 2906-2914.

Christen, V., Duong, F., Bernsmeier, C., Sun, D., Nassal, M. and Heim, M. H. (2007a)**.** Inhibition of alpha interferon signaling by hepatitis B virus. *J Virol* **81**, 159-165.

Christen, V., Treves, S., Duong, F. H. and Heim, M. H. (2007b)**.** Activation of endoplasmic reticulum stress response by hepatitis viruses up-regulates protein phosphatase 2A. *Hepatology* **46**, 558-565.

Chu, V. C., McElroy, L. J., Chu, V., Bauman, B. E. and Whittaker, G. R. (2006)**.** The avian coronavirus infectious bronchitis virus undergoes direct low-pH-dependent fusion activation during entry into host cells. *J Virol* **80**, 3180-3188.

Clementz, M. A., Kanjanahaluethai, A., O'Brien, T. E. and Baker, S. C. (2008)**.** Mutation in murine coronavirus replication protein nsp4 alters assembly of double membrane vesicles. *Virology* **375**, 118-129.

Cohen, E. A., Dehni, G., Sodroski, J. G. and Haseltine, W. A. (1990)**.** Human immunodeficiency virus vpr product is a virion-associated regulatory protein. *J Virol* **64**, 3097-3099.

Compton, S. R., Rogers, D. B., Holmes, K. V., Fertsch, D., Remenick, J. and McGowan, J. J. (1987)**.** In vitro replication of mouse hepatitis virus strain A59. *J Virol* **61**, 1814-1820.

Corse, E. and Machamer, C. E. (2000)**.** Infectious bronchitis virus E protein is targeted to the Golgi complex and directs release of virus-like particles. *J Virol* **74**, 4319-4326.

Corse, E. and Machamer, C. E. (2002)**.** The cytoplasmic tail of infectious bronchitis virus E protein directs Golgi targeting. *J Virol* **76**, 1273-1284.

Cox, G. J., Parker, M. D. and Babiuk, L. A. (1991)**.** Bovine coronavirus nonstructural protein ns2 is a phosphoprotein. *Virology* **185**, 509-512.

Dalton, K., Casais, R., Shaw, K., Stirrups, K., Evans, S., Britton, P., Brown, T. D. and Cavanagh, D. (2001)**.** cis-acting sequences required for coronavirus infectious bronchitis virus defective-RNA replication and packaging. *J Virol* **75**, 125-133.

Daniel, M. D., Kirchhoff, F., Czajak, S. C., Sehgal, P. K. and Desrosiers, R. C. (1992)**.** Protective effects of a live attenuated SIV vaccine with a deletion in the nef gene. *Science* **258**, 1938-1941.

Darbyshire, J. H. and Peters, R. W. (1984)**.** Sequential development of humoral immunity and assessment of protection in chickens following vaccination and challenge with avian infectious bronchitis virus. *Res Vet Sci* **37**, 77-86.

Davies, H. A. and Macnaughton, M. R. (1979)**.** Comparison of the morphology of three coronaviruses. *Arch Virol* **59**, 25-33.

de Haan, C. A., Masters, P. S., Shen, X., Weiss, S. and Rottier, P. J. (2002)**.** The group-specific murine coronavirus genes are not essential, but their deletion, by reverse genetics, is attenuating in the natural host. *Virology* **296**, 177-189.

de Haan, C. A., Smeets, M., Vernooij, F., Vennema, H. and Rottier, P. J. (1999)**.** Mapping of the coronavirus membrane protein domains involved in interaction with the spike protein. *J Virol* **73**, 7441-7452.

Decroly, E., Imbert, I., Coutard, B., Bouvet, M., Selisko, B., Alvarez, K., Gorbalenya, A. E., Snijder, E. J. and Canard, B. (2008). Coronavirus nonstructural protein 16 is a cap-0 binding enzyme possessing (nucleoside-2'O)-methyltransferase activity. *J Virol* **82**, 8071-8084.

Dediego, M. L., Pewe, L., Alvarez, E., Rejas, M. T., Perlman, S. and Enjuanes, L. (2008). Pathogenicity of severe acute respiratory coronavirus deletion mutants in hACE-2 transgenic mice. *Virology* **376**, 379-389.

Delmas, B., Gelfi, J., L'Haridon, R., Vogel, L. K., Sjostrom, H., Noren, O. and Laude, H. (1992). Aminopeptidase N is a major receptor for the entero-pathogenic coronavirus TGEV. *Nature* **357**, 417-420.

Delmas, B. and Laude, H. (1990). Assembly of coronavirus spike protein into trimers and its role in epitope expression. *J Virol* **64**, 5367-5375.

Di Fabio, J., Rossini, L. I., Orbell, S. J., Paul, G., Huggins, M. B., Malo, A., Silva, B. G. and Cook, J. K. (2000). Characterization of infectious bronchitis viruses isolated from outbreaks of disease in commercial flocks in Brazil. *Avian Dis* **44**, 582-589.

Dove, B., Brooks, G., Bicknell, K., Wurm, T. and Hiscox, J. A. (2006). Cell cycle perturbations induced by infection with the coronavirus infectious bronchitis virus and their effect on virus replication. *J Virol* **80**, 4147-4156.

Duarte, M., Gelfi, J., Lambert, P., Rasschaert, D. and Laude, H. (1993). Genome organization of porcine epidemic diarrhoea virus. *Adv Exp Med Biol* **342**, 55-60.

Eifart, P., Ludwig, K., Bottcher, C., de Haan, C. A., Rottier, P. J., Korte, T. and Herrmann, A. (2007). Role of endocytosis and low pH in murine hepatitis virus strain A59 cell entry. *J Virol* **81**, 10758-10768.

Elder, R. T., Yu, M., Chen, M., Zhu, X., Yanagida, M. and Zhao, Y. (2001). HIV-1 Vpr induces cell cycle G2 arrest in fission yeast (Schizosaccharomyces pombe) through a pathway involving regulatory and catalytic subunits of PP2A and acting on both Wee1 and Cdc25. *Virology* **287**, 359-370.

Elliott, J., Lynch, O. T., Suessmuth, Y., Qian, P., Boyd, C. R., Burrows, J. F., Buick, R., Stevenson, N. J., Touzelet, O., Gadina, M., Power, U. F. and Johnston, J. A. (2007). Respiratory syncytial virus NS1 protein degrades STAT2 by using the Elongin-Cullin E3 ligase. *J Virol* **81**, 3428-3436.

Engelsma, D., Bernad, R., Calafat, J. and Fornerod, M. (2004). Supraphysiological nuclear export signals bind CRM1 independently of RanGTP and arrest at Nup358. *EMBO J* **23**, 3643-3652.

Fielding, B. C., Gunalan, V., Tan, T. H., Chou, C. F., Shen, S., Khan, S., Lim, S. G., Hong, W. and Tan, Y. J. (2006)**.** Severe acute respiratory syndrome coronavirus protein 7a interacts with hSGT. *Biochem Biophys Res Commun* **343**, 1201-1208.

Fielding, B. C., Tan, Y. J., Shuo, S., Tan, T. H., Ooi, E. E., Lim, S. G., Hong, W. and Goh, P. Y. (2004)**.** Characterization of a unique group-specific protein (U122) of the severe acute respiratory syndrome coronavirus. *J Virol* **78**, 7311-7318.

Forgues, M., Marrogi, A. J., Spillare, E. A., Wu, C. G., Yang, Q., Yoshida, M. and Wang, X. W. (2001)**.** Interaction of the hepatitis B virus X protein with the Crm1-dependent nuclear export pathway. *J Biol Chem* **276**, 22797-22803.

Fornerod, M., Ohno, M., Yoshida, M. and Mattaj, I. W. (1997)**.** CRM1 is an export receptor for leucine-rich nuclear export signals. *Cell* **90**, 1051-1060.

Freundt, E. C., Yu, L., Park, E., Lenardo, M. J. and Xu, X. (2009)**.** Molecular Determinants for Subcellular Localization of the Severe Acute Respiratory Syndrome Coronavirus ORF 3b Protein. *J Virol*. 83, 6631-6640.

Frieman, M., Yount, B., Heise, M., Kopecky-Bromberg, S. A., Palese, P. and Baric, R. S. (2007)**.** Severe acute respiratory syndrome coronavirus ORF6 antagonizes STAT1 function by sequestering nuclear import factors on the rough endoplasmic reticulum/Golgi membrane. *J Virol* **81**, 9812-9824.

Frost, J. A., Alberts, A. S., Sontag, E., Guan, K., Mumby, M. C. and Feramisco, J. R. (1994)**.** Simian virus 40 small t antigen cooperates with mitogen-activated kinases to stimulate AP-1 activity. *Mol Cell Biol* **14**, 6244-6252.

Fu, D. X., Kuo, Y. L., Liu, B. Y., Jeang, K. T. and Giam, C. Z. (2003)**.** Human T-lymphotropic virus type I tax activates I-kappa B kinase by inhibiting I-kappa B kinase-associated serine/threonine protein phosphatase 2A. *J Biol Chem* **278**, 1487-1493.

Fujii, Y., Sakaguchi, T., Kiyotani, K., Huang, C., Fukuhara, N. and Yoshida, T. (2002)**.** Identification of mutations associated with attenuation of virulence of a field Sendai virus isolate by egg passage. *Virus Genes* **25**, 189-193.

Gabuzda, D. H., Lawrence, K., Langhoff, E., Terwilliger, E., Dorfman, T., Haseltine, W. A. and Sodroski, J. (1992)**.** Role of vif in replication of human immunodeficiency virus type 1 in CD4+ T lymphocytes. *J Virol* **66**, 6489-6495.

Garaigorta, U. and Ortin, J. (2007)**.** Mutation analysis of a recombinant NS replicon shows that influenza virus NS1 protein blocks the splicing and nucleo-cytoplasmic transport of its own viral mRNA. *Nucleic Acids Res* **35**, 4573-4582.

Garcia-Barrio, M., Dong, J., Ufano, S. and Hinnebusch, A. G. (2000). Association of GCN1-GCN20 regulatory complex with the N-terminus of eIF2alpha kinase GCN2 is required for GCN2 activation. *EMBO J* **19**, 1887-1899.

Garcia-Sastre, A., Egorov, A., Matassov, D., Brandt, S., Levy, D. E., Durbin, J. E., Palese, P. and Muster, T. (1998). Influenza A virus lacking the NS1 gene replicates in interferon-deficient systems. *Virology* **252**, 324-330.

Geilhausen, H. E., Ligon, F. B. and Lukert, P. D. (1973). The pathogenesis of virulent and avirulent avian infectious bronchitis virus. *Arch Gesamte Virusforsch* **40**, 285-290.

Geng, H., Liu, Y. M., Chan, W. S., Lo, A. W., Au, D. M., Waye, M. M. and Ho, Y. Y. (2005). The putative protein 6 of the severe acute respiratory syndrome-associated coronavirus: expression and functional characterization. *FEBS Lett* **579**, 6763-6768.

Goldsmith, C. S., Tatti, K. M., Ksiazek, T. G., Rollin, P. E., Comer, J. A., Lee, W. W., Rota, P. A., Bankamp, B., Bellini, W. J. and Zaki, S. R. (2004). Ultrastructural characterization of SARS coronavirus. *Emerg Infect Dis* **10**, 320-326.

Gonzalez, J. M., Gomez-Puertas, P., Cavanagh, D., Gorbalenya, A. E. and Enjuanes, L. (2003). A comparative sequence analysis to revise the current taxonomy of the family Coronaviridae. *Arch Virol* **148**, 2207-2235.

Gosert, R., Kanjanahaluethai, A., Egger, D., Bienz, K. and Baker, S. C. (2002). RNA replication of mouse hepatitis virus takes place at double-membrane vesicles. *J Virol* **76**, 3697-3708.

Gotoh, B., Takeuchi, K., Komatsu, T., Yokoo, J., Kimura, Y., Kurotani, A., Kato, A. and Nagai, Y. (1999). Knockout of the Sendai virus C gene eliminates the viral ability to prevent the interferon-alpha/beta-mediated responses. *FEBS Lett* **459**, 205-210.

Graham, R. L., Sims, A. C., Brockway, S. M., Baric, R. S. and Denison, M. R. (2005). The nsp2 replicase proteins of murine hepatitis virus and severe acute respiratory syndrome coronavirus are dispensable for viral replication. *J Virol* **79**, 13399-13411.

Guttridge, D. C., Albanese, C., Reuther, J. Y., Pestell, R. G. and Baldwin, A. S., Jr. (1999). NF-kappaB controls cell growth and differentiation through transcriptional regulation of cyclin D1. *Mol Cell Biol* **19**, 5785-5799.

Hahn, W. C., Dessain, S. K., Brooks, M. W., King, J. E., Elenbaas, B., Sabatini, D. M., DeCaprio, J. A. and Weinberg, R. A. (2002). Enumeration of the simian virus 40 early region elements necessary for human cell transformation. *Mol Cell Biol* **22**, 2111-2123.

Haijema, B. J., Volders, H. and Rottier, P. J. (2004)**.** Live, attenuated coronavirus vaccines through the directed deletion of group-specific genes provide protection against feline infectious peritonitis. *J Virol* **78**, 3863-3871.

Hanel, K., Stangler, T., Stoldt, M. and Willbold, D. (2006)**.** Solution structure of the X4 protein coded by the SARS related coronavirus reveals an immunoglobulin like fold and suggests a binding activity to integrin I domains. *J Biomed Sci* **13**, 281-293.

Hanel, K. and Willbold, D. (2007)**.** SARS-CoV accessory protein 7a directly interacts with human LFA-1. *Biol Chem* **388**, 1325-1332.

Haoudi, A., Daniels, R. C., Wong, E., Kupfer, G. and Semmes, O. J. (2003)**.** Human T-cell leukemia virus-I tax oncoprotein functionally targets a subnuclear complex involved in cellular DNA damage-response. *J Biol Chem* **278**, 37736-37744.

Harcourt, B. H., Jukneliene, D., Kanjanahaluethai, A., Bechill, J., Severson, K. M., Smith, C. M., Rota, P. A. and Baker, S. C. (2004)**.** Identification of severe acute respiratory syndrome coronavirus replicase products and characterization of papain-like protease activity. *J Virol* **78**, 13600-13612.

Harrison, S. M., Dove, B. K., Rothwell, L., Kaiser, P., Tarpey, I., Brooks, G. and Hiscox, J. A. (2007)**.** Characterisation of cyclin D1 down-regulation in coronavirus infected cells. *FEBS Lett* **581**, 1275-1286.

Hatada, E., Saito, S. and Fukuda, R. (1999)**.** Mutant influenza viruses with a defective NS1 protein cannot block the activation of PKR in infected cells. *J Virol* **73**, 2425-2433.

Hayman, A., Comely, S., Lackenby, A., Hartgroves, L. C., Goodbourn, S., McCauley, J. W. and Barclay, W. S. (2007)**.** NS1 proteins of avian influenza A viruses can act as antagonists of the human alpha/beta interferon response. *J Virol* **81**, 2318-2327.

Heinzinger, N. K., Bukinsky, M. I., Haggerty, S. A., Ragland, A. M., Kewalramani, V., Lee, M. A., Gendelman, H. E., Ratner, L., Stevenson, M. and Emerman, M. (1994)**.** The Vpr protein of human immunodeficiency virus type 1 influences nuclear localization of viral nucleic acids in nondividing host cells. *Proc Natl Acad Sci U S A* **91**, 7311-7315.

Herold, A., Teixeira, L. and Izaurralde, E. (2003)**.** Genome-wide analysis of nuclear mRNA export pathways in Drosophila. *EMBO J* **22**, 2472-2483.

Herrewegh, A. A., Vennema, H., Horzinek, M. C., Rottier, P. J. and de Groot, R. J. (1995)**.** The molecular genetics of feline coronaviruses: comparative sequence analysis of the ORF7a/7b transcription unit of different biotypes. *Virology* **212**, 622-631.

Hilton, A., Mizzen, L., MacIntyre, G., Cheley, S. and Anderson, R. (1986)**.** Translational control in murine hepatitis virus infection. *J Gen Virol* **67 (Pt 5)**, 923-932.

Hiscox, J. A., Wurm, T., Wilson, L., Britton, P., Cavanagh, D. and Brooks, G. (2001)**.** The coronavirus infectious bronchitis virus nucleoprotein localizes to the nucleolus. *J Virol* **75**, 506-512.

Hodgson, T., Britton, P. and Cavanagh, D. (2006)**.** Neither the RNA nor the proteins of open reading frames 3a and 3b of the coronavirus infectious bronchitis virus are essential for replication. *J Virol* **80**, 296-305.

Horisberger, M. A., Staeheli, P. and Haller, O. (1983)**.** Interferon induces a unique protein in mouse cells bearing a gene for resistance to influenza virus. *Proc Natl Acad Sci U S A* **80**, 1910-1914.

Hu, M. C., Mo, R., Bhella, S., Wilson, C. W., Chuang, P. T., Hui, C. C. and Rosenblum, N. D. (2006)**.** GLI3-dependent transcriptional repression of Gli1, Gli2 and kidney patterning genes disrupts renal morphogenesis. *Development* **133**, 569-578.

Huang, C., Ito, N., Tseng, C. T. and Makino, S. (2006)**.** Severe acute respiratory syndrome coronavirus 7a accessory protein is a viral structural protein. *J Virol* **80**, 7287-7294.

Huang, C., Peters, C. J. and Makino, S. (2007)**.** Severe acute respiratory syndrome coronavirus accessory protein 6 is a virion-associated protein and is released from 6 protein-expressing cells. *J Virol* **81**, 5423-5426.

Huang, Y. P. and Wang, C. H. (2007)**.** Sequence changes of infectious bronchitis virus isolates in the 3' 7.3 kb of the genome after attenuating passage in embryonated eggs. *Avian Pathol* **36**, 59-67.

Imbert, I., Guillemot, J. C., Bourhis, J. M., Bussetta, C., Coutard, B., Egloff, M. P., Ferron, F., Gorbalenya, A. E. and Canard, B. (2006)**.** A second, non-canonical RNA-dependent RNA polymerase in SARS coronavirus. *EMBO J* **25**, 4933-4942.

Ito, N., Mossel, E. C., Narayanan, K., Popov, V. L., Huang, C., Inoue, T., Peters, C. J. and Makino, S. (2005)**.** Severe acute respiratory syndrome coronavirus 3a protein is a viral structural protein. *J Virol* **79**, 3182-3186.

Itoh, M., Isegawa, Y., Hotta, H. and Homma, M. (1997)**.** Isolation of an avirulent mutant of Sendai virus with two amino acid mutations from a highly virulent field strain through adaptation to LLC-MK2 cells. *J Gen Virol* **78 (Pt 12)**, 3207-3215.

Ivanov, K. A., Thiel, V., Dobbe, J. C., van der Meer, Y., Snijder, E. J. and Ziebuhr, J. (2004)**.** Multiple enzymatic activities associated with severe acute respiratory syndrome coronavirus helicase. *J Virol* **78**, 5619-5632.

Jamieson, B. D., Aldrovandi, G. M., Planelles, V., Jowett, J. B., Gao, L., Bloch, L. M., Chen, I. S. and Zack, J. A. (1994). Requirement of human immunodeficiency virus type 1 nef for in vivo replication and pathogenicity. *J Virol* **68**, 3478-3485.

Janse, E. M., van Roozelaar, D. and Koch, G. (1994). Leukocyte subpopulations in kidney and trachea of chickens infected with infectious bronchitis virus. *Avian Pathol* **23**, 513-523.

Jia, W. and Naqi, S. A. (1997). Sequence analysis of gene 3, gene 4 and gene 5 of avian infectious bronchitis virus strain CU-T2. *Gene* **189**, 189-193.

Jin, H., Cheng, X., Zhou, H. Z., Li, S. and Seddiqui, A. (2000a). Respiratory syncytial virus that lacks open reading frame 2 of the M2 gene (M2-2) has altered growth characteristics and is attenuated in rodents. *J Virol* **74**, 74-82.

Jin, H., Zhou, H., Cheng, X., Tang, R., Munoz, M. and Nguyen, N. (2000b). Recombinant respiratory syncytial viruses with deletions in the NS1, NS2, SH, and M2-2 genes are attenuated in vitro and in vivo. *Virology* **273**, 210-218.

Jowett, J. B., Planelles, V., Poon, B., Shah, N. P., Chen, M. L. and Chen, I. S. (1995). The human immunodeficiency virus type 1 vpr gene arrests infected T cells in the G2 + M phase of the cell cycle. *J Virol* **69**, 6304-6313.

Kamibayashi, C., Estes, R., Lickteig, R. L., Yang, S. I., Craft, C. and Mumby, M. C. (1994). Comparison of heterotrimeric protein phosphatase 2A containing different B subunits. *J Biol Chem* **269**, 20139-20148.

Kamitani, W., Narayanan, K., Huang, C., Lokugamage, K., Ikegami, T., Ito, N., Kubo, H. and Makino, S. (2006). Severe acute respiratory syndrome coronavirus nsp1 protein suppresses host gene expression by promoting host mRNA degradation. *Proc Natl Acad Sci U S A* **103**, 12885-12890.

Kanjanahaluethai, A., Chen, Z., Jukneliene, D. and Baker, S. C. (2007). Membrane topology of murine coronavirus replicase nonstructural protein 3. *Virology* **361**, 391-401.

Kato, A., Kiyotani, K., Sakai, Y., Yoshida, T. and Nagai, Y. (1997). The paramyxovirus, Sendai virus, V protein encodes a luxury function required for viral pathogenesis. *EMBO J* **16**, 578-587.

Kawase, M., Shirato, K., Matsuyama, S. and Taguchi, F. (2009). Protease-mediated entry via the endosome of human coronavirus 229E. *J Virol* **83**, 712-721.

Keng, C. T., Choi, Y. W., Welkers, M. R., Chan, D. Z., Shen, S., Gee Lim, S., Hong, W. and Tan, Y. J. (2006)**.** The human severe acute respiratory syndrome coronavirus (SARS-CoV) 8b protein is distinct from its counterpart in animal SARS-CoV and down-regulates the expression of the envelope protein in infected cells. *Virology* **354**, 132-142.

Kennedy, D. A. and Johnson-Lussenburg, C. M. (1975)**.** Isolation and morphology of the internal component of human coronavirus, strain 229E. *Intervirology* **6**, 197-206.

Khan, S., Fielding, B. C., Tan, T. H., Chou, C. F., Shen, S., Lim, S. G., Hong, W. and Tan, Y. J. (2006)**.** Over-expression of severe acute respiratory syndrome coronavirus 3b protein induces both apoptosis and necrosis in Vero E6 cells. *Virus Res* **122**, 20-27.

Kienzle, T. E., Abraham, S., Hogue, B. G. and Brian, D. A. (1990)**.** Structure and orientation of expressed bovine coronavirus hemagglutinin-esterase protein. *J Virol* **64**, 1834-1838.

Kimura, T., Hashimoto, I., Nagase, T. and Fujisawa, J. (2004)**.** CRM1-dependent, but not ARE-mediated, nuclear export of IFN-alpha1 mRNA. *J Cell Sci* **117**, 2259-2270.

Kiyotani, K., Sakaguchi, T., Kato, A., Nagai, Y. and Yoshida, T. (2007)**.** Paramyxovirus Sendai virus V protein counteracts innate virus clearance through IRF-3 activation, but not via interferon, in mice. *Virology* **359**, 82-91.

Klimkait, T., Strebel, K., Hoggan, M. D., Martin, M. A. and Orenstein, J. M. (1990)**.** The human immunodeficiency virus type 1-specific protein vpu is required for efficient virus maturation and release. *J Virol* **64**, 621-629.

Klumperman, J., Locker, J. K., Meijer, A., Horzinek, M. C., Geuze, H. J. and Rottier, P. J. (1994)**.** Coronavirus M proteins accumulate in the Golgi complex beyond the site of virion budding. *J Virol* **68**, 6523-6534.

Knoops, K., Kikkert, M., Worm, S. H., Zevenhoven-Dobbe, J. C., van der Meer, Y., Koster, A. J., Mommaas, A. M. and Snijder, E. J. (2008)**.** SARS-coronavirus replication is supported by a reticulovesicular network of modified endoplasmic reticulum. *PLoS Biol* **6**, e226.

Kochs, G., Garcia-Sastre, A. and Martinez-Sobrido, L. (2007)**.** Multiple anti-interferon actions of the influenza A virus NS1 protein. *J Virol* **81**, 7011-7021.

Komatsu, T., Takeuchi, K., Yokoo, J. and Gotoh, B. (2004)**.** C and V proteins of Sendai virus target signaling pathways leading to IRF-3 activation for the negative regulation of interferon-beta production. *Virology* **325**, 137-148.

Kopecky-Bromberg, S. A., Martinez-Sobrido, L., Frieman, M., Baric, R. A. and Palese, P. (2007)**.** Severe acute respiratory syndrome coronavirus open reading frame (ORF) 3b, ORF 6, and nucleocapsid proteins function as interferon antagonists. *J Virol* **81**, 548-557.

Kopecky-Bromberg, S. A., Martinez-Sobrido, L. and Palese, P. (2006)**.** 7a protein of severe acute respiratory syndrome coronavirus inhibits cellular protein synthesis and activates p38 mitogen-activated protein kinase. *J Virol* **80**, 785-793.

Krahling, V., Stein, D. A., Spiegel, M., Weber, F. and Muhlberger, E. (2009)**.** Severe acute respiratory syndrome coronavirus triggers apoptosis via protein kinase R but is resistant to its antiviral activity. *J Virol* **83**, 2298-2309.

Krauss, S., Foerster, J., Schneider, R. and Schweiger, S. (2008)**.** Protein phosphatase 2A and rapamycin regulate the nuclear localization and activity of the transcription factor GLI3. *Cancer Res* **68**, 4658-4665.

Krishnamoorthy, J., Mounir, Z., Raven, J. F. and Koromilas, A. E. (2008)**.** The eIF2alpha kinases inhibit vesicular stomatitis virus replication independently of eIF2alpha phosphorylation. *Cell Cycle* **7**, 2346-2351.

Kubo, H., Yamada, Y. K. and Taguchi, F. (1994)**.** Localization of neutralizing epitopes and the receptor-binding site within the amino-terminal 330 amino acids of the murine coronavirus spike protein. *J Virol* **68**, 5403-5410.

Kuo, L. and Masters, P. S. (2003)**.** The small envelope protein E is not essential for murine coronavirus replication. *J Virol* **77**, 4597-4608.

Kurotani, A., Kiyotani, K., Kato, A., Shioda, T., Sakai, Y., Mizumoto, K., Yoshida, T. and Nagai, Y. (1998)**.** Sendai virus C proteins are categorically nonessential gene products but silencing their expression severely impairs viral replication and pathogenesis. *Genes Cells* **3**, 111-124.

Law, P. T., Wong, C. H., Au, T. C., Chuck, C. P., Kong, S. K., Chan, P. K., To, K. F., Lo, A. W., Chan, J. Y., Suen, Y. K., Chan, H. Y., Fung, K. P., Waye, M. M., Sung, J. J., Lo, Y. M. and Tsui, S. K. (2005)**.** The 3a protein of severe acute respiratory syndrome-associated coronavirus induces apoptosis in Vero E6 cells. *J Gen Virol* **86**, 1921-1930.

Le, T. M., Wong, H. H., Tay, F. P., Fang, S., Keng, C. T., Tan, Y. J. and Liu, D. X. (2007)**.** Expression, post-translational modification and biochemical characterization of proteins encoded by subgenomic mRNA8 of the severe acute respiratory syndrome coronavirus. *FEBS J* **274**, 4211-4222.

Li, S., Brignole, C., Marcellus, R., Thirlwell, S., Binda, O., McQuoid, M. J., Ashby, D., Chan, H., Zhang, Z., Miron, M. J., Pallas, D. C. and Branton, P. E. (2009)**.** The Adenovirus E4orf4 Protein Induces G2/M Arrest and Cell Death by Blocking PP2A Activity Regulated by the B55 Subunit. *J Virol*. **83**, 8340-8352.

Li, W., Moore, M. J., Vasilieva, N., Sui, J., Wong, S. K., Berne, M. A., Somasundaran, M., Sullivan, J. L., Luzuriaga, K., Greenough, T. C., Choe, H. and Farzan, M. (2003)**.** Angiotensin-converting enzyme 2 is a functional receptor for the SARS coronavirus. *Nature* **426**, 450-454.

Liao, C. L. and Lai, M. M. (1994)**.** Requirement of the 5'-end genomic sequence as an upstream cis-acting element for coronavirus subgenomic mRNA transcription. *J Virol* **68**, 4727-4737.

Lichty, J. J., Malecki, J. L., Agnew, H. D., Michelson-Horowitz, D. J. and Tan, S. (2005)**.** Comparison of affinity tags for protein purification. *Protein Expr Purif* **41**, 98-105.

Lin, C. N., Su, B. L., Huang, H. P., Lee, J. J., Hsieh, M. W. and Chueh, L. L. (2008)**.** Field strain feline coronaviruses with small deletions in ORF7b associated with both enteric infection and feline infectious peritonitis. *J Feline Med Surg*. **11**, 413-419.

Lin, Y. J., Liao, C. L. and Lai, M. M. (1994)**.** Identification of the cis-acting signal for minus-strand RNA synthesis of a murine coronavirus: implications for the role of minus-strand RNA in RNA replication and transcription. *J Virol* **68**, 8131-8140.

Ling, Z., Tran, K. C. and Teng, M. N. (2009)**.** Human respiratory syncytial virus nonstructural protein NS2 antagonizes the activation of beta interferon transcription by interacting with RIG-I. *J Virol* **83**, 3734-3742.

Liu, D. X., Cavanagh, D., Green, P. and Inglis, S. C. (1991)**.** A polycistronic mRNA specified by the coronavirus infectious bronchitis virus. *Virology* **184**, 531-544.

Liu, D. X. and Inglis, S. C. (1991)**.** Association of the infectious bronchitis virus 3c protein with the virion envelope. *Virology* 185, 911-917.

Liu, D. X. and Inglis, S. C. (1992a)**.** Identification of two new polypeptides encoded by mRNA5 of the coronavirus infectious bronchitis virus. *Virology* **186**, 342-347.

Liu, D. X. and Inglis, S. C. (1992b)**.** Internal entry of ribosomes on a tricistronic mRNA encoded by infectious bronchitis virus. *J Virol* **66**, 6143-6154.

Liu, S., Zhang, Q., Chen, J., Han, Z., Shao, Y., Kong, X. and Tong, G. (2008)**.** Identification of the avian infectious bronchitis coronaviruses with mutations in gene 3. *Gene* **412**, 12-25.

Lontok, E., Corse, E. and Machamer, C. E. (2004)**.** Intracellular targeting signals contribute to localization of coronavirus spike proteins near the virus assembly site. *J Virol* **78**, 5913-5922.

Lu, W., Zheng, B. J., Xu, K., Schwarz, W., Du, L., Wong, C. K., Chen, J., Duan, S., Deubel, V. and Sun, B. (2006). Severe acute respiratory syndrome-associated coronavirus 3a protein forms an ion channel and modulates virus release. *Proc Natl Acad Sci U S A* **103**, 12540-12545.

Lu, Y. and Denison, M. R. (1997). Determinants of mouse hepatitis virus 3C-like proteinase activity. *Virology* **230**, 335-342.

Ludowyke, R. I., Holst, J., Mudge, L. M. and Sim, A. T. (2000). Transient translocation and activation of protein phosphatase 2A during mast cell secretion. *J Biol Chem* **275**, 6144-6152.

Machamer, C. E., Mentone, S. A., Rose, J. K. and Farquhar, M. G. (1990). The E1 glycoprotein of an avian coronavirus is targeted to the cis Golgi complex. *Proc Natl Acad Sci U S A* **87**, 6944-6948.

Macneughton, M. R. and Davies, H. A. (1978). Ribonucleoprotein-like structures from coronavirus particles. *J Gen Virol* **39**, 545-549.

Madan, V., Garcia Mde, J., Sanz, M. A. and Carrasco, L. (2005). Viroporin activity of murine hepatitis virus E protein. *FEBS Lett* **579**, 3607-3612.

Makino, S., Joo, M. and Makino, J. K. (1991). A system for study of coronavirus mRNA synthesis: a regulated, expressed subgenomic defective interfering RNA results from intergenic site insertion. *J Virol* **65**, 6031-6041.

Malakhov, M. P., Mattern, M. R., Malakhova, O. A., Drinker, M., Weeks, S. D. and Butt, T. R. (2004). SUMO fusions and SUMO-specific protease for efficient expression and purification of proteins. *J Struct Funct Genomics* **5**, 75-86.

Mardani, K., Noormohammadi, A. H., Hooper, P., Ignjatovic, J. and Browning, G. F. (2008). Infectious bronchitis viruses with a novel genomic organization. *J Virol* **82**, 2013-2024.

Marion, R. M., Aragon, T., Beloso, A., Nieto, A. and Ortin, J. (1997). The N-terminal half of the influenza virus NS1 protein is sufficient for nuclear retention of mRNA and enhancement of viral mRNA translation. *Nucleic Acids Res* **25**, 4271-4277.

Marra, M. A., Jones, S. J., Astell, C. R., Holt, R. A., Brooks-Wilson, A., Butterfield, Y. S., Khattra, J., Asano, J. K., Barber, S. A., Chan, S. Y., Cloutier, A., Coughlin, S. M., Freeman, D., Girn, N., Griffith, O. L., Leach, S. R., Mayo, M., McDonald, H., Montgomery, S. B., Pandoh, P. K., Petrescu, A. S., Robertson, A. G., Schein, J. E., Siddiqui, A., Smailus, D. E., Stott, J. M., Yang, G. S., Plummer, F., Andonov, A., Artsob, H., Bastien, N., Bernard, K., Booth, T. F., Bowness, D., Czub, M., Drebot, M., Fernando, L., Flick, R., Garbutt, M., Gray, M., Grolla, A., Jones, S., Feldmann, H., Meyers, A., Kabani, A., Li, Y., Normand, S., Stroher, U., Tipples, G. A., Tyler, S., Vogrig, R., Ward, D., Watson, B., Brunham, R.

C., Krajden, M., Petric, M., Skowronski, D. M., Upton, C. and Roper, R. L. (2003)**.** The Genome sequence of the SARS-associated coronavirus. *Science* **300**, 1399-1404.

Marton, M. J., Crouch, D. and Hinnebusch, A. G. (1993)**.** GCN1, a translational activator of GCN4 in Saccharomyces cerevisiae, is required for phosphorylation of eukaryotic translation initiation factor 2 by protein kinase GCN2. *Mol Cell Biol* **13**, 3541-3556.

Marton, M. J., Vazquez de Aldana, C. R., Qiu, H., Chakraburtty, K. and Hinnebusch, A. G. (1997)**.** Evidence that GCN1 and GCN20, translational regulators of GCN4, function on elongating ribosomes in activation of eIF2alpha kinase GCN2. *Mol Cell Biol* **17**, 4474-4489.

Mazumder, R., Iyer, L. M., Vasudevan, S. and Aravind, L. (2002)**.** Detection of novel members, structure-function analysis and evolutionary classification of the 2H phosphoesterase superfamily. *Nucleic Acids Res* **30**, 5229-5243.

McCright, B., Rivers, A. M., Audlin, S. and Virshup, D. M. (1996)**.** The B56 family of protein phosphatase 2A (PP2A) regulatory subunits encodes differentiation-induced phosphoproteins that target PP2A to both nucleus and cytoplasm. *J Biol Chem* **271**, 22081-22089.

McGoldrick, A., Lowings, J. P. and Paton, D. J. (1999)**.** Characterisation of a recent virulent transmissible gastroenteritis virus from Britain with a deleted ORF 3a. *Arch Virol* **144**, 763-770.

Mehle, A., Strack, B., Ancuta, P., Zhang, C., McPike, M. and Gabuzda, D. (2004)**.** Vif overcomes the innate antiviral activity of APOBEC3G by promoting its degradation in the ubiquitin-proteasome pathway. *J Biol Chem* **279**, 7792-7798.

Meier, C., Aricescu, A. R., Assenberg, R., Aplin, R. T., Gilbert, R. J., Grimes, J. M. and Stuart, D. I. (2006)**.** The crystal structure of ORF-9b, a lipid binding protein from the SARS coronavirus. *Structure* **14**, 1157-1165.

Mihindukulasuriya, K. A., Wu, G., St Leger, J., Nordhausen, R. W. and Wang, D. (2008)**.** Identification of a novel coronavirus from a beluga whale by using a panviral microarray. *J Virol* **82**, 5084-5088.

Minskaia, E., Hertzig, T., Gorbalenya, A. E., Campanacci, V., Cambillau, C., Canard, B. and Ziebuhr, J. (2006)**.** Discovery of an RNA virus 3'->5' exoribonuclease that is critically involved in coronavirus RNA synthesis. *Proc Natl Acad Sci U S A* **103**, 5108-5113.

Moshynskyy, I., Viswanathan, S., Vasilenko, N., Lobanov, V., Petric, M., Babiuk, L. A. and Zakhartchouk, A. N. (2007)**.** Intracellular localization of the SARS coronavirus protein 9b: evidence of active export from the nucleus. *Virus Res* **127**, 116-121.

Muneer, M. A., Newman, J. A., Halvorson, D. A., Sivanandan, V., Nagaraja, K. V. and Coon, C. N. (1988)**.** Efficacy of infectious bronchitis virus vaccines against heterologous challenge. *Res Vet Sci* **45**, 22-27.

Nakamura, K., Cook, J. K., Otsuki, K., Huggins, M. B. and Frazier, J. A. (1991)**.** Comparative study of respiratory lesions in two chicken lines of different susceptibility infected with infectious bronchitis virus: histology, ultrastructure and immunohistochemistry. *Avian Pathol* **20**, 241-257.

Narayanan, K., Maeda, A., Maeda, J. and Makino, S. (2000)**.** Characterization of the coronavirus M protein and nucleocapsid interaction in infected cells. *J Virol* **74**, 8127-8134.

Navas-Martin, S., Brom, M., Chua, M. M., Watson, R., Qiu, Z. and Weiss, S. R. (2007)**.** Replicase genes of murine coronavirus strains A59 and JHM are interchangeable: differences in pathogenesis map to the 3' one-third of the genome. *J Virol* **81**, 1022-1026.

Navas, S., Seo, S. H., Chua, M. M., Das Sarma, J., Lavi, E., Hingley, S. T. and Weiss, S. R. (2001)**.** Murine coronavirus spike protein determines the ability of the virus to replicate in the liver and cause hepatitis. *J Virol* **75**, 2452-2457.

Nelson, C. A., Pekosz, A., Lee, C. A., Diamond, M. S. and Fremont, D. H. (2005)**.** Structure and intracellular targeting of the SARS-coronavirus Orf7a accessory protein. *Structure* **13**, 75-85.

Nelson, G. W., Stohlman, S. A. and Tahara, S. M. (2000)**.** High affinity interaction between nucleocapsid protein and leader/intergenic sequence of mouse hepatitis virus RNA. *J Gen Virol* **81**, 181-188.

Netland, J., Ferraro, D., Pewe, L., Olivares, H., Gallagher, T. and Perlman, S. (2007)**.** Enhancement of murine coronavirus replication by severe acute respiratory syndrome coronavirus protein 6 requires the N-terminal hydrophobic region but not C-terminal sorting motifs. *J Virol* **81**, 11520-11525.

Neuman, B. W., Joseph, J. S., Saikatendu, K. S., Serrano, P., Chatterjee, A., Johnson, M. A., Liao, L., Klaus, J. P., Yates, J. R., 3rd, Wuthrich, K., Stevens, R. C., Buchmeier, M. J. and Kuhn, P. (2008)**.** Proteomics analysis unravels the functional repertoire of coronavirus nonstructural protein 3. *J Virol* **82**, 5279-5294.

Newby, C. M., Sabin, L. and Pekosz, A. (2007)**.** The RNA binding domain of influenza A virus NS1 protein affects secretion of tumor necrosis factor alpha, interleukin-6, and interferon in primary murine tracheal epithelial cells. *J Virol* **81**, 9469-9480.

Nguyen, V. P. and Hogue, B. G. (1997)**.** Protein interactions during coronavirus assembly. *J Virol* **71**, 9278-9284.

Niemann, H., Boschek, B., Evans, D., Rosing, M., Tamura, T. and Klenk, H. D. (1982)**.** Post-translational glycosylation of coronavirus glycoprotein E1: inhibition by monensin. *EMBO J* **1**, 1499-1504.

Oostra, M., de Haan, C. A. and Rottier, P. J. (2007a)**.** The 29-nucleotide deletion present in human but not in animal severe acute respiratory syndrome coronaviruses disrupts the functional expression of open reading frame 8. *J Virol* **81**, 13876-13888.

Oostra, M., Hagemeijer, M. C., van Gent, M., Bekker, C. P., te Lintelo, E. G., Rottier, P. J. and de Haan, C. A. (2008)**.** Topology and membrane anchoring of the coronavirus replication complex: not all hydrophobic domains of nsp3 and nsp6 are membrane spanning. *J Virol* **82**, 12392-12405.

Oostra, M., te Lintelo, E. G., Deijs, M., Verheije, M. H., Rottier, P. J. and de Haan, C. A. (2007b)**.** Localization and membrane topology of coronavirus nonstructural protein 4: involvement of the early secretory pathway in replication. *J Virol* **81**, 12323-12336.

Opitz, B., Rejaibi, A., Dauber, B., Eckhard, J., Vinzing, M., Schmeck, B., Hippenstiel, S., Suttorp, N. and Wolff, T. (2007)**.** IFNbeta induction by influenza A virus is mediated by RIG-I which is regulated by the viral NS1 protein. *Cell Microbiol* **9**, 930-938.

Opstelten, D. J., Raamsman, M. J., Wolfs, K., Horzinek, M. C. and Rottier, P. J. (1995)**.** Envelope glycoprotein interactions in coronavirus assembly. *J Cell Biol* **131**, 339-349.

Ortego, J., Ceriani, J. E., Patino, C., Plana, J. and Enjuanes, L. (2007)**.** Absence of E protein arrests transmissible gastroenteritis coronavirus maturation in the secretory pathway. *Virology* **368**, 296-308.

Ortego, J., Sola, I., Almazan, F., Ceriani, J. E., Riquelme, C., Balasch, M., Plana, J. and Enjuanes, L. (2003)**.** Transmissible gastroenteritis coronavirus gene 7 is not essential but influences in vivo virus replication and virulence. *Virology* **308**, 13-22.

Padhan, K., Minakshi, R., Towheed, M. A. and Jameel, S. (2008)**.** Severe acute respiratory syndrome coronavirus 3a protein activates the mitochondrial death pathway through p38 MAP kinase activation. *J Gen Virol* **89**, 1960-1969.

Padhan, K., Tanwar, C., Hussain, A., Hui, P. Y., Lee, M. Y., Cheung, C. Y., Peiris, J. S. and Jameel, S. (2007)**.** Severe acute respiratory syndrome coronavirus Orf3a protein interacts with caveolin. *J Gen Virol* **88**, 3067-3077.

Pendleton, A. R. and Machamer, C. E. (2005)**.** Infectious bronchitis virus 3a protein localizes to a novel domain of the smooth endoplasmic reticulum. *J Virol* **79**, 6142-6151.

Pendleton, A. R. and Machamer, C. E. (2006)**.** Differential localization and turnover of infectious bronchitis virus 3b protein in mammalian versus avian cells. *Virology* **345**, 337-345.

Pereira, C. M., Sattlegger, E., Jiang, H. Y., Longo, B. M., Jaqueta, C. B., Hinnebusch, A. G., Wek, R. C., Mello, L. E. and Castilho, B. A. (2005)**.** IMPACT, a protein preferentially expressed in the mouse brain, binds GCN1 and inhibits GCN2 activation. *J Biol Chem* **280**, 28316-28323.

Pewe, L., Zhou, H., Netland, J., Tangudu, C., Olivares, H., Shi, L., Look, D., Gallagher, T. and Perlman, S. (2005)**.** A severe acute respiratory syndrome-associated coronavirus-specific protein enhances virulence of an attenuated murine coronavirus. *J Virol* **79**, 11335-11342.

Pinon, J. D., Teng, H. and Weiss, S. R. (1999)**.** Further requirements for cleavage by the murine coronavirus 3C-like proteinase: identification of a cleavage site within ORF1b. *Virology* **263**, 471-484.

Prentice, E., Jerome, W. G., Yoshimori, T., Mizushima, N. and Denison, M. R. (2004a)**.** Coronavirus replication complex formation utilizes components of cellular autophagy. *J Biol Chem* **279**, 10136-10141.

Prentice, E., McAuliffe, J., Lu, X., Subbarao, K. and Denison, M. R. (2004b)**.** Identification and characterization of severe acute respiratory syndrome coronavirus replicase proteins. *J Virol* **78**, 9977-9986.

Purcell, D. A. and Clarke, J. K. (1972)**.** The replication of infectious bronchitis virus in fowl trachea. *Arch Gesamte Virusforsch* **39**, 248-256.

Qiu, M., Shi, Y., Guo, Z., Chen, Z., He, R., Chen, R., Zhou, D., Dai, E., Wang, X., Si, B., Song, Y., Li, J., Yang, L., Wang, J., Wang, H., Pang, X., Zhai, J., Du, Z., Liu, Y., Zhang, Y., Li, L., Sun, B. and Yang, R. (2005)**.** Antibody responses to individual proteins of SARS coronavirus and their neutralization activities. *Microbes Infect* **7**, 882-889.

Raaben, M., Groot Koerkamp, M. J., Rottier, P. J. and de Haan, C. A. (2007)**.** Mouse hepatitis coronavirus replication induces host translational shutoff and mRNA decay, with concomitant formation of stress granules and processing bodies. *Cell Microbiol* **9**, 2218-2229.

Reichelt, M., Stertz, S., Krijnse-Locker, J., Haller, O. and Kochs, G. (2004)**.** Missorting of LaCrosse virus nucleocapsid protein by the interferon-induced MxA GTPase involves smooth ER membranes. *Traffic* **5**, 772-784.

Ricagno, S., Egloff, M. P., Ulferts, R., Coutard, B., Nurizzo, D., Campanacci, V., Cambillau, C., Ziebuhr, J. and Canard, B. (2006)**.** Crystal structure and mechanistic determinants of SARS coronavirus nonstructural protein 15 define an endoribonuclease family. *Proc Natl Acad Sci U S A* **103**, 11892-11897.

Rimondi, A., Craig, M. I., Vagnozzi, A., Konig, G., Delamer, M. and Pereda, A. (2009)**.** Molecular characterization of avian infectious bronchitis virus strains from outbreaks in Argentina (2001-2008). *Avian Pathol* **38**, 149-153.

Romanova, L. I., Lidsky, P. V., Kolesnikova, M. S., Fominykh, K. V., Gmyl, A. P., Sheval, E. V., Hato, S. V., van Kuppeveld, F. J. and Agol, V. I. (2009)**.** Antiapoptotic activity of the cardiovirus leader protein, a viral "security" protein. *J Virol* **83**, 7273-7284.

Roth-Cross, J. K., Martinez-Sobrido, L., Scott, E. P., Garcia-Sastre, A. and Weiss, S. R. (2007)**.** Inhibition of the alpha/beta interferon response by mouse hepatitis virus at multiple levels. *J Virol* **81**, 7189-7199.

Roth-Cross, J. K., Stokes, H., Chang, G., Chua, M. M., Thiel, V., Weiss, S. R., Gorbalenya, A. E. and Siddell, S. G. (2009)**.** Organ-Specific Attenuation of Murine Hepatitis Virus (MHV-A59) by Replacement of Catalytic Residues in the Putative Viral Cyclic Phosphodiesterase NS2. *J Virol*. **83**, 3743-3753.

Rottier, P. J., Horzinek, M. C. and van der Zeijst, B. A. (1981)**.** Viral protein synthesis in mouse hepatitis virus strain A59-infected cells: effect of tunicamycin. *J Virol* **40**, 350-357.

Rottier, P. J. and Rose, J. K. (1987)**.** Coronavirus E1 glycoprotein expressed from cloned cDNA localizes in the Golgi region. *J Virol* **61**, 2042-2045.

Rottier, P. J., Welling, G. W., Welling-Wester, S., Niesters, H. G., Lenstra, J. A. and Van der Zeijst, B. A. (1986)**.** Predicted membrane topology of the coronavirus protein E1. *Biochemistry* **25**, 1335-1339.

Rowland, R. R., Chauhan, V., Fang, Y., Pekosz, A., Kerrigan, M. and Burton, M. D. (2005)**.** Intracellular localization of the severe acute respiratory syndrome coronavirus nucleocapsid protein: absence of nucleolar accumulation during infection and after expression as a recombinant protein in vero cells. *J Virol* **79**, 11507-11512.

Rowland, R. R., Kervin, R., Kuckleburg, C., Sperlich, A. and Benfield, D. A. (1999)**.** The localization of porcine reproductive and respiratory syndrome virus nucleocapsid protein to the nucleolus of infected cells and identification of a potential nucleolar localization signal sequence. *Virus Res* **64**, 1-12.

Saikatendu, K. S., Joseph, J. S., Subramanian, V., Clayton, T., Griffith, M., Moy, K., Velasquez, J., Neuman, B. W., Buchmeier, M. J., Stevens, R. C. and Kuhn, P. (2005)**.** Structural basis of severe acute respiratory syndrome coronavirus ADP-ribose-1"-phosphate dephosphorylation by a conserved domain of nsP3. *Structure* **13**, 1665-1675.

Sakai, H., Shibata, R., Sakuragi, J., Sakuragi, S., Kawamura, M. and Adachi, A. (1993)**.** Cell-dependent requirement of human immunodeficiency virus type 1 Vif protein for maturation of virus particles. *J Virol* **67**, 1663-1666.

Salvatore, M., Basler, C. F., Parisien, J. P., Horvath, C. M., Bourmakina, S., Zheng, H., Muster, T., Palese, P. and Garcia-Sastre, A. (2002)**.** Effects of influenza A virus NS1 protein on protein expression: the NS1 protein enhances translation and is not required for shutoff of host protein synthesis. *J Virol* **76**, 1206-1212.

Sanchez, C. M., Izeta, A., Sanchez-Morgado, J. M., Alonso, S., Sola, I., Balasch, M., Plana-Duran, J. and Enjuanes, L. (1999)**.** Targeted recombination demonstrates that the spike gene of transmissible gastroenteritis coronavirus is a determinant of its enteric tropism and virulence. *J Virol* **73**, 7607-7618.

Sattlegger, E. and Hinnebusch, A. G. (2000)**.** Separate domains in GCN1 for binding protein kinase GCN2 and ribosomes are required for GCN2 activation in amino acid-starved cells. *EMBO J* **19**, 6622-6633.

Sattlegger, E. and Hinnebusch, A. G. (2005)**.** Polyribosome binding by GCN1 is required for full activation of eukaryotic translation initiation factor 2{alpha} kinase GCN2 during amino acid starvation. *J Biol Chem* **280**, 16514-16521.

Schaecher, S. R., Diamond, M. S. and Pekosz, A. (2008)**.** The transmembrane domain of the severe acute respiratory syndrome coronavirus ORF7b protein is necessary and sufficient for its retention in the Golgi complex. *J Virol* **82**, 9477-9491.

Schaecher, S. R., Mackenzie, J. M. and Pekosz, A. (2007a)**.** The ORF7b protein of severe acute respiratory syndrome coronavirus (SARS-CoV) is expressed in virus-infected cells and incorporated into SARS-CoV particles. *J Virol* **81**, 718-731.

Schaecher, S. R., Touchette, E., Schriewer, J., Buller, R. M. and Pekosz, A. (2007b)**.** Severe acute respiratory syndrome coronavirus gene 7 products contribute to virus-induced apoptosis. *J Virol* **81**, 11054-11068.

Schultze, B., Cavanagh, D. and Herrler, G. (1992)**.** Neuraminidase treatment of avian infectious bronchitis coronavirus reveals a hemagglutinating activity that is dependent on sialic acid-containing receptors on erythrocytes. *Virology* **189**, 792-794.

Schutz, S., Chemnitz, J., Spillner, C., Frohme, M., Hauber, J. and Kehlenbach, R. H. (2006)**.** Stimulated expression of mRNAs in activated T cells depends on a functional CRM1 nuclear export pathway. *J Mol Biol* **358**, 997-1009.

Schwarz, B., Routledge, E. and Siddell, S. G. (1990)**.** Murine coronavirus nonstructural protein ns2 is not essential for virus replication in transformed cells. *J Virol* **64**, 4784-4791.

Seybert, A., Hegyi, A., Siddell, S. G. and Ziebuhr, J. (2000)**.** The human coronavirus 229E superfamily 1 helicase has RNA and DNA duplex-unwinding activities with 5'-to-3' polarity. *RNA* **6**, 1056-1068.

Sharma, K., Surjit, M., Satija, N., Liu, B., Chow, V. T. and Lal, S. K. (2007)**.** The 3a accessory protein of SARS coronavirus specifically interacts with the 5'UTR of its genomic RNA, Using a unique 75 amino acid interaction domain. *Biochemistry* **46**, 6488-6499.

Sheehy, A. M., Gaddis, N. C., Choi, J. D. and Malim, M. H. (2002)**.** Isolation of a human gene that inhibits HIV-1 infection and is suppressed by the viral Vif protein. *Nature* **418**, 646-650.

Shen, S., Lin, P. S., Chao, Y. C., Zhang, A., Yang, X., Lim, S. G., Hong, W. and Tan, Y. J. (2005)**.** The severe acute respiratory syndrome coronavirus 3a is a novel structural protein. *Biochem Biophys Res Commun* **330**, 286-292.

Shen, S., Wen, Z. L. and Liu, D. X. (2003)**.** Emergence of a coronavirus infectious bronchitis virus mutant with a truncated 3b gene: functional characterization of the 3b protein in pathogenesis and replication. *Virology* **311**, 16-27.

Shi, S. T., Schiller, J. J., Kanjanahaluethai, A., Baker, S. C., Oh, J. W. and Lai, M. M. (1999)**.** Colocalization and membrane association of murine hepatitis virus gene 1 products and De novo-synthesized viral RNA in infected cells. *J Virol* **73**, 5957-5969.

Shieh, C. K., Soe, L. H., Makino, S., Chang, M. F., Stohlman, S. A. and Lai, M. M. (1987)**.** The 5'-end sequence of the murine coronavirus genome: implications for multiple fusion sites in leader-primed transcription. *Virology* **156**, 321-330.

Sims, A. C., Ostermann, J. and Denison, M. R. (2000)**.** Mouse hepatitis virus replicase proteins associate with two distinct populations of intracellular membranes. *J Virol* **74**, 5647-5654.

Snijder, E. J., Bredenbeek, P. J., Dobbe, J. C., Thiel, V., Ziebuhr, J., Poon, L. L., Guan, Y., Rozanov, M., Spaan, W. J. and Gorbalenya, A. E. (2003)**.** Unique and conserved features of genome and proteome of SARS-coronavirus, an early split-off from the coronavirus group 2 lineage. *J Mol Biol* **331**, 991-1004.

Snijder, E. J., van der Meer, Y., Zevenhoven-Dobbe, J., Onderwater, J. J., van der Meulen, J., Koerten, H. K. and Mommaas, A. M. (2006)**.** Ultrastructure and origin of membrane vesicles associated with the severe acute respiratory syndrome coronavirus replication complex. *J Virol* **80**, 5927-5940.

Sola, I., Alonso, S., Zuniga, S., Balasch, M., Plana-Duran, J. and Enjuanes, L. (2003)**.** Engineering the transmissible gastroenteritis virus genome as an expression vector inducing lactogenic immunity. *J Virol* **77**, 4357-4369.

Sontag, E., Sontag, J. M. and Garcia, A. (1997)**.** Protein phosphatase 2A is a critical regulator of protein kinase C zeta signaling targeted by SV40 small t to promote cell growth and NF-kappaB activation. *EMBO J* **16**, 5662-5671.

Sood, R., Porter, A. C., Olsen, D. A., Cavener, D. R. and Wek, R. C. (2000)**.** A mammalian homologue of GCN2 protein kinase important for translational control by phosphorylation of eukaryotic initiation factor-2alpha. *Genetics* **154**, 787-801.

Spann, K. M., Tran, K. C., Chi, B., Rabin, R. L. and Collins, P. L. (2004)**.** Suppression of the induction of alpha, beta, and lambda interferons by the NS1 and NS2 proteins of human respiratory syncytial virus in human epithelial cells and macrophages [corrected]. *J Virol* **78**, 4363-4369.

Sparks, J. S., Lu, X. and Denison, M. R. (2007)**.** Genetic analysis of Murine hepatitis virus nsp4 in virus replication. *J Virol* **81**, 12554-12563.

Spiegel, M., Pichlmair, A., Martinez-Sobrido, L., Cros, J., Garcia-Sastre, A., Haller, O. and Weber, F. (2005)**.** Inhibition of Beta interferon induction by severe acute respiratory syndrome coronavirus suggests a two-step model for activation of interferon regulatory factor 3. *J Virol* **79**, 2079-2086.

Stade, K., Ford, C. S., Guthrie, C. and Weis, K. (1997)**.** Exportin 1 (Crm1p) is an essential nuclear export factor. *Cell* **90**, 1041-1050.

Staeheli, P. and Haller, O. (1985)**.** Interferon-induced human protein with homology to protein Mx of influenza virus-resistant mice. *Mol Cell Biol* **5**, 2150-2153.

Stohlman, S. A., Baric, R. S., Nelson, G. N., Soe, L. H., Welter, L. M. and Deans, R. J. (1988)**.** Specific interaction between coronavirus leader RNA and nucleocapsid protein. *J Virol* **62**, 4288-4295.

Strebel, K., Klimkait, T., Maldarelli, F. and Martin, M. A. (1989)**.** Molecular and biochemical analyses of human immunodeficiency virus type 1 vpu protein. *J Virol* **63**, 3784-3791.

Suarez, D. L. and Perdue, M. L. (1998)**.** Multiple alignment comparison of the non-structural genes of influenza A viruses. *Virus Res* **54**, 59-69.

Sung, S. C., Chao, C. Y., Jeng, K. S., Yang, J. Y. and Lai, M. M. (2009)**.** The 8ab protein of SARS-CoV is a luminal ER membrane-associated protein and induces the activation of ATF6. *Virology* **387**, 402-413.

Swigut, T., Iafrate, A. J., Muench, J., Kirchhoff, F. and Skowronski, J. (2000)**.** Simian and human immunodeficiency virus Nef proteins use different surfaces to downregulate class I major histocompatibility complex antigen expression. *J Virol* **74**, 5691-5701.

Tahara, S. M., Dietlin, T. A., Bergmann, C. C., Nelson, G. W., Kyuwa, S., Anthony, R. P. and Stohlman, S. A. (1994)**.** Coronavirus translational regulation: leader affects mRNA efficiency. *Virology* **202**, 621-630.

Tahara, S. M., Dietlin, T. A., Nelson, G. W., Stohlman, S. A. and Manno, D. J. (1998)**.** Mouse hepatitis virus nucleocapsid protein as a translational effector of viral mRNAs. *Adv Exp Med Biol* **440**, 313-318.

Tan, Y. J., Fielding, B. C., Goh, P. Y., Shen, S., Tan, T. H., Lim, S. G. and Hong, W. (2004a)**.** Overexpression of 7a, a protein specifically encoded by the severe acute respiratory syndrome coronavirus, induces apoptosis via a caspase-dependent pathway. *J Virol* **78**, 14043-14047.

Tan, Y. J., Teng, E., Shen, S., Tan, T. H., Goh, P. Y., Fielding, B. C., Ooi, E. E., Tan, H. C., Lim, S. G. and Hong, W. (2004b)**.** A novel severe acute respiratory syndrome coronavirus protein, U274, is transported to the cell surface and undergoes endocytosis. *J Virol* **78**, 6723-6734.

Tan, Y. J., Tham, P. Y., Chan, D. Z., Chou, C. F., Shen, S., Fielding, B. C., Tan, T. H., Lim, S. G. and Hong, W. (2005)**.** The severe acute respiratory syndrome coronavirus 3a protein up-regulates expression of fibrinogen in lung epithelial cells. *J Virol* **79**, 10083-10087.

Tan, Y. X., Tan, T. H., Lee, M. J., Tham, P. Y., Gunalan, V., Druce, J., Birch, C., Catton, M., Fu, N. Y., Yu, V. C. and Tan, Y. J. (2007)**.** Induction of apoptosis by the severe acute respiratory syndrome coronavirus 7a protein is dependent on its interaction with the Bcl-XL protein. *J Virol* **81**, 6346-6355.

Tangudu, C., Olivares, H., Netland, J., Perlman, S. and Gallagher, T. (2007)**.** Severe acute respiratory syndrome coronavirus protein 6 accelerates murine coronavirus infections. *J Virol* **81**, 1220-1229.

Tekes, G., Hofmann-Lehmann, R., Stallkamp, I., Thiel, V. and Thiel, H. J. (2008)**.** Genome organization and reverse genetic analysis of a type I feline coronavirus. *J Virol* **82**, 1851-1859.

Teng, M. N. and Collins, P. L. (1999)**.** Altered growth characteristics of recombinant respiratory syncytial viruses which do not produce NS2 protein. *J Virol* **73**, 466-473.

Tesfay, M. Z., Yin, J., Gardner, C. L., Khoretonenko, M. V., Korneeva, N. L., Rhoads, R. E., Ryman, K. D. and Klimstra, W. B. (2008)**.** Alpha/beta interferon inhibits cap-dependent translation of viral but not cellular mRNA by a PKR-independent mechanism. *J Virol* **82**, 2620-2630.

Thiel, V. and Siddell, S. G. (1994)**.** Internal ribosome entry in the coding region of murine hepatitis virus mRNA 5. *J Gen Virol* **75 (Pt 11)**, 3041-3046.

Tibbles, K. W., Cavanagh, D. and Brown, T. D. (1999)**.** Activity of a purified His-tagged 3C-like proteinase from the coronavirus infectious bronchitis virus. *Virus Res* **60**, 137-145.

Tooze, J., Tooze, S. A. and Fuller, S. D. (1987)**.** Sorting of progeny coronavirus from condensed secretory proteins at the exit from the trans-Golgi network of AtT20 cells. *J Cell Biol* **105**, 1215-1226.

Tresnan, D. B., Levis, R. and Holmes, K. V. (1996)**.** Feline aminopeptidase N serves as a receptor for feline, canine, porcine, and human coronaviruses in serogroup I. *J Virol* **70**, 8669-8674.

Tung, F. Y., Abraham, S., Sethna, M., Hung, S. L., Sethna, P., Hogue, B. G. and Brian, D. A. (1992)**.** The 9-kDa hydrophobic protein encoded at the 3' end of the porcine transmissible gastroenteritis coronavirus genome is membrane-associated. *Virology* **186**, 676-683.

van der Hoek, L., Pyrc, K., Jebbink, M. F., Vermeulen-Oost, W., Berkhout, R. J., Wolthers, K. C., Wertheim-van Dillen, P. M., Kaandorp, J., Spaargaren, J. and Berkhout, B. (2004)**.** Identification of a new human coronavirus. *Nat Med* **10**, 368-373.

van der Meer, Y., Snijder, E. J., Dobbe, J. C., Schleich, S., Denison, M. R., Spaan, W. J. and Locker, J. K. (1999)**.** Localization of mouse hepatitis virus nonstructural proteins and RNA synthesis indicates a role for late endosomes in viral replication. *J Virol* **73**, 7641-7657.

van Hemert, M. J., van den Worm, S. H., Knoops, K., Mommaas, A. M., Gorbalenya, A. E. and Snijder, E. J. (2008)**.** SARS-coronavirus replication/transcription complexes are membrane-protected and need a host factor for activity in vitro. *PLoS Pathog* **4**, e1000054.

van Marle, G., Dobbe, J.C., Gultyaev, A. P., Luytjes, W., Spaan, W. J. and Snijder, E. J. (1999). Arterivirus discontinuous mRNA transcription is guided by base pairing between sense and antisense transcription-regulating sequences. *Proc Natl Acad Sci USA* **96**, 12056-61.

Van Neck, T., Pannecouque, C., Vanstreels, E., Stevens, M., Dehaen, W. and Daelemans, D. (2008)**.** Inhibition of the CRM1-mediated nucleocytoplasmic transport by N-azolylacrylates: structure-activity relationship and mechanism of action. *Bioorg Med Chem* **16**, 9487-9497.

van Pesch, V., van Eyll, O. and Michiels, T. (2001)**.** The leader protein of Theiler's virus inhibits immediate-early alpha/beta interferon production. *J Virol* **75**, 7811-7817.

Vandekerchove, D., Herdt, P. D., Laevens, H., Butaye, P., Meulemans, G. and Pasmans, F. (2004)**.** Significance of interactions between Escherichia coli and respiratory pathogens in layer hen flocks suffering from colibacillosis-associated mortality. *Avian Pathol* **33**, 298-302.

Vazquez de Aldana, C. R., Marton, M. J. and Hinnebusch, A. G. (1995)**.** GCN20, a novel ATP binding cassette protein, and GCN1 reside in a complex that mediates activation of the eIF-2 alpha kinase GCN2 in amino acid-starved cells. *EMBO J* **14**, 3184-3199.

Vennema, H., Godeke, G. J., Rossen, J. W., Voorhout, W. F., Horzinek, M. C., Opstelten, D. J. and Rottier, P. J. (1996)**.** Nucleocapsid-independent assembly of coronavirus-like particles by co-expression of viral envelope protein genes. *EMBO J* **15**, 2020-2028.

Vennema, H., Heijnen, L., Zijderveld, A., Horzinek, M. C. and Spaan, W. J. (1990)**.** Intracellular transport of recombinant coronavirus spike proteins: implications for virus assembly. *J Virol* **64**, 339-346.

Versteeg, G. A., Bredenbeek, P. J., van den Worm, S. H. and Spaan, W. J. (2007a)**.** Group 2 coronaviruses prevent immediate early interferon induction by protection of viral RNA from host cell recognition. *Virology* **361**, 18-26.

Versteeg, G. A., van de Nes, P. S., Bredenbeek, P. J. and Spaan, W. J. (2007b)**.** The coronavirus spike protein induces endoplasmic reticulum stress and upregulation of intracellular chemokine mRNA concentrations. *J Virol* **81**, 10981-10990.

Vlach, J., Garcia, A., Jacque, J. M., Rodriguez, M. S., Michelson, S. and Virelizier, J. L. (1995)**.** Induction of Sp1 phosphorylation and NF-kappa B-independent HIV promoter domain activity in T lymphocytes stimulated by okadaic acid. *Virology* **208**, 753-761.

Voorhoeve, P. M., Watson, R. J., Farlie, P. G., Bernards, R. and Lam, E. W. (1999)**.** Rapid dephosphorylation of p107 following UV irradiation. *Oncogene* **18**, 679-688.

Weber, F., Bridgen, A., Fazakerley, J. K., Streitenfeld, H., Kessler, N., Randall, R. E. and Elliott, R. M. (2002)**.** Bunyamwera bunyavirus nonstructural protein NSs counteracts the induction of alpha/beta interferon. *J Virol* **76**, 7949-7955.

Westphal, R. S., Anderson, K. A., Means, A. R. and Wadzinski, B. E. (1998)**.** A signaling complex of Ca2+-calmodulin-dependent protein kinase IV and protein phosphatase 2A. *Science* **280**, 1258-1261.

Wheat, W. H., Roesler, W. J. and Klemm, D. J. (1994)**.** Simian virus 40 small tumor antigen inhibits dephosphorylation of protein kinase A-phosphorylated CREB and regulates CREB transcriptional stimulation. *Mol Cell Biol* **14**, 5881-5890.

Wilhelmsen, K. C., Leibowitz, J. L., Bond, C. W. and Robb, J. A. (1981)**.** The replication of murine coronaviruses in enucleated cells. *Virology* **110**, 225-230.

Willey, R. L., Maldarelli, F., Martin, M. A. and Strebel, K. (1992)**.** Human immunodeficiency virus type 1 Vpu protein induces rapid degradation of CD4. *J Virol* **66**, 7193-7200.

Williams, R. K., Jiang, G. S. and Holmes, K. V. (1991)**.** Receptor for mouse hepatitis virus is a member of the carcinoembryonic antigen family of glycoproteins. *Proc Natl Acad Sci U S A* **88**, 5533-5536.

Wilson, L., McKinlay, C., Gage, P. and Ewart, G. (2004)**.** SARS coronavirus E protein forms cation-selective ion channels. *Virology* **330**, 322-331.

Winter, C., Herrler, G. and Neumann, U. (2008a)**.** Infection of the tracheal epithelium by infectious bronchitis virus is sialic acid dependent. *Microbes Infect* **10**, 367-373.

Winter, C., Schwegmann-Wessels, C., Cavanagh, D., Neumann, U. and Herrler, G. (2006)**.** Sialic acid is a receptor determinant for infection of cells by avian Infectious bronchitis virus. *J Gen Virol* **87**, 1209-1216.

Winter, C., Schwegmann-Wessels, C., Neumann, U. and Herrler, G. (2008b)**.** The spike protein of infectious bronchitis virus is retained intracellularly by a tyrosine motif. *J Virol* **82**, 2765-2771.

Woo, P. C., Lau, S. K., Lam, C. S., Lai, K. K., Huang, Y., Lee, P., Luk, G. S., Dyrting, K. C., Chan, K. H. and Yuen, K. Y. (2009)**.** Comparative analysis of complete genome sequences of three avian coronaviruses reveals a novel group 3c coronavirus. *J Virol* **83**, 908-917.

Woo, P. C., Wang, M., Lau, S. K., Xu, H., Poon, R. W., Guo, R., Wong, B. H., Gao, K., Tsoi, H. W., Huang, Y., Li, K. S., Lam, C. S., Chan, K. H., Zheng, B. J. and Yuen, K. Y. (2007)**.** Comparative analysis of twelve genomes of three novel group 2c and group 2d coronaviruses reveals unique group and subgroup features. *J Virol* **81**, 1574-1585.

Woods, R. D. (2001)**.** Efficacy of a transmissible gastroenteritis coronavirus with an altered ORF-3 gene. *Can J Vet Res* **65**, 28-32.

Wurm, T., Chen, H., Hodgson, T., Britton, P., Brooks, G. and Hiscox, J. A. (2001)**.** Localization to the nucleolus is a common feature of coronavirus nucleoproteins, and the protein may disrupt host cell division. *J Virol* **75**, 9345-9356.

Xu, K., Zheng, B. J., Zeng, R., Lu, W., Lin, Y. P., Xue, L., Li, L., Yang, L. L., Xu, C., Dai, J., Wang, F., Li, Q., Dong, Q. X., Yang, R. F., Wu, J. R. and Sun, B. (2009)**.** Severe acute respiratory syndrome coronavirus accessory protein 9b is a virion-associated protein. *Virology* **388**, 279-285.

Yang, S. I., Lickteig, R. L., Estes, R., Rundell, K., Walter, G. and Mumby, M. C. (1991)**.** Control of protein phosphatase 2A by simian virus 40 small-t antigen. *Mol Cell Biol* **11**, 1988-1995.

Yang, Z. Y., Huang, Y., Ganesh, L., Leung, K., Kong, W. P., Schwartz, O., Subbarao, K. and Nabel, G. J. (2004)**.** pH-dependent entry of severe acute respiratory syndrome coronavirus is mediated by the spike glycoprotein and enhanced by dendritic cell transfer through DC-SIGN. *J Virol* **78**, 5642-5650.

Yao, K., Goodwin, M. A. and Vakharia, V. N. (1998)**.** Generation of a mutant infectious bursal disease virus that does not cause bursal lesions. *J Virol* **72**, 2647-2654.

Yao, K. and Vakharia, V. N. (2001)**.** Induction of apoptosis in vitro by the 17-kDa nonstructural protein of infectious bursal disease virus: possible role in viral pathogenesis. *Virology* **285**, 50-58.

Ye, Z., Wong, C. K., Li, P. and Xie, Y. (2008)**.** A SARS-CoV protein, ORF-6, induces caspase-3 mediated, ER stress and JNK-dependent apoptosis. *Biochim Biophys Acta* **1780**, 1383-1387.

Yeager, C. L., Ashmun, R. A., Williams, R. K., Cardellichio, C. B., Shapiro, L. H., Look, A. T. and Holmes, K. V. (1992)**.** Human aminopeptidase N is a receptor for human coronavirus 229E. *Nature* **357**, 420-422.

Yoo, D. W., Parker, M. D. and Babiuk, L. A. (1991)**.** The S2 subunit of the spike glycoprotein of bovine coronavirus mediates membrane fusion in insect cells. *Virology* **180**, 395-399.

You, J., Dove, B. K., Enjuanes, L., DeDiego, M. L., Alvarez, E., Howell, G., Heinen, P., Zambon, M. and Hiscox, J. A. (2005)**.** Subcellular localization of the severe acute respiratory syndrome coronavirus nucleocapsid protein. *J Gen Virol* **86**, 3303-3310.

Youn, S., Collisson, E. W. and Machamer, C. E. (2005)**.** Contribution of trafficking signals in the cytoplasmic tail of the infectious bronchitis virus spike protein to virus infection. *J Virol* **79**, 13209-13217.

Young, D. F., Didcock, L., Goodbourn, S. and Randall, R. E. (2000)**.** Paramyxoviridae use distinct virus-specific mechanisms to circumvent the interferon response. *Virology* **269**, 383-390.

Yount, B., Roberts, R. S., Sims, A. C., Deming, D., Frieman, M. B., Sparks, J., Denison, M. R., Davis, N. and Baric, R. S. (2005)**.** Severe acute respiratory syndrome coronavirus group-specific open reading frames encode nonessential functions for replication in cell cultures and mice. *J Virol* **79**, 14909-14922.

Yuan, X., Li, J., Shan, Y., Yang, Z., Zhao, Z., Chen, B., Yao, Z., Dong, B., Wang, S., Chen, J. and Cong, Y. (2005a)**.** Subcellular localization and membrane association of SARS-CoV 3a protein. *Virus Res* **109**, 191-202.

Yuan, X., Shan, Y., Yao, Z., Li, J., Zhao, Z., Chen, J. and Cong, Y. (2006a)**.** Mitochondrial location of severe acute respiratory syndrome coronavirus 3b protein. *Mol Cells* **21**, 186-191.

Yuan, X., Shan, Y., Zhao, Z., Chen, J. and Cong, Y. (2005b)**.** G0/G1 arrest and apoptosis induced by SARS-CoV 3b protein in transfected cells. *Virol J* **2**, 66.

Yuan, X., Wu, J., Shan, Y., Yao, Z., Dong, B., Chen, B., Zhao, Z., Wang, S., Chen, J. and Cong, Y. (2006b)**.** SARS coronavirus 7a protein blocks cell cycle progression at G0/G1 phase via the cyclin D3/pRb pathway. *Virology* **346**, 74-85.

Yuan, X., Yao, Z., Shan, Y., Chen, B., Yang, Z., Wu, J., Zhao, Z., Chen, J. and Cong, Y. (2005c)**.** Nucleolar localization of non-structural protein 3b, a protein specifically encoded by the severe acute respiratory syndrome coronavirus. *Virus Res* **114**, 70-79.

Yuan, X., Yao, Z., Wu, J., Zhou, Y., Shan, Y., Dong, B., Zhao, Z., Hua, P., Chen, J. and Cong, Y. (2007)**.** G1 phase cell cycle arrest induced by SARS-CoV 3a protein via the cyclin D3/pRb pathway. *Am J Respir Cell Mol Biol* **37**, 9-19.

Zhai, Y., Sun, F., Li, X., Pang, H., Xu, X., Bartlam, M. and Rao, Z. (2005)**.** Insights into SARS-CoV transcription and replication from the structure of the nsp7-nsp8 hexadecamer. *Nat Struct Mol Biol* **12**, 980-986.

Zhang, X., Hasoksuz, M., Spiro, D., Halpin, R., Wang, S., Stollar, S., Janies, D., Hadya, N., Tang, Y., Ghedin, E. and Saif, L. (2007)**.** Complete genomic sequences, a key residue in the spike protein and deletions in nonstructural protein 3b of US strains of the virulent and attenuated coronaviruses, transmissible gastroenteritis virus and porcine respiratory coronavirus. *Virology* **358**, 424-435.

Zhang, X., Liao, C. L. and Lai, M. M. (1994)**.** Coronavirus leader RNA regulates and initiates subgenomic mRNA transcription both in trans and in cis. *J Virol* **68**, 4738-4746.

Zhao, J., Falcon, A., Zhou, H., Netland, J., Enjuanes, L., Perez Brena, P. and Perlman, S. (2009a)**.** Severe acute respiratory syndrome coronavirus protein 6 is required for optimal replication. *J Virol* **83**, 2368-2373.

Zhao, Y., Kurian, D., Xu, H., Petherbridge, L., Smith, L. P., Hunt, L. and Nair, V. (2009b)**.** Interaction of Marek's disease virus oncoprotein Meq with heat shock protein 70 in lymphoid tumour cells. *J Gen Virol*. **90**, 2201-2208.

Zhao, Z., Thackray, L. B., Miller, B. C., Lynn, T. M., Becker, M. M., Ward, E., Mizushima, N. N., Denison, M. R. and Virgin, H. W. t. (2007)**.** Coronavirus replication does not require the autophagy gene ATG5. *Autophagy* **3**, 581-585.

Zhou, H. and Perlman, S. (2007)**.** Mouse hepatitis virus does not induce Beta interferon synthesis and does not inhibit its induction by double-stranded RNA. *J Virol* **81**, 568-574.

Ziebuhr, J. and Siddell, S. G. (1999)**.** Processing of the human coronavirus 229E replicase polyproteins by the virus-encoded 3C-like proteinase: identification of proteolytic products and cleavage sites common to pp1a and pp1ab. *J Virol* **73**, 177-185.

Zoll, J., Galama, J. M., van Kuppeveld, F. J. and Melchers, W. J. (1996)**.** Mengovirus leader is involved in the inhibition of host cell protein synthesis. *J Virol* **70**, 4948-4952.

Zoltick, P. W., Leibowitz, J. L., Oleszak, E. L. and Weiss, S. R. (1990)**.** Mouse hepatitis virus ORF 2a is expressed in the cytosol of infected mouse fibroblasts. *Virology* **174**, 605-607.

Zuniga, S., Sola, I., Alonso, S. and Enjuanes, L. (2004)**.** Sequence motifs involved in the regulation of discontinuous coronavirus subgenomic RNA synthesis. *J Virol* **78**, 980-994.

Zuo, X., Mattern, M. R., Tan, R., Li, S., Hall, J., Sterner, D. E., Shoo, J., Tran, H., Lim, P., Sarafianos, S. G., Kazi, L., Navas-Martin, S., Weiss, S. R. and Butt, T. R. (2005)**.** Expression and purification of SARS coronavirus proteins using SUMO-fusions. *Protein Expr Purif* **42**, 100-110.

Guidelines for this thesis taken from the Guide to Postgraduate Study 29th September 2008, Department of Biological Sciences, University of Warwick.